Vol. 55, No.2 / 2018

e: ISSN 2068 – 2239
p: ISSN 2068 – 4215

INMATEH -

AGRICULTURAL ENGINEERING

MAY - AUGUST

Editorial

The National Institute of Research-Development for Machines and Installations designed to Agriculture and Food Industry - INMA Bucharest has the oldest and most prestigious research activity in the field of agricultural machinery and mechanizing technologies in Romania.

Short History

- In 1927, the first research **Center for Agricultural Machinery** in Agricultural Research Institute of Romania - ICAR (Establishing Law was published in O.D. no. 97/05.05.1927) was established;
- In 1930, was founded **The Testing Department of Agricultural Machinery and Tools** by transforming Agricultural Research Centre of ICAR - that founded the science of methodologies and experimental techniques in the field (Decision no. 2000/1930 of ICAR Manager - GHEORGHE IONESCU ŞIŞEŞTI);
- In 1952, was established the Research Institute for Mechanization and Electrification of Agriculture - ICMA Bănеasa, by transforming the Department of Agricultural Machines and Tools Testing;
- In 1979, the Research Institute of Scientific and Technological Engineering for Agricultural Machinery and Tools – ICSITMUA was founded - subordinated to Ministry of Machine Building Industry - MICM, by unifying ICMA subordinated to MAA with ICPMA subordinated to MICM;
- In 1996 the National Institute of Research-Development for Machines and Installations designed to Agriculture and Food Industry – INMA was founded – according to G.D. no.1308/25.11.1996, by reorganizing ICSITMUA, G.D no. 1308/1996 coordinated by the Ministry of Education and Research G.D. no. 823/2004;
- In 2008 INMA has been accredited to carry out research and developing activities financed from public funds under G.D. no. 551/2007, Decision of the National Authority for Scientific Research - ANCSno. 9634/2008.

As a result of widening the spectrum of communication, dissemination and implementation of scientific research results, in 2000 was founded the institute magazine, issued under the name of SCIENTIFIC PAPERS **(INMATEH)**, ISSN 1583 – 1019.

Starting with volume 30, no. 1/2010, the magazine changed its name to **INMATEH - Agricultural Engineering**, appearing both in print format (ISSN 2068 - 4215), and online (ISSN online: 2068 - 2239). The magazine is bilingual, abstract being published in native language and English, with a rhythm of three issues / year: January-April, May-August, September-December and is recognized by CNCSIS – with B^+ category. Published articles are from the field of AGRICULTURAL ENGINEERING: technologies and technical equipment for agriculture and food industry, renewable energy, machinery testing, environment, transport in agriculture etc. and are evaluated by specialists inside the country and abroad, in mentioned domains.

Technical level and performance processes, technology and machinery for agriculture and food industry increasing, according to national requirements and European and international regulations, as well as exploitation of renewable resources in terms of efficiency, life, health and environment protection represent referential elements for the magazine „**INMATEH - Agricultural Engineering**".

We are thankful to all readers, publishers and assessors.

Editor in chief,

Ph. D. Eng. **Vladut Nicolae-Valentin**

Managing Editorial Board - INMA Bucharest

In the present, *INMATEH - Agricultural Engineering* journal is indexed in the next international databases:
ELSEVIER /SciVerse SCOPUS, CLARIVATE ANALYTICS' WEB OF SCIENCE- Emerging Sources Citation Index (ESCI), ULRICHS Web: Global Serials Directory, CABI, SCIPIO, Index COPERNICUS International, EBSCO Publishing, Elektronische Zeitschriftenbibliothek

INMATEH - Agricultural Engineering
vol. 55, no.2 / 2018
NATIONAL INSTITUTE OF RESEARCH-DEVELOPMENT FOR MACHINES AND INSTALLATIONS DESIGNED TO AGRICULTURE AND FOOD INDUSTRY - INMA Bucharest
6 Ion Ionescu de la Brad Blvd., sector 1, Bucharest

Three issues per year,
e-ISSN: 2068 – 2239
p ISSN: 2068 – 4215

Edited by: INMA Bucharest

CONTENT

RESEARCH ON A BOILER FURNACE MODULE EFFECTIVENESS WORKING ON SMALL FRACTURE WASTES

/

ДОСЛІДЖЕННЯ ЕФЕКТИВНОСТІ РОБОТИ ТОПКОВОГО ПРИСТРОЮ КОТЛОАГРЕГАТУ НА ПАЛИВІ З ДРІБНОЗЕРНИСТИХ ВІДХОДІВ

Prof. D.Sc. Golub G.A.[1)], Prof. D.Sc. Kukharets S.M.[2)], S.Lect. Ph.D. Tsyvenkova N.M.[2)], Teach. Assis. Grad.Stud. Golubenko A.A.[2)], Grad.Stud. Kalenichenko P.S.[2)]

[1)]National University of Life and Environmental Sciences of Ukraine / Ukraine,

[2)]Zhytomyr National Agroecological University / Ukraine

Tel: +380503138903, E-mail: nataliyatsyvenkova@gmail.com

Keywords: *furnace module, flue gases temperature, small fracture wastes, aerodynamic resistance*

ABSTRACT

A method of defining an optimal blowing mode for the boiler when burning agricultural plant residues with varying moisture content, by measuring flue gases temperature was proposed. A multifactor experiment was planned to interconnect the above-mentioned parameters. A tuning chart for the boiler was built based on the results. It was defined that maximum flue gases temperature is an indicator of optimal air supply, i.e. flue gases temperature is an estimate indicator of combustion completeness. As a result of researching regime parameters when burning different plant residue mixtures and analysing received response surfaces, the parameters for maximized heat productivity were obtained.

РЕЗЮМЕ

Представлено метод визначення оптимальних технологічних режимів дуття в процесі експлуатації котлоагрегату при спалюванні рослинних залишків аграрного походження змінної вологості дослідженням температури димових газів. Спланований багатофакторний експеримент, який пов'язує означені вище параметри, за його результатами побудовані регулювальні характеристики котлоагрегату. Встановлено, що найвищі значення температури димових газів є показником оптимального значення питомих витрат повітря, тобто температура димових газів є оціночним показником горіння. В результаті дослідження режимних параметрів спалювання складних сумішей рослинних відходів та аналізу отриманих поверхонь відгуку отримано режими, що забезпечують їх спалювання з найбільшою тепловіддачею.

INTRODUCTION

One of the ways of integrated use of bioenergy conversion technologies in agroecosystems is burning plant residues in boilers *(Golub et al., 2017; Geletuha and Zheleznaya, 2014; Roy and Dias, 2017; Sippula et al., 2017).*

Combustion – is a complex physicochemical process, the basis of which is a quick oxidization process with intense energy releasing via heat and light radiation *(Cao et al., 2017; Didura and Struchaev, 2008; Lavrenuk et al., 2014; Nussbaumer, 2003).* To support continuous and long-lasting combustion in a furnace one has to provide such conditions: permanent fuel feeding and air blowing and their extensive mixing with each other; proper temperature needed for ignition and constant intensive burning; continuous combustion products extraction *(Branco and Costa, 2017; Porteiro et al., 2006).*

When burning solid fuels several stages can be separated: heating fresh fuel portions; humidity evaporation; volatiles sublimation and coke formation; volatile and coke combustion; ash formation. *(Yin et al., 2008).* Herewith while increasing fuel layer height, an oxidant concentration in combustion gases goes down (*Didura and Struchaev, 2008; Lavrenuk et al., 2014)*.

When burning plant raw material in thermotechnical equipment (a boiler) the thermal balance looks like the following (*Stepanov et al., 2011)*:

$$Q_{LCV} = Q_1 + Q_2 + Q_3 + Q_4 + Q_5 + Q_6 \quad (1)$$

where

Q_{LCV} is lower calorific value of a fuel, MJ/kg.

Dividing both parts of (1) by Q_{LCV} and multiplying by 100% we receive a boiler thermal balance in %:

$$100 = q_1 + q_2 + q_3 + q_4 + q_5 + q_6 \quad (2)$$

where q_1 – is useful thermal energy; q_2 – thermal loses with flue gases; q_3 – loses from chemical combustion incompleteness; q_4 – loses from mechanical combustion incompleteness; q_5 – loses through the outer shell into environment; q_6 – loses with the heat of the ash.

A characteristic of furnace, as a part of thermotechnical equipment, effectiveness is a combustible components combustion completeness. Therefore, the furnace coefficient of performance (CoP), when q_5 and q_6 are constant, is calculated like *(Carvalho et al., 2013; Kær, 2004; Lerkkasemsan, 2017):*

$$\eta = 1 - \frac{(q_3 + q_4)}{100} \quad (3)$$

Indicator q_3 is conditioned by incomplete combustion of such fuel components as CO, CH_4 and H_2, the calorific value of which is evacuated from furnace module with flue gases in a chemically bonded state.

A chemical incompleteness of combustion is conditioned by multiple phenomenon: a lack of air, supplied into combustion chamber of furnace module; unsatisfactory mixing of fuel and air in the chamber; low temperature in boiler`s combustion chamber, which can't provide persistent combustion *(Bhuiyan and Naser, 2015; Karim and Naser, 2014; Masud et al., 2016)*. Indicator q_3 is going low while excess air coefficient is going up but to a certain extent, which is explained as when oxidant concentration in combustion zone of gaseous fuel components, which are extracted in gas producing process, rises, a combustion reaction runs more completely. For modern boiler designs q_3 can reach 3-5%, but even despite its little value, loses of fuel combustion incompleteness are significant (*Bhuiyan and Naser, 2015; Van Der Lans et al., 2000)*.

Indicator q_4 depends on loses connected with: fuel particles extraction with flue gases; fuel particles falling through the grates to ashtray; part of fuel carbon is not burning out and is extracted with ash (*Bhuiyan and Naser, 2015; Lavrenuk et al., 2014; Stepanov et al., 2011)*. The loses of q_4 raise while air excess coefficient α deviate from optimal value *(Tóth et al., 2017)*. While α is growing, q_4 is going low because of fuel and air mixing intensification but to a certain extent, with the further α growing q_4 began growing up because of fuel particles extraction from combustion zone intensification. Summing loses in combustion chamber for different α values we can determine optimal α value, which responds to minimal loses *(Kær, 2004; Porteiro et al., 2009; Ström and Thunman, 2013).*

As it is known α - is a real quantity of air, needed for complete combustion of fuel, to theoretical quantity, Q_{theor}, ratio. The Q_{theor} value is calculated from combustion equation provided that we know fuel elementary composition. Elementary composition is well known for traditional fuels (gas, petrol, fuel oil etc.), but considering fuels from agricultural plant raw material, it is determined only for few of them. For the fuels the elementary composition of which is unknown (buckwheat husk, millet husk), it is impossible to calculate theoretical air supply, as well as α, that is why when calculating oxidant supply for such fuels a specific air supply $Q_{specific}$ instead of α is used. It tells how much air is needed for the most complete burning of 1 kg of fuel. We must admit that the only way of determining $Q_{specific}$ is experimental.

$$Q_{specific} = \alpha \cdot Q_{theor} \quad (4)$$

where Q_{theor} – is theoretical air quantity needed for complete burning of 1 kg of fuel, m^3/kg.

Furnace module always works in pair with some thermotechnical equipment (boiler, heat producer etc.), that is why when burning fuel in furnace module the requirements of that equipment must be taken into account.

Heat which is transferred from/to any caloric media by means of thermotechnical equipment is transferred by radiation and convection:

$$Q = Q_{rad} + Q_{conv} \quad (5)$$

Heat flux for radiation heat exchange is defined by (*Lavrenuk et al., 2014; Stepanov et al., 2011):*

$$Q_{rad} = \frac{C_0}{\frac{1}{\varepsilon_w} + \frac{1}{\varepsilon} - 1}\left[\frac{\varepsilon}{\varepsilon_r}\left(\frac{T}{100}\right)^4 - \left(\frac{T_r}{100}\right)^4\right] \cdot F_1 \quad (6)$$

where C_0 – black body radiation coefficient, $W/(m^2 \cdot K^4)$; T – flue gases absolute temperature, °K; ε_w –wall blackness grade, T_r – rays acceptor absolute temperature, °K; ε, ε_r – gases blackness grade for temperature T and T_r; F_1 – ray acceptor surface area, m^2.

Convectional heat flux is defined by:

$$Q_{conv} = k \cdot \Delta T \cdot F_2 \quad (7)$$

Where:

k – heat transfer coefficient, W/(m^2·^{0}K); $\Delta T = T - T_{c.m.}$ – temperature difference between flue gases and caloric media heated by thermotechnical equipment, $^\circ$K; F_2 – convection heat exchanger surface area, m^2.

The (6) and (7) shows that in order to raise quantity of useful heat, which is transferred through thermotechnical equipment, flue gases temperature should be raised, while other conditions being constant. The ratio for flue gases temperature is the following (*Stepanov et al., 2011)*:

$$T = \frac{Q_{LCV} \cdot \eta_f + q_{air} + q_{fuel}}{Q_{RO_2} \cdot c_{CO_2} + Q_{N_2} \cdot c_{N_2} + Q_{H_2O} \cdot c_{H_2O} + Q_{theor}(\alpha - 1) \cdot c_{air}} \quad (8)$$

where

Q_{LCV} – fuel lower calorific value, kJ/kg; q_{air} – heat evacuated with air, kJ/kg; q_{fuel} – heat evacuated with fuel, kJ/kg; Q_{RO2}, Q_{N2}, Q_{H2O} – combustion products volumes, m^3/kg; c_{CO2}, c_{N2}, c_{H2O} – combustion products heat capacity for mean temperature *0* to T $^\circ$C, kJ/(m^3·$^\circ$K); $Q_{theor}(\alpha\text{-}1)$ – excessive air volume, m^3/kg; c_{air} – air heat capacity for mean temperature *0* to T_{air} $^\circ$C, kJ/(m^3·$^\circ$K).

Considering (4) equation (8) becomes:

$$T = \frac{Q_{LCV} \cdot \eta_f + q_{air} + q_{fuel}}{Q_{RO_2} \cdot c_{CO_2} + Q_{N_2} \cdot c_{N_2} + Q_{H_2O} \cdot c_{H_2O} + (Q_{specific} - Q_{theor}) \cdot c_{air}} \quad (9)$$

Thus, the furnace module CoP, which is the function of α ($\eta=f(\alpha)$), considering $Q_{specific}$ is constant for this fuel, will be determined as:

$$\eta=f(Q_{specific}) \quad (10)$$

From (9) considering (10) we draw the conclusion that, while other conditions are constant, flue gases temperature on the output of furnace module depends on specific air supply. Therefore, maximum flue gases temperature value is an indicator of optimal specific air supply value, i.e. flue gases temperature is an indirect indicator of combustion process quality.

Since we can't define specific air supply optimal value theoretically – then the only simple and reliable method is the experiment.

The main requirement for the furnace module is providing maximum fuel calorific value, which, in turn, depends on air quantity supplied for combustion. Air supply is calculated with stoichiometric combustion equations which determine minimal air quantity needed to complete combustion of 1 kg of fuel providing that the entire oxygen in the air will react with fuel combustible components. In real conditions, real air quantity supplied for combustion process is always more than theoretically defined, because of imperfect air and fuel mixing and technical imperfection *(Bhuiyan and Naser, 2015; Cao and Li, 2017; Carvalho et al., 2013)*.

So, the less is the value of specific air supply provided complete fuel combustion the more perfect the combustion process is *(Kiselev, 1971; Nussbaumer, 2003)*. Lowering specific air supply raises furnace module CoP and lowers air blowers' actuators consumption. Further lowering, to less than optimal, leads to fuel under burning and lowers the economic effect of thermotechnical equipment *(Melnichuk et al., 2011).*

The research defines experimentally specific air supply for optimal combustion of the buckwheat husk and millet husk. According to theoretical research while raising air supply, flue gases temperature raises, at first, because of lowering of chemical and mechanical under burning, but then, after certain value, lowers because of raising of unburned fuel particles evacuation and flue gases dilution by excessive air *(Stepanov et al., 2011; Van Der Lans et al., 2000).* So, the highest flue gases temperature on the output of furnace module let us talk about the highest combustion completeness, and that correspondent specific air supply is optimal for this type of fuel.

Therefore, the agenda of the research is to develop a method for defining optimal combustion modes for biomass of an arbitrary chemical and fractional composition, by means of multifactor experiment and received data processing. To check effectiveness of this method, that is oriented for usage in small farming without engagement of an outside specialist.

MATERIALS AND METHODS

Experiments were made on boiler designed in NUBIP of Ukraine (fig.1) with laboratory measuring equipment of NUBIP of Ukraine and Institute of Gas NAS of Ukraine according to the accepted methods and branch standards *(DSTU 3581-97).*

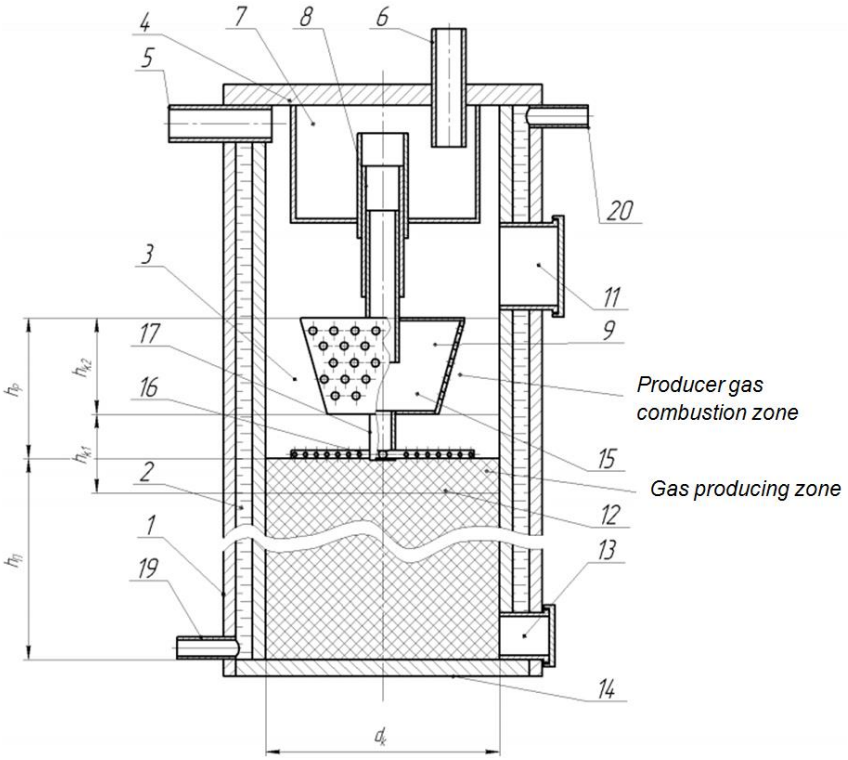

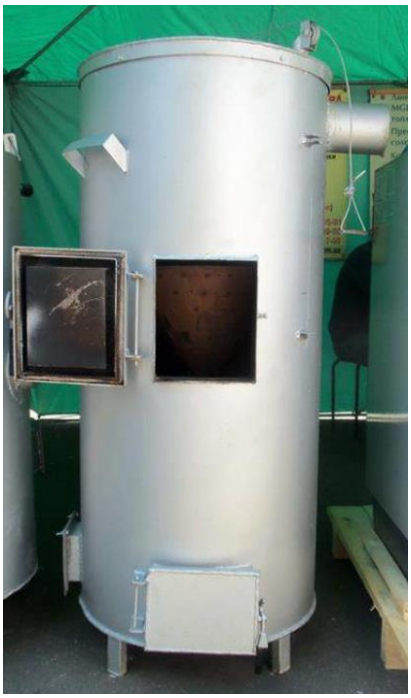

Fig. 1 – Boiler for straw, general view *(Kukharets, 2014)*

1 – outer shell; 2 – cavity; 3 – combustion chamber; 4 – lid; 5 – combustion product evacuation pipe; 6 – air supply pipe, 7 – intermediate capacity; 8 – guider; 9 – air diffuser; 10 – holes, 11 – doors for fuel; 12 – fuel; 13 – doors for ash; 14 – the bottom; 15 – air diffuser upper section; 16 – air diffuser lower section; 17,18 – pipe parts 19 –cold water supply pipe; 20 – hot water evacuation pipe; d_K – boiler diameter; $h_П$ – fuel layer height; h_p – air diffuser height; h_{K1} – gas producing area height; h_{K2} – producer gas combustion area height

Multifactor experiment *(Adler, 1976; Melnikov et al., 1980)* is about mutual influence of such factors as: flue gases temperature, air supply for the initial fuel combustion, producer gas combustion air supply, fuel mixture moisture content.

Experiment was held for different kind of mixtures. Mixture 1 – 50% buckwheat husk + 50% millet husk; mixture 2 – 20% chopped straw + 40% chopped sunflower disks + 40% sunflower husk.

Choosing variation intervals, we were thinking as follows. Total air supply was defined for nominal furnace module productivity based on the manufacturer`s recommendation for approximate calculations – 0.01846 m^3/s air supply for boiler nominal productivity of 50 kW (working heat productivity is 37.5 kW) *(Kiselev, 1971),* for the agricultural plant wastes with lower calorific value of 13.4 – 16.5 MJ/kg *(Kiselev, 1971; Roy and Dias, 2017).*

So, the total air supply will be (considering air excess coefficient recommended for boilers of spherical type α=1,3): max – 80 m^3/h, min – 50 m^3/h. Thus, multifactor experiment planning needs three levels and equal intervals we assume: 50, 65 та 80 m^3/h. Fuel moisture content variation levels were 10%, 25%, 40% *(Geletuha and Zheleznaya, 2014).* Variation levels of above-mentioned factors are given in table 1.

Table 1

Variable factors and limits of their variation for defining the combustion process technological parameters

Factor variation level	Fuel moisture content W, [%]	Fuel air supply Q_{air}, [m^3/h]	Producer gas air supply Q_{pg}, [m^3/h]
	X_1	X_2	X_3
Lower level (-)	10	11	39
Middle level (0)	25	14	51
Upper level (+)	40	17	63

Factors encoding: X_1=W, X_2=Q_{air}, X_3=$Q_{pg.}$

To reduce the number of experiments and obtain the regression equation, the mathematical method of the experiment planning based on Box-Behnken quadric plan *(Adler, 1976; Melnikov et al., 1980)* was used.

Planning stage included the following steps: factor encoding, scheduling, randomization tests, implementation plan of the experiment, testing the reproducibility of the experiments, calculation of regression coefficients, assessment of regression coefficients significance and test model adequacy.

The experiment consisted in 15 tests at threefold repetition in each of them.

Main measuring equipment were: fuel quantity Q_{fuel} (kg) was measured on technical scales VLR-1 (ВЛР-1) GOST 11219-71 (error 0,1%); air supply for fuel Q_{air} (m^3/h) and for producer gas Q_{pg} (m^3/h) was measured with differential pitot-static tube with micro manometer DSP-160-M1 (ДСП-160-М1) (error 0.025%) ТУ 25-7310.0063 (technical conditions of Ukraine); flue gases temperature T (^0C) was measured with a K-type thermocouple paired with EPP-093 m^3 (ЄПП-093 m^3) (error 1%); time τ (c) was measured with a mechanical stopwatch СОСпр-25-2-000±4 (error 0.02%) GOST 5072-79.

RESULTS

As a result of laboratory experiments and statistical computation a heat productivity data array was obtained; it is given in table 2.

Table 2

Planning matrix of a multifactor experiment for determining combustion parameters for two mixtures

№	Experiment planning method				Mixture 1							Mixture 2						
	X_0	X_1	X_2	X_3	T_1	T_2	T_3	T_{med}	$T_{med.com}$	$(T_{med} - T_{med.com})$	$(T_{med} - T_{med.com})^2$	T_1	T_2	T_3	T_{med}	$T_{med.com}$	$(T_{med} - T_{med.com})$	$(T_{med} - T_{med.com})^2$
1	+	+	+	0	340	335	338	337.5	341.1	-3.6	12.96	496	478	484	486	492.3	-6.2	38.69
2	+	+	–	0	339	335	188	287.2	315.4	-28.3	800.89	474	462	471	469	472.4	-3.4	11.70
3	+	–	+	0	376	373	376	374.7	346.4	28.2	795.24	496	496	508	500	496.4	3.4	11.70
4	+	–	–	0	371	368	369	369.0	365.4	3.6	12.96	492	486	479	485	479.3	6.2	38.69
5	+	0	0	0	389	390	388	388.8	390.8	-1.9	3.61	517	529	513	520	521.6	-2.0	3.88
6	+	+	0	+	334	325	332	330.0	331.4	-1.4	1.96	488	480	493	487	491.8	-4.7	22.28
7	+	+	0	–	365	371	370	368.5	359.1	9.4	88.36	489	492	512	498	498.2	-0.6	0.32
8	+	–	0	+	378	377	376	376.5	385.9	-9.4	88.36	493	511	517	507	506.5	0.6	0.32
9	+	–	0	–	365	359	360	361.2	359.8	1.4	1.96	488	507	503	499	494.6	4.7	22.28
10	+	0	0	0	388	385	388	386.8	390.8	-3.9	15.21	524	522	521	522	521.6	0.6	0.36
11	+	0	+	+	375	378	370	374.2	368.6	5.6	31.36	499	514	495	503	501.2	1.6	2.46
12	+	0	+	–	375	370	373	372.5	377.7	-5.2	27.04	504	502	500	502	504.2	-2.6	6.71
13	+	0	–	+	379	380	378	378.7	373.5	5.2	27.04	486	496	491	491	488.5	2.6	6.71
14	+	0	–	–	363	359	360	360.5	366.1	-5.6	31.36	483	473	479	478	479.9	-1.6	2.46
15	+	0	0	0	395	398	398	396.7	390.8	5.9	34.81	522	523	523	523	521.6	1.4	1.90
Regression coefficients:					b_0=390.78; b_1=-13.81; b_2=1.688; b_3=-0.416; b_{12}=11.17; b_{13}=-13.46; b_{23}=-4.125; b_{11}=-30.55; b_{22}=-18.14; b_{33}=-1.18							b_0=521.61; b_1=-2.759; b_2=9.25; b_3=1.394; b_{12}=0.67; b_{13}=-4.552; b_{23}=-2.9; b_{11}=-16.1; b_{22}=-20.42; b_{33}=-7.757						

Received data was processed according to multifactor experiment planning method, with making polynomial regressions of flue gases temperature on factors which influence combustion process.

Experiment results were processed using the software “Statistica”. Homogeneity of variances was tested by the Cochrane criterion. Since $G^{com}=6.67<G^{tabl}(0.05;\ 15;\ 2)=19.3$ – for mixture 1 and $G^{com}=8.87<G^{tabl}(0.05;\ 15;\ 2)=19.3$ – for mixture 2, the process is reproduced.

When we determined the confidence intervals for regression coefficients, the Student test was used, the tabulated value of which at a 5% level of significance and the number of degrees of freedom of experiment variance reproducibility $f_1=2$ was $t=4.3$ (*Melnikov et al., 1980*). The significance of regression coefficients was tested according to the established confidence intervals and covariance. As a result, the regression equation had the form:

- for mixture 1:

$$T=390.78-13.81\cdot X_1+1.69\cdot X_2-0.42\cdot X_3+11.17\cdot X_1\cdot X_2-13.46\cdot X_1\cdot X_3-4.13\cdot X_2\cdot X_3-30.55\cdot X_1^2-18.14\cdot X_2^2-1.18\cdot X_3^2 \quad (11)$$

- for mixture 2:

$$T=521.61-2.76\cdot X_1+9.25\cdot X_2+1.4\cdot X_3+0.67\cdot X_1\cdot X_2-4.55\cdot X_1\cdot X_3-2.9\cdot X_2\cdot X_3-16.1\cdot X_1^2-20.42\cdot X_2^2-7.56\cdot X_3^2 \quad (12)$$

where: X_1 - encoded value of initial fuel moisture value W, %; X_2 - encoded value of the air supply for fuel combustion Q_{air}, m³/h; X_3 - encoded value of the air supply for producer gas combustion Q_{pg}, m³/h.

Adequacy test of hypotheses of obtained regression equation was performed by the Fisher criterion. The estimated value of this criterion in the dispersion of inadequacy $S^2_{inadeq}=27.05$ and dispersion $S_y^2=54.01$ *(mixture 1) and* $S^2_{inadeq}=3.08$, $S_y^2=6.15$ *(mixture 2)* reproducibility of the experiment was: $F^{com}=0.5$. Tabular value of Fisher's exact test adopted by the 5% of significance, according to (*Melnikov et al., 1980*), was: $F^{tabl}(0.05;\ f_1;\ f_2)=19.38$, where $f_2=8$ variance inadequacy degrees of freedom $f_1=2$ – variance experiment reproducibility degrees of freedom. Since, $F^{com}=0.5<F^{tabl}(0.05;\ f_1;\ f_2)=19.38$, the hypothesis by the adequacy of the regression equation is confirmed.

Graphical representations of the above-mentioned equation are given in fig. 2.

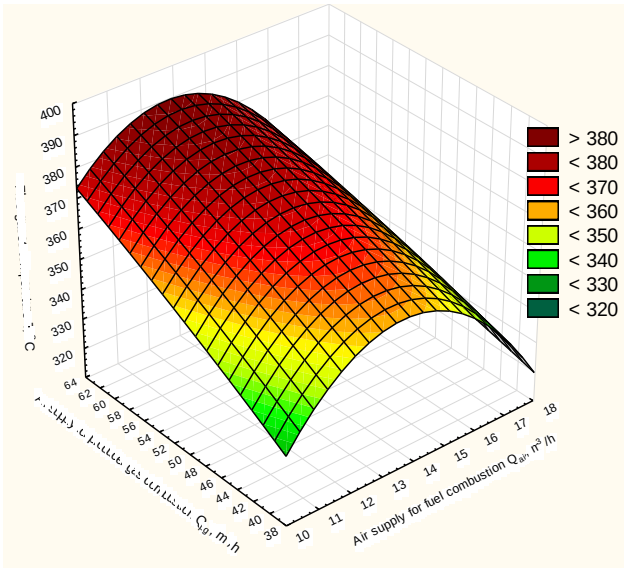

a)

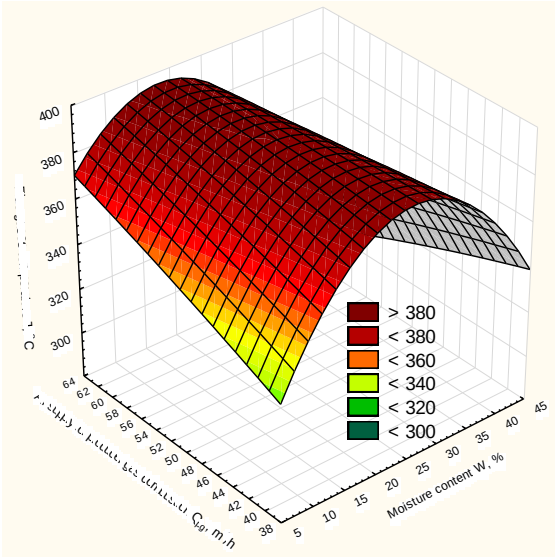

b)

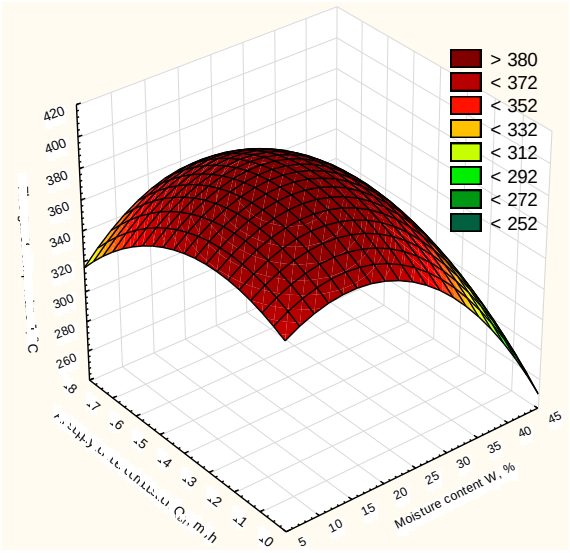

c)

Fig. 2 – Response surfaces of flue gases temperature for mixture 1

a – W=10%, b – Q_{air}=14 m³/h, c – Q_{pg}=63 m³/h

Response surfaces comparison shows that flue gases temperature rises with producer gas combustion air supply and reaches maximum value when Q_{pg}=58 m³/h, fuel combustion (pyrolysis) air supply Q_{air}=14.8 m³/h and fuel moisture content W=28% (fig. 2.a, 2.b). The graphs also show the exact borders of the fuel moisture content when its burning is most effective for this particular boiler design. When moisture content is less than 20% fuel deflagrates and a very little pyrolysis gas produced that, in turn, gives lower flue gases temperature.

When moisture content grows, too much heat is expended for moisture evaporation and as a result flue gases temperature goes down. Maximum temperature in fig. 2.c is a bit lower but more clearly allocated and reached at fuel air supply Q_{air}=15.5 m³/h and moisture content 28%. Therefore, total air supply for mixture 1 is 73 m³/h, herewith it is expedient to supply 79…80% of air to gas combustion and 20…21% to fuel pyrolysis process. Such air distribution differs from what is recommended by manufacturer and is explained by fuel mixture peculiarity.

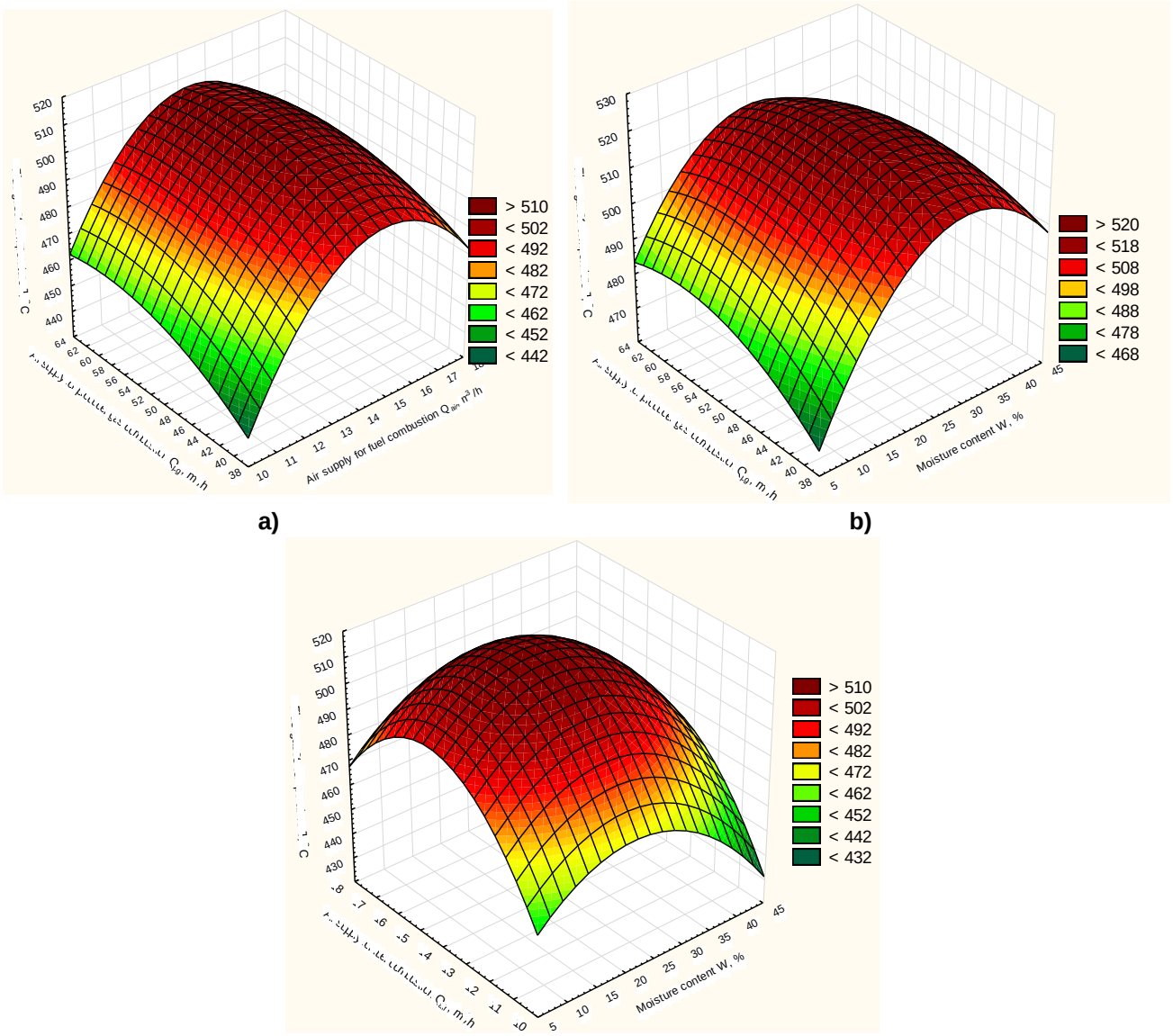

Fig. 3 – Response surfaces of flue gases temperature for mixture 2

a – W=10%, b – Q_{air}=14 m³/h, c – Q_{pg}=63 m³/h

For the fuel mixture 2 response surfaces gives clear maximums for flue gases temperature within optimal parameters values. If we fixate moisture content on the minimal level of 10%, the highest flue gases temperature is observed when fuel combustion air supply is 15.5 m³/h i (fig. 3.a). When fuel combustion air supply Q_{air} is fixed at 14 m³/h, maximized flue gases temperature is located within producer gas combustion air supply value 51 m³/h and fuel moisture content 27% (fig. 3.b).

For this mixture total air supply, for effective boiler functioning, is 66.5 m³/h, herewith it is expedient to supply around 76% of air for producer gas combustion process and the rest 24% for the process of fuel pyrolysis. Such distribution matches manufacturer's recommendations so this fuel mixture is well suited for the chosen boiler design.

To prove the research hypothesis about defining optimal combustions modes for biomass by maximized flue gases temperature a control experiment was carried out. The point of this experiment was in

defining boiler's heat productivity when changing blowing modes while burning an optimal, for this type of boiler, fuel mixture with 27% moisture content.

Based on these results there were built:

- flue gases temperature response surface for mixture 2 with moisture content W=27% (fig. 4.a) and a contour plot with the highlighted area of maximized temperature values (fig. 4.b);

- boilers heat productivity response surface against blowing mode for the same fuel mixture 2 and *W*=27% (fig. 5.a) and contour plot with highlighted area of maximum heat productivity values (fig. 5.b).

Comparing fig. 4 and fig. 5 we can see that areas with maximum values matches. This fact proves our hypothesis.

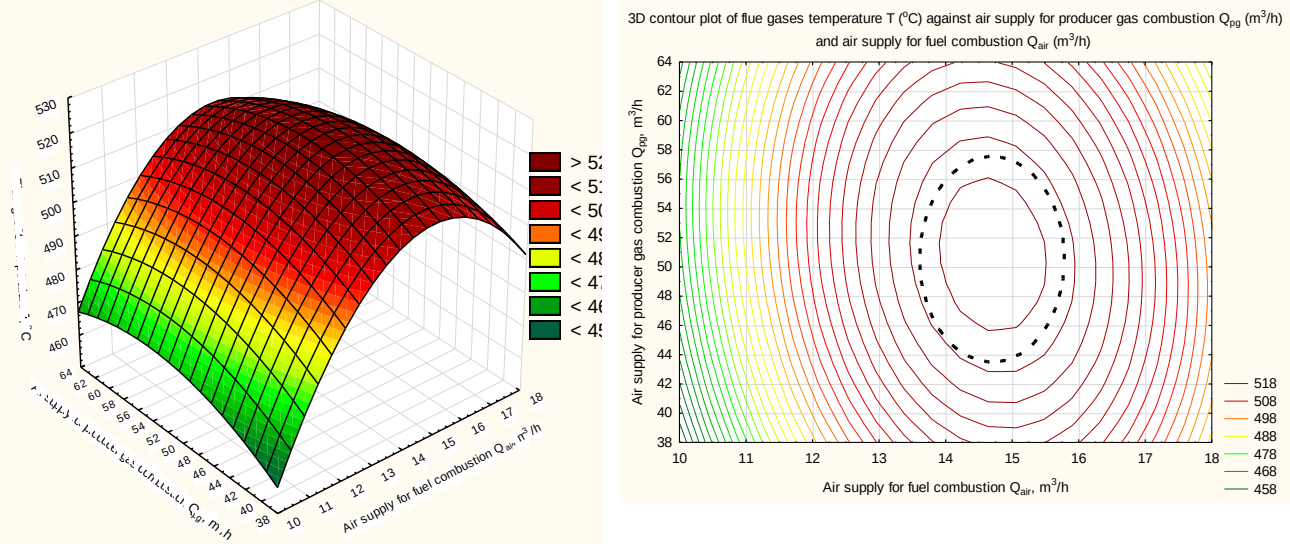

a) **b)**

Fig. 4 – response surfaces for flue gases temperature for mixture 2 with *W=27%*

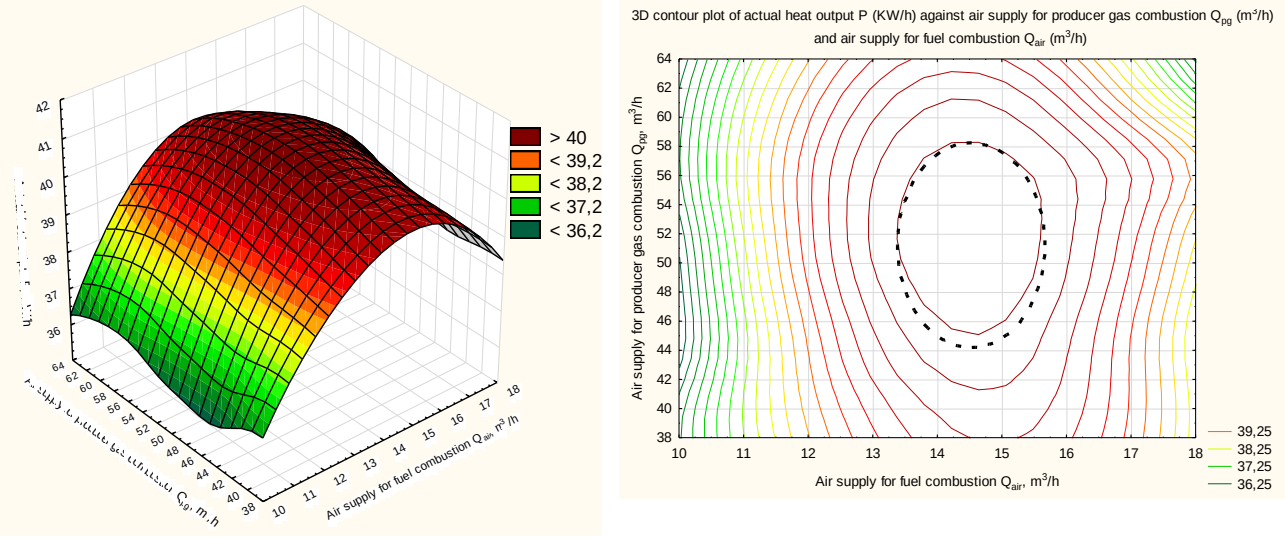

a) **b)**

Fig. 5 – Response surfaces for real boiler's heat productivity for mixture 2 with *W=27%*

CONCLUSIONS

Summing all we can say that:

1. It is defined that for any mixture of agricultural plant residues despite of its type, composition, growing, picking and storing conditions exact optimal combustion modes exists. They can be defined without elementary composition research;

2. Experimentally substantiated mode and design parameters of boiler for effective combustion of the small fracture plant wastes:

– total air supply for mixture 1 is 73 m^3/h with optimal moisture content W=28%, herewith 79…80% of air should be supplied for gas combustion and 20…21% – for the fuel pyrolysis process;

– total air supply for mixture 2 is 66.5 m^3/h with optimal moisture content W=27%, herewith 76% of air should be supplied for gas combustion and 24% – for the fuel pyrolysis process;

– chemical and mechanical combustion incompleteness for mixture 1 was 1.9% and 3.7% respectively, and for mixture 2 – 1.7% and 2.3%;

– the hypothesis that we can define upper and lower air supply by measuring flue gases temperature is confirmed by control experiment of measuring maximum heat productivity. Maximum of heat productivity was seen between the same air blowing mode values as for flue gases temperature.

Since flue gases temperature is easier to measure than heat productivity, then the described method can be recommended for defining optimal combustion parameters for complex fuel mixtures without defining its chemical composition, calorific value or any features that can influence combustion effectiveness exactly in the boilers with upper combustion. Proposed method gives us possibility to burn any fuel biomass mixtures with maximum effectiveness and heat productivity.

A perspective direction of researches is creating an automatic air blowing mode regulation system dependent on flue gases temperature, based on these results.

REFERENCES

[1] Adler U.P., (1976), *Planning experiment when searching for optimal conditions (Планирование эксперимента при поиске оптимальных условий),* "Nauka", p. 279, Moscow / Russia;

[2] Bhuiyan A.A., Naser J., (2015), CFD modelling of co-firing of biomass with coal under oxy-fuel combustion in a large scale power plant, *Fuel,* no.159, ISSN 0016-2361, pp. 150-168;

[3] Bhuiyan A.A., Naser J., (2015), Computational modelling of co-firing of biomass with coal under oxy-fuel condition in a small scale furnace, *Fuel,* no.43, ISSN 0016-2361, pp. 455-466;

[4] Bhuiyan A.A., Naser J., (2015), Numerical Modelling of Biomass Co–combustion with Pulverized coal in a Small-Scale Furnace, *Procedia Engineering,* no.105, ISSN: 1877-7058, pp. 504-511;

[5] Branco V., Costa M., (2017), Effect of particle size on the burnout and emissions of particulate matter from the combustion of pulverized agricultural residues in a drop tube furnace, *Energy conversion and management,* Elsevier Ltd., ISBN10:0123964881, pp 1-7, San Diego / U.S.A.;

[6] Cao W., Li J., Lue L., (2017), Study on the ignition behaviour and kinetics of combustion of biomass, *Energy Procedia*, vol.142, Elsevier Ltd, ISSN: 1876-6102, pp. 136-141, San Diego / USA;

[7] Carvalho L., Wopienka E., Pointner C., Lundgren J., Kumar Verma V., Haslinger W., Schmidl Ch., (2013), Performance of a pellet boiler fired with agricultural fuels, *Applied Energy,* vol.104, Elsevier Ltd., ISBN10:0123964881, pp. 286-296, San Diego / USA;

[8] Didura V., Struchaev M., (2008), *Heat engineering (Теплотехніка)*, "Agrarian education", ISBN 966-7906-43-4, 233 p., Kyiv/Ukraine;

[9] Geletuha G., Zheleznaya T., (2014), World experience of using agricultural residues for energy production (Мировой опыт использования отходов сельского хозяйства для производства энергии), *Enterprise Environment (Экология предприятия),* no. 3, pp.56-69, Kiev/Ukraine;

[10] Golub G., Kukharets S., Yarosh Y., Kukharets V., (2017), Integrated use of bioenergy conversion technologies in agroecosystems (Комплексне використання технологій біоенергетичної конверсії у агроекосистемах), *INMATEH-Agricultural Engineering*, vol. 51, no.1, pp. 93-100, Bucharest/Romania;

[11] Kær S.K., (2004), Numerical modelling of a straw-fired grate boiler, *Fuel,* no. 83(9), ISSN 0016-2361, pp. 1183-1190;

[12] Karim M., Naser J., (2014), Progress in Numerical Modelling of Packed Bed Biomass Combustion, *Proceedings of the 19th Australasian Fluid Mechanics Conference* (19 AFMC), pp. 390-395, Melbourne / Australia;

[13] Kiselev N., (1971), *Boilers and heat generators in agriculture (Котлы и теплогенераторы в сельском хозяйстве),* "High school", p. 135, Moscow / Russia;

[14] Kukharets S.M., (2014), Rationale the main parameters of upper combustion boilers (Обгрунтування основних параметрів котлів із верхнім горінням), *Engineering and Energetics in agriculture (Техніка та енергетика АПК)*, no. 196, part 2, ISSN 2222-8594, pp 238-250, Kiev/Ukraine;

[15] Lavrenuk O., Balanuk V., Muhalichko B., (2014), *The combustion and explosion theory (Теорія горіння та вибуху)*, "VONDRVR LSU LS", 130 p., Lviv/Ukraine;

[16] Lerkkasemsan N., (2017), Fuzzy logic-based predictive model for biomass pyrolysis, *Applied Energy,* vol. 185, part 2, Elsevier Ltd, ISBN10:0123964881, pp. 1019-1030, San Diego / USA;

[17] Masud M., Khan K., Hassan Nur, (2016), *Thermofluid Modelling for Energy Efficiency Applications*, ed. 1, "Academic Press", Publishing House, ISBN: 9780128023976, 360 p., Queensland/Australia;
[18] Melnichuk M., Dubrovin V., Mironenko V. et al., (2011), *Alternative energy (Альтернативна енергетика)*, "Agrar media group", Kiev/Ukraine;
[19] Melnikov S.V., Atselkin V.R., Roshchin P.M., (1980), *Planning experiment of agricultural process research (Планирование эксперимента в исследованиях сельскохозяйственных процессов),* "Kolos", p. 168, Leningrad / Russia;
[20] Nussbaumer T., (2003), Combustion and co-combustion of biomass: fundamentals, technologies, and primary measures for emission reduction, *Energy & fuels*, no.17(6), ISSN 0887-0624, pp. 1510-1521, Washington / USA.;
[21] Porteiro J., Collazo J., Patiño D., Granada E., Gonzalez J.C.M., Míguez J.L., (2009), Numerical modelling of a biomass pellet domestic boiler, *Energy and Fuels,* ISSN 0887-0624, no. 23(2), pp. 1067-1075;
[22] Porteiro J., Míguez J.L., Granada E., Moran J.C., (2006), Mathematical modelling of the combustion of a single wood particle, *Fuel Processing Technology,* no. 87(2), ISSN: 0378-3820, pp. 169-175;
[23] Roy P., Dias G., (2017), Prospects for pyrolysis technologies in the bioenergy sector: A review, *Renewable and Sustainable Energy Reviews,* vol. 77, Elsevier Ltd., ISBN10:0123964881, pp. 59-69, San Diego/USA;
[24] Sippula O., Lamberg H., Leskinen J., Tissari J., Jokiniemi J., (2017), Emissions and ash behaviour in a 500 kW pellet boiler operated with various blends of woody biomass and peat, *Fuel,* no. 202, ISSN 0016-2361, pp. 144-153;
[25] Stepanov D., Korzhenko E., Bondar L., (2011), *Boiler installations for small enterprises (Котельні установки малих підприємств)*, "VNTU", p. 120, Vinnitsa/Ukraine;
[26] Ström H., Thunman H., (2013), CFD simulations of biofuel bed conversion: A submodel for the drying and devolatilization of thermally thick wood particles, *Combustion and Flame*, no. 160(2), ISSN: 0010-2180, pp. 417-431;
[27] Tóth P., Garami A., Csordás B., (2017), Image-based deep neural network prediction of the heat output of a step-grate biomass boiler, *Applied Energy*, vol. 200, Elsevier Ltd., ISBN10:0123964881, pp. 155-169, San Diego/USA;
[28] Van Der Lans R.P., Pedersen L.T., Jensen A., Glarborg P., Dam-Johansen K., (2000), Modelling and experiments of straw combustion in a grate furnace, *Biomass and Bioenergy,* no. 19(3), ISSN: 0961-9534, pp. 199-208;
[29] Yin C., Rosendahl L.A., Kær S.K., (2008), Grate-firing of biomass for heat and power production. *Progress in Energy and Combustion Science*; no. 34(6), ISSN: 0360-1285, pp. 725-754, Netherlands;
[30] ***DSTU 3581-97, *Energy efficiency, Methods of measuring and calculating the heat of combustion (Енергозбереження. Методи вимірювання і розрахунку теплоти згоряння палива)*, Kiev/Ukraine.

DESIGN AND EXPERIMENTAL STUDY OF A RAPESEED BROADCAST SPREADER OF SCREW-DROP TYPE
/
螺旋排种式油菜籽撒播机设计及试验

Prof. Ph.D. Eng. Xie S.Y., Ms. Stud. Eng. Yu T., Ms. Stud. Eng. Chen T.H., Ms. Stud. Eng. Yang Z.R., Prof. Ph.D. Eng. Yang L., Prof. Ph.D. Eng. Yang M.J.*)

Southwest University, College of Engineering and Technology, Chongqing Key Laboratory of Agricultural Equipment for Hilly and Mountainous Regions / P. R. China
Tel: 8613883002509; E-mail: ymingjin@swu.edu.cn

Keywords: *broadcast spreader, screw-drop type, direct drilling, distribution uniformity, rapeseed*

ABSTRACT

A small-scale rapeseed broadcast spreader of screw-drop type was developed in this study. The effect of process parameters on broadcast sowing performance of rapeseed was tested and investigated. The metering rate and spreading width of the broadcast spreader were adjustable. The metering rate linearly increased with the increase of screw auger revolution and the spreading width logarithmically increased with the increase of rotary disk revolution and height. Rotary disk revolution had the highest significant level of impact on distribution uniformity of rapeseed broadcast sowing of the broadcast spreader, and it was followed by screw auger revolution, rotary disk height and the spreader forward speed, sequentially. The optimal process parameters for distribution uniformity of rapeseed broadcast sowing were the rotary disk revolution 180 rpm, rotary blade height 800 mm, forward speed 2 km/h, and screw auger revolution 40 rpm.

摘要

本研究开发了一套小型螺旋排种式油菜籽撒播机，并测试和验证了工艺参数对油菜籽撒播性能的影响。研究表明，撒播机的排种速率和撒播幅宽可调，排种速率随着螺旋排种搅龙转速的增加而呈线性增加，撒播幅宽随着圆盘转速和圆盘高度的增加而呈对数关系增加。圆盘转速对油菜籽撒播均匀性的影响最显著，其次是螺旋排种搅龙转速和圆盘高度，前进速度影响最小。对于撒播均匀性而言，最优的工艺参数是：圆盘转速 180 rpm，圆盘高度 800 mm，前进速度 2 km/h，排种搅龙转速 40 rpm。

INTRODUCTION

Rape is a bright-yellow flowering member of the family *Brassicaceae* (mustard or cabbage family), cultivated mainly for its oil-rich seed. Rapeseed is the third-largest source of vegetable oil in the world *(Yang et al., 2017)*. China is one of the top rapeseed producers and accounts for about 20% of world production. Rapeseed is more likely to achieve increased yield in high-density plantings since high-density planting can increase index of plant leaf area, improve efficiency of light energy use and nitrogen use, and promote transformation of nitrogen to grain *(Hu et al., 2017)*.

Direct drilling is an effect method of rapeseed planting in high-density planting model and greatly reduces labour cost and improves soil structure. By means of direct drilling, rapeseed is metered and dropped into farming lands, namely mechanical seedling nursery is not required, which simplifies the planting process and benefits its mechanization of rapeseed production *(Zhang et al., 2012)*. Direct drilling falls into 4 categories: broadcast sowing, strip sowing, dibble sowing and precision sowing, and their sowing precision increases sequentially. No-till farming of rape is newly encouraged in Southern China. Broadcast sowing is one of the key links of no-till farming of rape. Compared to traditional transplanting method, broadcast sowing shows good performance of high efficiency and low labour cost. The main obstacles for advocating broadcast sowing are high amount of seed use and low distribution uniformity of sowing *(Sun et al., 2017)*.

The application of broadcast spreader to broadcast sowing gave direct reference to fertilizer spreader. Centrifugal spreader was the main type of broadcast spreader used in fertilizer broadcasting, and as a result, the corresponding study, design, optimization, and improvement matured a lot. Theoretical

studies on centrifugal spreader dated back to the 60s of last century. While neglecting particle bounce, motion and force of a single spherical particle on a flat rotary disk equipped with radial straight vanes were examined, particle trajectories escaping from the disk were investigated. According to these theoretical studies, many centrifugal spreaders for fertilizer use were developed and their broadcasting performances were examined *(Wu, 2007; Zhang et al., 2012; Dong et al., 2013; Kobets et al., 2017)*. To optimize spreading process and improve broadcasting performance, innovative image-based techniques were employed to measure the spread pattern and identify the particle dispersion, and showed good agreement with experiments *(Cool et al., 2017; Chen et al., 2017)*.

Nevertheless, as for centrifugal spreader for rapeseed broadcast purpose, few reports or literatures were available. The main objectives of this study were to develop a small-scale rapeseed broadcast spreader, investigate the effect of process parameters on rapeseed broadcast sowing performance, and optimize process parameters of the broadcast spreader.

MATERIALS AND METHODS

Mature and dry rapeseed was bought from market in Beibei, Chongqing, China. The impurities, cracked, germinated, mouldy seed and seed of small size were manually removed to obtain test samples of a uniform size.

Design of broadcast spreader

A schematic diagram of the broadcast spreader designed for rapeseed broadcast sowing was presented, as shown in fig.1. The main components of the spreader were seed hopper, screw auger for metering rapeseed, seed chute, and rotary disk for spreading rapeseed. Rapeseed in seed hopper was screw-dropped onto the flat rotary disk of diameter 200 mm, through a screw auger of diameter 100 mm and seed chute. The rotary disk was evenly equipped with 6 radial straight vanes. Rapeseed on the rotary disk was accelerated by the resultant of forces such as gravity, inertia transfer, Coriolis' inertia, frictional forces interaction with disk and vane edge, disk reaction *(Kobets et al., 2017)*. An initial throw velocity off the rotary disk was obtained, with rapeseed passing through a 120° exit. Other rapeseed, blocked by the shield, was dropped into the seed collector for later sowing. The screw auger and rotary disk were driven by different motors to obtain revolutions of ω_1 and ω_2. The screw auger rotated counter-clockwise on the top view.

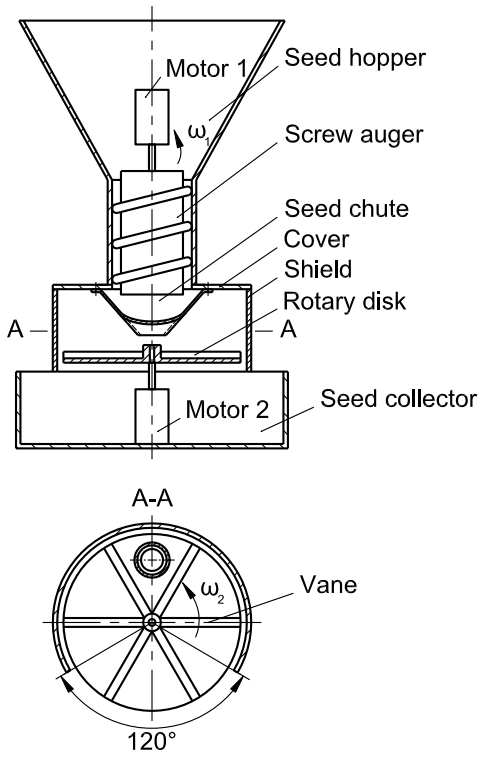

Fig. 1 – Structure diagram of broadcast spreader of screw-drop type

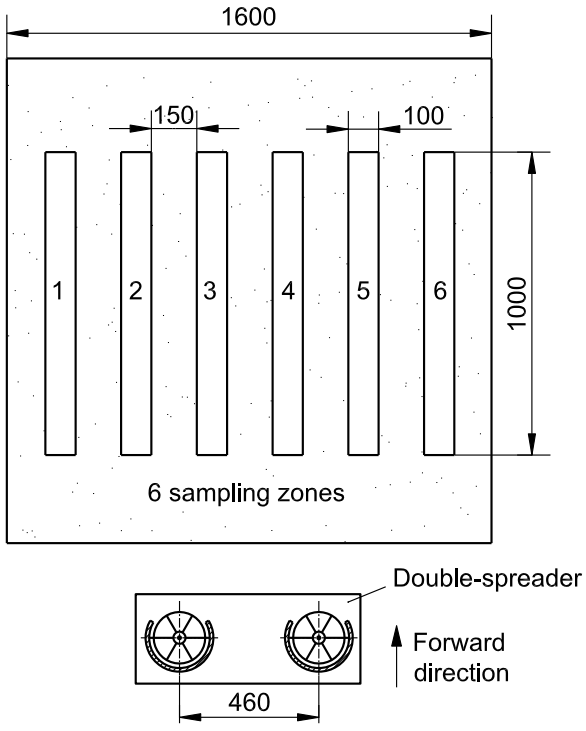

Fig. 2 – Outline of experiments on double-spreader

Experiments on single-spreader

(1) Metering rate with revolution of screw auger. In order to obtain a defined constant broadcast sowing rate of rapeseed, it is necessary to examine the metering rate of screw auger. The revolution of screw auger was controlled by motor *1* with Pulse Width Modulation (PWM) method, and it was tested by a portable tachometer. The rapeseed was metered under constant revolution of screw auger. Seven revolutions were adopted for the experiment, at an increasing revolution of 10 rpm from 10 rpm to 70 rpm. To reduce errors of metering test, only rapeseed in the medium stage was sampled by a container. The sampling time was from 0.5 min to 1.5 min.

(2) Spreading width with revolution of rotary disk. A flannelette cloth of dimensions 1.6 m width and 10.0 m length was covered on a flat field for the spreading width test. The height of rotary disk above the flat field was set as 160 mm, and revolution of screw auger was set as 40 rpm. Seventeen revolutions of rotary disk were adopted for the experiment. The rotary disk minimum revolution was set as 118 rpm, and the maximum revolution was set as 584 rpm. Five grams of rapeseed were used for each test. The revolution of rotary disk was controlled by motor *2* with PWM method.

(3) Spreading width with height of rotary disk. The revolutions of screw auger and rotary disk were set as 40 rpm and 417 rpm, separately. Eight heights of rotary disk were set for the experiment. The minimum height was set as 160 mm, and the maximum height was set as 1500 mm. Five grams of rapeseed were used for each test as well.

Experiments on double-spreader

(1) Experimental setup. To improve efficiency and distribution uniformity of rapeseed broadcast sowing, an overall design of double-spreader was adopted for the rapeseed broadcast spreader. The span of the two spreaders was set as 460 mm, an approximate span of an adult's shoulders. Six sampling zones were marked on the flannelette, with dimensions of 1000 mm length and 100 mm width, and there were spaces of 150 mm between neighbour zones, as shown in fig. 2. Five grams of rapeseed per spreader, namely 10 g of rapeseed altogether, were used for each test.

(2) Experimental procedures. Experiments of distribution uniformity of single-factor sowing were initially conducted to obtain an overall performance of the double-spreader. According to the tested distribution uniformity, control factors and their levels of multi-factor sowing for distribution uniformity could be defined. Parameters of the single-factor sowing for distribution uniformity were listed in Table 1.

Table 1

Parameters of single-factor sowing for distribution uniformity

Experiment Item	Fixed parameters				
	Revolution of rotary disk	Height of rotary disk	Span of spreaders	Revolution of screw auger	Forward speed
	[rpm]	[mm]	[mm]	[rpm]	[km/h]
Effect of revolution of rotary disk on distribution uniformity	/	160	460	40	0
Effect of height of rotary disk on distribution uniformity	435	/	460	40	0
Effect of span of spreaders on distribution uniformity	435	160	/	40	0
Effect of forward speed on distribution uniformity	435	410	460	40	/

For experiments on distribution uniformity of multi-factor sowing, orthogonal Factorial Experiment Design technique based on Taguchi methodology was employed to arrange experiments. Taking revolution of rotary disk, height of rotary disk, forward speed of broadcast spreader, and revolution of screw auger as control factors, and sowing distribution uniformity as evaluation index, levels of control factors were defined, as shown in Table 2. Experiments were designed in accordance with appropriate orthogonal array $L_9(3^4)$, a 3-level 4-factor array with 9 runs, and their arrangement was shown in Table 3. The span of spreaders was set as 460 mm for the multi-factor sowing.

Table 2

Levels of control factor

Level	Revolution of rotary disk A	Height of rotary disk B	Forward speed C	Revolution of screw auger D
	[rpm]	[mm]	[km/h]	[rpm]
1	180	400	1	10
2	360	800	2	40
3	540	1200	3	70

Table 3

Experiment arrangements and results of distribution uniformity

No.	Factor A	Factor B	Factor C	Factor D	Distribution uniformity
1	1	1	1	1	0.713
2	1	2	2	2	0.761
3	1	3	3	3	0.656
4	2	1	2	3	0.556
5	2	2	3	1	0.657
6	2	3	1	2	0.669
7	3	1	3	2	0.688
8	3	2	1	3	0.697
9	3	3	2	1	0.701

The experiments of distribution uniformity of broadcast sowing were conducted according to standard of American Society of Agricultural and Biological Engineers ASAE S341.3, namely "Procedure for measuring distribution uniformity and calibrating granular broadcast spreaders" *(American Society of Agricultural and Biological Engineers, 2005)*. Distribution uniformity was calculated by the following expression:

$$D = 1 - CV \quad (1)$$

where:

D is distribution uniformity, [dimensionless];

CV – coefficient of variation, [dimensionless].

Coefficient of variation was calculated as follows:

$$CV = \frac{s}{\mu} \quad (2)$$

where:

s is standard deviation of samples;

μ – mean accumulated sample per sampling zone, [particles].

RESULTS

Performance of Single-spreader

Metering rate with revolution of screw auger, at an increasing revolution of 10 rpm from 10 rpm to 70 rpm, was obtained and depicted. As shown in fig. 3, metering rate of the broadcast spreader linearly increases with the increase of screw auger revolution. A regression equation, with coefficient of determination R^2 0.9820, was obtained by means of software SPSS as:

$$M = 0.1293 R_a + 2.5571 \text{ [g/min]} \quad (3)$$

where: M is metering rate, [g/min];

R_a – auger revolution, [rpm].

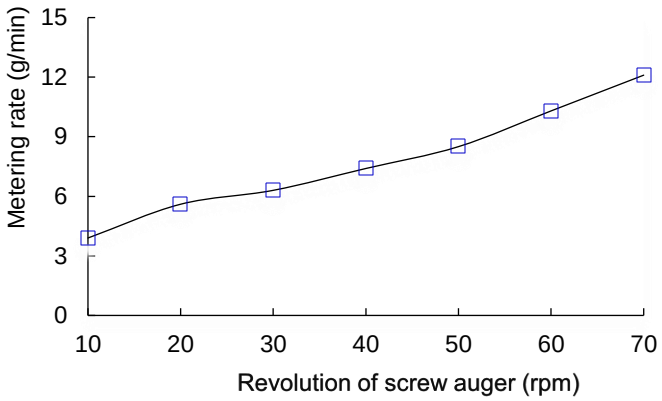

Fig. 3 – Metering rate with screw auger revolution

Spreading width with rotary disk revolution, starting from 118 rpm to 584 rpm, was obtained and depicted. As shown in Fig. 4, spreading width of the broadcast spreader logarithmically increases with the increase of rotary disk revolution. A regression equation, with coefficient of determination R^2 0.9830, was obtained as:

$$W = 768.87 \ln\left(R_d\right) - 3489.7 \quad [\text{mm}] \tag{4}$$

where:

W is spreading width, [mm];

R_d – rotary disk revolution, [rpm].

Similarly, spreading width with the height of rotary disk, starting from 160 mm to 1500 mm, was obtain and depicted. As shown in fig. 5, spreading width of the broadcast spreader logarithmically increases with the increase of rotary disk height. A regression equation, with coefficient of determination R^2 0.9840, was obtained as:

$$W = 600.7 \ln\left(H\right) - 2001.3 \quad [\text{mm}] \tag{5}$$

where:

H is rotary disk height, [mm].

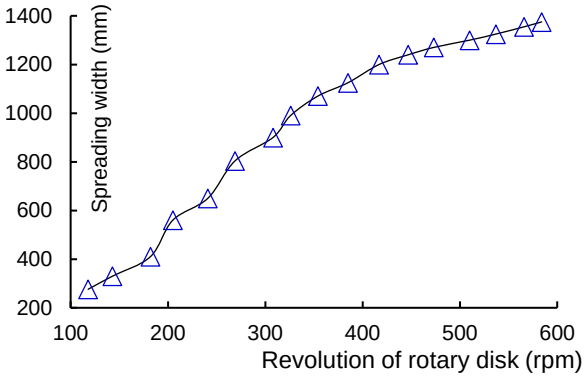

Fig. 4 – Spreading width with revolution of rotary disk

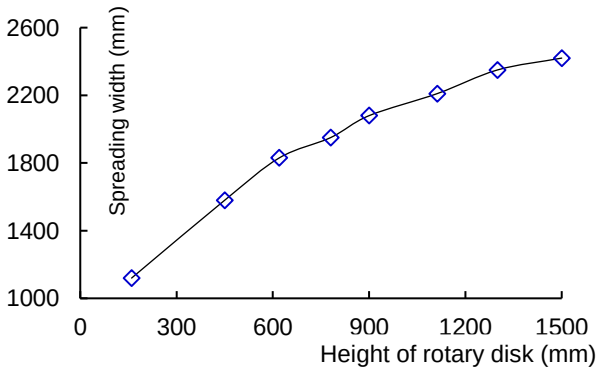

Fig. 5 – Spreading width with height of rotary disk

Performance of Double-spreader

Distribution uniformity of single-factor sowing

Distribution uniformity of single-factor sowing was obtained and depicted, as shown in fig. 6. While keeping height of rotary disk 160 mm, span of spreaders 460 mm, revolution of screw auger 40 rpm, and forward speed of the double-spreader 0 km/h constant, the maximum distribution uniformity obtained was 0.757 at rotary disk revolution 435 rpm, and the minimum was 0.502 at 260 rpm, with a difference of 0.255 (fig. 6 (a)). While keeping rotary disk revolution 435 rpm, span of spreaders 460 mm, screw auger

revolution 40 rpm, and forward speed of the double-spreader 0 km/h constant, the maximum distribution uniformity obtained was 0.812 at rotary disk height 475 mm, and the minimum was 0.665 at 550 mm, with a difference of 0.147 (fig. 6 (b)). While keeping rotary disk revolution 435 rpm, rotary disk height 160 mm, screw auger revolution 40 rpm, and forward speed of the double-spreader 0 km/h constant, the maximum distribution uniformity obtained was 0.851 at span of spreaders 860 mm, and the minimum was 0.613 at 660 mm, with a difference of 0.238 (fig. 6 (c)). While keeping rotary disk revolution 435 rpm, rotary disk height 160 mm, span of spreaders 460 mm, and screw auger revolution 40 rpm constant, the maximum distribution uniformity obtained was 0.820 at forward speed of the double-spreader 2 km/h, and the minimum was 0.684 at 1.5 km/h, with a difference of 0.136 (fig. 6 (d)).

According to Chinese standard JB/T 6274.1-2013, namely "Grain drill - Part 1: Specifications", the distribution uniformity of a grain drill should be higher than 0.55 *(Ministry of Industry and Information Technology of the P. R. China, 2013)*. The overall performance of the double-spreader is good, especially for application of rapeseed broadcast sowing in hilly and mountainous regions of Chongqing, China. But for practical promotion of the broadcast spreader, some parameters or specifications should be adjusted, so as to obtain convenience, easy-operation and portability of the rapeseed broadcast sowing.

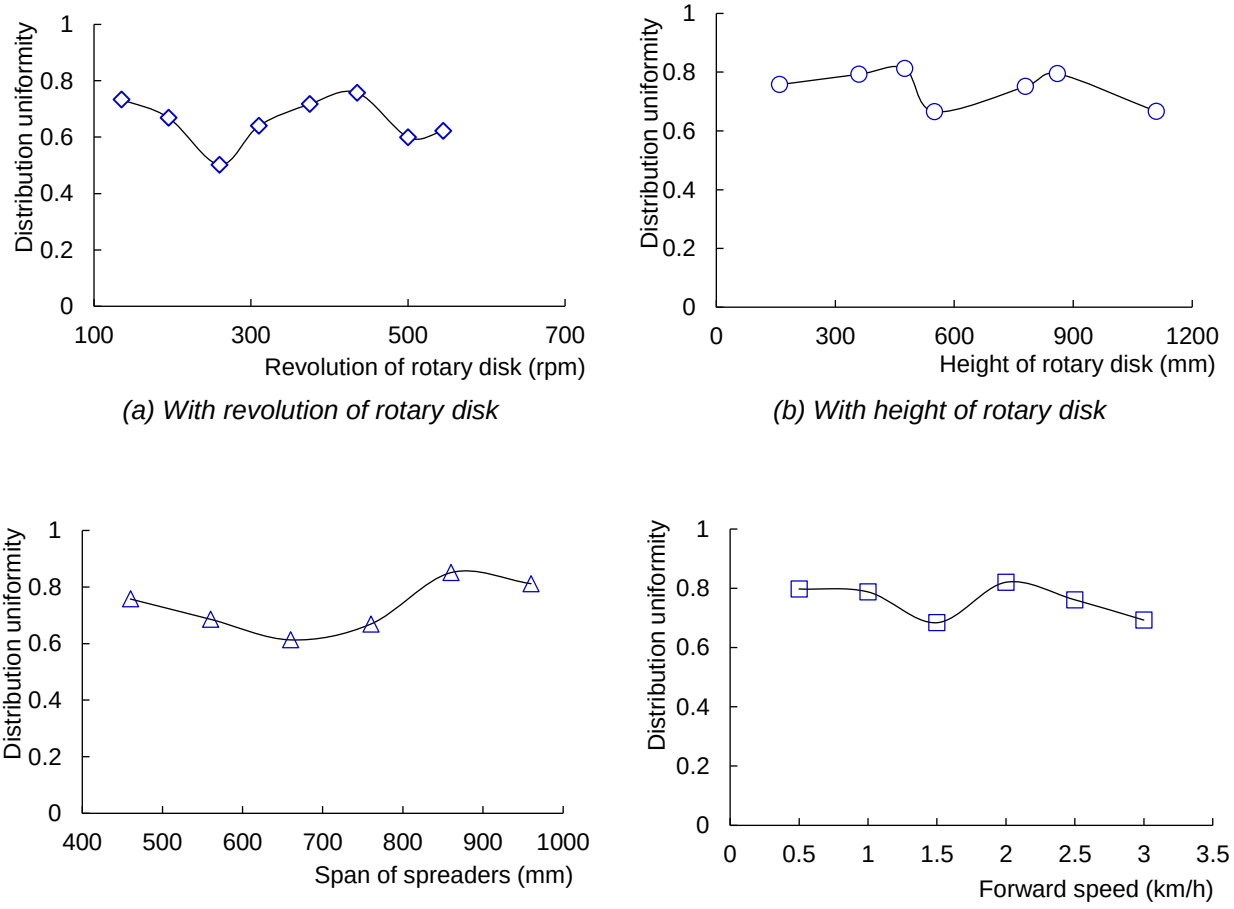

(a) With revolution of rotary disk *(b) With height of rotary disk*

(c) With span of spreaders *(d) With forward speed*

Fig. 6 – Distribution uniformity of single-factor sowing

Distribution uniformity of multi-factor sowing

Experimental results of distribution uniformity of multi-factor sowing were obtained, as listed in Table 3. Statistical analyses of range and variance were performed to obtain the impacts and their significance of each control factor on distribution uniformity of rapeseed broadcast sowing. Range analysis results were listed in Table 3, and variance analysis results were listed in Table 4. The values in cells of each level of the control factors in Table 3 represented mean values of distribution uniformity of the corresponding levels and factors. The delta values of each factor represented the biggest change of mean distribution uniformity of the factor, namely the impact level of each factor. The numbers in the rank row indicated the impact significance of the control factors.

Table 4

Range analysis

Level	Factor A	Factor B	Factor C	Factor D
1	0.7100	0.6523	0.6930	0.6903
2	0.6273	0.7050	0.6727	0.7060
3	0.6953	0.6.53	0.6670	0.6363
Delta	0.0827	0.0527	0.0260	0.0697
Rank	1	3	4	2

Table 5

Variance analysis

Source of variance	Degree of freedom	Sum of squares	Mean sum of squares	*F*-ratio	Critical *F*-ratio
Factor A	2	0.011673	0.005836	10.41	$F_{0.088}(2,2)=10.41$
Factor B	2	0.004183	0.002091	3.73	$F_{0.211}(2,2)=3.73$
Factor C	2	0.001122	0.000561	Error	/
Factor D	2	0.008015	0.004007	7.15	$F_{0.123}(2,2)=7.15$
Total	8	/	/	/	/

Range analysis and variance analysis showed that: factor of rotary disk revolution had the highest significant level of impact on distribution of rapeseed broadcast sowing of the double-spreader, and it was followed by factors of screw auger revolution, rotary disk height and forward speed of the double-spreader, sequentially. By taking the column of control factor with the minimum sum of squares, namely factor of forward speed, as the error column of orthogonal array, the *F*-ratio of each control factor was compared to a critical value corresponding to a certain pre-selected probability. Then, there were probabilities of 91.2 %, 87.7 %, and 78.9 % that control factors were in fact due to chance because of rotary disk revolution, screw auger revolution and rotary disk height, respectively. The probabilities were quite high for the outdoor experiments. $A_1B_2C_2D_2$ was the optimal level combination for good performance of distribution uniformity, namely rotary disk revolution 180 rpm, rotary blade height 800 mm, forward speed 2 km/h, and screw auger revolution 40 rpm.

CONCLUSIONS

A rapeseed broadcast spreader of screw-drop type was developed. The metering rate with screw auger revolution, spreading width with rotary disk revolution and rotary disk height were examined for the single-spreader. The performance of distribution uniformity of single-factor sowing and multi-factor sowing was investigated for the double-spreader.

The main conclusions are as follows:

- The metering rate of the broadcast spreader was adjustable with Pulse Width Modulation method, and it linearly increased with the increase of screw auger revolution. Spreading width of the broadcast spreader was also adjustable by means of altering rotary disk revolution or rotary disk height, and it logarithmically increased with the increase of rotary disk revolution and rotary disk height.
- Factor of rotary disk revolution had the highest significant level of impact on distribution uniformity of rapeseed broadcast sowing of the double-spreader, and it was followed by factors of screw auger revolution, rotary disk height and forward speed of the double-spreader, sequentially. There were probabilities of 91.2 %, 87.7 % and 78.9 % that control factors were in fact due to chance because of rotary disk revolution, screw auger revolution and rotary disk height, respectively.
- The optimal process parameters for distribution uniformity of rapeseed broadcast sowing were rotary disk revolution 180 rpm, rotary blade height 800 mm, forward speed 2 km/h and screw auger revolution 40 rpm.

ACKNOWLEDGEMENTS

The study was funded by National Natural Science Foundation of China (No. 31301575), Research Project of Southwest University (No. GZRY20170057) and National Key R&D Program of China (No. 2017YFD071101-3).

REFERENCES

[1] Chen W, Williams K.C., Donohue T.J. and Katterfeld A., (2017), Application of the image processing technique in identify the particle dispersion from a centrifugal fertilizer spreader, *Particulate Science and Technology*, vol. 35, issue 5, pp. 607-615, Ed. Taylor & Francis Inc., Philadelphia/U.S.A.;

[2] Cool S.R., Pieters, J.G., Seatovic D., Mertens K.C., Nuyttens D., Van De Gucht T.C. and Vangeyte, J., (2017), Development of a stereovision-based technique to measure the spread patterns of granular fertilizer spreaders, *Sensors*, vol. 17, issue 6, pp. 1-23, Ed. MDPI, Basel/Switzerland;

[3] Dong X.Q., Song J.N., Zhang J.K., Junkui, Kang X.J. and Wang J.C., (2013), Working performance and experiment on granular fertilizer spreader with cone disk (锥盘式颗粒肥撒施机构抛撒性能分析与试验), *Transactions of the Chinese Society of Agricultural Engineering*, vol. 29, issue 19, pp. 33-40, Ed. Chinese Society of Agricultural Engineering, Beijing/P.R.C.;

[4] Hu Q., Hua W., Yin Y., Zhang X.K., Liu L.J., Shi J.Q., Zhao Y.G., Qin L., Chen C. and Wang H.Z., (2017), Rapeseed research and production in China, *The Crop Journal*, issue 5, pp. 127-135, Ed. Crop Science Society of China, Beijing/P.R.C.;

[5] Kobets A.S., Naumenko M.M., Ponomarenko N.O., Kharytonov M.M., Velychko O.P. and Yaropud V.M., (2017), Design substantiation of the three-tier centrifugal type mineral fertilizers spreader, *INMATEH Agricultural Engineering*, vol. 53, issue 3, pp. 13-20, INMA Bucharest/Romania;

[6] Sun C., Lin L.B., Tang W.J., Sui L.B., Zhang H., Xia Z.T. Zhao H.Y. Han Y.X. and Li L.P., (2017), Rape planting technology of convenient and simple method and some considerations (关于轻简化油菜种植技术和几点思考), *China Southern Agricultural Machinery*, issue 19, pp. 17-20, Ed. Jiangxi Academy of Agricultural Machinery Research, Nanchang/P.R.C.;

[7] Wu H., (2007), *Development and distribution study on the spreading test system for a spinner spreader (圆盘式施肥机抛撒试验系统开发与撒肥规律研究)*, Master thesis, Agricultural University of Hebei, Baoding/P.R.C.;

[8] Yang M.J., Liu B., Yang Z.R., Ding Z.Y., Yang L., Xie S.Y. and Chen X.B., (2017), Development and experimental study of infrared belt dryer for rapeseed, *INMATEH Agricultural Engineering*, vol. 53, issue 3, pp. 71-80, INMA Bucharest/Romania;

[9] Zhang N., Liao Q.X., (2012), Research progress of seeding technology and equipment for small seeds in China (我国小粒径种子播种技术与装备的应用与研究进展), *Chinese Agricultural Mechanization*, issue 1, pp. 93-96, 103, Ed. Nanjing Research Institute for Agricultural Mechanization Ministry of Agriculture, Nanjing/P.R.C.;

[10] Zhang R., Wang X., Zhao C.J., Bai Y.L., Meng Z.J. and Chen L.P., (2012), Design and experiment of variable rate fertilizer spreader with conveyor chain (链条输送式变量施肥抛撒机的设计与试验), *Transactions of the Chinese Society of Agricultural Engineering*, vol. 28, issue 6, pp. 20-25, Ed. Chinese Society of Agricultural Engineering, Beijing/P.R.C.;

[11] *** American Society of Agricultural and Biological Engineers, (2005), *Procedure for measuring distribution uniformity and calibrating granular broadcast spreaders, ASAE S341.3*, American Society of Agricultural and Biological Engineers, Joseph/U.S.A.;

[12] *** Ministry of Industry and Information Technology of the P. R. China, (2013), *Grain drill- Part 1: Specifications, JB/T 6274.1-2013 (谷物播种机 第 1 部分: 技术条件, JB/T 6274.1-2013)*, China Machine Press, Beijing/P.R.C.

EXPERIMENTAL RESEARCHES ON THE WORKING PROCESS OF A SEEDBED PREPARATION EQUIPMENT FOR HEAVY SOILS

/

CERCETĂRI EXPERIMENTALE PRIVIND PROCESUL DE LUCRU AL UNUI ECHIPAMENT DE PREGĂTIT PATUL GERMINATIV PENTRU SOLURI GRELE

PhD. Stud. Vlăduţ D.I.[1)], Prof. PhD. Eng. Biriş S.[1)], PhD. Eng. Vlăduţ V.[2*)], PhD. Stud. Eng. Cujbescu D.[2)], Lect. PhD. Eng. Ungureanu N.[1)], PhD. Stud. Eng. Găgeanu I.[2)]

[1)]University "POLITEHNICA" Bucharest / Romania; [2)]INMA Bucharest / Romania

E-mail: valentin_vladut@yahoo.com

Keywords: *soil, tillage, chisel, force, penetration, humidity*

ABSTRACT

The paper presents the results obtained from experimental researches carried out under exploitation conditions in order to determinate the qualitative working indices of an equipment used for preparing the seedbed for heavy soils: the vegetal debris coverage degree and the soil crushing degree, as well as the energy indices: slipping, traction and fuel consumption, depending on the depth, soil moisture and working speed.

REZUMAT

Lucrarea prezintă rezultatele obţinute ca urmare a cercetărilor experimentale realizate în condiţii de exploatare pentru determinarea indicilor calitativi de lucru ai unui echipament de pregătit patul germinativ pentru soluri grele: gradul de acoperire cu resturi vegetale şi gradul de mărunţire a solului, precum şi a indicilor energetici: patinarea, forţa de tracţiune şi consumul de combustibil, funcţie de adâncime, umiditatea solului şi viteza de lucru.

INTRODUCTION

Conservative soil cultivation works are an alternative to classical soil processing (ploughing) in the context of current drought-induced climate change. The use of the equipment for processing the seedbed for heavy soils is an alternative, this equipment being able to process the soils up to depths of 25-30 cm (*Budoi and Penescu, 1996; Constantin et al., 2008*).

Under the need to apply conservative tillage, it became widely used the cultivator, an equipment for conservative processing of soil that can also perform soil crumbling in a single pass (*Koloszvary*, *2008*).

The cultivator can be fitted with active bodies, type notched disks, chisel and levelling; of these types, the chisel type active bodies are subjected to an intense wear due to the shape that comes directly in contact with the soil, resulting in a high wear (*Constantin et al, 2012*). Such equipment for conservative processing of soil is designed as a complex aggregate, consisting of 4 modules with different active bodies, mounted one after another so that in a single pass to perform several operations which will ultimately lead to a high quality of soil processing (*Croitoru et al 2016; Vladuţoiu L. et al, 2017*).

This equipment must be checked and tested from the point of view of stress and strains distribution in the frame of agricultural cultivators using the finite element method (*Biriş et al, 2016*), of transportation stress of agricultural implements within laboratory (*Matache et al, 2016*), respectively of structural and kinematic analysis of the mechanism deep soil loosening (*Croitoru et al, 2017*), so that to enhance the performance of cultivators' working bodies (*Biriş et al, 2017*).

MATERIALS AND METHODS

The experimental researches for the determination of the qualitative and energetic indices with the soil processing equipment (seedbed preparation) in a conservative system, were made in the Zerind locality, Arad County (Fig. 1), about 12 km away from Chisinau Cris, on an area of about 30 ha, using a 250 HP tractor (Fig. 2). In order to determine the experimental data, a National Instruments acquisition system, tensometric marks, humidity meter, penetrometer, stopwatch, fuel consumption meter, furrowmeter, metric frame, 100 kg scale, bags and milestones were used (*Uceanu et al, 2008; Vlăduţ et al, 2012*).

Fig. 1 - Polygon 1 used for experiments (Zerind locality, Arad county)

Fig. 2 - Soil processing equipment working in a conservative system during experiments

RESULTS

- ***Soil moisture determination***

According to the working depth set for the experiments: 5 / 10 / 15 / 20 / 25 / 30 cm, the relative humidity of the soil (Fig. 3) was determined for these 6 horizons: 0 – 5 / 5 – 10 / 10 – 15 / 15 – 20 / 20 - 25 / 25 - 30 cm (Table 1).

Fig. 3 - Aspects during soil determination in the polygon used for experimentation

Table 1

Soil humidity depending on the depth of the horizons

SOIL HUMIDITY [%]											
Depth [cm]	**Sample**										***Average***
	1	**2**	**3**	**4**	**5**	**6**	**7**	**8**	**9**	**10**	
0 – 5	17.4	19.6	18.2	17.7	18.4	20.3	20	19	18.1	18.3	*18.7*
5 – 10	25.3	28.8	22.9	27.6	25.8	26.7	29.4	27	28.7	25.8	*26.8*
10 – 15	37.2	38.9	36.9	34.5	36.8	35.9	34.4	32.8	33.7	31.9	*35.3*
15 – 20	21.8	40.8	42.2	39.9	41.7	42.6	43.1	40.5	41.3	42.1	*39.6*
20 - 25	38.6	42.3	40.9	41.5	41.9	40.7	42.2	41.6	42.2	42.1	*41.4*
25 - 30	39.1	43	41.2	42.8	42.7	42.7	44.1	40.9	41.3	41.2	*41.9*

- ***Soil compactness determination (resistance to penetration)***

The soil compactness was determined, for the working depth of the equipment set between: 0…30 cm, (Fig. 4), Table 2.

Fig. 4 - Soil compactness determination (resistance to penetration) in polygon 1

Table 2

Compactness of the soil corresponding to the working depth of the equipment

Depth [cm]	SOIL COMPACTNESS [kPa]				
	Sample I	Sample II	Sample III	Sample IV	*AVERAGE*
2.5	1088	3054	1860	3025	*2256.75*
5.0	1369	2036	2212	2011	*1907.00*
7.5	1193	3265	1931	3210	*2399.75*
10.0	1334	4318	1966	4290	*2977.00*
12.5	2247	4213	1896	4280	*3159.00*
15.0	2387	3581	1899	3560	*2856.75*
17.5	1931	3511	1860	3480	*2695.5*
20.0	2071	3195	1755	3090	*2527.75*
22.5	1966	3300	1931	3281	*2619.5*
25.0	1755	2738	2001	2711	*2301.25*
27.5	1746	2685	1995	2657	*2270.75*
30.0	1723	2611	1952	2613	*2224.75*

Determination of qualitative and energetic indices

- ***Determination of the vegetal debris coverage degree***

This step has been done in order to identify the average values of the existing vegetal mass present on the soil surface per 1m^2, before (Fig. 5) and after the passing of the aggregate, and in order to check how the cultivator incorporates as much as possible of the vegetal debris into the soil (Table 3).

The existing vegetal mass on the soil surface (per 1m^2) before the passing of the aggregate

Existing soil mass on the soil surface (per 1m^2) after the cultivator-tractor aggregate has passed

Fig. 5 - Aspects on how to determine the degree of vegetal debris coverage

Table 3

Determination of vegetal debris coverage degree

A. BEFORE THE PASSING OF THE AGGREGATE						
Repetition 1 [kg/m^2]	**Repetition 2** [kg/m^2]	**Repetition 3** [kg/m^2]	**Repetition 4** [kg/m^2]	**Repetition 5** [kg/m^2]	**Repetition 6** [kg/m^2]	***AVERAGE*** [kg/m^2]
0.445	0.494	0.364	0.612	0.533	0.481	*0.488*
B: AFTER THE PASSING OF THE AGGREGATE						
Repetition 1 [kg/m^2]	**Repetition 2** [kg/m^2]	**Repetition 3** [kg/m^2]	**Repetition 4** [kg/m^2]	**Repetition 5** [kg/m^2]	**Repetition 6** [kg/m^2]	***AVERAGE*** [kg/m^2]
0.034	0.038	0.028	0.048	0.042	0.037	*0.0378*
Incorporation of plant residues degree						
92.36	92.31	92.31	92.16	92.12	92.31	**92.25**

- ***Determination of soil compactness***

This step was done in order to determine how the working parts of the cultivator dislodge and crush the soil (Fig.6) in order to make a seedbed, as uniform as possible with the smallest bulges (Table 4).

Fig. 6 - Aspects on how to determine the degree of soil shredding

Table 4

Determination of soil compactness

Particle size [mm]	**The grading degree by size [%]**					
	Sample 1	**Sample 2**	**Sample 3**	**Sample 4**	**Sample 5**	***Average***
>100	8.20	5.90	6.93	8.54	6.23	*7.160*
>50	66.63	71.64	68.69	72.64	71.88	*70.296*
>20	22.66	21.02	23.01	23.15	22.88	*22.544*

- ***Determination of tractor slipping and fuel consumption***

The tractor slipping (Table 5) that occurs when the tractor is towing the cultivator while working is necessary to calculate the traction power requirement of the power source used (tractor). The average fuel consumption of the tractor, obtained by processing the 80 ha of scarified land (including double crossings at the ends of the plot and for turning at the end of the furrow, etc.), correlated with the working width of the equipment, speed and working depth, allows to determine cultivator productivity, which varies depending on working conditions: humidity, soil compactness, depth of work, etc. (*Uceanu et al, 2008*).

Table 5

Slipping of the tractor during the working process with the "DRACULA" cultivator

Slipping [%]*)											
Sample 1		**Sample 2**		**Sample 3**		**Sample 4**		**Sample 5**		**AVERAGE**	
left	right	left	right	left	right	left	right	left	right	left	right
9.50	9.50	9.75	9.50	10.0	10.0	10.25	10.50	10.50	10.50	-	-
6.31%		7.54%		11.21%		14.22%		15.23%		*10.9%*	

**) The measurement has been done on a lenght of 50 m*

- *Average fuel consumption: 25.81 l / ha*

In order to highlight the energetic indices according to the variation of the main working parameters: depth, speed and soil humidity, experiments were carried out following their variation: traction, slipping and fuel consumption (Table 6).

Table 6

Variation of the energetic indices depending on: depth and working speed, respectively soil humidity

Parameters		d_1 [5 cm]; S.U. = 18.7%				d_2 [10 cm]; S.U. = 26.8%				d_3 [15 cm]; S.U. = 35.3%			
		R1	R2	R3	*Average*	R1	R2	R3	*Average*	R1	R2	R3	*Average*
s_1 = 2 [m/s] 7.2 [km/h]	Slipping [%]	6.15	6.15	6.18	*6.16*	7.42	7.43	7.47	*7.44*	9.43	9.42	9.38	*9.41*
	Traction force T_r [daN]	100.3	100.8	100.1	*100.4*	108.9	101.2	105.8	*105.3*	119.2	114.3	116.7	*116.73*
	Fuel consumption [l/ha]	5.98	6.02	6.03	*6.01*	10.44	10.42	10.4	*10.42*	13.13	12.9	12.73	*12.92*
s_2 = 2.5 [m/s] 9 [km/h]	Slipping [%]	6.26	6.26	6.23	*6.25*	7.49	7.49	7.49	*7.49*	9.51	9.49	9.5	*9.5*
	Traction force T_r [daN]	102.48	102.89	101.96	*102.44*	110.22	105.77	107.46	*107.82*	118.95	121.35	119.24	*119.85*
	Fuel consumption [l/ha]	6.12	6.12	6.18	*6.14*	10.35	10.31	10.33	*10.33*	12.72	12.81	12.9	*12.81*
s_3 = 3 [m/s] 10.8 [km/h]	Slipping [%]	6.36	6.32	6.34	*6.34*	7.58	7.58	7.55	*7.57*	9.5	9.51	9.55	*9.52*
	Traction force T_r [daN]	103.95	104.12	103.98	*104.02*	112.87	111.56	111.21	*111.88*	122.33	124.01	121.89	*122.74*
	Fuel consumption [l/ha]	6.26	6.26	6.23	*6.25*	10.24	10.22	10.26	*10.24*	12.73	12.74	12.72	*12.73*
s_4 = 3.5 [m/s] 12.6 [km/h]	Slipping [%]	6.48	6.49	6.5	*6.49*	7.67	7.67	7.64	*7.66*	9.52	9.53	9.51	*9.52*
	Traction force T_r [daN]	105.21	106.03	104.32	*105.19*	114.34	114.88	113.98	*114.40*	122.33	124.01	121.89	*122.74*
	Fuel consumption [l/ha]	6.36	6.37	6.35	*6.36*	10.13	10.13	10.07	*10.11*	12.61	12.71	12.51	*12.61*

Parameters		d_4 [20 cm]; S.U. = 39.6%				d_5 [25 cm]; S.U. = 41.4%				d_6 [30 cm]; S.U. = 41.9%			
		R1	R2	R3	*Average*	R1	R2	R3	*Average*	R1	R2	R3	*Average*
s_1 = 2 [m/s] 7.2 [km/h]	Slipping [%]	11.07	11.09	11.08	*11.08*	14.3	14.1	13.9	*14.1*	15.07	15.08	15.12	*15.09*
	Traction force T_r [daN]	118.72	121.21	124.54	*121.49*	123.51	126.17	127.32	*125.67*	128.85	129.04	129.65	*129.18*
	Fuel consumption [l/ha]	25.42	25.44	25.4	*25.42*	21.67	21.67	21.64	*21.66*	26.1	26.1	26.1	*26.1*
s_2 = 2.5 [m/s] 9 [km/h]	Slipping [%]	11.16	11.16	11.16	*11.16*	14.19	14.19	14.16	*14.18*	15.19	15.21	15.2	*15.2*
	Traction force T_r [daN]	120.75	124.33	125.04	*123.37*	131.52	130.26	132.2	*131.33*	139.12	138.62	137.52	*138.42*
	Fuel consumption [l/ha]	17.6	17.52	17.56	*17.56*	21.42	21.42	21.45	*21.43*	25.81	25.83	25.82	*25.82*
s_3 = 3 [m/s] 10.8 [km/h]	Slipping [%]	12.27	11.27	11.24	*11.26*	14.25	14.27	14.29	*14.27*	15.28	15.27	15.29	*15.28*
	Traction force T_r [daN]	127.55	126.89	128.19	*127.54*	136.95	137.53	135.88	*136.79*	143.62	145.52	146.06	*145.07*
	Fuel consumption [l/ha]	17.49	17.5	17.45	*17.48*	21.33	21.32	21.34	*21.33*	25.69	25.69	25.72	*25.7*
s_4 = 3.5 [m/s] 12.6 [km/h]	Slipping [%]	11.35	11.35	11.32	*11.34*	14.33	14.33	14.33	*14.33*	15.36	15.36	15.33	*15.35*
	Traction force T_r [daN]	130.14	131.56	130.61	*130.77*	140.56	142.06	141.32	*141.31*	151.69	154.32	152.54	*152.85*
	Fuel consumption [l/ha]	14.4	14.41	14.45	*14.42*	21.28	21.27	21.223	*21.26*	25.6	25.63	25.63	*25.62*

s-speed; d-depth; S.U.-soil humidity; R-repetition

T_f [daN] Speed: 7.2 km/h; depth: 15 cm; sample 1

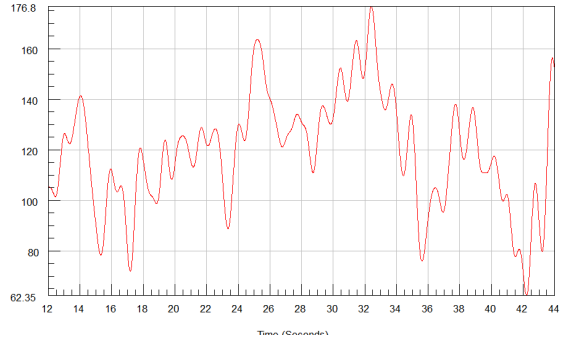

Speed: 7.2 km/h; depth: 15 cm; sample 1

viteza - 7,5km/h, adancime- 15cm, nr. proba - 1

Marker	Y Max	Y Min	Y Mean
	176.8	62.35	119.2

T_f [daN] Speed: 7.2 km/h; depth: 15 cm; sample 2

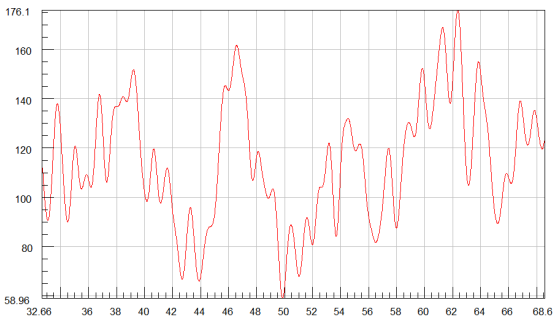

Speed: 7.2 km/h; depth: 15 cm; sample 2

viteza - 7,5km/h, adancime- 15cm, nr. proba - 2

Marker	Y Max	Y Min	Y Mean
	176.1	58.96	114.3

T_f [daN] Speed: 7.2 km/h; depth: 15 cm; sample 3

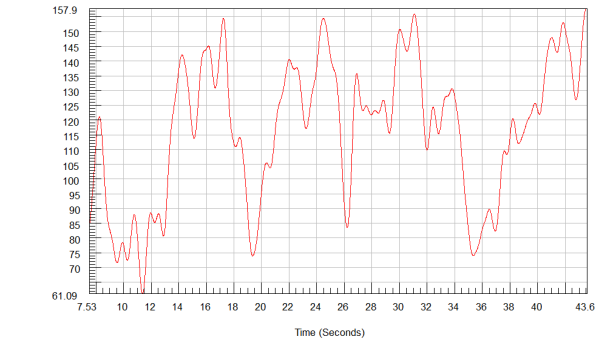

Speed: 7.2 km/h; depth: 15 cm; sample 3

Marker	Y Max	Y Min	Y Mean
	157.9	61.09	116.7

T_f [daN] Speed: 7.2 km/h; depth: 10 cm; sample 3

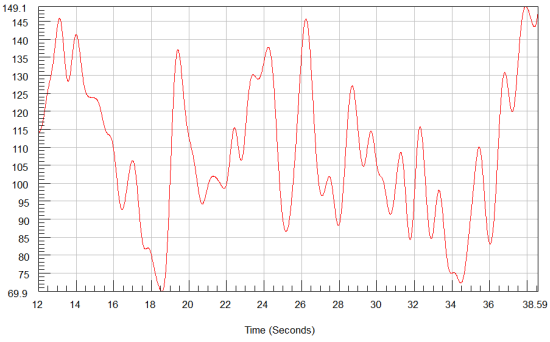

Speed: 7.2 km/h; depth: 10 cm; sample 3

Marker	Y Max	Y Min	Y Mean
	149.1	69.9	108.9

Tf [daN] Speed: 7.2 km/h; depth: 10 cm; sample 2

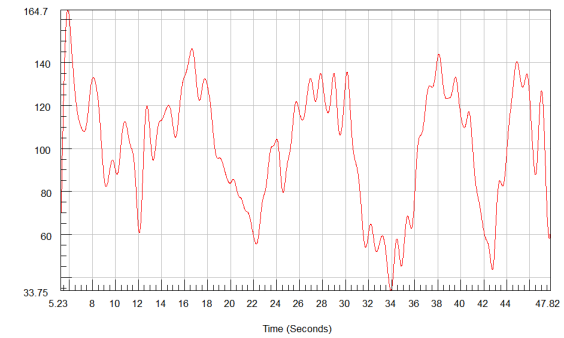

Speed: 7.2 km/h; depth: 10 cm; sample 2

Marker	Y Max	Y Min	Y Mean
	164.7	33.75	101.2

Tf [daN] Speed: 7.2 km/h; depth: 10 cm; sample 1

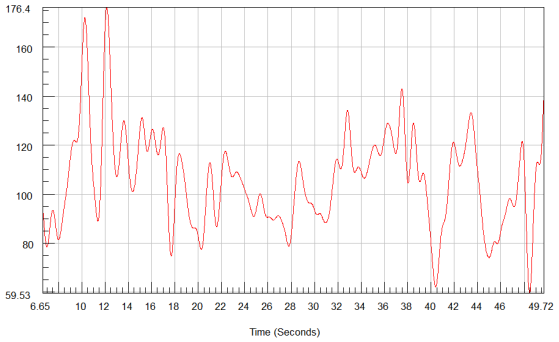

Speed: 7.2 km/h; depth: 10 cm; sample 1

Marker	Y Max	Y Min	Y Mean
	176.4	59.53	105.8

T_f [daN] Speed: 7.2 km/h; depth: 5 cm; sample 3

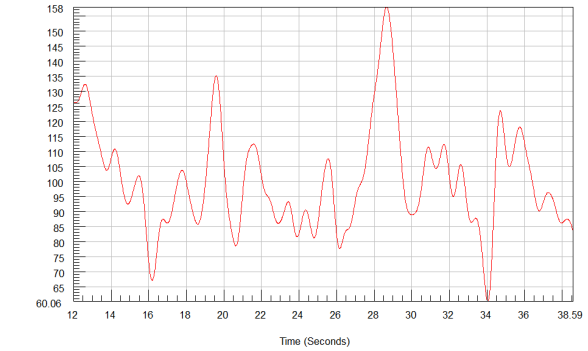

Speed: 7.2 km/h; depth: 5 cm; sample 3

Marker	Y Max	Y Min	Y Mean
	158	60.06	100.3

T_f [daN] Speed: 7.2 km/h; depth: 5 cm; sample 2

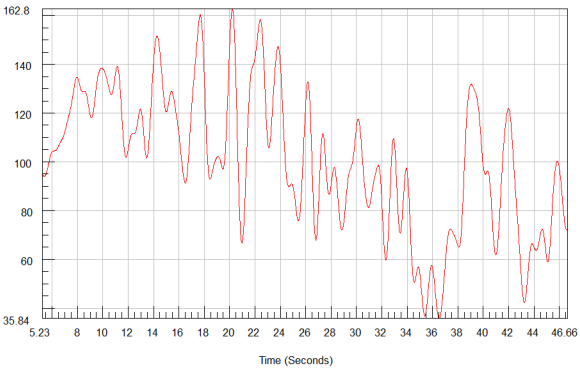

Speed: 7.2 km/h; depth: 5 cm; sample 2

Marker	Y Max	Y Min	Y Mean
	162.8	35.84	100.8

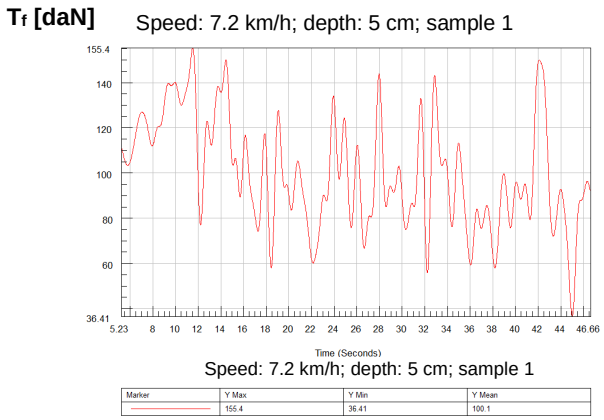

Fig. 7 – Grafic representation of the traction force, for each registration

CONCLUSIONS

Soil humidity and compactness are two very important factors that have a great influence on the data obtained while determining the qualitative working or energetic indices of the "DRACULA" cultivator, because any variation of one or both of these factors leads to variations in measured data, as a result of the experimental research and implicitly of the obtained results.

That is why it is very important that the qualitative and energetic indices determined for the tractor unit + DRACULA cultivator to be accomplished within a short period of time (maximum 3-4 days) on the same site (plot), and also, during this experimental period no variations were accepted (precipitations) because they have the ability to change the input parameters (soil humidity and compactness) and therefore the measured output data will not be comparable to those measured prior to the occurrence of these improper conditions.

The experimental researches presented in this report respected these conditions and by analysing the data obtained it is observed that:

- soil humidity determined on 6 horizons (0 – 5 / 5 – 10 / 10 – 15 / 15 – 20 / 20 – 25 / 25 - 30 cm), corresponding to the working depths previously defined, varies with depth, growing with it;
- the soil compactness (penetration resistance) for the depth of 0 ÷ 30 cm (the maximum working depth of the cultivator) increases with the depth (not uniformly due to the inhomogeneity and unevenness of the soil) reaching a maximum of 12.5 cm, after that it decreases continuously, (in these horizons the humidity is higher and the soil is not as rough);
- the vegetal debris coverage degree of the soil after the passing of the aggregate (incorporation of vegetal debris into the soil) by the active parts of the "DRACULA" cultivator is very good (92.25%), since this equipment does not overturn the soil;
- the soil grinding degree made by the "DRACULA" cultivator has a comparative value with those made by the other seedbed preparation equipment (disc grabs, tines, etc.), the results obtained with this equipment were made on a land that has been unprocessed for 20 years and scarified, so under very difficult working conditions; unlike conventional bedding equipment, this cultivator is normally used directly in non-terrain (conservative soil treatment system);
- among all the determined energetic indices, the slipping and tensile strength (for different working speeds and depths, respectively humidities) had increasing values with increasing working depth and humidity, respectively working speed, but fuel consumption decreased with the increasing of the working speed and increasing of the working depth, while soil moisture had higher values.

ACKNOWLEDGEMENTS

This work was supported by Grant of the Romanian National Authority for Scientific Research, CNCS, UEFISCDI, PN-III-P2-2.1-BG-2016, Project number: 78BG/2016, SC Artecom SRL upgraded competences through deep soil tillage machinery optimization.

REFERENCES

[1] Biriş S.Şt., Maican E., Vlăduț V., Bungescu S.T., Ungureanu N., Vlăduț D.I., (2016), Stress and strains distribution in the frame of agricultural cultivators using the finite element method, *Proceedings of the 44th International Symposium on Agricultural Engineering "Actual Tasks on Agricultural Engineering"*, pp.111-118, Opatija / Croatia;

[2] Biriş S. Şt., Ungureanu N., Gheorghiță N. E., Maican E., Vlăduț V., (2017), Theoretical research on enhancing the performance of cultivators working bodies, *Proceedings of the 45th International Symposium on Agricultural Engineering "Actual Tasks on Agricultural Engineering"*, pp.121-130, Opatija / Croatia;

[3] Budoi Gh., Penescu A., (1996), Agrotechnica, *Ceres Publishing House*, Bucharest / Romania;

[4] Constantin N., Cojocaru I., Pirna I., Nitescu V., Leu I., (2008), Independent disc harrow for the stubble-turning and prepared the germinative bed, on all soil types, for the tractors designed tractors 120÷220HP, *SCIENTIFIC PAPERS (INMATEH III),* pp.139-143, Bucharest / Romania;

[5] Constantin N., Irimia D., Persu C., Cociu A., Atanasov At., Usenko M., (2012), Experimenting the multifunctional machine to worked - MATINA, *INMATEH – Agricultural Engineering*, no. 1/2012, vol. 36, pp.5-12, Bucharest / Romania;

[6] Croitoru St., Marin E., Badescu M., Vladut V., Ungureanu N., Manea D., Boruz S., Matei Gh., (2016), Agrotechnical and energetic characteristics of new designed subsoiler, *Proceedings of the 44th International Symposium on Agricultural Engineering "Actual Tasks on Agricultural Engineering"*, pp.165-176, Opatija / Croatia;

[7] Croitoru Şt., Vladut V., Voicea I., Gheorghe Gh., Marin E., Vlăduţoiu L., Moise V., Boruz S., Pruteanu A., Andrei S., Păunescu D., (2017), Structural and kinematic analysis of the mechanism for arable deep soil loosening, *Proceedings of the 45th International Symposium on Agricultural Engineering "Actual Tasks on Agricultural Engineering"*, pp.207-216, Opatija / Croatia;

[8] Koloszvari C., (2008), Studies and research on the optimization of constructive and functional parameters of a disc harrow for high power tractors, *PhD thesis*, Transilvania University of Brasov / Romania;

[9] Matache M., Voicu Gh., Vladut V., Voicea I., Persu C., (2016), Simulation of transportation stress of agricultural implements within laboratory, *Proceedings of the 44th International Symposium on Agricultural Engineering "Actual Tasks on Agricultural Engineering"*, pp.119-128, Opatija / Croatia;

[10] Uceanu E., Bolintineanu Gh., Voicea I., Matache M., (2008), Research regarding the determination, qualitative and energetic indices of the soil works, in the conditions of using the new tractor-agricultural machinery aggregates, *SCIENTIFIC PAPERS (INMATEH III)*, pp.87-93, Bucharest / Romania;

[11] Vlăduţ V., Matache M., Nicolescu M., Biriş S., Paraschiv G., Voicu Gh., Danciu A., Persu C., (2012), Assisted Testing of Biotechnical Systems, *Terra Nostra Publishing House*, Iasi / Romania;

[12] Vlăduţoiu L., Cârdei P., Vlăduţ V., Fechete L., (2017), Modern trends in designing and selecting the machine/equipment for deep soil tillage, *16th International Scientific Conference "Engineering for Rural Development"*, pp.1415-1420, Jelgava / Latvia.

MATHEMATICAL MODEL OF BENDING VIBRATIONS OF A HORIZONTAL FEEDER-MIXER ALONG THE FLOW OF GRAIN MIXTURE

/

МАТЕМАТИЧНА МОДЕЛЬ ЗГИННИХ КОЛИВАНЬ ГОРИЗОНТАЛЬНОГО ЗАВАНТАЖУВАЧА-ЗМІШУВАЧА ВЗДОВЖ ПОТОКУ ЗЕРНОВОЇ СУМІШІ

DSc. Eng. Lyashuk O.L[1)]., Lect. Ph.D. Eng. Sokil M.B. [3)], PhD Eng. Klendiy V.M. [1)], PhD Eng. Skyba O.P. [1)], Tretiakov O.L. [1)], Slobodian L.M. [1)], PhD Econ. Slobodian N.O. [2)]

[1)]Ternopil Ivan Pul'uj National Technical University/ Ukraine

[2)]SHEI "Ternopil State Medical University named after I.Ya. Gorbachevskiy Ministry of Health of Ukraine"/ Ukraine;

[3)]National University Lviv Polytechnic / Ukraine

E-mail: oleglashuk@ukr.net

***Keywords**: mathematical model, feeder-mixer, horizontal screw, bending vibrations*

ABSTRACT

During the grain mixture motion along the working body of the feeder, the transverse (bending) vibrations occur. To deduce a differential equation describing bending vibrations of the feeder-mixer horizontal screw, a physical model is developed; the distribution of forces acting on the element of the horizontal working body during the grain mixture movement is defined.

РЕЗЮМЕ

При русі зернової суміші вздовж робочого органу завантажувача виникають поперечні (згинні) коливання. Для отримання диференціального рівняння, яке описує згинні коливання горизонтального гвинта завантажувача-змішувача розроблена фізична модель та розподіл сил, які діють на елемент горизонтального робочого органу під час переміщення зернової суміші.

INTRODUCTION

Screw transport and technological mechanisms are widely used in various industries. The effectiveness of many sections, shops and enterprises in general depends on their reliable work. Therefore, in order to ensure the reliability and quality of the technological processes implementation by means of screw mechanisms, the dynamic stresses caused by vibration processes should be considered.

The foundations of designing and researching screw conveyors have been laid by the scholars (*Hevko B.M., 1989; Hevko B.M., Pavelchuk Yu.F., 2017; Rohatynskyi R., and others, 2012; Hevko R.B., and others, 2012; Hevko R.B., Klendiy O.M. 2014; Hevko R.B., and others, 2015; Lyashuk O.L., and others, 2015;* Tian Y., Cheng Q., and others, (2018*)*. The vibration theory has been studied in the works of (Bulgakov V., *and others,* 2017*;* Hewko B.M., and others, 2015; *Loveykin V.S., Nesterov A.P., 2002; Chen L.Q. 2009 and others; Sokil M.B., and others, 2016)*. However, the dynamic stresses in screw working bodies that arise under different modes of their operation in non-resonant and resonant zones are not sufficiently studied; and the reliability of screw transport and technology systems is not assessed. Therefore, the need for further research is indisputable.

The objective of the work is to develop a mathematical model of bending vibrations of the feeder-mixer horizontal working body.

MATERIALS AND METHODS

To deduce a differential equation describing the bending vibrations of an auger of the feeder-mixer horizontal screw, along which a homogeneous grain flow moves, the following assumptions should be considered:

- the cross-sectional area, mass per unit length, rigidity of the screw-mixer (together with a cylindrical casing) are slowly variable values along the length;
- the elastic properties of the working screw, together with the casing, satisfy the close to linear law of elasticity;
- during the vibration of the working body, the resistance force is proportional to its motion velocity in degree S ;

- the grain mixture flows at a constant velocity relative to the screw-mixer and does not affect its roughness;
- the normal sections of the screw-mixer remain perpendicular to its neutral axis (there is no deplanation of the cross-section);
- the deflection of separate parts of the screw-mixer occurs in the direction perpendicular to its neutral line, that is, the longitudinal displacements are neglected (deflections of the axis points of the elastic body of an arbitrary normal section occur in the horizontal plane);

These assumptions allow to unambiguously determining the position of the feeder-mixer horizontal branch by a function that describes the horizontal displacement of the screw working body neutral axis. Obviously, the specified function will depend on two variables - the linear coordinate x and the time t. The linear coordinate X will be deduced from the point of loading the grain mixture in a horizontal cylindrical casing; and the axis OX is directed along the undeformed axis of the screw. The record $y(x,t)$ denotes the deflection of the neutral axis point of the working screw with the coordinate X in the horizontal direction at an arbitrary time (Fig. 1 a). The forces acting on the conditionally specified element of the deformed screw are shown in Fig. 1 b.

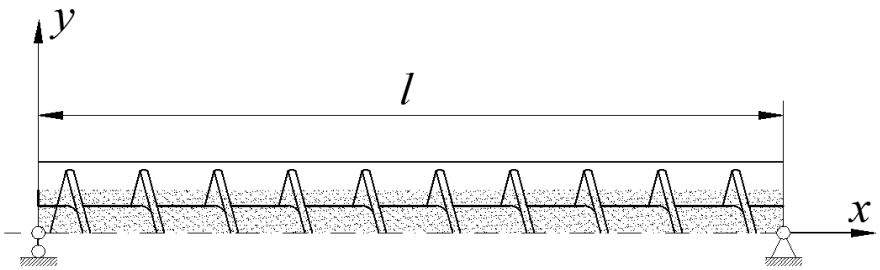

a)

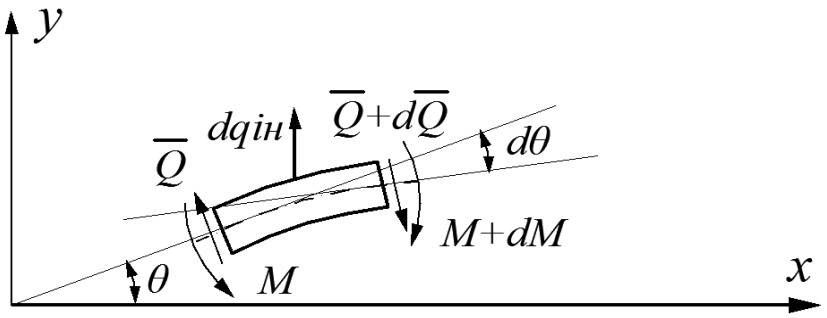

b)

Fig. 1 - Physical model and distribution of forces acting on the element of the horizontal working body during the grain mixture displacement

Providing that:

ρ- the mass per unit length of the horizontal working body;

m - the mass per unit length of the grain mixture continuous flow, which moves relative to the working body at a constant velocity u;

$E(x)$ and $I(x)$ - accordingly, the elasticity modulus of the working body material and the inertia moment of the cross-section relative to the neutral axis;

$M+\frac{\partial M}{\partial x}dx$ and $M+\frac{\partial M}{\partial x}dx$ - bending moments at the beginning and at the end of the conditionally specified element;

Q and $Q+\frac{\partial Q}{\partial x}dx$ - cross-cutting forces in the above-mentioned places of the conditionally specified element;

θ - and $\theta+d\theta$ - angles formed by a tangent to the neutral line with the OX axis at the beginning and at the end of the specified element;

$dq = q(x,t)dx$ - the resulting force component of the external forces in the plane OXZ (plane of vibrations) acting on the conditionally specified element of the working body; $q(x,t)$ - the forces intensity.

$\frac{\partial^2 y}{\partial t^2}$ - a projection of the acceleration of the specified element centre on the axis OY;

$\frac{d^2 y}{dt^2}$ - a projection on the same axis of the absolute acceleration of the grain mixture element, which coincides with the screw auger element under study at the given time;

then, for the case of small ($\sin\theta = \frac{\partial y}{\partial x}$, $\sin(\theta + d\theta) = \frac{\partial y}{\partial x} + \frac{\partial^2 y}{\partial x^2}dx$) bending vibrations of the working body horizontal part, the equation of "dynamic equilibrium" acquires the form

$$Q\cos\theta - (Q + dQ)\cos(\theta + d\theta) + dq_{i\text{H}} + q(x,t)dx = 0 \quad (1)$$

The inertia force (*Chen, L.Q., 2009)* of the element $dq_{i\text{H}}$ under study together with the grain mixture is determined by the dependence

$$dq_{i\text{H}} = m\frac{d^2 y(x,t)}{dt^2}dx + \rho\frac{\partial^2 y(x,t)}{\partial t^2}dx + (m+\rho)\omega^2 \quad (2)$$

where ω - angular velocity of the screw working body rotation.

Connecting the cross-cutting force to the bending moment (*Hevko I., 2012; Hevko I.B., 2013; Oleg Lyashuk, and others, 2016)* ($Q = \frac{dM}{dx}$) by the known ratio, the following formula is derived from equation (1)

$$m\frac{d^2 y(x,t)}{dt^2} + \rho\frac{\partial^2 y(x,t)}{\partial t^2} + (m+\rho)\omega^2 y + \delta\left(\frac{\partial y(x,t)}{\partial t}\right)^s = \\ + \frac{\partial}{\partial x}\left[\frac{\partial}{\partial x}\left(E(x)I(x)\left(\frac{\partial^2 y(x,t)}{\partial x^2} + \mu\left(\frac{\partial^2 y(x,t)}{\partial x^2}\right)^3\right)\right)\right] = f(x,\mathrm{y},\theta). \quad (3)$$

The addend $\delta\left(\frac{\partial y(x,t)}{\partial t}\right)^s$ in equation (3) describes the external force of the resistance, which is proportional to the motion velocity in degree s, and δ is the coefficient of proportionality at the given force during vibration of the feeder-mixer working body.

The function $f(x,\mathrm{y},\theta)$ is somewhat different in nature (nonlinear and periodic in θ), and it will be further considered.

The grain mixture moves relative to the screw working body with a constant relative linear velocity u, so the body's inertia equals

$$m\frac{d^2 y(x,t)}{dt^2} = m\frac{\partial^2 y(x,t)}{\partial t^2} + m\frac{\partial^2 y(x,t)}{\partial x^2}(u)^2 + 2m\frac{\partial^2 y(x,t)}{\partial t \partial x}u. \quad (4)$$

Based on the above, the following formula is deduced from equation (3)

$$(m+\rho)\left(\frac{\partial^2 y(x,t)}{\partial t^2}-\omega^2 y(x,t)\right)+2mu\frac{\partial^2 y(x,t)}{\partial t\partial x}+mu^2\frac{\partial^2 y(x,t)}{\partial x^2}+\delta\left(\frac{\partial y(x,t)}{\partial t}\right)^S+$$
$$+\frac{\partial}{\partial x}\left[\frac{\partial}{\partial x}\left(EI(x)\left(\frac{\partial^2 y(x,t)}{\partial x^2}+\mu\left(\frac{\partial^2 y(x,t)}{\partial x^2}\right)^3\right)\right)\right]=f(x,y,\theta). \quad (5)$$

Considering the physical process of the system, the boundary conditions for the last equation can be presented as

$$y(x,t)\Big|_{\substack{x=0,\\ x=l}}=0,\ \frac{\partial^2 y}{\partial x^2}(x,t)\Big|_{\substack{x=0,\\ x=l}}=0. \quad (6)$$

Notes:

1. In dependence (3), the condition of nonlinear-elastic properties of the screw working body material together with the cylindrical casing is applied in the form of a nonlinear technical law of elasticity (*Mytropolskyi Y.A., Lymarchenko O.S. 1998)*: $\sigma=E(\varepsilon_1+\mu\varepsilon_1^3)$ $\varepsilon_1=\frac{\partial y(x,t)}{\partial x}$ - relative deformation of the screw working body, μ defines the deflation of its elastic properties from the linear law and $\mu<<1$;

2. The grain mixture motion is complex. The first summand of the right-hand side of the dependence (4) expresses the inertial forces of the mixture in the transportation motion, the second - in the relative motion, and the third summand expresses Coriolis components. Based on the above, inertial forces of the grain mixture can be defined.

The influence of the whole set of parameters describing the dynamics of the system under study could be defined only by solving the boundary problems (5), (6). It is difficult to find the analytical solution even for the corresponding linear model (without considering the nonlinearly elastic properties of the working screw material). Therefore, the dynamic process of the system 'an elastic body - a continuous flow of grain mixture' at a limited velocity of the mixture should be studied. Based on the above, the proposed model of the dynamic process can be presented as

$$\frac{\partial^2 y}{\partial t^2}+\alpha^2\frac{\partial^4 y}{\partial x^4}-\omega^2 y=-\mu F\left(y,\theta,\frac{\partial y}{\partial t},\frac{\partial^2 y}{\partial x^2},\frac{\partial^3 y}{\partial x^3},\frac{\partial^4 y}{\partial x^4}\right) \quad (7)$$

$\alpha^2=\frac{EI}{m+\rho}$, $F\left(y,\theta,\frac{\partial y}{\partial t},\frac{\partial^2 y}{\partial x^2},\frac{\partial^3 y}{\partial x^3},\frac{\partial^4 y}{\partial x^4}\right)$ – analytical 2π - periodical θ function:

$$\mu F\left(y,\theta,...,\frac{\partial^4 y}{\partial x^4}\right)=-\eta\frac{EI}{m+\rho}\frac{\partial^2}{\partial x^2}\left(\frac{\partial^2 y}{\partial x^2}\right)^2+\frac{1}{m+\rho}f(x,y,\theta)-\frac{1}{m+\rho}(mu^2\frac{\partial^2 y(x,t)^2}{\partial x^2}+2m\frac{\partial^2 u}{\partial x\partial t}u+-\delta\left(\frac{\partial y(x,t)}{\partial t}\right)^S$$

Thus, the dynamic process of the given system can be considered as the overlap of two waves of the same length with time-varying amplitudes and frequencies, that is, the first approximation of the asymptotic solution (*Mytropolskyi Y.A., Lymarchenko O.S. 1998*;) of the boundary value problem (7), (6) can be submitted as

$$y(x,t)=C_1\cos(\kappa x+\psi)+C_2\cos(\kappa x-\psi)+\mu\, y_1(a,x,\psi,\theta) \quad (8)$$

where $C_1, C_2,$ - the constant content and appearance of the waves will be set below, ψ - the phase of the indicated waves, $\mu\, y_1(a,x,\psi,\theta)$ - the perturbation of the vibration process is caused by nonlinear and other forces.

The representation of the solution in the form (8) must satisfy the boundary conditions (6). Therefore, $C_1=-C_2=a$, and for the periodic by ψ and θ function $y_1(a,x,\psi,\theta)$, the ratios must be satisfied

$$y_1(a,x,\psi,\theta)_{|x=0}=y_1(a,x,\psi,\theta)_{|x=l}=0 \quad (9)$$

In addition, if we impose on a periodic by ψ and θ function a condition of absence in its representation by harmonics ψ the first component

$$\int_0^{2\pi} y_1(a,x,\psi,\theta)\begin{Bmatrix}\cos\psi\\ \sin\psi\end{Bmatrix}d\psi = 0 \tag{10}$$

then, the parameter will be considered the amplitude of the direct or reverse wave. The wave number κ is related to the frequency Ω of the dynamic process by the dispersion ratio

$$\Omega^2 - \alpha^2\kappa^4 + \omega^2 = 0 \tag{11}$$

The representation of the solution in the form (8), as well as the boundary conditions (9), allow determining the set of values of the wave number $\kappa_k = \frac{k\pi}{l}, k = 1,2,\ldots.$. Simultaneously, the obtained dispersion ratio determines the frequency Ω of the process as a function of a wave number in the form $\Omega = \sqrt{\frac{EI}{m+\rho}\kappa^4 - \omega^2}$.

Considering the obtained values κ_k, the eigenfrequencies spectrum of the working body of the conveyor horizontal branch is obtained

$$\Omega_k = \sqrt{\frac{EI}{m+\rho}\left(\frac{k\pi}{l}\right)^4 - \omega^2} \tag{12}$$

Typically, in nonlinear systems, a dynamic process with a frequency close to the main frequency ($k=1$) of the system frequency spectrum *(Mytropolskyi Y.A., Lymarchenko O.S. 1998)* is developed; therefore, the unperturbed motion of the considered conveyor branch is defined by the dependence

$$y(x,t) = a\left[\cos\left(\frac{\pi}{l}x + \sqrt{\frac{EI}{m+\rho}\left(\frac{\pi}{l}\right)^4 - \omega^2}t + \psi\right) - \cos\left(\frac{\pi}{l}x - \sqrt{\frac{EI}{m+\rho}\left(\frac{\pi}{l}\right)^4 - \omega^2}t - \psi\right)\right] \tag{13}$$

or

$$y(x,t) = 2a\sin\frac{\pi}{l}x\cos\left(\sqrt{\frac{EI}{m+\rho}\left(\frac{\pi}{l}\right)^4 - \omega^2}t + \psi\right) \tag{14}$$

The ratios (13) and (14) do not contradict each other; only for (14), the parameter a will be nothing more than a half of the vibrations amplitude.

In Fig. 2, the dependence of the internal vibrations frequency Ω_k of the feeder-mixer horizontal working body on the angular velocity of the working body rotation at different values of the grain mixture mass per unit length (the elastic modulus of the material - $E = 2,06\cdot10^{11} N/m^2$, $l = 6 \div 10\, m$, $m = 0 \div 40\, kg/m$, $\rho = 30\, kg/m$) is presented:

Obviously, the higher are the angular rotational velocities of the working body of the feeder-mixer horizontal branch, the lower is the actual frequency of its vibrations.

Moreover, the decay velocity from the angular rotational velocity is higher provided the values of the mass per unit length of the grain mixture are, For a non-perturbed case in (13) or (14), the parameters a and ϕ are stable; in perturbing motion larger they are variables in time, and the laws of their changes are determined by the right-hand side of equation (7) - the nonlinear-elastic properties of the auger screw material, the physical-mechanical and kinematic parameters of the grain mixture and the speed of its movement.

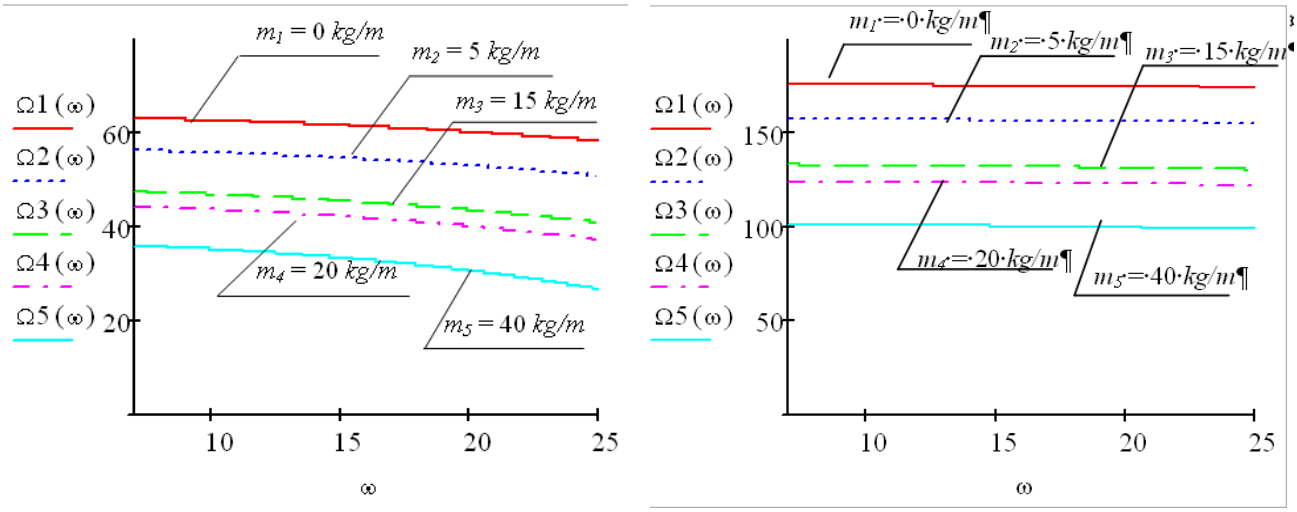

Fig. 2 - Dependence of the eigenfrequency on the working body length on the angular velocity of its rotation
a) $l = 10\,m$; *b)* $l = 6\,m$

To find the influence of these factors on the process dynamics, a function $y_1\left(a, x, \psi, \theta\right)$ in the asymptotic representation (8) should be developed. As the screw working body can be exposed to external periodic perturbation by frequency ν, then the dangerous resonant vibrations may occur provided $p\nu \approx q\Omega_k$ (p and q are relatively simple numbers). This fact is a prerequisite for considering two cases of perturbed vibrations of the horizontal working body: resonant ($p\nu \approx q\Omega_k$) and non-resonant ($p\nu \neq q\Omega_k$). First, a simpler non-resonant case should be considered, for which, as shown in (*Mytropolskyi Y.A., Lymarchenko O.S., 1998; Hevko I.B., 2013; Oleg Lyashuk, 2016; Sokil M.B., and others, 2016, Sun X.X.; Meng W.J., Yuan Y., 2017*), the amplitude and frequency of the process must be determined by the ratio:

$$\frac{da}{dt} = \mu A_1\left(a\right) + ...,$$
$$\frac{d\psi}{dt} = \Omega + \varepsilon B_1\left(a\right) + ..., \tag{15}$$

The unknown functions $A_1\left(a\right)$ and $B_1\left(a\right)$ are found in the following way: the representation (15) should satisfy the original equation (7) and boundary conditions (6) with the accurate size of order μ inclusively. Therefore, by differentiating on independent variables x and t (7), the formula for the first approximation is deduced:

$$\frac{\partial y}{\partial t} = \mu A_1\left(a\right)\left(\cos\left(\kappa x + \psi\right) - \cos\left(\kappa x - \psi\right)\right) - a\left(\Omega + \varepsilon B_1\left(a\right)\right)\left(\sin\left(\kappa x + \psi\right) + \sin\left(\kappa x - \psi\right)\right)$$
$$+\mu\left(\Omega\frac{\partial y_1\left(a, x, \psi, \theta\right)}{\partial \psi} + \frac{\partial y_1\left(a, x, \psi, \theta\right)}{\partial \theta}\nu\right), \tag{16}$$

$$\frac{\partial^2 y}{\partial t^2} = -a\,\omega_k{}^2\left(\sin\left(\kappa x + \psi\right) + \sin\left(\kappa x - \psi\right)\right) -$$
$$-2\mu\left(A_1\left(a\right) + a B_1\left(a\right)\Omega\right)\left(\cos\left(\kappa x + \psi\right) - \cos\left(\kappa x - \psi\right)\right) +$$
$$+\varepsilon\left(\frac{\partial^2 y_1}{\partial \psi^2}\omega^2 + \frac{\partial^2 y_1}{\partial \theta^2}\nu^2 + 2\frac{\partial^2 y_1}{\partial \psi \partial \theta}\Omega\nu\right), \tag{17}$$

$$\frac{\partial y}{\partial x} = -a\kappa\left(\sin\left(\kappa x+\psi\right)-\sin\left(\kappa x-\psi\right)\right)+\mu\frac{\partial y_1}{\partial x},$$
$$\frac{\partial^2 y}{\partial x^2} = -a\kappa^2\left(\cos\left(\kappa x+\psi\right)-\cos\left(\kappa x-\psi\right)\right)+\mu\frac{\partial^2 y_1}{\partial x^2}$$
$$\frac{\partial^3 y}{\partial x^3} = a\kappa^3\left(\sin\left(\kappa x+\psi\right)+\sin\left(\kappa x-\psi\right)\right)+\varepsilon\frac{\partial^3 y_1}{\partial x^3}, \quad (18)$$
$$\frac{\partial^4 y}{\partial x^4} = a\kappa^4\left(\cos\left(\kappa x+\psi\right)-\cos\left(\kappa x-\psi\right)\right)+\varepsilon\frac{\partial^4 y_1}{\partial x^4}.$$

Substituting in the base equation (7) the above dependences after the equalization of the coefficients at μ, a differential equation for determining the desired functions $A_1(a)$, $B_1(a)$ is deduced.

$$L\left(\frac{\partial^2 y_1}{\partial\psi^2},\frac{\partial^2 y_1}{\partial\theta^2},...,\frac{\partial^4 y_1}{\partial x^4}\right)=\frac{\partial^2 y_1}{\partial\psi^2}\Omega^2+\frac{\partial^2 y_1}{\partial\theta^2}\nu^2+2\frac{\partial^2 y_1}{\partial\psi\partial\theta}\Omega\nu+\alpha^2\frac{\partial^4 y_1}{\partial x^4}+\omega^2 y_1=$$
$$=4a\Omega A_1(a)\sin\frac{\pi x}{l}\sin\psi+4a\Omega B_1(a)\sin\frac{\pi x}{l}\cos\psi--u^2a\left(\frac{\pi}{l}\right)^2\sin\frac{\pi x}{l}\cos\psi+ \quad (19)$$
$$+2ua\Omega\frac{\pi}{l}\cos\frac{\pi x}{l}\sin\psi+F\left(a,\psi,x\right).$$

If a function $y_1\left(a,\psi,\vartheta,x\right)$ is periodic by an argument ψ, then its partial derivatives are the same by the noted argument. Consequently, the left-hand side of differential equation (19) does not contain the summands that are proportional to $\sin\psi$ and $\cos\psi$. This is the basis for finding the functions $A_1(a), B_1(a)$

$$A_1(a)=-\frac{1}{p}\frac{1}{4\Omega\pi^2}\int_0^l\int_0^{2\pi}\int_0^{2\pi}F\left(a,x,\psi,\theta\right)\sin\frac{k\pi}{l}x\sin\psi\,dxd\psi\,d\theta,$$
$$B_1(a)=-\frac{1}{p}\frac{1}{4\Omega\pi^2 a}\int_0^l\int_0^{2\pi}\int_0^{2\pi}F\left(a,x,\psi,\theta\right)\sin\frac{k\pi}{l}x\cos\psi\,dxd\psi\,d\theta, \quad (20)$$

where $p=\frac{l}{2}$.

As the elastic body material satisfies the nonlinear technical law of elasticity (*Owen, Philip J., Cleary, Paul W., 2010; Sun X.X.; Meng W.J., Yuan Y., 2017*) then the resistance to the motion is proportional to the velocity, and the right-hand sides of the equation (17), that is, the functions $A_1(a)$ $B_1(a)$ acquire the form

$$\mu A_1(a)=-\frac{\bar{\delta}}{m+\rho}\left(\Omega\right)^{s-1}a^s,$$
$$\mu B_1(a)=-\frac{3\mu}{32}\frac{\pi^2}{l^2}\frac{a^2}{\Omega}-\left(\frac{\pi}{l}\right)^2\frac{m}{m+\rho}\frac{u^2}{8\Omega}. \quad (21)$$

RESULTS

In Fig. 3, the dependence in time of the amplitude and frequency of nonlinear vibrations of the feeder-mixer horizontal working body at its various geometric dimensions, the angular velocity of the working body rotation, the grain mixture mass per unit length, and the speed of its transportation are presented.

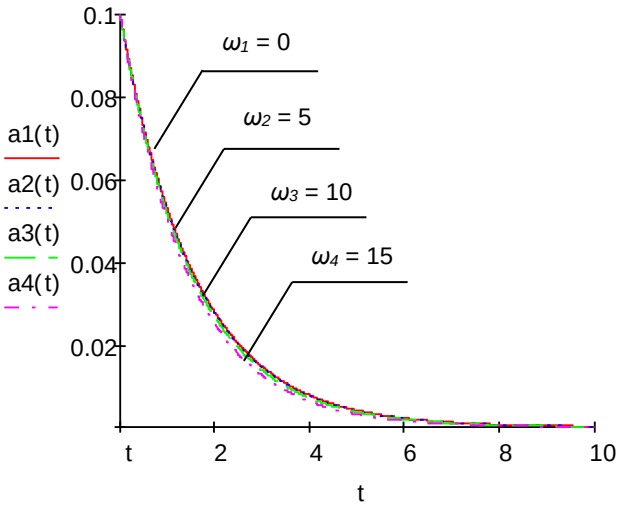

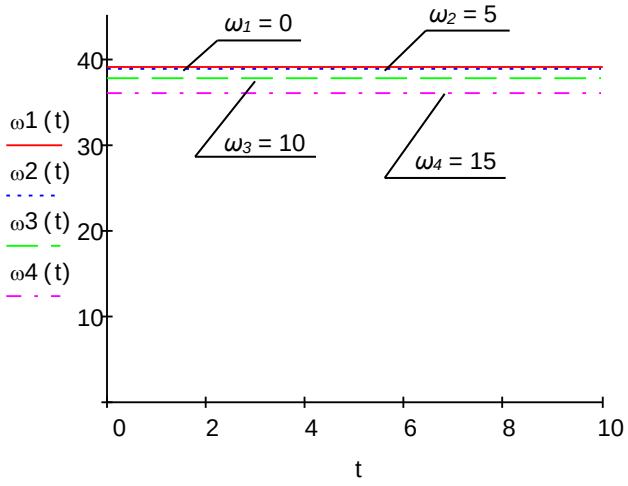

$\rho = 10 kg/m,\ m = 0, kg/m\ I = 6 \cdot 10^{-6} m^2,\ E = 2.06 \cdot 10^{11} N/m^2,\ l = 10m, u = 10 m/s$

a) ***b)***

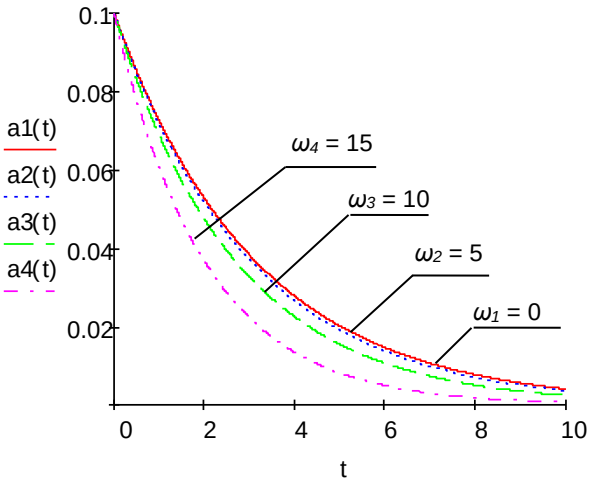

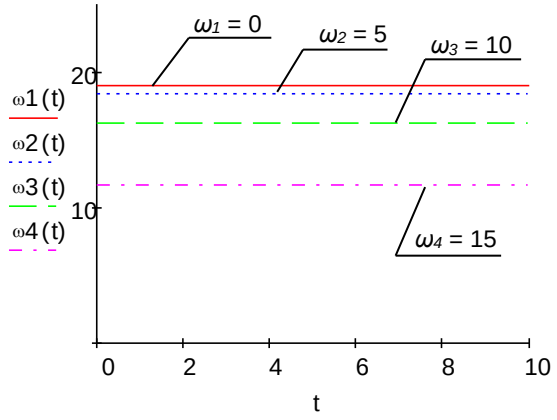

$\rho = 10, kg/m,\ m = 30 kg/m,\ I = 6 \cdot 10^{-6} m^2,\ E = 2.06 \cdot 10^{11} N/m^2, l = 10m,\ u = 10 m/s$

c) ***d)***

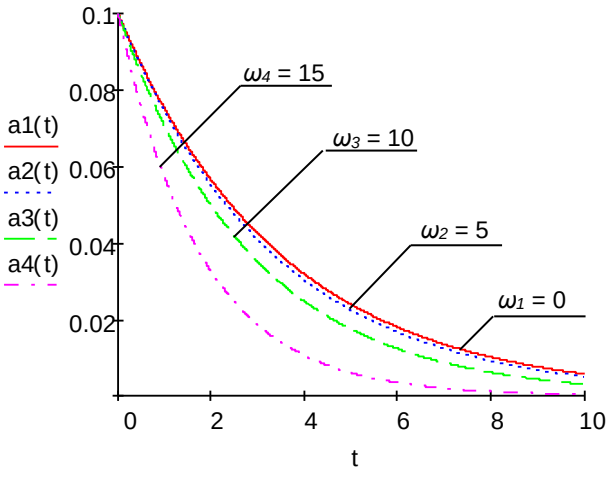

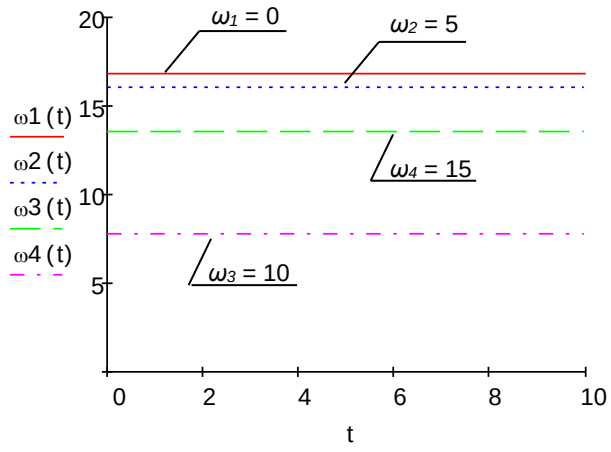

$\rho = 10 kg/m,\ m = 40 kg/m,\ I = 6 \cdot 10^{-6} m^2,\ E = 2.06 \cdot 10^{11} N/m^2, l = 10m,\ u = 10 m/s$

e) ***f)***

Fig. 3 - Laws of variation in time of the amplitude and frequency of bending vibrations of the feeder-mixer horizontal branch

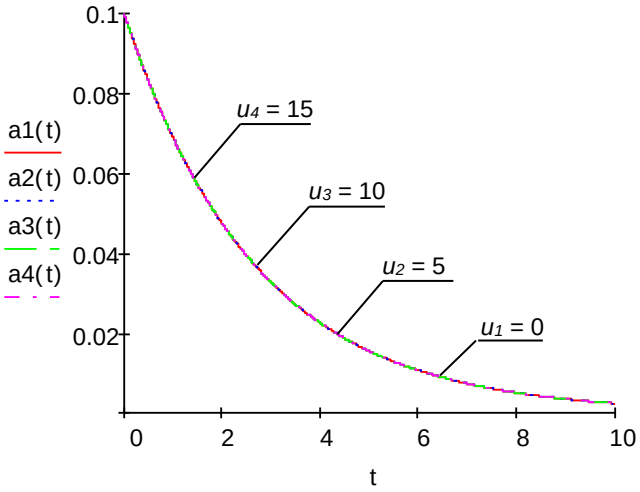

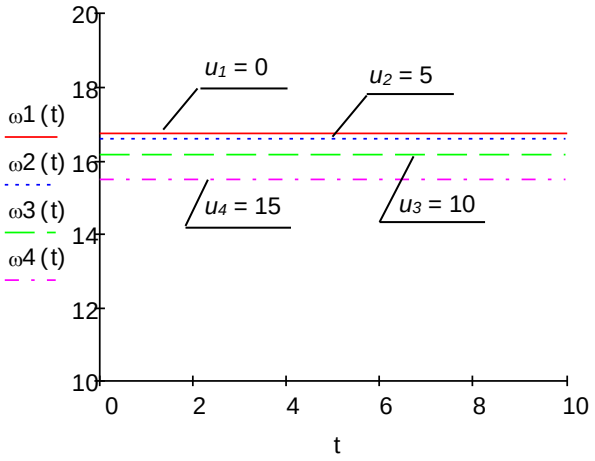

$\rho = 10 kg/m,\ m = 30 kg/m,\ I = 6 \cdot 10^{-6} m^2,\ E = 2.06 \cdot 10^{11} N/m^2,\ \omega = 10 rad/s$

g) ***h)***

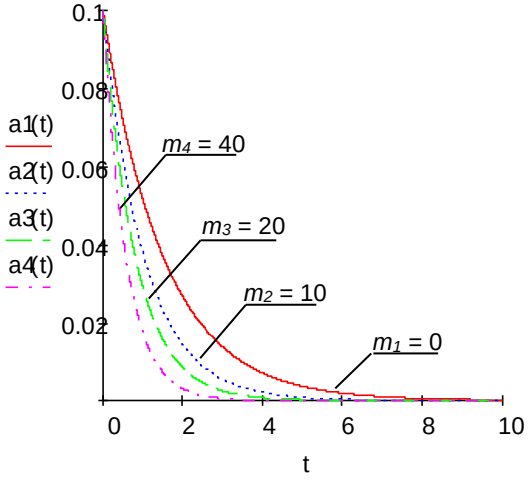

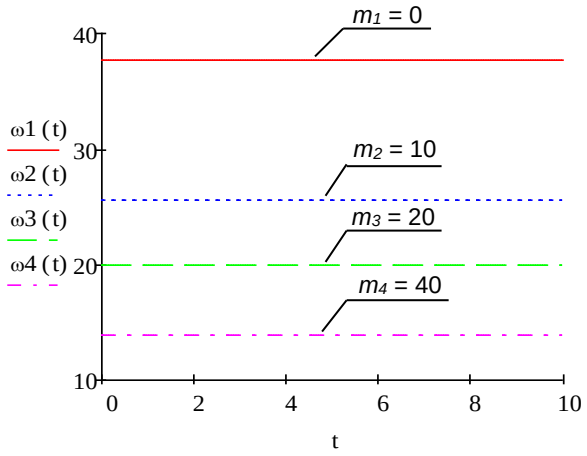

$\rho = 10 kg/m,\ u = 7.5 m/s,\ I = 6 \cdot 10^{-6}\ m^2,\ E = 2.06 \cdot 10^{11} N/m^2,\ \omega = 10 rad/s$

i) ***j)***

Fig. 3 - Laws of variation in time of the amplitude and frequency of bending vibrations of the feeder-mixer horizontal branch

CONCLUSIONS

Based on the analytical and graphical results, the following conclusions should be made:

- the higher are the angular rotational velocities of the feeder-mixer working body and the values of the grain mixture mass per unit length, the lower is the actual frequency of the horizontal branch with the grain mixture; at the same time, the rate of closing the amplitude is higher;
- if the velocities of the grain mixture motion along the feeder-mixture horizontal branch are higher, the actual frequency of vibrations is somewhat lower;
- the effect of the amplitude variation in time on the change in actual frequency of vibrations of the horizontal branch with the grain mixture is insignificant. The above can be justified by the fact that the mathematical model is considered with a small non-linearity.
- the results are very important in the study of more complex - resonant vibrations of the feeder-mixer working body.

REFERENCES

[1] Bulgakov V., Adamchuk V., Nozdrovicky L., Krocko V., Korenko M., Kiurchev V., Ihnatiev Y., (2017), Mathematical model of complex movement of a material point on a surface of agricultural machine working body, *V International scientific Congress "Agricultural machinery*", Vol.1, pp. 64-71;

[2] Chen L.Q., (2009), Nonlinear parametric vibration of axially moving beams: asymptotic analysis and differential quadrature verification, *Journal of Physics: Conference,* Series 181, pp.1–8;
[3] Hevko B.M., Pavelchuk Yu.F., (2017), Modeling of fluctuations of the mechanical system 'suspension hole': theoretical analysis, *Innovative solutions in modern science*, № 1(10), pp.1-9;
[4] Hevko B.M., Rohatynskyi R.M., (1989), Screw feeders of agricultural machines, *Vyshcha shkola*, p.176, Lviv/Ukraine;
[5] Hevko B.M. and others, (2015), The study of bulk material kinematics in a screw conveyor-mixer *INMATEH -Agricultural Engineering,* vol. 47, no.3, pp.155-163, Bucharest/Romania;
[6] Hevko R.B. and others, (2012), Improvement of the technical level of flexible screw conveyors*, Monograph, Aston*, p.204, Ternopil/ Ukraine;
[7] Hevko R.B. and others, (2015), Development and investigation of reciprocating screw with flexible helical surface, *INMATEH - Agricultural engineering,* vol. 46, no.2. pp. 133-138, Bucharest/Romania;
[8] Hevko R.B. and others, (2016), Investigation of a transfer branch of a flexible screw conveyer, *INMATEH - Agricultural Engineering*, vol. 48, no. 1, pp. 29-34, Bucharest/Romania;
[9] Hevko R.B., Klendiy O.M., (2014), The investigation of the process of a screw conveyer safety device actuation*, INMATEH - Agricultural Engineering*, vol. 42, no.1, pp. 55-60, Bucharest/Romania;
[10] Hevko I., (2012), Mathematical model of nonlinear bending oscillations of a screw, *Bulletin of TNTU*, № 4 (68), pp.141–154, Ternopil/ Ukraine;
[11] Hevko I., (2012), Mathematical model of torsional oscillations of a screw, *Materials of the Sixteenth Scientific Conference of TNTU named after I. Pul'uj,* p. 15, Ternopil/ Ukraine;
[12] Hevko I.B., (2013), Scientific and Applied Fundamentals of Screw Transport and Technological Mechanisms Production: author's abstract of doctor's diss. (*Techn. Sciences: 05. 02.02 "Machine Knowledge*", p. 42, Lviv/Ukraine;
[13] Hevko B.M. and others, (2015), The study of bulk material kinematics in a screw conveyor-mixer, *INMATEH - Agricultural Engineering*, vol. 45, no. 3, pp. 197–205, Bucharest/Romania;
[14] Loveykin V.S., Nesterov A.P., (2002), Dynamic optimization of lifting machines, *Publishing house of SNU,* p. 387, Luhansk/ Ukraine;
[15] Lyashuk O.L. and others, (2015), Modeling of the vertical screw conveyer loading, *INMATEH - Agricultural Engineering,* vol. 45, no. 1, pp. 87-95, Bucharest/Romania;
[16] Mytropolskyi Y.A., Lymarchenko O.S., (1998), On the question of the asymptotic approximation for the slow wave processes in nonlinear dispersive media, *Ukr. mat. journal*, №3 (59), pp. 357–371, Kiev/Ukraine;
[17] Oleg Lyashuk, (2016), The study on nonlinear model of dynamics of a system 'extruder elastic auger working body', *In acta technologica agriculturae*, no. 4, pp. 102-107, Nitra/Slovak Republic;
[18] Owen Philip J., Cleary Paul W., (2010), Screw conveyor performance: comparison of discrete element modelling with laboratory experiments, Progress in computational fluid dynamics, 10(5/6), pp.327-333.
[18] Rohatynskyi R. and others, (2012), Investigation of the torque fluctuations of a screw, *Scientific works of the Russian University "Angel Кънчев ": Agricultural machinery and technology. Agrarian Sciences and Veterinary Medicine. Repair and reliability*, Vol.51, Series 1.1, pp. 42-46;
[19] Sokil M.B. and others, (2016), Dynamics of flexible elements of drive systems with variable contact point to the pulleys, *INMATEH - Agricultural Engineering,* vol.48, no.1, pp.119-124, Bucharest/Romania;
[20] Sun X.X., Meng W.J., Yuan Y., (2017), Design method of a vertical screw conveyor based on Taylor-Couette-Poiseuille stable helical vortex, *Advances in mechanical engineering*, 9(7);
[21] Tian Y., Cheng Q. and others, (2018), Research on the Principle of a New Flexible Screw Conveyor and Its Power Consumption, *Applied Sciences*, 8(7).

INVESTIGATION OF OIL EXTRACTION FROM THE CANOLA AND SOYBEAN SEEDS, USING A MICROWAVE INTENSIFIER

/

ДОСЛІДЖЕННЯ ЕКСТРАКЦІЇ ОЛІЇ З НАСІННЯ РІПАКУ ТА СОЇ ПРИ ВИКОРИСТАННІ МІКРОХВИЛЬОВОГО ІНТЕНСИФІКАТОРА

Prof. PhD. Bandura V.[1)], Prof. Ph.D. Eng. Bulgakov V.[2)], Prof. Ph.D. Eng. Adamchuk V.[3)], Ph.D. Eng. Ivanovs S.[4)]
[1)] Vinnytsia National Agrarian University/ Ukraine; [2)] National University of Life and Environmental Sciences of Ukraine / Ukraine, [3)] National Scientific Centre "Institute for Agricultural Engineering and Electrification" / Ukraine;
[4)] Latvia University of Agriculture / Latvia
Tel.+37129403708, E-mail: semjons@apollo.lv

Keywords*: soybean, canola, extraction, ethanol, microwaves, tocopherols.*

ABSTRACT

Intensification of the technological processes in the production of vegetable oils is a topical scientific and practical task. It is assumed that extracts from the plant raw materials obtained by exposure to the electromagnetic microwave field possess qualitatively new biochemical and biological properties in comparison with similar extracts obtained by means of the conventional extraction methods. The article deals with possibilities to reduce the duration of the extraction process of the soybean and canola seeds, to achieve great output of the target component, to increase the number of valuable components (tocopherols) in the finished product. It has been established that in the microwave intensifier, in contrast to the classic method of extraction, the extraction time of the soybean and canola seeds is reduced to 70%, but the output of the target component increases within the limits of 30%.

РЕЗЮМЕ

Інтенсифікація технологічних процесів при отриманні рослинних олій є актуальною науково-практичною задачею. Передбачається, що екстракти з рослинної сировини, отримані з використанням впливу мікрохвильового електромагнітного поля, набувають якісно нові біохімічні та біологічні властивості у порівнянні з аналогами, отриманими традиційними методами екстракції. У роботі досліджувалися можливості скорочення тривалості процесу екстракції насіння сої та ріпаку, одержання більшого виходу цільового компонента, збільшення кількості цінних компонентів (токоферолів) в готовому продукті. Встановлено, що в мікрохвильовому інтенсифікаторі, порівняно з класичним методом екстрагування, час проведення екстрагування насіння сої та ріпаку зменшується до 70%, а вихід цільового компонента збільшується в межах 30%.

INTRODUCTION

Vegetable oils are an important food product and a raw material for the chemical, machine-building, metallurgical industry, as well as for the production of biodiesel fuel *(Thiyam-Holländer et al., 2016)*. Owing to the presence of fatty acids and absence of cholesterol, vegetable oils have an ability to reduce the risk of cardiovascular diseases. The properties of the oils and the ability to preserve their valuable qualities depend on many factors, including the biologically active components, particularly tocopherols, which are antioxidants preventing and protecting polyunsaturated fatty acids from oxidation *(Loganes et al, 2016; Burdo, 2013)*.

Canola seeds contain 40-45% of oil and, in contrast to other vegetable oils, it has a series of advantages from the point of view of the physiology of human nutrition. It also contains 18-22% of crude protein and other physiologically important acids in an optimal ratio, as well as α and β tocopherols. By the volume of production, rapeseed oil became the third in the world after palm and soybean oils.

Soybean seeds are also used to produce very valuable edible oil, which belongs to the group of linoleic-oleic oils. A very important group of compounds in soybean seeds are phosphatides, as well as tocopherols and pigments. These substances play an active role in metabolic processes, serving as one of the best sources of the natural antioxidant – vitamin E. Soybean seeds contain from 14 to 25% of oil and belong to the group of low-oil crops.

When processing low-oil raw materials, direct extraction of oil is applied (without preliminary extraction of oil by pressing).

The extraction process is based on the ability of vegetable oils to dissolve in organic solvents. The extraction rate depends on the condition of the oilseed material, its temperature, the degree of crushing, etc. In the process of extracting oil from the crushed raw material, a miscela (an oil solution in a solvent) and a defatted residue (meal, solvent cake) is obtained. In order to extract oil, the solvent is subsequently evaporated from the miscela. The resulting vapours of the solvent are condensed and their recovery is conducted to convert the solvent into a liquid state.

Extraction of oil from seeds (considered in the process of these studies) is an important process which determines the degree of extraction of valuable components from the raw materials and the quality of the finished product. However, at the moment, in all industries, including the food industry, the classical extraction is a rather labour-intensive and inefficient process *(Thiyam-Holländer et al., 2016; Burdo et al, 2016)*. Among the existing problems, one can note the low output of the target component, the long duration of the process, the use of high pressure, large overall dimensions and the high metal intensity of the apparatus.

The search for new technologies to improve the extraction process allowed discovering methods by which intensification of the extraction process is achieved using electro-pulse technologies characterized by high impacts, specific by their power, upon the biomass placed in the reactor. They may include the shock wave, ultrasound, the electromagnetic field, etc. Application of these impacts allows significant improvement in the efficiency of the process even at room temperatures, reduction of the mass-transfer characteristics of the equipment, dramatic decrease in the electricity consumption.

Ultrasound has a destructive, crushing effect on the plant cells. A negative aspect of this impact is also the relatively high-power consumption. Besides, it is recommended to add surfactants to the extracting agent retarding the formation of cavitation, which is not always consistent with the production technology. When extracting, it is necessary to consider an increase in the extracting agent temperature due to the absorption of the ultrasonic energy and to ensure that the temperature of the extracting agent did not exceed the allowed values *(Burdo, 2015; Orlov, 2002).*

The positive aspects of the CO_2 – extraction technology are *(Salgin et al., 2006; Eggers, 1996, Bozan and Temelli, 2003)* production of native extracts, elimination of high temperatures, raising the quality of the target products, versatility of the CO_2 solvent (not combustible, not explosive, with a low cost).

To increase the extraction rate, catalysts, surfactants, chemical modifiers are used. Despite the fact that supercritical extraction has significant advantages, its application in the food production is still insufficient. This is because the solution of each specific extraction task requires an individual approach to the optimization of a certain technological process, its productivity specifying its raw material, extracting agent and the final product. Naturally, all these tasks are solved if the necessary unification level of the equipment is ensured.

Application of microwave heating makes it possible to intensify considerably the thermal treatment process of the raw material and extraction of stable soluble substances by an aqueous medium. Positive results from the application of electromagnetic pulsed radiation were obtained: in the production of food grade dyes from beets, fruit and berry raw materials, in the scheme of accelerated ripening (aging) of cognac spirits, when extracting cedar oil from the seeds of the Siberian pine, to accelerate the extraction of fungicides from wood materials under laboratory conditions, when extracting the oil from the mint leaves, rosemary, the tea tree (manuka), sandalwood and other plants, when extracting nicotine from the tobacco raw material, when extracting coffee beans *(Rekas et al, 2017; Burdo et al., 2007)*.

The aim of the work is to study possibilities of intensifying extraction of the soybean oil and rape seed oil by using microwave exposure and increasing the number of valuable components (tocopherols) in the finished product.

MATERIALS AND METHODS

The extraction process was carried out on the test bench which is described in more detail in works *(Bandura and Kaljanovska, 2011)*. Extraction of oil from the miscela to determine the concentrations was carried out arbitrarily by evaporating the solvent. The contents of tocopherols and other components in the oil samples were carried out under the factory laboratory conditions in accordance with accepted standards and compared with current standards. The methods of investigation are based on a thermophysical analysis of the structure of the material and the solvent.

In experimental studies, control instrumentation, modern methodologies and devices were used, among which there are the authors' developments. For analytical research and processing of experimental research results, a PC and the corresponding software packages MathCAD and Excel were used.

Studies on the oil extraction of the canola seeds, the "Champion" variety, and the soybean seeds, varieties "Vinnichanka", using ethyl alcohol, were carried out on elaborated experimental equipment with a microwave intensifier. In order to study the process, the solution concentration was determined depending on the extraction time, etc. For determine oil concentration in the miscela, a HP 1100 chromatograph (Agilent Technologies (USA) was used.

After a series of preliminary experiments were conducted on the extraction of the micromodel *(Koljanovska and Bandura, 2012)*, a larger installation was created (Fig. 1).

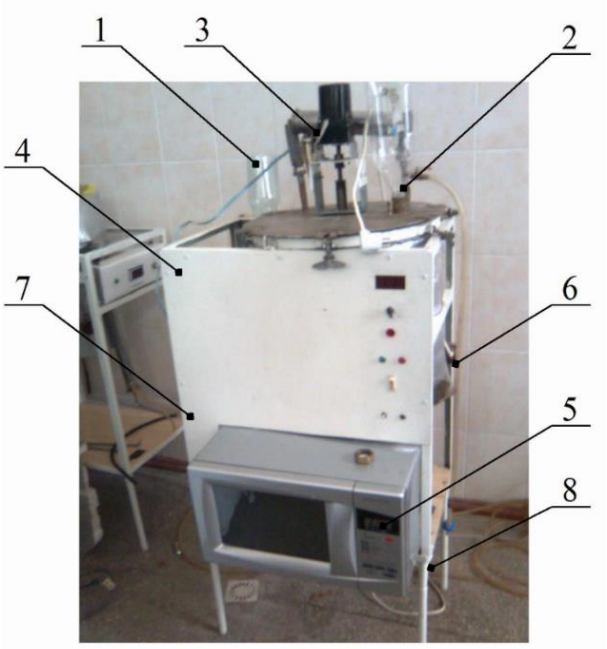

Fig. 1 - Laboratory equipment (extractor with a microwave intensifier)

1 – an orifice with a vessel for filling the extractor with the solvent;2 – an orifice with a vessel for filling the reaction vessel with a solid phase; 3 – a reflux condenser; 4 – the extractor; 5 – the electromagnetic intensifier (MWI; 6 – a sensor for taking the temperature of the intermediate heat carrier; 7 – a sensor for taking the temperature of the product at the inlet into the microwave intensifier; 8 – a sensor for taking the temperature of the product at the outlet from the microwave intensifier

In the laboratory installation, the power of the microwave intensifier can be varied within the limits from 0.4 to 1.6 kW, the volume of the solvent is from 0.008 to 0.015 m^3, the mass of the canola and soybean seeds was from 2 to 5 kg. The frequency of the microwaves was 2450 MHz.

In the preliminary investigations, we estimated the impact of the power of the microwave intensifier 0.4; 0.6; 0.8; 1.0; 1.2; 1.4; 1.6 kW upon the oil output. The results of the extraction studies with the help of a microwave intensifier at different capacities showed that the concentration of the canola and soybean oil increased in the range from 0.4 to 0.8 kW, and then, starting from 0.8 kW and higher, practically did not change. Therefore, in order to save energy, the applied capacity of the intensifier in the following experiments was 0.8 kW. In this paper, there are presented the results of research on the extraction process of the canola seeds, the "Champion" variety (the oil content – 43%) and soy bean, the "Vinnichanka" variety (the oil content - 21%), with ethyl alcohol, using the self-developed experimental equipment on the basis of a microwave intensifier (MWI). The laboratory equipment works as follows: the seeds of the investigated oil crops are fed into the extractor *4* through the orifice *2*, and the solvent – through the orifice *1*. The solvent is condensed in the reflux condenser *3*. The extraction intensification takes place in the electromagnetic intensifier (MWI) *5*.

Temperature measurements by the sensors of the intermediate heat carrier, of the miscela at the inlet into and the outlet from the microwave intensifier were carried out with a 2 minutes' interval; after every 2 minutes samples were taken to determine the concentration of the miscela. To increase the validity of the results, the experiments were conducted in 6-fold replicates. Where the results were obtained with significant deviations (with a coefficient of variation of more than 10%), the number of measurements was increased to 12.

During the study, temperature indicators of the product were taken using of sensors at the inlet *7* and the outlet *8* from the microwave intensifier, as well as temperatures of the intermediate heat carrier *6*. The characteristics of the laboratory equipment during the experiments were as follows (Table 1).

The processing of the experimental data about the change in the concentration of the solid and the liquid phases under different condition parameters in the ethyl alcohol medium was carried out using the MathCad system.

Table 1

Characteristics of the extractor with a microwave intensifier

Characteristics of the equipment	Unit of measurement	Quantity
Volume of the solvent (V)	m^3	0.008
Mass of the canola seeds (Mc_p)	kg	2
Mass of the soybean seeds (Mc_c)	kg	2
Duration of extraction (t)	min	32
MWI efficiency (N)	kW	0.8

RESULTS

During the research, the temperature indicators of the miscela (the solution of oil in the solvent) at the inlet *7* and at the outlet *8* from the microwave intensifier, as well as the temperature of the intermediate heat carrier *6* were taken with the help of sensors. The graph (Fig. 2) shows experimentally obtained dependences of the temperature of the miscela on time in the process of extracting the canola seeds and soybean seeds using ethyl alcohol in the extractor with a microwave intensifier.

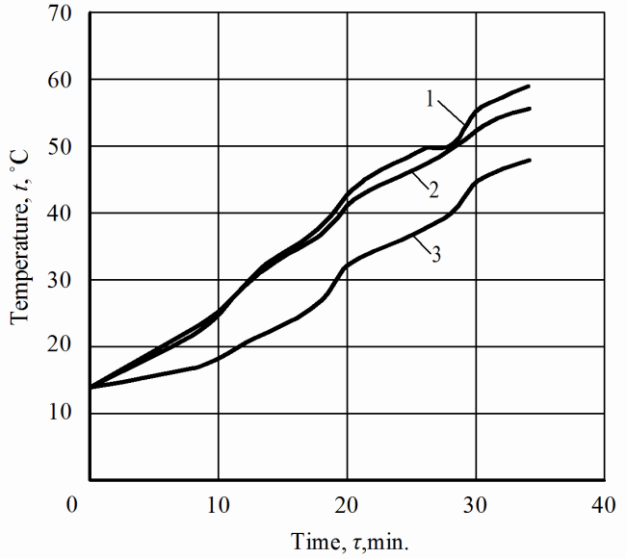

Fig. 2 - The value of the miscela temperature depending on the time of the canola and soybean seeds using ethyl alcohol, in the extractor with a microwave intensifier

1 - temperature at the outlet; 2 - temperature at the inlet; 3 - temperature of the heat carrier

As it can be seen from Fig. 2, the temperature of the miscela at the outlet of the microwave intensifier was high, while during the investigation its maximum value was 59°C, the maximum value at the inlet was 56°C and the temperature of the intermediate heat carrier at the end of the study was not more than 48°C. The graph was created on basis experimental data (the obtained dependences do not have a strictly linear form), and in the present paper its further approximation has not been fulfilled.

Fig. 3 shows the concentration of the miscela of the soybean seeds, the "Vinnichanka" variety, and of the "Champion" canola seeds, depending on the extraction time using the microwave intensifier. In contrast with the traditional technology, the use of a microwave intensifier contributes to a significant reduction in time and an increase in the amount of the extracted oil (about 30%) *(Bandura et al., 2011, Burdo et al., 2016).* The output of the extracted canola seed oil with 2 kg of the loaded canola seed grain, crushed to the size of a fraction of 0.5-1 mm with an initial oil content of 43%, was 0.83 kg, i.e. 41.5% (i.e. only 1.5% of the canola oil remains in the residue). The concentration of the soybean oil at the end of the experiment, using the MWI, was 5.0%. The output of the soybean oil from 2 kg of seeds, crushed to the fraction size of 0.5-1 mm and the initial oil content of 21%, was 0.40 kg, i.e. 20%. This means that only 1.0% of the soybean oil remains in the residue after the seed processing. Intensification of the extraction process by means of the microwave field is

more efficient than the classical method of boiling. Intensification of the extraction process, using the microwave field, takes place by increasing pressure (barodiffusion) inside the capillaries of the plant raw material, followed by their destruction and the maximum arrival of the target component into the extracting agent. A barodiffusion current arises which contributes to significant reduction in the duration of the extraction process and substantial increase in the extraction of valuable components from the raw material.

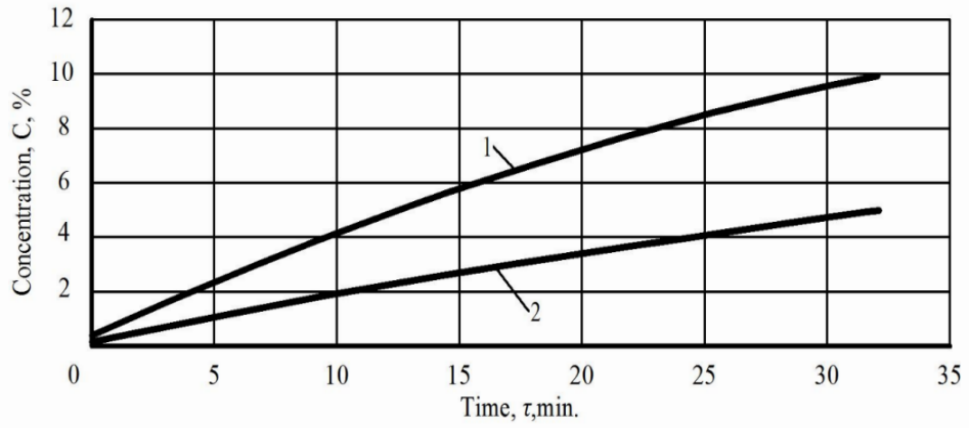

Fig. 3 - Dependence of the oil concentration in the miscela on the time in the extraction process of oil from the canola and soybean seeds using alcohol, in a microwave intensifier

1) - colza + alcohol, fraction of grain 0.5-1 mm, hydromodule 1: 4, output power 800 W;
2) - soybean + alcohol, fraction of grain 0.5-1 mm, hydromodule 1: 4, output power 800 W.

As it is known *(Bogaert et al., 2018, Bredeson, 1983; Karaj and Müller, 2011; Ward, 1976),* increasing temperature raises the intensity of the oil release, both by a mechanical method of obtaining oil from the seeds and by extraction. However, high temperature can adversely affect the quality of the product to be obtained, and therefore the maximum allowed temperature is limited by certain requirements of the standard. Particularly, for the crops under consideration (canola and soybean) the maximum allowed temperature should be not more than 60°C. In order to obtain a compatible comparison for the oil production intensification by means of a microwave field and by raising temperature, research was carried out of both crops.

The experimental research shows that, when extracting crushed canola and soybean grains by alcohol in the conventional way (in a thermostat by infusion) at different temperatures (12°C, 40°C, 50°C, 60°C), the process can also be intensified by moderate increase in temperature to 60°C.

By the way, after extracting canola for 5 hours the oil concentration in the miscel was 8.1% at a temperature of 12°C, 15.2% at 40°C, 20.9% at 50°C and 24.3% at 60°C (fig.4). The process becomes practically stable for all the investigated temperatures after 10 hours of extraction, the oil concentration at 12°C being 12.3%, at 40°C – 21.4%, at 50°C – 24.7%, and at 60°C – 28.3%.

The tendency of increasing the oil concentration, when temperature increases, was preserved for soybeans too. So, when extracting for 5 hours, the oil concentration was at a temperature of 12ºC – 3.7%, at 40ºC – 13.1%, at 50ºC – 14.9% and at 60ºC – 21.5%. At temperatures of 40-60°C extraction was carried out for 5 hours and at a temperature of 12°C – 24 hours. At a temperature of 12°C – 24 hours the concentration of the soybean oil reaching only 8.9%, i.e. it was by 6% lower than at a 5-hours' extraction at 50°C (Fig. 5).

However, when comparing the data obtained by the conventional method (extracting in a thermostat) with the data obtained using a microwave intensifier, it is evident that the proposed method allows at the same time increasing the oil concentration by about 30%.

An important parameter is also time consumed for the production of oil. The results of the research show that, in order to achieve a concentration equal to that reached by the conventional method, the time required, when using a microwave intensifier, is reduced almost twofold (1.96 times).

An important indicator of the quality of the canola and soybean oil is the amount of the acid and the peroxide value, which contain common tocopherols, etc. The obtained experimental samples fully corresponded (Table 2) to the requirements of the standards (*State Standard of Ukraine No 4534: 2006; State Standard of Ukraine No 46.072: 2005*).

The efficiency of the use of a non-standard for the given process polar solvent of ethyl alcohol is confirmed by the results of the gas-liquid chromatography, which show that under the influence of the electromagnetic field, this solvent intensifies extraction from the canola and soy bean seeds not only fatty acids but also biologically active substances, in particular, tocopherol $C_{29}H_{50}O_2$.

As it is evident from the data in Table 3, in contrast with the classical method of extraction, when using a microwave intensifier, the content of tocopherols increased in the canola oil, on the average, 1.8 times, and

in the soybean oil - 2.6 times. This indicates promising prospects for the application of microwave radiation to produce better quality products from the canola and soybean seeds.

Table 2

Compliance of the tested samples of oils with the requirements of state standards of Ukraine

Indicators	Canola oil (a sample)	Requirements of the standard: DSTU 46.072: 2005 "Canola oil"	Soybean oil (a sample)	Requirements of the standard: DSTU 4534: 2006 "Soybean oil"
Acidity number, mg KOH/g	3.9	not more than 6.0	4.0	not more than 6.0
Mass fraction of moisture and volatile substances, %	0.25	not more than 0.25	0.19	not more than 0.2
Peroxide number, 0.5·*O* mmol·kg^{-1}	8.9	not more than 10.0	9.1	not more than 10.0
Mass fraction of phosphorus-containing substances in terms of stearo-oleo-lecithin, %	1.9	not more than 2.0	4.0	not more than 6.0
Mass fraction of erucic acid, %, to the sum of fatty acids	0.8	not more than 2.0	-	-

Table 3

Content of tocopherols in the canola and soybean oil samples

Oil	Content of common tocopherols after extraction in the MWI,%	Content of common tocopherols after classical extraction, %
Canola	92	51
Soybean	301.2	137

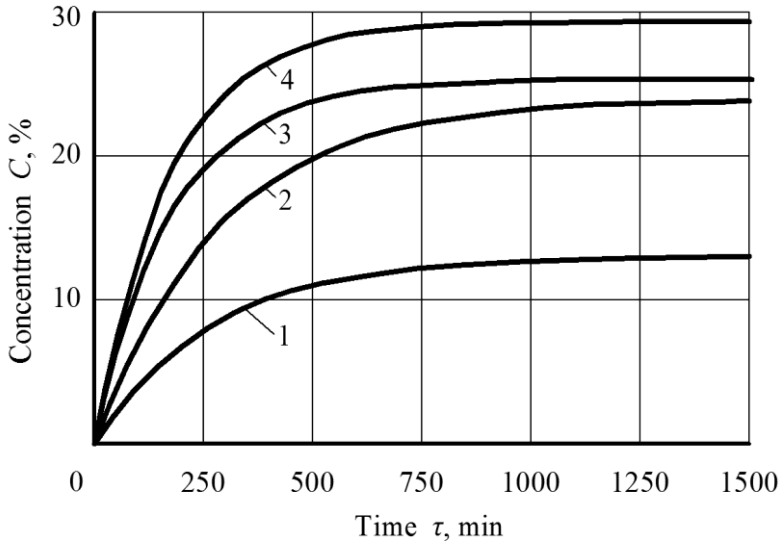

Fig.4 - Dependence of the oil concentration in the miscela on the time in the extraction process of oil from the canola using the conventional method (in a thermostat by the infusion method)

(colza + alcohol, fraction of grain 0.5-1 mm, hydromodule 1: 4)

On the basis of these studies, a technological scheme for extraction of oil from the rapeseed and soybean seeds, using a microwave intensifier was developed and recommended; functional dependences were found that allowed to determine the rational operating conditions of extractors depending on the influence of intensifying factors; the efficiency was established of the use of a more safe, non-toxic ethyl alcohol (as opposed to the toxic explosive hexane, which is used now in production). The proposed technology will provide an opportunity to obtain a product that meets the requirements of the existing national standards.

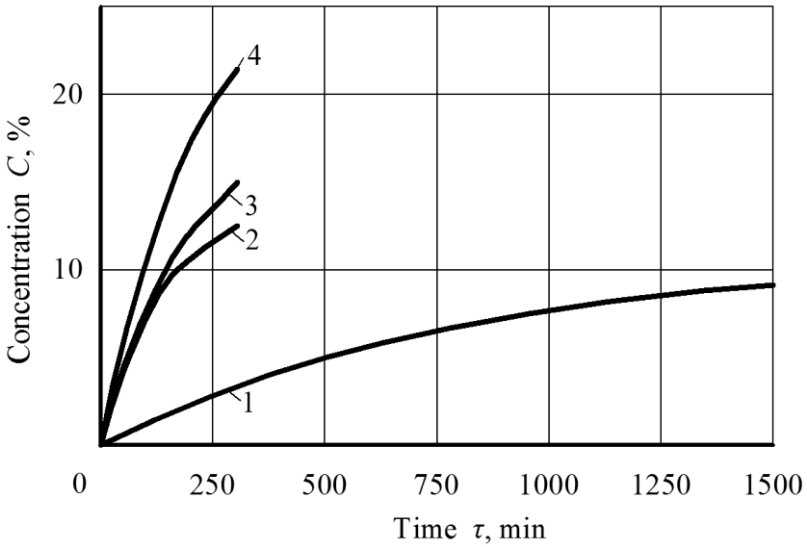

Fig. 5 - Dependence of the oil concentration in the miscela on the time in the extraction process of oil from the soya seeds using the conventional method (in a thermostat by the infusion method)

(soya + alcohol, fraction of grain 0.5-1 mm, hydromodule 1: 4)

CONCLUSIONS

1. In contrast with the traditional extraction method, the use of a microwave intensifier to extract oil from the canola and soy been seeds makes it possible to accelerate the process and allows obtaining a better-quality product.

2. In experiments using a microwave intensifier, the output of the extracted canola oil was 41.5% and the soy bean oil 20%.

3. In contrast with the classical extraction method, when using a microwave intensifier, the content of tocopherols increased in the canola oil, on the average, 1.8 times, and in the soybean oil – 2.6 times.

REFERENCES

[1] Bandura V., Koljanovska L., (2011), Intensification of vegetable oil extraction by electromagnetic field,*Scientific works of the Odessa National Academy of Food Technologies,* Vol.39 (2), pp. 186-190, Odessa/Ukraine;

[2] Bandura V., Koljanovska L., Ruzhicka N., (2011), Intensification of extraction in the technology of the canola oil production, Vibrations in engineering and technologies, Vol. 61(1), pp. 98-102, Vinnica/Ukraine;

[3] Bogaert L., Mathieu H., Mhemdi H., Vorobiev E., (2018), Characterization of oilseeds mechanical expression in an instrumented pilot screw press, *Industrial Crops and Products,* Vol.121, pp.1 06-113. Wageningen/Netherlands;

[4] Bredeson D.K., (1983), Mechanical oil extraction, *Journal of the American Oil Chemists' Society*, Vol. 60, pp. 211-213, Piqua/USA;

[5] Burdo O., (2013), *Food nanotechnologies*, 294 p., Herson/Ukraine;

[6] Burdo O., (2015), Technologies of directed energy action in agroindustrial complexes, *Scientific works of the Odessa National Academy of Food Technologies,* 2015, Vol.47(1), pp. 4-10. Odessa/Ukraine;

[7] Burdo O., Terziev S., Bandura V., Jaravoj I., (2016), The mechanodiffusion effect-a new phenomenon in heat and mass transfer, *Materials of the XV Minsk International Forum on Heat and Mass Transfer)*, 23-26 May 2016, Vol. 2, pp. 224-228, Minsk/Belarus;

[8] Burdo O., Rjashko G., (2007), *Extraction in the "coffee-water" system*, 176 p., Odessa/Ukraine;

[9] Bozan B., Temelli F., (2003), Extraction of Poppy Seed Oil Using Supercritical CO_2, *Journal of Food Science,* 68(2), pp. 422–426;

[10] Eggers R., (1996), Supercritical fluid extraction (SFE) of oilseeds/lipids, *Supercritical Fluid Technology in Oil and Lipid Chemistry*, p.34, AOCS Press, Illinois/USA;

[11] Orlov I., (2002), Infusions obtained by aqueous and ultrasound extraction from the herbs of oregano, motherwort, peppermint, *Storage and processing of agricultural raw materials*, Vol. 12, pp. 26-27, Moskow/Russia;

[12] Karaj S., Müller J., (2011), Optimizing mechanical oil extraction of Jatropha curcas L. seeds with respect to press capacity, oil recovery and energy efficiency, *Industrial Crops and Products*, 34(1), pp. 1010-1016, Piqua/USA;
[13] Koljanovska L., Bandura V., (2012), Kinetics of extraction of oil from soya and canola, *Proceedings of the Odessa National Academy of Food Technologies*, Vol. 41(2), pp. 101-106, Odessa/Ukraine;
[14] Loganes C., Ballali S., Minto C., (2016), Main properties of canola oil components: A descriptive review of current knowledge. *Open Agriculture Journal*, Vol. 10, pp. 69-74;
[15] Rekas A., Scibisz I., Siger A., Wroniak M., (2017), The effect of microwave pre-treatment of seeds on the stability and degradation kinetics of phenolic compounds in rapeseed oil during long-term storage, *Food Chemistry,* Vol. 222, pp. 43-52;
[16] Salgın Uğur, Döker Onur, Ҫalımli Ayla, (2006), Extraction of sunflower oil with supercritical CO_2: Experiments and modelling, *Journal of Supercritical Fluids,* Vol. 38, pp. 326–331;
[17] Thiyam-Holländer U., Eskin M., Matthäus B., (2016), Canola and Rapeseed: Production, Processing, *Food Quality and Nutrition*, Retrieved, 2016, 40 p. Boca Raton/USA;
[18] Ward J.A., (1976), Processing high oil continuous screw preses, *Journal of the American Oil Chemists' Society*, Vol.53 (6), pp. 261-264, Piqua/USA;
[19] ***State Standard of Ukraine (DSTU) 46.072: 2005, Rapeseed oil, Kiev/Ukraine;
[20] ***State Standard of Ukraine (DSTU) 4534: 2006, Soy bean oil, Kiev/Ukraine.

HOT-AIR DRYING CHARACTERISTICS AND QUALITY EVALUATION OF BITTER MELON SLICE
/
苦瓜片热风干燥特性及品质评价

Ms.Eng. Liang Yang, Ms.Eng. Zhonghuan Hu, Prof. Ling Yang, Prof. Shouyong Xie, Prof. Mingjin Yang*)
Southwest University, College of Engineering and Technology, Chongqing Key Laboratory of Agricultural Equipment for Hilly and Mountainous Regions / P. R. China
Tel: 8613883002509; E-mail: ymingjin@swu.edu.cn

Keywords: *bitter melon slice, drying characteristics, mathematical model, quality evaluation, hot-air drying*

ABSTRACT

Hot-air drying experiments and quality evaluation were conducted to obtain drying characteristics and overall evaluation of hot-air drying of bitter melon slice in this study. The evaluation indexes included effective moisture diffusivity, total colour difference, retention rate of vitamin C and mass fraction of total saponins, etc. Results showed that: drying rate decreased with decrease of moisture content, and moisture removal was mainly processed during the falling rate drying stage; Page model and Modified Page model gave the best fit to experimental data of moisture ratio, and Page model was preferred for hot-air drying of bitter melon slice for convenience of process control and optimization; Air temperature had the highest level of influence on the synthetic evaluation index, and it was followed by air velocity, layer thickness and initial mass, sequentially, and the confidence levels of air temperature, air velocity and layer thickness were 99.6%, 98.1%, and 96.5%, respectively.

摘要

本文以有效水分扩散系数、色差、维生素 C 保留率和总皂苷质量分数等为评价指标，进行了苦瓜片的热风干燥实验，得到了苦瓜片的热风干燥特性和干燥质量的总体评价。研究结果表明：干燥速率随着含水率的降低而降低，水分的去除主要发生在降速干燥阶段；Page 模型和修正 Page 模型对苦瓜片水分比实验数据的拟合性能最好，但是基于工艺控制和优化的方便性，优选 Page 模型；热风温度对苦瓜片热风干燥综合性能的影响最显著，其次是热风速度和物料厚度，初始质量影响最小，热风温度、热风速度和物料厚度的置信度分别为 99.6%、98.1%和 96.5%。

INTRODUCTION

Bitter melon (*Momordica charantia* L.), also known as bitter gourd (named because of its special bitterness), is a member of the Cucurbitaceae family and mostly cultivated for its edible fruits as well as medicinal usages. Bitter melon originated in India and was introduced into China in the 14th century, and it is planted worldwide at present (*Horax et al., 2010*). In Chinese and Western cuisine, bitter melon is valued for its bitter flavour, and it is consumed by means of dishes, soups, dim sum, and herbal teas. The ingredients of bitter flavour are cucurbitane-type triterpenoids. Cucurbitane-type triterpenoids are primarily sub-divided into types of sapogenin and saponin which possess medicinal values to human beings, such as bacteriostasis and relief of diabetes (*Donya et al., 2007; Cui et al., 2015*). The nutrients of bitter melon mainly include amino acid, folic acid, carotenoid, vitamin A, vitamin C (Vc), magnesium, calcium and other microelements (*Xiang et al., 2000*). Vc is an important and essential nutrient and it is often taken as an index of nutrient quality of processes. Fresh bitter melon has Vc content of 56-120 (mg/100g), ranking the first in gourd vegetables (*Zhu et al., 2015*).

Bitter melon, as an economic crop, has been widely cultivated in Chongqing, China. The production of bitter melon is seasonal, and the fresh bitter melon is easy to become ripped and rotten after harvest. Timely dehydration or drying is crucial for bitter melon so as to guarantee the yearly supply and consumption. Dried bitter melon slice is usually consumed as dishes or bitter tea after rehydration. At present, several drying methods are available for drying of bitter melon slice, and some examples are solar/sun drying, hot-air drying, microwave drying, freeze drying, vacuum drying, infrared drying, and some of their combinations (*Santos and Silva, 2008*). Hot-air drying is the most commonly employed method to dry bitter melon slice, because of such advantages as good convenience in operation, low invest in equipment, and high efficiency

in process (*Yu et al., 2013*). But for hot-air drying, if inappropriate process parameters are adopted, quality of dried bitter melon slice may be degraded, especially resulting in loss of ingredients of bitter flavour and nutrients of bitter melon. Currently, the study of hot-air drying of bitter melon slice is mainly focused on drying characteristics, and mathematical models to fit its moisture ratio change (*Mudgal and Vishakha, 2009*). As to ingredients of bitter flavour and nutrients of bitter melon, few published studies were available for good reference.

This study aimed to investigate the effects of process parameters on hot-air drying characteristics of bitter melon slice, to compare applicability of different mathematical models to the drying process, and to evaluate effective moisture diffusivity (EMD), total colour difference, retention rate of Vc, and mass fraction of total saponins, etc., in order to provide a fundamental basis for drying process optimization and quality improvement of the final product.

MATERIALS AND METHODS

Materials

Sample preparation

Fresh bitter melon (*Momordica charantia* L.) of 70-80% maturity was bought from local market. It was washed with clean water and blotted with absorbing paper. The average initial moisture content was 95%w.b. (wet basis), namely 1900%d.b. (dry basis), as determined by direct drying method (Dryer DHG-9140A, Shanghai Jing Hong Laboratory Instrument Co., Ltd.), according to Chinese standard GB 5009.3-2016 “Determination of moisture in foods” (*China National standardizing committee, 2016a*) as follows: sliced fresh bitter melon (slice thickness 3mm) of 5-10g were dried at 105±1°C for 4h first; then, the bitter melon was weighed every 1h, sequentially; finally, the drying process was ended when neighbour mass change was less than 2mg. Other bitter melon was stored in a refrigerator at 4±1°C for the later use.

Thin-layer drying test-bench

Thin-layer drying test-bench (BC-2, Changchun Jida Science instrument Equipment Co., Ltd.) was adopted for hot-air drying of bitter melon slice. The test-bench consisted of cubic drying chamber, hot-air tunnel, heating unit, draft fan, airflow control set, sensors of air temperature and velocity, and control unit, etc. Air temperature and air velocity were adjustable, and their stable control ranges were 20-80°C and 0.1-1.5m/s, respectively. Detailed information of the test-bench can be found in the published literature (*Yang, 2014*).

Methods

Experimental arrangement

Orthogonal Factorial Experiment Design technique based on Taguchi methodology was adopted to arrange experiments (*Yang et al., 2017*). Main control factors affecting hot-air drying of bitter melon slice were defined as: factor A: air temperature; factor B: layer thickness; factor C: air velocity; factor D: initial mass. Levels of each control factor were defined, as shown in Table 1. Experimental arrangement was detailed in accordance with appropriate orthogonal array $L_9(3^4)$, a 3-level 4-factor array with 9 runs, as shown in Table 2, with EMD, total colour difference, retention rate of Vc, and mass fraction of total saponins of bitter melon as evaluation indexes.

Table 1

Levels of control factor

Level	Air temperature A	Layer thickness B	Air velocity C	Initial mass D
	[°C]	[mm]	[m/s]	[g]
1	45	3	0.6	30
2	55	6	0.9	40
3	65	9	1.2	50

The bitter melon slice of required thickness was prepared using a small-scale cutter. The slice thickness was adjustable. The samples of bitter melon slice were weighed every 5 min during the 1st hour of hot-air drying, every 10 min during the 2nd and 3rd hour, and every 30 min by the end of drying. The drying process was ended when neighbour mass change was less than 5mg for each drying experiment. All experiments were replicated three times. The mass of bitter melon slice was measured by a digital balance (AL204 electronic balance, Mettler Toledo) with accuracy of ±0.1mg.

Moisture ratio (MR) and drying rate (DR) were calculated by expressions as:

$$MR = \frac{M_t - M_e}{M_0 - M_e}, \text{ [dimensionless]} \quad (1)$$

where MR – moisture ratio, [dimensionless]; M_t – instantaneous moisture content, [%d.b.]; M_e – equilibrium moisture content, [%d.b.]; M_0 – initial moisture content, [%d.b.].

$$DR = \frac{M_{t+\Delta t} - M_t}{\Delta t}, \text{ [%d.b./min]} \quad (2)$$

where DR – drying rate, [%d.b./min]; t – time elapsed, [min].

Equilibrium moisture content could be determined only under conditions of constant temperature and air humidity. Due to low values of equilibrium moisture relative to M_0 or M_t and due to change of temperature and air humidity during drying, the moisture ratio neglecting equilibrium moisture content was expressed as $MR = M_t / M_0$.

EMD at each corresponding moisture ratio and time was calculated by the expression as (*Falade and Solademi, 2014*):

$$\ln MR = \ln \frac{8}{\pi^2} - \frac{\pi^2 D_{eff} t}{4L^2}, \text{ [dimensionless]} \quad (3)$$

where D_{eff} – effective moisture diffusivity, [m^2/s]; L – half of layer thickness, [m]; t – time elapsed, [s].

The average EMD was calculated from all positive EMD values by the expression as (*Singh and Gupta, 2006*):

$$D_{ave} = \frac{\sum_{i=1}^{n} D_{eff\_i}}{n}, \text{ [m}^2\text{/s]} \quad (4)$$

where D_{ave} – average EMD, [m^2/s]; D_{eff_i} –positive EMD, [m^2/s]; n – number of positive D_{eff_i} values of each experiment, [dimensionless].

Mathematical modelling of drying curve

Moisture ratio vs. drying time were fitted to five drying mathematical models of hot-air drying of bitter melon slice. The models for the fit were Page model, Modified Page model, Logarithmic model, Henderson and Pabis model, and Two term exponential model (*Xin et al., 2018; Doymaz, 2004*). Nonlinear regression equations were adopted for the fit by using software Origin 8.0. Coefficient of determination (R^2), reduced Chi-square (χ^2) and root mean square error (RMSE) were applied to evaluate appropriateness of the fit.

Method for quality analysis

Chromatic aberration. The colour of dried bitter melon slice was measured using a colorimeter with 8 replications (UltraScan PRO, USA). The chromatic aberration, defined by total colour difference (ΔE), was determined by the expression as (*Deng et al., 2017*):

$$\Delta E = \sqrt{\Delta L^2 + \Delta a^2 + \Delta b^2}, \text{ [dimensionless]} \quad (5)$$

where ΔE – total colour difference; ΔL – deviation value of black and white; Δa – deviation value of red and green; Δb – deviation value of yellow and blue. ΔL, Δa, Δb are dimensionless.

Retention rate of Vc. Vc content of bitter melon slice was measured by the 2, 6-dichloro-indophenol titration method, according to regulations described in Chinese standard GB 5009.86-2016 “Determination of ascorbic acid in foods” (*China National standardizing committee, 2016b*). Vc content and retention rate of Vc were calculated by expressions (*Zhu et al., 2015*):

$$X = \frac{VT}{m_0} \times 100, \text{ [mg/100g]} \quad (6)$$

where X – Vc content, [mg/100g]; V – dyestuff volume used in titration, [ml]; T – Vc content that can be oxidized by one millilitre of dyestuff, [mg/ml]; m_0 – mass of bitter melon sample used in the titration measurement, [g].

$$R_C = \frac{C_1}{C_0} \times 100, \text{ [\%]} \quad (7)$$

where R_C – retention rate of Vc, [%]; C_1 – Vc content of dried bitter melon slice, [mg/100g]; C_0 – Vc content of fresh bitter melon, [mg/100g].

Total saponins. To obtain total saponins of bitter melon slice, main steps were normally followed as: determination of wavelength for maximum absorption, establishment of regression equation of standard

momordicoside A, and measurement of total saponins of bitter melon slice. The momordicoside A was bought from Cheng Du Purechem-Standard Co., Ltd, China.

(1) Determination of wavelength for maximum absorption. Wavelength for maximum absorption of momordicoside was measured by spectrometric method (*Xu and Dong, 2005*), using UV-spectrometer (Shimadzu UV-2550, Japan). The wavelength for maximum absorption of momordicoside A was measured as 551nm. The UV-spectrometer pattern of Momordicoside A was plotted within wavelength 440-700nm, as shown in Fig. 1. The wavelength for maximum absorption of total saponins of bitter melon slice was tested and ranged from 549nm to 586nm, which demonstrated that the wavelength for maximum absorption of momordicoside A, namely 551nm, was acceptable for measurement of total saponins of bitter melon slice.

(2) Establishment of regression equation of Momordicoside A. In order to obtain total saponins of bitter melon slice, it was indispensable to establish an equation of absorption of the Momordicoside A with mass. Standard solutions of Momordicoside A of 40, 100, 160, 220 and 280μL were used for measurement of absorption, and their corresponding mass were 40, 100, 160, 220 and 280μg, respectively. Standard curve of Momordicoside A (namely curve of absorption vs. mass of Momordicoside A) was plotted, as shown in Fig. 2. The regression equation, with coefficient of determination 0.9975, was obtained as expressed:

$$A=0.0035m-0.099\text{ , [dimensionless]} \tag{8}$$

Where:

A – absorption, [dimensionless];

m – mass of Momordicoside A, [μg].

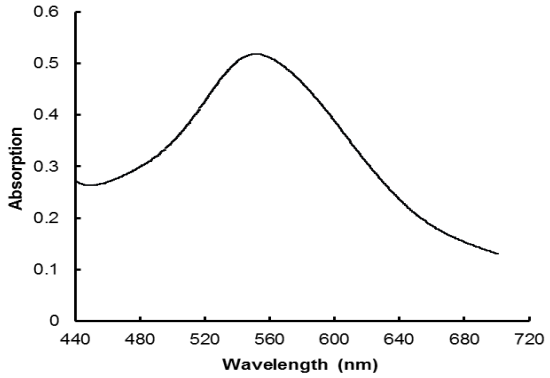

Fig. 1 - UV-spectrometer pattern of Momordicoside A

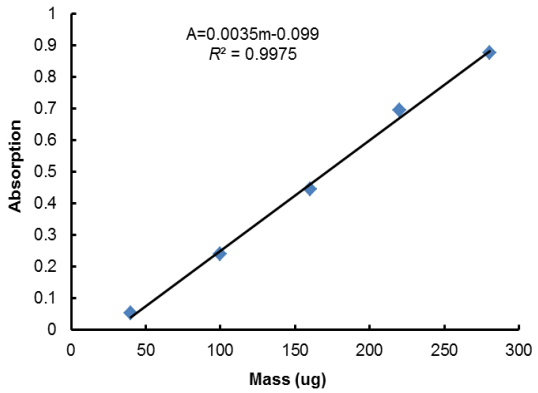

Fig. 2 - Standard curve of Momordicoside A

(3) Measurement of total saponins of bitter melon slice. The procedures for preparation of solution of bitter melon slice were outlined as follows: sample of dried bitter melon slice was powdered, and 1g of the powder, with precision of ±1mg, was placed in 500 ml round flask; 60% ethanol was used as solvent, and reflux extraction of 3 times was conducted at 60°C for 3h; the solution of extraction was fully evaporated, and the substance of extraction was dissolved into distilled water; by adding water saturated n-butanol into the resultant solution, total saponins were extracted 3 times by method of liquid-liquid extraction; the n-butanol solution of total saponins was obtained, and it was concentrated to dried saponins by reduced pressure concentration method; total saponins were dissolved with methanol, centrifuged with 3000rpm, and moved to 10mL volumetric flask; it was available to measure the absorption of total saponins of bitter melon slice (*Xu and Dong, 2005*). Then, mass fraction of total saponins of bitter melon slice was calculated by:

$$M_s=\frac{m}{m_0}\times 100\text{ , [%]} \tag{9}$$

where M_s – mass fraction of total saponins, [%]; *m* – mass of total saponins of bitter melon slice, [μg]; m_0 – mass of bitter melon powder, [μg].

RESULTS

Drying Characteristics

The moisture ratio vs. drying time and drying rate vs. moisture content were obtained, as shown in Figs. 3 and 4, respectively. The EMD values of bitter melon slice of different runs were listed in Table 2.

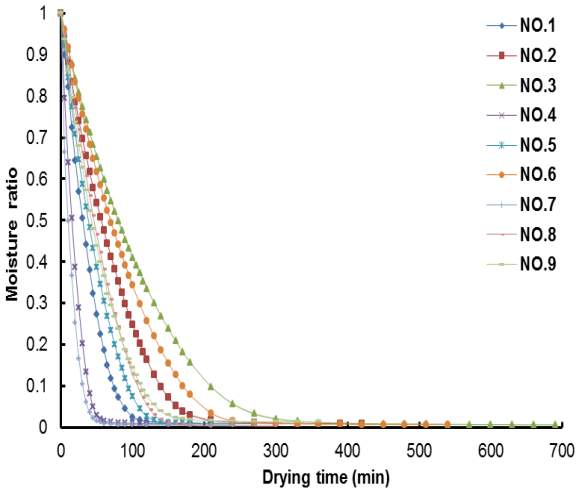

Fig. 3 - Moisture ratio vs. drying time

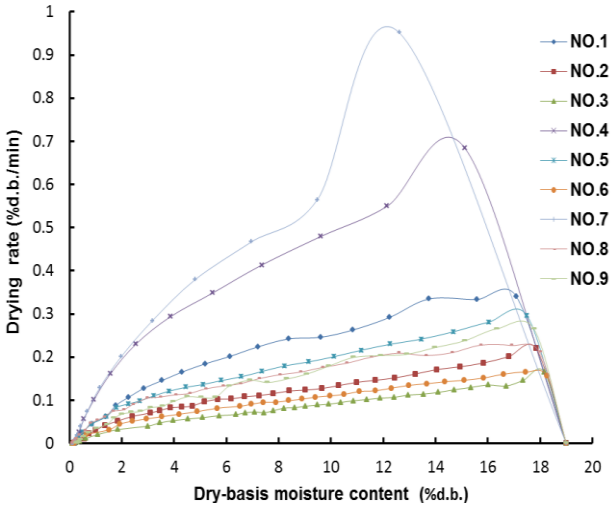

Fig. 4 - Drying rate vs. moisture content

Table 2

Experimental arrangement and results of experiment

No.	Factor A	Factor B	Factor C	Factor D	Effective moisture diffusivity	Total colour difference	Retention rate of Vc	Mass fraction of total saponins	Synthetic evaluation index
					[10^{-10}m^2/s]	*I*	[%]	[%]	*I*
1	1	1	1	1	3.55	26.31	35.69	2.28	0.3237
2	1	2	2	2	7.00	26.45	30.80	2.35	0.4103
3	1	3	3	3	10.14	26.72	29.99	2.43	0.5246
4	2	1	2	3	6.44	24.14	45.38	2.50	0.7961
5	2	2	3	1	11.58	25.46	28.69	2.55	0.7214
6	2	3	1	2	12.59	25.36	31.33	2.45	0.7138
7	3	1	3	2	8.43	24.99	35.52	2.18	0.4820
8	3	2	1	3	10.70	27.71	19.01	2.22	0.2248
9	3	3	2	1	11.91	26.49	27.90	2.32	0.4955

Moisture ratio of each run in the experiment decreased rapidly in the early stage of hot-air drying of bitter melon slice, it decreased with a gradually slower downward trend in the following stage and it approached to a relatively low value in the final stage, as shown in Fig. 3.

The drying rate of each run decreased with the decrease of moisture content, except for the early stage which had a lower drying rate. During the early stage of the hot-air drying, the heat was mainly used to heat samples of bitter melon slice to levels of air temperature, which resulted in the lower drying rate in this stage, as shown in Fig. 4. Moreover, no constant drying rate stage was observed during hot-air drying of bitter melon slice, and moisture removal was mainly processed during the falling rate drying stage; the time to heat the bitter melon slice in the early stage was short, which had small effect on the change of moisture ratio during the early stage.

The result of variance analysis of EMD was listed in Table 3. The control factor with the lowest sum of squares was treated as error column while computing *F*-ratio. According to variance analysis, layer thickness had the highest level of influence on the EMD during hot-air drying of bitter melon slice, and it was followed by air temperature, air velocity, and initial mass, sequentially; the *F*-ratio of each control factor was compared to a critical value corresponding to a certain pre-selected probability, resulting in probabilities, namely confidence levels, of 99.6%, 99.3%, and 95.9% that control factors were in fact due to chance because of layer thickness, air temperature, and air velocity, respectively. The mean EMD of all runs in Table 2 was 9.15×10^{-10}m^2/s.

Table 3

Variance analysis

Experiment indexes	Source of variance	Degree of freedom	Sum of squares	Mean sum of squares	*F*-ratio	Critical *F*-ratio
Effective moisture diffusivity	Factor A	2	22.857	11.429	131.396	$F_{0.007}(2,2)=131.396$
	Factor B	2	45.529	22.764	261.726	$F_{0.004}(2,2)=261.726$
	Factor C	2	4.024	2.012	23.132	$F_{0.041}(2,2)=23.132$
	Factor D	2	0.174	0.087	Error	/
	Total	8	72.584	/	/	/
Total colour difference	Factor A	2	4.257	2.128	7.165	$F_{0.122}(2,2)=7.165$
	Factor B	2	3.162	1.581	5.323	$F_{0.158}(2,2)=5.323$
	Factor C	2	1.124	0.562	1.892	$F_{0.346}(2,2)=1.892$
	Factor D	2	0.593	0.297	Error	/
	Total	8	9.136	/	/	/
Retention rate of Vc	Factor A	2	89.398	44.699	18.311	$F_{0.052}(2,2)=18.311$
	Factor B	2	257.209	128.605	52.685	$F_{0.019}(2,2)=52.685$
	Factor C	2	54.462	27.231	11.155	$F_{0.082}(2,2)=11.155$
	Factor D	2	4.882	2.441	Error	/
	Total	8	405.951	/	/	/
Mass Fraction of total saponins	Factor A	2	0.10196	0.05098	15.881	$F_{0.059}(2,2)=15.881$
	Factor B	2	0.00996	0.00498	1.551	$F_{0.392}(2,2)=1.551$
	Factor C	2	0.01029	0.00514	1.601	$F_{0.384}(2,2)=1.601$
	Factor D	2	0.00642	0.00321	Error	/
	Total	8	0.12863	/	/	/
Synthetic evaluation index	Factor A	2	2231.628	1115.814	252.161	$F_{0.004}(2,2)=252.161$
	Factor B	2	244.576	122.288	27.636	$F_{0.035}(2,2)=27.635$
	Factor C	2	456.420	228.210	51.573	$F_{0.019}(2,2)=51.573$
	Factor D	2	8.850	4.425	Error	/
	Total	8	2941.474	/	/	/

The experimental drying data of bitter melon slice moisture ratio of each run were fitted into the selected drying mathematical models, and the corresponding model parameters and evaluation indexes of appropriateness of the fit were shown in Table 4. The higher the R^2 values and the lower the χ^2 and *RMSE* values, the better the fit appropriateness *(Wang et al., 2007)*. As shown in Table 4, Page model and Modified Page model gave the best fit to experimental data of moisture ratio, with R^2 0.99782, χ^2 0.0002, and *RMSE* 0.01360, and they were followed by Two-term Exponential model, Logarithmic model, Henderson and Pabis model. Although Page and Modified Page model had the same R^2, χ^2, and *RMSE*, in view of simplicity of mathematical model, convenience of process control and optimization, Page model was preferred for hot-air drying of bitter melon slice.

Overall Evaluation of Drying Process

Total colour difference, retention rate of Vc, mass fraction of total saponins, and their synthetic evaluation index were employed as indexes to evaluate the quality of dried bitter melon slice. The results of evaluation indexes were shown in Table 2, and their variance analysis were shown in Table 3.

Total colour difference

Air temperature had the highest level of influence on total colour difference during hot-air drying of bitter melon slice, and it was followed by layer thickness, air velocity, and initial mass sequentially; the confidence levels of air temperature, layer thickness and air velocity were 87.8%, 84.2%, and 65.4%, respectively. The mean total colour difference of all runs in Table 2 was 25.96.

The colour of bitter melon was largely showed as green, which was mainly influenced by chlorophyll. Chlorophyll easily oxidized and decomposed by heating, and the higher the temperature, the faster the oxidization and decomposition. While at the same temperature, the degree of oxidization and decomposition of chlorophyll became severe with the increase of layer thickness or the decrease of air velocity. Therefore, air temperature and layer thickness had some high significant levels of influence on the total colour difference of bitter melon slice. Moreover, with increase of temperature, enzymatic browning and non-enzymatic browning intensified during the drying process, which made colour of bitter melon slice changed from green to yellowish brown. The visual observation of dried bitter melon slice under different drying conditions was shown in Fig. 5.

Retention rate of Vc

Layer thickness had the highest level of influence on retention rate of Vc during hot-air drying of bitter melon slice, and it was followed by air temperature, air velocity, and initial mass sequentially; the confidence levels of layer thickness, air temperature and air velocity were 98.1%, 94.8%, and 91.8%, respectively. The mean retention rate of Vc of all runs in Table 2 was 31.59%.

Statistical analysis of mathematical models **Table 4**

Model	Parameter									Mean value
	Run 1	Run 2	Run 3	Run 4	Run 5	Run 6	Run 7	Run 8	Run 9	
1 Page: $MR=\exp(-kt^n)$										
k	0.01012	0.00605	0.00521	0.02667	0.00809	0.00433	0.07019	0.00421	0.00849	/
n	1.24894	1.18601	1.12269	1.21018	1.23016	1.20487	1.00988	1.33875	1.17770	/
R^2	0.99819	0.99717	0.99859	0.99758	0.99738	0.99836	0.99719	0.99738	0.99851	0.99782
χ^2	0.000179	0.000267	0.000144	0.000200	0.000249	0.000173	0.000194	0.000261	0.000134	0.000200
RMSE	0.01284	0.01593	0.01174	0.01350	0.01530	0.01282	0.01328	0.01571	0.01127	0.01360
2 Modified Page: $MR=\exp[-(kt)^n]$										
k	0.02529	0.01348	0.00925	0.05004	0.01993	0.01092	0.07200	0.01681	0.01743	/
n	1.24894	1.18601	1.12268	1.21018	1.23016	1.20486	1.01184	1.33876	1.17770	/
R^2	0.99819	0.99717	0.99859	0.99758	0.99738	0.99836	0.99719	0.99738	0.99851	0.99782
χ^2	0.000179	0.000267	0.000144	0.000200	0.000249	0.000173	0.000194	0.000261	0.000134	0.000200
RMSE	0.01284	0.01593	0.01173	0.01350	0.01530	0.01282	0.01328	0.01571	0.01127	0.01360
3 Logarithmic: $MR=a\exp(-kt)+c$										
a	1.07771	1.05930	1.03639	1.04213	1.0806	1.06664	0.99484	1.12721	1.06074	/
k	0.02549	0.01341	0.00913	0.01257	0.01955	0.01086	0.07164	0.01637	0.01771	/
c	-0.03015	-0.02502	-0.01519	-0.00758	-0.03969	-0.02413	-0.00086	-0.06181	-0.02026	/
R^2	0.99152	0.99317	0.99693	0.99200	0.99284	0.99436	0.99705	0.98942	0.99481	0.99357
χ^2	0.000836	0.000644	0.000313	0.000661	0.000682	0.000594	0.000203	0.001060	0.000467	0.000607
RMSE	0.02713	0.02441	0.01714	0.02397	0.02486	0.02347	0.01325	0.03112	0.02072	0.02290
4 Henderson and Pabis: $MR=a\exp(-kt)$										
a	1.05716	1.04222	1.02592	1.03715	1.05559	1.04982	0.99432	1.08651	1.04821	/
k	0.02740	0.01422	0.00946	0.05368	0.02158	0.01147	0.07184	0.01890	0.01864	/
R^2	0.98980	0.99196	0.99644	0.99203	0.98976	0.99328	0.99719	0.98331	0.99395	0.99197
χ^2	0.00101	0.000758	0.000364	0.000658	0.000975	0.000709	0.000194	0.001670	0.000544	0.000765
RMSE	0.03042	0.02683	0.01866	0.02451	0.03023	0.02597	0.01326	0.03968	0.02269	0.02581
5 Two-term exponential: $MR=a\exp(-kt)+(1-a)\exp(-kat)$										
a	1.78403	1.70686	1.62603	1.73317	1.75879	1.73545	1.35196	1.86710	1.70306	/
k	0.03616	0.01837	0.01199	0.06948	0.02807	0. 1513	0.07928	0.02531	0.02370	/
R^2	0.99787	0.99730	0.99887	0.99744	0.99709	0.99835	0.99734	0.99591	0.99855	0.99764
χ^2	0.000210	0.000255	0.000116	0.000211	0.000277	0.000174	0.000183	0.000408	0.000131	0.000218
RMSE	0.01389	0.01556	0.01053	0.01388	0.01612	0.01286	0.01290	0.01964	0.01111	0.01405

Notes: k, n, a and c are model constants.

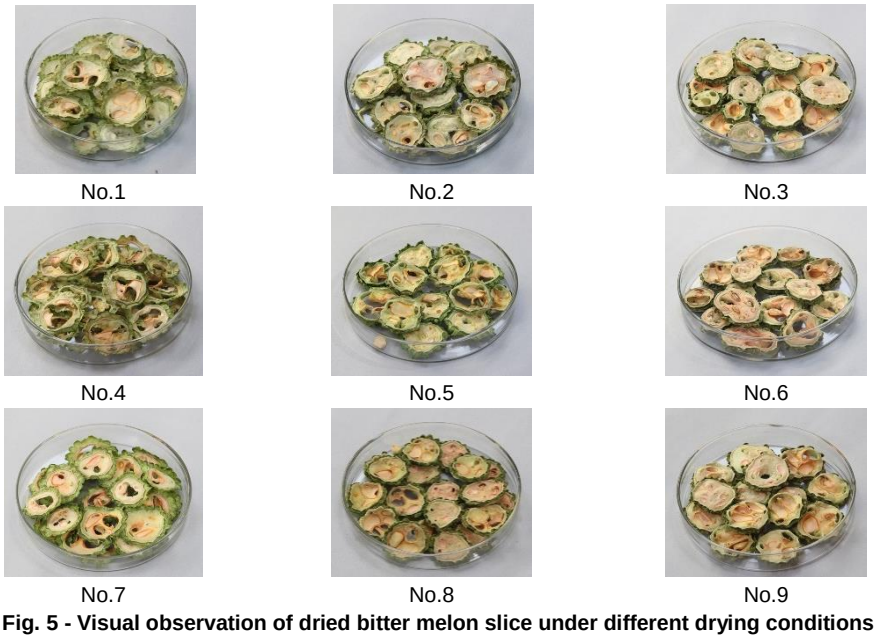

Fig. 5 - Visual observation of dried bitter melon slice under different drying conditions

Vitamin C was a thermal sensitive substance, and it easy oxidized and decomposed by heating, which showed a similar trend as the change of total colour difference. The higher the temperature, the faster the oxidization and decomposition of Vc. While at the same temperature, the degree of oxidization and decomposition of Vc also became severe with increase of layer thickness or decrease of air velocity. Under the dual influence of temperature and air velocity, retention rate of Vc first increased and then decreased.

Mass fraction of total saponins

Air temperature had the highest level of influence on mass fraction of total saponins during hot-air drying of bitter melon slice, and it was followed by air velocity, layer thickness, and initial mass sequentially; the confidence levels of air temperature, air velocity and layer thickness were 94.1%, 61.6%, and 60.8%, respectively. The mean mass fraction of total saponins of all runs in Table 2 was 2.36%. There was a trend that mass fraction of total saponins first increased and then decreased as well, with the increase of air temperature.

Synthetic evaluation

To obtain the overall influence of control factors on hot-air drying of bitter melon slice, it was necessary to give weights to different factors. Normalization was applied to all evaluation indexes since these indexes had different units. The equation of normalization was expressed as (*Li et al., 2007*):

$$q' = \frac{q - q_{\min}}{q_{\max} - q_{\min}}, \text{ [dimensionless]} \quad (10)$$

where q' – the characteristic parameters after normalization, [dimensionless]; q – characteristic parameters before normalization, [dimensionless]; $q_{\max}$ – the maximum value in the corresponding parameters, $q_{\max}=\max(q)$, [dimensionless]; $q_{\min}$ – the minimum value in the corresponding parameters, $q_{\min}=\min(q)$, [dimensionless].

Same weight of 0.25 was given to each evaluation index, and synthetic evaluation index was expressed as:

$$E_s = 0.25D_e' + 0.25(1 - C_r') + 0.25R_c' + 0.25M_s', \text{ [dimensionless]} \quad (11)$$

where E_s – synthetic evaluation index, [dimensionless]; D_e', C_r', R_c', and M_s' – normalized values of EMD, total colour difference, retention rate of Vc, and mass fraction of total saponins, respectively, [dimensionless].

According to variance analysis, air temperature had the highest level of influence on synthetic evaluation index during hot-air drying of bitter melon slice, and it was followed by air velocity, layer thickness, and initial mass sequentially; the confidence levels of air temperature, air velocity and layer thickness were 99.6%, 98.1%, and 96.5%, respectively. The mean synthetic evaluation index of all runs in Table 2 was 0.5214.

Range analysis was applied to synthetic evaluation indexes of all runs and analysis results were shown in Table 5. The values in cells of each level of control factors in Table 5 represent synthetic evaluation index of the corresponding levels and factors. The delta values of each factor represent the biggest change of synthetic evaluation index of the factor, namely the impact level of each factor. The numbers in the rank row indicate the impact significance sequence of control factors. According to range analysis, there were same sequences of influence significance on synthetic evaluation index as variance analysis; the optimal combination for the highest synthetic evaluation index was A2B3C3D2 which showed a value of synthetic evaluation index 0.7490, according to optimal engineering average strategy (*Wang, 2004*). But it was less than the maximum value 0.7961 of synthetic evaluation index of run 4, namely A2B1C2D3, with a relative difference 5.92% which might result from experimental errors during the multi-factor multi-index drying process.

Table 5

Range analysis of synthetic evaluation index

Level	Factor A	Factor B	Factor C	Factor D
1	0.4195	0.5339	0.4208	0.5135
2	0.7438	0.4521	0.5673	0.5353
3	0.4007	0.5780	0.5760	0.5152
Delta	0.3430	0.1258	0.1552	0.0218
Rank	1	3	2	4

CONCLUSIONS

In this study, effects of process parameters on hot-air drying characteristics of bitter melon slice were investigated, applicability of different mathematical models to the drying process was compared, and overall evaluation was conducted by using synthetic evaluation index. Main conclusions were drawn as follows:

- Moisture ratio of bitter melon slice decreased rapidly in the early stage of hot-air drying of bitter melon slice. Drying rate decreased with decrease of moisture content. No constant drying rate stage was observed during the drying process, and moisture removal was mainly processed during falling rate drying stage.
- Page model and Modified Page model gave the best fit to experimental data of moisture ratio, with coefficient of determination 0.99782, reduced Chi-square 0.0002 and root mean square error 0.01360. For convenience of process control and optimization, Page model was preferred for hot-air drying of bitter melon slice.
- Air temperature had the highest level of influence on synthetic evaluation index during hot-air drying of bitter melon slice, and it was followed by air velocity, layer thickness, and initial mass sequentially; the confidence levels of air temperature, air velocity and layer thickness were 99.6%, 98.1%, and 96.5%, respectively. The optimal combination for hot-air drying of bitter melon slice was obtained, with synthetic evaluation index 0.7490.

ACKNOWLEDGEMENTS

The study was funded by the National Natural Science Foundation of China (No. 31301575), and Fundamental Research Funds for the Central Universities of China (No. SWU115011).

REFERENCES

[1] Cui J.J., Li B., Cheng J.W., and Hu K.L., (2015), Progress on bitter principles and its biosynthesis in bitter gourd (*苦瓜苦味物质及其生物合成研究进展*), *Acta Horticulturae Sinica*, vol. 42, issue 9, pp. 1707-1718, Ed. Chinese Society for Horticultural Science, Beijing / P.R.C.;

[2] Deng Y.Y., Tang Q., Zhang R.F., Zhang Y., Liu L., Wei Z.C., Ma Y.X. and Zhang M.W., (2017), Effects of different drying methods on the nutrition and physical properties of *Momordica charantia* (*不同干燥方式对苦瓜营养与品质特性的影响*), *Scientia Agricultura Sinica*, vol. 50, issue 2, pp. 362-371, Ed. Chinese Academy of Agricultural Sciences, Beijing / P.R.C.;

[3] Donya A., Hettiarachchy N., Liyanage R., Lay J., Chen P.Y. and Jalaluddin M., (2007), Effects of processing methods on the proximate composition and momordicosides K and L content of bitter melon vegetable, *Journal of Agricultural and Food Chemistry*, vol. 55, issue 14, pp. 5827-5833, Ed. American Chemical Society, Washington, D.C./U.S.A.;

[4] Doymaz I., (2004), Effect of dipping treatment on air drying of plums. *Journal of Food Engineering,* vol. 64, issue 4, pp. 465-470, Ed. Elsevier Sci Ltd, Oxford/England;

[5] Falade K.O., Solademi O.J., (2010), Modelling of air drying of fresh and blanched sweet potato slices, *International Journal of Food Science and Technology*, vol. 45, issue 2, pp. 278-288, Ed.Wiley Blackwell Publishing, Inc., Malden/U.S.A.;

[6] Horax R., Hettiarachchy N., Kannan A. and Chen P.Y., (2010), Proximate composition and amino acid and mineral contents of *Mormordica charantia* L. pericarp and seeds at different maturity stages, *Food Chemistry*, vol. 122, issue 4, pp. 1111-1115, Ed. Elsevier Sci Ltd, Oxford/England;

[7] Li X.W., Yang M.J., Xie S.Y. and Yang S.Z., (2007), Wear condition monitoring of helical cutters based on neural network information infusion method (*基于神经网络信息融合的铣刀磨损状态监测*), *Transactions of the Chinese Society for Agricultural Machinery*, vol. 38, issue 7, pp. 160-163, Ed. Chinese Society for Agricultural Machinery, Beijing/ P.P.C.;

[8] Mudgal V.D., Vishakha K.P., (2009), Thin-layer drying kinetics of bitter gourd (*Momordica charantia* L.). *Journal of Food Science and Technology - Mysore*, vol. 46, issue 3, pp. 236-239, Ed. Association of Food Scientists and Technologists of India, Mysore/India;

[9] Santos P.H.S., Silva M.A., (2008), Retention of Vitamin C in drying processes of fruits and vegetables-a review, *Drying Technology*, vol. 26, issue 12, pp. 1421-1437, Ed. Taylor & Francis Inc, Philadelphia/U.S.A.;

[10] Singh B., Gupta A.K., (2006), Mass transfer kinetics and determination of effective diffusivity during convective dehydration of pre-osmosed carrot cubes, *Journal of Food Engineering*, vol. 79, issue 2, pp. 459-470, Ed. Elsevier Sci Ltd, Oxford/England;

[11] Wang W.Z., (2004), Design of experiments and analysis (*试验设计与分析*), Higher Education Press, Beijing / P.R.China;

[12] Wang Z.F., Sun J.H., Liao X.J., Chen F., Zhao G.H., Xu J.H. and Hu X.S., (2007), Mathematical modelling on hot air drying of thin layer apple pomace, *Food Research International*, vol. 40, pp. 39-46, Ed. Elsevier Science Bv, Amsterdam/Netherlands;

[13] Xiang C.P., Wu C.Y. and Wang L.P., (2000), Analysis and utilization of nutrient composition in bitter gourd (*苦瓜营养成分分析及利用评价*), *Journal of Huazhong Agricultural University*, vol. 19, issue 4, pp. 388-390, Ed. Huazhong Agricultural University, Wuhan/P.R.China;

[14] Xin Y.N., Zhang J.W. and Li B, (2018). Drying kinetics of tobacco strips at different air temperatures and relative humidities, *Journal of Thermal Analysis & Calorimetry*, vol. 132, issue 2, pp. 1347-1358, Ed. Springer, Dordrecht/Netherlands;

[15] Xu B., Dong Y., (2005), Determination on total saponins of *Momordica charantia* L. by spectrophotometry (*分光光度法测定苦瓜总皂甙含量*), *Food Science*, vol. 26, issue 10, pp. 165-169, Ed. Beijing Academy of Food Science, Beijing/P.R.China;

[16] Yang L., (2014), *Heat & Mass transfer characteristics and model of hot-air drying for seed of rape* (*Brassica napus* L.) (*甘蓝型油菜籽热风干燥传热传质特性及模型研究*), PhD dissertation, Southwest University, Chongqing / P.P.China;

[17] Yang M.J., Liu B., Yang Z.R., Ding Z.Y., Yang L., Xie S.Y. and Chen X.B., (2017), Development and experimental study of infrared belt dryer for rapeseed, *INMATEH - Agricultural Engineering*, vol. 53, issue 3, pp. 71-80, Ed. INMA, Bucharest/Romania;

[18] Yu M.J., Zhang X.J., Mu G.L., Yan J.S., Zhang H. and Shi Z.L., (2013), Research progress on the application of hot air-drying technology in China (*我国热风干燥技术的应用研究进展*), *Agricultural Science & Technology and Equipment*, issue 8, pp. 14-16, Ed. Liaoning Provincial Institute of Agricultural Mechanization, Shenyang/ P.R.China;

[19] Zhu X.Y., Zhang J., He Y.Y. and Deng F.M., (2015), Effects of hot air and far-infrared drying temperatures on quality of bitter gourd (*Momordica charantia* L.) powder (*热风与远红外干燥温度对苦瓜全粉品质的影响*), *Modern Food Science and Technology*, vol. 31, issue 7, pp. 265-269, 325, Ed. South China University of Technology, Guangzhou/P.R.China;

[20] *** China National standardizing committee, (2016a), *Determination of moisture in foods, GB 5009.3-2016* (*食品安全国家标准食品中水分的测定, GB 5009.3-2016*), Chinese Standard Press, Beijing / P.R.China;

[21] *** China National standardizing committee, (2016b), *Determination of ascorbic acid in foods, GB 5009.86-2016* (*食品安全国家标准食品中抗坏血酸的测定, GB 5009.86-2016*), Chinese Standard Press, Beijing / P.R.China.

ONION BULBS ORIENTATION DURING ALIGNED PLANTING OF SEED-ONION USING VIBRATION-PNEUMATIC PLANTING DEVICE

/

ОРИЕНТИРОВАНИЕ ЛУКОВИЦ ПРИ ПОСАДКЕ ВИБРАЦИОННО-ПНЕВМАТИЧЕСКИМ ВЫСАЖИВАЮЩИМ АППАРАТОМ ДЛЯ ПОСАДКИ ЛУКОВИЦ ЛУКА-СЕВКА

PhD. Eng.Sc., Aksenov A.G., Prof. PhD. Eng.Sc. Izmaylov A.Iu., Prof. PhD. Eng.Sc., Dorokhov. A.S., PhD. Eng.Sc., Sibirev A.V.

FSBSI "Federal Scientific Agronomic and Engineering Centre VIM"/ Russian

Telephone: 89645843518; E-mail: sibirev2011@yandex.ru

Keywords: *planting device, vibration-pneumatic, forward velocity, machine height*

ABSTRACT

The existing seed-onion planting machines provide that the sowing machines select bulbs from the total mass by group rather than by piece. As a result, the bulbs are not planted with their stems down and at a preset spacing. Therefore, new solutions are needed to maintain bulb stems downward position in the furrow. The article discusses various designs of planting devices for planting machines and highlights their main advantages and disadvantages. It also provides an overview of an engineering sample design of the planting machine equipped with vibration-pneumatic planting device for oriented seed-onion planting in the furrow.

РЕЗЮМЕ

Существующие машины для посадки лука-севка обеспечивают групповой отбор луковиц из общей массы высевающими аппаратами, а не поштучный, вследствие чего не обеспечивается посадка луковиц донцем вниз и заданный шаг посадки. Следовательно, необходим поиск новых решений по сохранению положения луковиц в борозде донцем вниз. В статье проведен анализ конструкций высаживающих аппаратов посадочных машин, выявлены их основные достоинства и недостатки. Представлена конструкция опытного образца посадочной машины, оснащенная вибрационно-пневматическим высаживающим аппаратом для ориентированной посадки лука-севка в борозду.

INTRODUCTION

Meeting optimal deadlines and applicable recommendations when planting seed-onion is essential for yield enhancement. In central and northern parts of Russia, onion-turnip is grown mostly from seed-onion (*Aksenov A.G., Sibirev A.V., Emelianov P.A., 2016*).

Lack of equipment for mechanical bulbs planting that could meet the agronomic and engineering requirements (uniformity of bulbs distribution in the furrow, orienting and embedding them into the soil with their stems down), serve as a deterrent for increasing commercial production of onion-turnip from seed-onion *(Aksenov A.G., Sibirev A.V., Emelianov P.A., 2018)*.

When analyzing the designs of existing planting machines as well as patent and technical literature as described herein below, we managed to reveal the disadvantages of sowing and planting machines for bulbs planting which hinder quality process of seed-onion planting (*Aksenov A.G., Sibirev A.V., Emelianov P.A., 2016*). In a disk sowing machine *(Nilesh N. Jadhav, Harshal R. Aher, Amol P. Ghode, 2015)* with a horizontal axis of rotation (Fig. 1), the sowing disks are mounted on the rotary shaft to form cells for gripping seed-onion bulbs. The seed-box sides have cuts for mounting the sowing shaft.

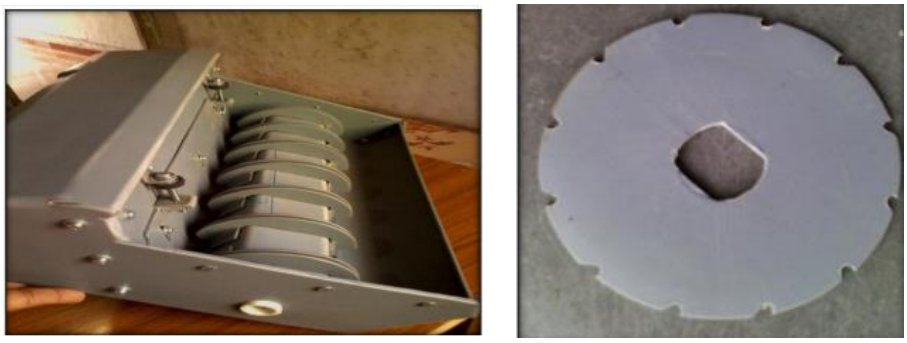

a) *b)*

Fig. 1 – Disk sowing machine

a) – general view of the sowing device; b) – sowing disk

Technological process of seed-onion planting with the disk sowing machine equipped with the horizontal axis of rotation is as follows:

The bulbs are taken from the seed-box and fed into the space formed by the sowing disks and the sowing machine body. When rotating, the sowing disks carry and turn the bulbs, their growing points upward, along the sowing machine drum rotation. Further rotation of the disk sowing machine makes the bulbs fall from the cells due to its rotation clockwise and turn them growing points upward.

Disadvantages of the sowing machine design include incapability to fix the bulb which can make the bulb loose its preset oriented position.

Another type of disk sowing machines is a sowing machine with peripheral cells on the seed disk *(Amol B. Rohokale, Pavan D. Shewale, Sumit B. Pokharkar, Keshav K. Sanap, 2014).*

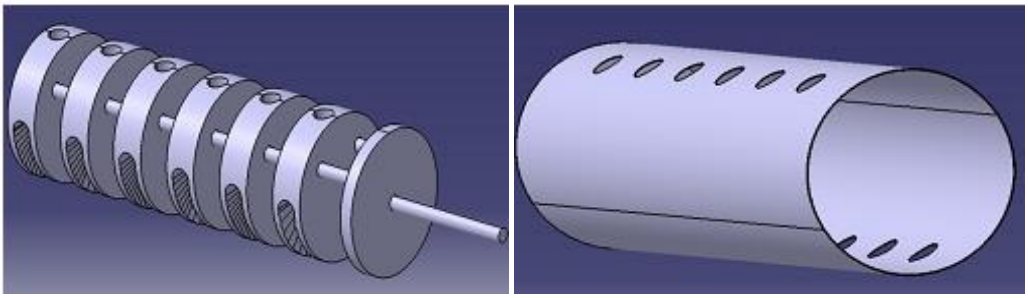

a) *b)*

Fig. 2 – Scheme of disk sowing machine with peripheral cells

a) – general view of sowing discs; b) – cylindrical body

The sowing disc rotates inside the cylindrical body which has sowing holes to ensure that the seeds are sowed smoothly.

A disadvantage of this sowing machine involves higher damage of the seeds being sowed, since they fall in between the sowing disk and the cylindrical body.

There also exists a disk seeder (Fig.3), wherein operating components involve the blades diametrically located on the planting disk *(Thorat Swapnil V, Madhu L. Kasturi, Patil Girish V, Patil Rajkumarn, 2017)* mounted at the bottom of the seed-box on the shaft.

Fig. 3 – Disk seeder with diametrically located blades

MATERIALS AND METHODS

The existing planting machines ensure uniformity of bulbs distribution at the level of 60%, the number of bulbs oriented in stems down position at the level of 15-20 %, and those in stems upward position – about 10-15 %, which does not comply with the agronomic and technical requirements for bulb planting and entails reduction in yields.

We conducted several studies to check how seed-onion bulbs orientation affected the onion-turnip yields in Penza Oblast in 2014-2015.

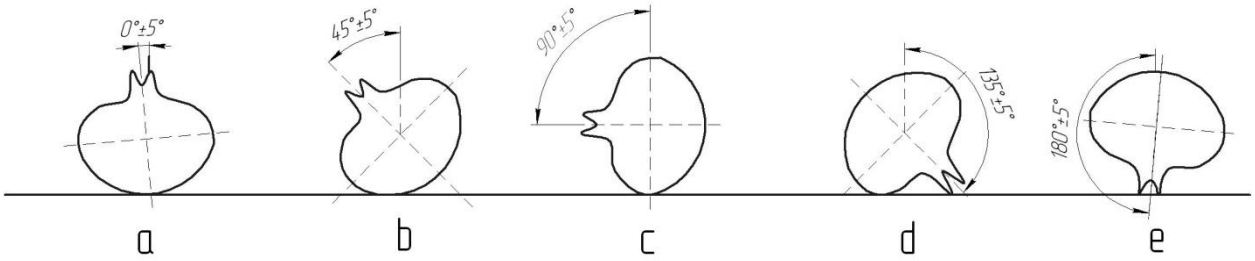

Fig. 4 – The position of the bulb on the reference plane

Seed-onion of nine varieties with different shape indices (*Bessonovskii Local, Odintsovets, Zolotnichok, Bordkovskii, Maiachkovskii 300, Danilovskii 301, Shtuttgarten Rizen, Centurion, Yubiliar*) was sized by 10-15 mm in diameter and planted in the trial field. Seed-onion was preceded by cabbage, soil acidity equalled to pH 5.6–6.7. The agronomic technology used is very common for Penza Oblast.

Planting system: 33+33 single row by 100 pieces in three replications. During the vegetation period, some phenological observations and biometric measurements were performed. The following seed-onion planting options were used:

- bulbs planted in the strictly upright position (control);
- bulbs planted with 45° deviation from upright position;
- bulbs planted with 90° deviation from upright position;
- bulbs planted with 135° deviation from upright position;
- bulbs planted with 180° deviation from upright position;

Research results are provided in Fig. 5.

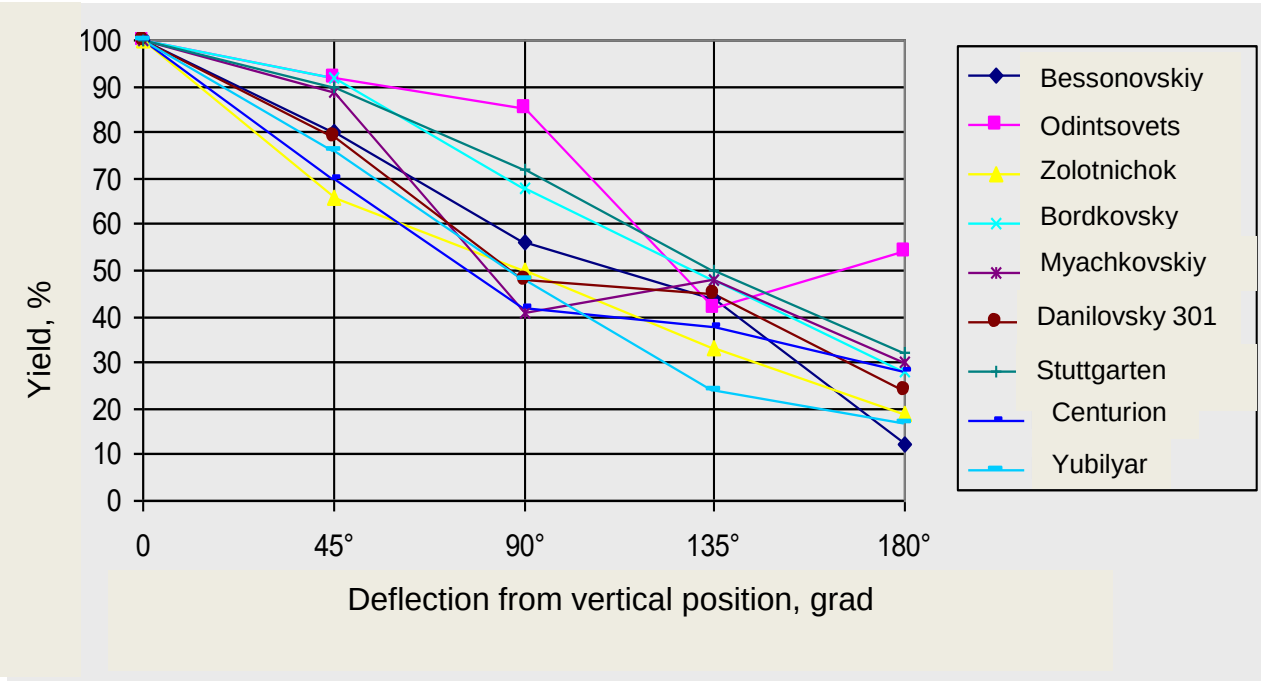

Fig. 5 – Influence of the bulbs position when planting on the yield of onion-turnip

Analysis of Fig. 5 proves that the increase in the angle of inclination leads to reduction in onion-turnip yield.

On the average, by the varieties it was established that planting of bulbs at different angles leads to the following reduction in onion-turnip yield: 45°–19%, 90°–44%, 135°–59%, and 180°–73%.

Such reduction in yield was caused by later and more thinned bulb shoots that deviate from upright position and as a consequence, lag behind the bulbs positioned with their stem-plates downward during vegetation.

Fig. 6 – Shoots of seed-onion planted at different angles:

1 – at the angle of 0°; 2 – at the angle of 45º; 3 – at the angle of 90º; 4 – at the angle of 135º; 5 – at the angle of 180º

In order to conduct research and develop the planting device for onion planting machines that would comply with the agricultural and technological requirements for bulbs position in the furrow, we analyzed the existing planting machines as well as patent and technical literature and obtained the following results:

- seed-onion is planted mostly with the use of sowing machines equipped with the mechanical sowing device. Their main advantages include simple design and high performance but these sowing devices do not ensure compliance with the agricultural and technical requirements related to the uniformity of bulbs distribution along the furrow and stem-plate downward orientation;

- the existing machines for seed-onion planting have the following major disadvantages: the sowing devices select bulbs from the total mass by group rather than by piece which does not ensure that the bulbs are planted with their stems down and at a preset spacing. In addition, the height of the sowing machines above the soil level does not provide for the required uniformity of bulbs distribution and stem-down orientation thereof.

Thus, in order to increase the quality of seed-onion planting with the use of planting machines, which ensure stem down orientation of the bulbs and uniform distribution thereof along the furrow, we need (i) to develop and justify the design and technological scheme as well as design of the planting machine for oriented seed-onion planting, (ii) to perform theoretical study concerning the operating process and obtain analytic dependences for determining its basic design and operating parameters, (iii) to manufacture a pilot model for the planting machine equipped with the device for oriented seed-onion planting, and (iv) to perform laboratory tests and field trials for the planting machine to determine its efficiency and profitability. The “oriented bulb planting” means that the bulbs are embedded into soil in the defined position but not at random. When planting with a planting machine, design and operation of the sowing device or installation of the orienter ensure that the bulbs position is changed from random to the defined one. To ensure oriented bulbs planting, we have suggested the scheme of the vibration-pneumatic seeder design the novelty of which is proved by the RF patent No. 2407271 *(Patent No. 2407271. Russia, IPC A01 C11/02. Vibration-Pneumatic Seeder for Seed-Onion Oriented Planting / P.A. Emelianov, A.G. Aksenov).*

A vibration-pneumatic seeder (Fig. 7) consists of a bunker *1*, a vibration trough *2*, a pneumatic drum *3* and an eccentric *4 (Patent No. 2407271. Russia, IPC A01 C11/02. Vibration-Pneumatic Seeder for Seed-Onion Oriented Planting / P.A. Emelianov, A.G. Aksenov).* The vibration trough *2* is fixed to the bunker bottom while the upper end of the vibration trough is mounted under the unloading window of the bunker *1*

and the lower one - above the groove of the pneumatic drum *3*. The vibration trough *2* is intended for single-piece bulbs feeding to the pneumatic drum *3* with their growing points facing downward. The trough's cross-section is shaped as a semicircle with the diameter exceeding the maximum bulb diameter. At one end of the trough, there is a slot that is wider than a growing point diameter and its length equals two bulb diameters. The other end of the trough is connected with the eccentric mechanism by a connecting rod. The trough is inclined to the horizon at the angle less than the friction angle of bulbs sliding along the trough material. The pneumatic drum groove shall be of such size that all the bulbs could be freely laid down therein and sticking to it without losing orientation. Taking into account the above, the groove shape taken as appropriate for a side surface of a bulb, is a semicircle. The diameter of pneumatic drum suction hole is 6 mm (d_{hole} = 6 mm).

The clearance between the trough and the drum groove bottom must be set of such a size that a bulb could not move along the groove in the direction opposite to the drum rotation and the trough could not touch the groove bottom during operation. So, the distance (clearance) must be less than the bulb diameter but should exceed the trough oscillation amplitude.

Air-stream velocity in the suction hole must be equal to the bulb hovering velocity, which is 15–31 m/s, in order to ensure that the bulbs are sucking to the suction holes with their growing points.

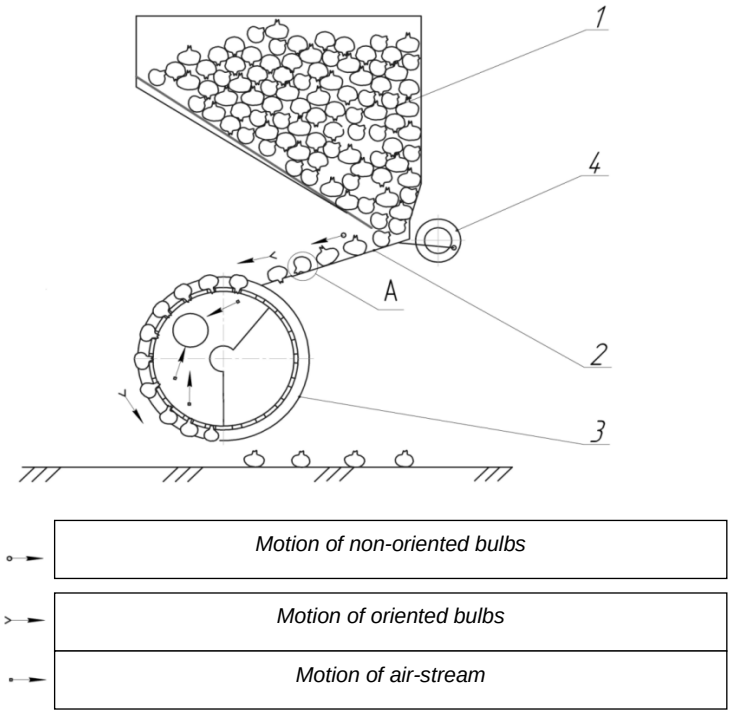

Fig. 7 – Scheme of the vibration-pneumatic seeder

1 – bunker; 2 – vibration trough; 3 – pneumatic drum; 4 – eccentric

To achieve these objectives, the experimental researches program included laboratory tests and field trials of the engineering sample of the planting machine equipped with the vibration-pneumatic seeder. The laboratory and field testing is aimed at setting the optimal operation mode and determining the quantitative performance indicators for the suggested engineering sample equipped with the vibration-pneumatic seeder for oriented seed-onion planting in the field conditions. To carry out the laboratory and field trials, Agroinzheneriia, LLC (the city of Penza) developed and manufactured a planting machine equipped with the vibration-pneumatic planting device (Fig. 8).

It consists of a frame *1*, support wheel *2*, bunker *3*, fan *5*, three vacuum lines *6* and three planting sections *4*. Each section includes a vibration-pneumatic planting device, a colter, a covering wheel and a guidance mechanism (the mechanism that makes the colters copy the field microrelief). The planting device is driven by the support wheel through the chain *7*, and the fan is driven by tractor PTO shaft through the prop shaft *8*. Conditions of carrying out the laboratory tests and field trials (plot and culture characteristics) have been studied on record land plots 50 m long and 1.4 m wide uniformly distributed along the field diagonal. The number of plots equals five.

A smooth, homogeneous, earlier prepared plot was chosen for planting, where on the days of testing, soil humidity and hardness were determined at the depth of 0–0.01; 0.01–0.02; 0.02–0.03 m on three spots *(Thorat Swapnil V, Madhu L. Kasturi, Patil Girish V, Patil Rajkumarn, 2017).*

Fig. 8 – General view of the planting machine equipped with vibration-pneumatic planting device
1 – frame; 2 – support wheel; 3 – bunker; 4 – planting section; 5 – the fan; 6 – vacuum line; 7 – a chain; 8 – prop shaft

The field microrelief is smooth, the slope does not exceed 3˚, furrow length equals 150 m, the field outline is close to the regular rectangular shape. When determining the planting quality, the following indicators were taken into account: the number of bulbs positioned with their stem-plates downward; uniformity of bulbs distribution along the furrow; percentage of damaged bulbs. When studying the engineering sample of the planting machine equipped with the vibration-pneumatic planting device, its forward velocity was changed from 0.8 to 1.2 m/s. The rotation frequency and the planting device height above ground (furrow) surface were constant and equalled 0.47 s^{-1} and 0.12 m, respectively. Actual (operation) aggregate motion velocity V_M was determined from the record plot length (50 m) taking into account the passing time according to the formula *(Thorat Swapnil V. et al., 2017; ***Vehicle Service Station AIST 5.6-2010 (2011)):*

$$V_{\mathrm{M}} = \frac{\mathrm{S_{agr}}}{\mathrm{t}_{agr}} \quad \text{[m/s]} \tag{1}$$

where: S_{agr} – is the distance passed by the aggregate, [m];

t_{agr} – time of passing the distance by the aggregate, [s].

Measurements were taken under the steady operation mode. Five samples were taken at each operation mode. The beginning and the end of the testing were determined by signals given at the beginning and at the end of a record plot. The testing duration was recorded by a stopwatch *(Thorat Swapnil V. et al., 2017)*.

After the sowing machine passed along each record plot, the following measurements were taken: the angle of a growing point inclination against the furrow bottom, degrees; the distance between the bulbs in a row, m; the number of damaged bulbs, pieces.

Measurements taken from each record plot were processed according to the following procedure.

The bulbs stem-plate position against the furrow bottom was determined both by sight and with the help of a goniometer. On the basis of the measurement results, three bulb positions were fixed: the bulbs positioned with their stems down (the angle of a growing point inclination $90 \pm 45°$); the bulbs positioned sideways (the angle of a growing point inclination$0 \pm 45°$); the bulbs positioned with stems upward (the angle of a growing point inclination $270 \pm 45°$);

Then the number of bulbs positioned with their stems down, K (%), was calculated:

$$\mathrm{K} = \frac{\mathrm{N}_{90\pm45}}{\mathrm{N_p}} \times 100 \tag{2}$$

where $\mathrm{N}_{90\pm45}$ is the number of bulbs positioned stems down, pieces;

$\mathrm{N_p}$ - total number of bulbs, pieces.

During the experimental testing, the depth of bulbs planting ranged from 3.0 to 5.0 cm. The distance between the rows of planted bulbs ranged from 25 to 33 cm. Uniformity of bulbs distribution was determined from the number of normal intervals. Normal interval is the distance between two neighbouring bulbs *L*, that

is equal to *M* ± 0.5 *M*, where *M* is the distance between the bulbs as provided for by the agronomic and engineering requirements (M=0.1 m). The distance between the bulbs was measured with a millimetre ruler and the following three types of intervals were fixed as a result of measurements:

- normal interval $L_H = M \pm 0{,}5M$;
- reduced interval $L_{yM} < M \pm 0{,}5M$;
- extended interval $L_{yB} > M \pm 0{,}5M$.

$$P = \frac{L_H}{L_{yM}+L_{yB}+L_H} \times 100 \quad (3)$$

Damaged bulbs were considered to be the bulbs that were bared and squashed when planting with the engineering sample of the vibration-pneumatic seeder. These were determined visually.

$$D = \frac{N_d}{N_p} \times 100 \quad (4)$$

where: N_d – is the number of damaged bulbs, pieces.

RESULTS

In the study aimed at determining the optimal speed value V_M for the planting machine engineering sample, all parameters and operation modes, except for V_M, were constant and equal to the optimal values obtained as a result of the laboratory studies. Motion speed was changed from 0.8 to 1.2 m/s with the interval of 0.1 m/s.

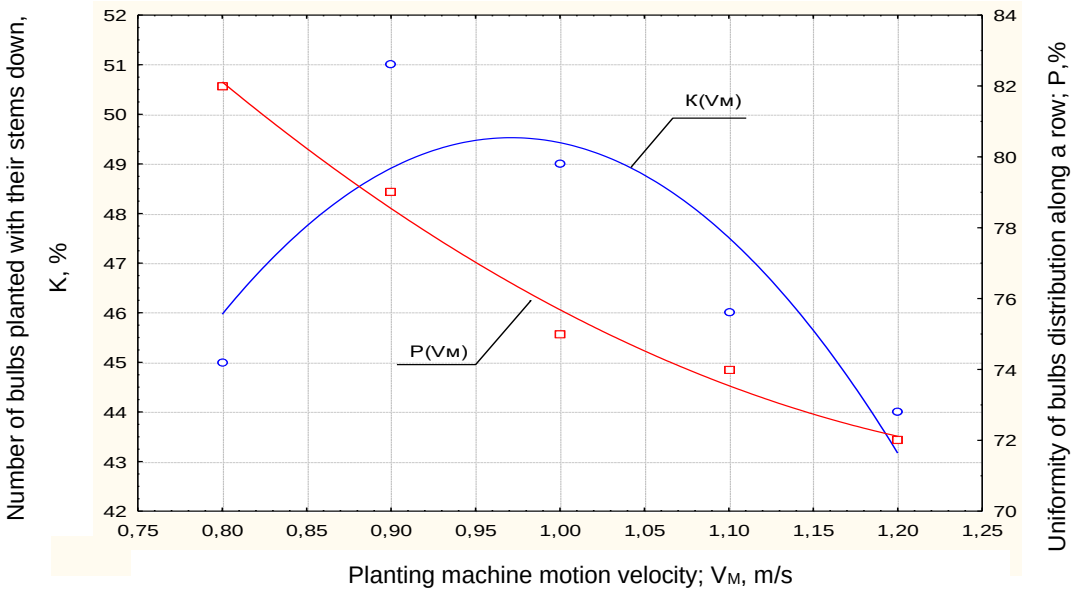

Fig. 9 – Dependence of bulbs number planted with their stems down, K, %, and the uniformity of bulbs distribution along the row P, % of the planting machine forward velocity

According to the results of testing data processing, the graphs were drawn to show how the planting machine motion speed influences the number of bulbs planted with their stem-plates downward, K [%], and the uniformity of bulbs distribution along the row P, % (Fig. 9). Correlation between the number of bulbs planted with their stems down, K [%], and the uniformity of bulbs distribution along the row P,%, depending on the planting machine speed, is expressed by the equation of cuspidal functions:

$$K = -65 + 235{,}8751 \cdot V_M - 121{,}4286 \cdot V_M^2$$
$$P = 136{,}4 - 96{,}4286 \cdot V_M + 35{,}7143 \cdot V_M^2 \quad (5)$$

Analyzing the graphs obtained, we can make the conclusion that the largest number of bulbs positioned with their stem-plates downward (51%) is reached at the velocity of 0.9–1.0 m/s; as the velocity increases, the number of properly positioned bulbs decreases significantly. The best indicators of uniformity are obtained at the lowest speed but increasing of uniformity due to further speed reduction will result in considerable slowdown in the planting aggregate performance. So, the motion speed cannot be optimized relative to the uniformity and it is necessary to take the rational value. Therefore, the best indicators were

obtained K = 51 %, P = 79 % at the speed value of V_M =0.9 – 1.0 m/s. The number of bulbs damaged by the planting device was 0.9% which complied with the agronomic and engineering requirements.

Similar studies carried out for the Koningsplanter planter with a belt planting mechanism showed that the best quality of planting for this machine corresponds to a speed of 1.3-1.4 m/s, the uniformity of planting is within the range of 60-70%, and the number of bulbs, planted with their stems down, does not exceed 20% *(Aksenov A.G., Sibirev A.V., Emelianov P.A., 2018)*.

CONCLUSIONS

The laboratory tests and field trials confirmed the expediency of using the engineering sample of the planting machine equipped with the vibration-pneumatic planting device. Uniformity of bulbs distribution was P = 79 % and the number of bulbs positioned with their stems down was K= 51%, those positioned sideways – 47 %, and those positioned stems upward – 2%, while the planting machine forward velocity was V_M= 0.9–1.0 m/s, the machine height above ground was H_A= 0.12 m, and the pneumatic drum rotation frequency was $n_Б$= 0.47 s^{-1}.

ACKNOWLEDGEMENTS

An experimental sample of a planting machine with a vibrating-pneumatic planting device for oriented seed-onion planting was manufactured at OJSC «Radiozavod» (Penza) and underwent an industrial inspection at «Novy Vyrzhai» LLC in the Penza Region.

The planting machine, equipped with a vibrating-pneumatic planting device, allows increasing the percentage of bulbs planted by the bottom up to 2 times and the uniformity of bulbs distribution along the row by 19% compared to the Koningsplanter planting machine equipped with a belt planter.

REFERENCES

[1] Aksenov A.G., Sibirev A.V., Emelianov P.A., (2016), Technical Equipment for Vegetable Growing, *Tractors and Agricultural Machines,* Issue number 8, pp. 25-30, Moscow / Russia;

[2] Aksenov A.G., Sibirev A.V., Emelianov P.A., (2018), Oriented Bulbs Planting with Forked-Roller Planting Apparatus, *Vestnik of Mordova University,* Issue number 1, pp. 20-24, Saransk / Russia;

[3] Aksenov A.G., (2018), Onion Set Bulb Position during Planting with Vibration-Pneumatic Planting Device*, Agri Res & Tech:Open Access J.*, Issue number 16 (3), pp. 1-6, California / United States;

[4] Brewster J., (2008), *Onions and Other Vegetable Alliums*: 2-nd edition. *Crop Production Science in Horticulture*, vol.15, 432 p, Cambridge / England;

[5] Emelianov P.A., Aksenov A.G., Patent No. 2407271. Russia, IPC A01 C11/02. *Vibration-Pneumatic Seeder for Seed-Onion Oriented Planting*, no.2008149668/21; Appl. 16.12.2008 Publ. 27.12.2010 Bul. No.36*;*

[6] Jarudchai Y., Sonluck K., Jiraporn B., (2002), Design and development of a garlic planter in Thailand, *Bachelor's thesis King Mongkut's Institute of Technology Ladkrabang,* vol. 2, pp. 1-10, Thailand;

[7] Nilesh N.J., Harshal R.A., Amol P.G., (2015), Design and Fabrication of Onion Seed Sowing Machine, *International Journal on Recent Technologies in Mechanical and Automobile Engineering*, Issue number 2, pp. 1-10, Pahang / Malaysia;

[8] Rohokale A.B., Shewale P.D., Pokharkar S.B., Sanap K.K., (2014), A review on multi-seed sowing machine, *International Journal of Mechanical Engineering and Technology (IJMET),* vol.5, pp.180-186, Tamil Nadu / India;

[9] Shen Qiang, Xu Li-li, Wang Jun-qiang, Yang Wei-min (2015)**.** The performance of Agricultural science and technology transformation Fund of different Technical Fields, *International Conference on Engineering Management, Engineering Education and Information Technology,* Issue number 1, pp. 94-98, Madrid / Spain;

[10] Thorat S.V., Madhu L.K., Patil G.V, Patil R., (2017), Design and Fabrication of Seed Sowing Machine // International Research Journal of Engineering and Technology, *International Research Journal of Engineering and Technology (IRJET),* Issue number 4, pp. 704-707, West Bengal / India;

[11] *** Vehicle Service Station AIST 5.6-2010 (2011), "Agricultural Equipment Testing. Sowing and Planting Machines." Purpose Indicators. General requirements. Introduced on 15.04.2001, M.: Standards Publishing House, 27 p.

NEW WORKING ELEMENT OF STRIPPER HEADER "OZON" / НОВЫЙ РАБОЧИЙ ОРГАН ОЧЕСЫВАЮЩЕЙ ЖАТКИ "ОЗОН"

Prof. PhD. Eng.Sc. Aldoshin N.V.[1)], Prof. PhD. Eng.Sc. Kravchenko I.N.[1)], Prof. PhD. Eng.Sc. Kuznetsov Y.A.*[2)], Prof. PhD. Phil.Sc. Kalashnikova L.V.[3)], Assoc. Prof. D.Eng.Sc. Korneev V.M.[1)]

[1)]Russian State Agrarian University – Moscow Agricultural Academy named after K.A. Timiryazev, Moscow / Russia;
[2)]Orel State Agrarian University named after N.V. Parakhin / Russia;
[3)]Orel State University named after I.S. Turgenev / Russia
Tel: +79208289219; E-mail: kentury@rambler.ru.

Keywords: *combine harvester, stripper header, construction, beater, fingers, tines*

ABSTRACT

New construction of working elements of combine harvester stripper header is suggested. The essence of technical solution consists in the construction alteration of stripper header fingers at the account of tine technological gap increase. The recommendations on the choice of rational kinematic operation mode of combine harvester header are developed. The improved construction allows increasing combine harvester stripping efficiency and decreasing grain material losses to 5% at harvesting.

РЕЗЮМЕ

Предложена новая конструкция рабочих органов комбайновых очесывающих жаток. Суть технического решения заключается в изменении устройства гребенок очесывающих барабанов, за счет увеличения технологического зазора между зубцами. Разработаны рекомендации по выбору рационального кинематического режима работы комбайновой жатки. Усовершенствованная конструкция позволяет повысить эффективность комбайнового очеса и снизить при уборке до 5 % потери зернового материала.

INTRODUCTION

Now there are questions of great importance regarding the construction development of stripping harvesting part of grain combine harvesters in many countries. A considerable amount of research papers is related to the investigations in the areas of grain harvesting optimization and combines header modernization *(Chegini G. and Mirnezami S.V., 2016; Henry W.B. et al, 2008; Ince A. et al, 2011).*

In the structure of grain production, grain legumes occupy a significant place *(Stagnari F. et al, 2017; Zotikov V.I., 2017).* In the world agricultural farming, leguminous crops occupy about 13% of grain crops. In the Russian Federation, the share of these crops in the structure is less than 1%. Leguminous are the source of plant protein. Increase of their sowing area allows solving the problem of fodder shortage. Leguminous in the Russian Federation are cultivated on areas of 1300…2000 thous. ha *(Sergeeva V.A. et al, 2016).*

At the present time, on the country territory white lupine sowings are expanded wider. This crop peculiarities require the reasoned recommendations on carrying out all kinds of different mechanized works and particularly harvesting *(Aldoshin N., (2016); Zotikov V.I., 2017).*

In this respect, the experimental researches of white lupine harvesting process with usage of stripper headers are of particular interest.

Stripper headers operate steadily in large range of harvested crops humidity. The maximum humidity level is limited to biological grain ripening, and that is why stripper headers provide good harvesting results even at 30% crop humidity. The minimum humidity level is limited with equilibrium humidity of grain storage, which is 12-15% *(Aladyev N.A., 2015; Sergeeva V.A. et al, 2016).*

It should be emphasized that the applied stripper headers are divided into mounted and trailed, which differ in terms of stripping equipment, working elements, method of stripping products harvesting. Herewith, the machines are produced with or without the plant supplying equipment, that feeds the stripping zone *(Ince A. et al, 2011; Mkrtchyan S.R. et al, 2013; Mosyakov M.A., 2016).*

On the Russian market the stripper headers of trademarks "Ozon" (Russia), "Slavyanka" (Ukraine), and also "Shelbourne" (Great Britain) are the best known.

The main difference of all presented models is in number of stripping rotors (beaters), but the headers operation principle is the same.

OJSC “Penzmash” (Russia) produces mounted stripper headers of type “OZON”. Header “Ozon” is designed to harvest grain crops and grass seeds with direct combining by grain stripping and feeding stripping mass into combine harvester. The technological process of header operation is presented in fig. 1.

On average, the grain mass harvested from one field area unit with a conventional header consists of one mass part of grain and one-and-a-half part of straw. Grain mass harvested by stripper header from the same field area unit on an average consists of one mass part of grain and just a quarter of mass part of straw. Thus, the decrease of grain mass fed to combine harvester in half at the expense of reduction of straw amount in grain heap, results in combine threshing drum operation in underload mode. The reserve in threshing drum capacity appears. This enhances the speed of combine harvester movement. At harvesting, the usage of stripper headers enables combine harvester to move in 1.5-2 times faster *(Aldoshin N., 2016).*

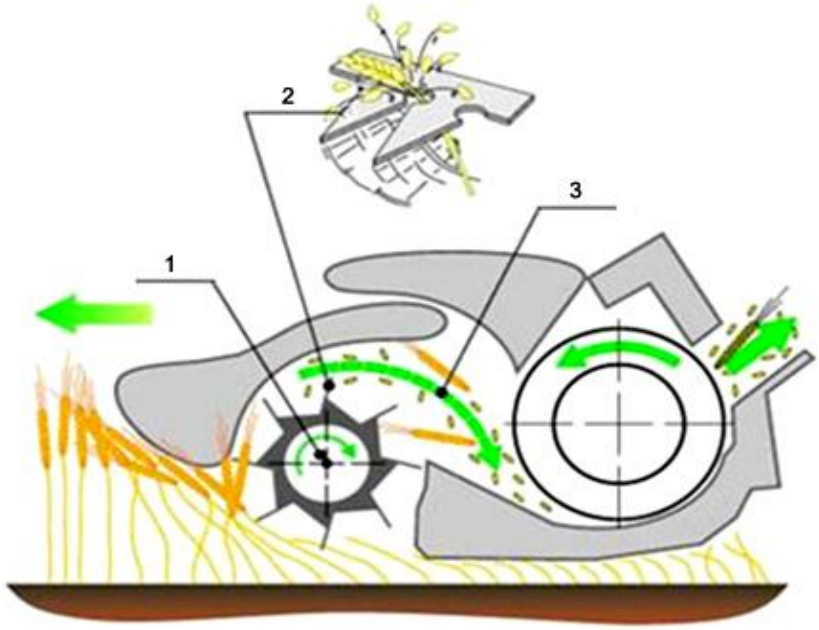

Fig. 1 - Technological process of stripper header “OZON” operation

1 – stripping rotors; 2 – stripping tines; 3 – grain and turned away grain heads

Stripper headers operate steadily in a large range of harvested crops humidity. The upper humidity limit is limited only by biological ripeness of grain and that is why stripper headers are able to harvest grains with good results, even at 30% crop humidity. The lower humidity limit depends on the equilibrium humidity of grain storage, which is 12-15%. At lower humidity the fixation of grain in head grows weak. Some extra grain losses appear at mechanical impact of header on plant stand. However, due to the 3-5 days earlier start of harvesting the total duration of stripper header usage in harvesting time is longer in comparison with the usage of conventional headers *(Aldoshin N., 2016; Mkrtchyan S.R. et al, 2013; Mosyakov M.A., 2016)*.

It should be pointed out, that it is impossible to confuse biological plant humidity with surface moisture from rain or dew. In this case, the connection of root system and soil grows weak and at stripping, some plants can be pulled out with roots. Thus, after rain, soil should get dry but anyway harvesting can be started by 2-3 - hours earlier than with conventional header.

Stripping operating principle provides that qualitative plant threshing (stripping) is done in the open space. In this case, the grains (seeds) separated after stripping do not affect plant stand and move in the open space into the intended direction. Thus, the losses of the stripped grains are minimal. Such stripping levels are possible only in the case when plant inflorescences are compact and are located at the end of the stem top, i.e. in the area close to the open space. The cereals and headings crops, such as wheat, barley, rye, oat, triticale, rice, sorgo, flax and others correspond to these requirements first (fig. 2).

If plant inflorescences are located along the whole stem (leguminous crops) or they are located incompact (rape), grains being separated after stripping from lower stem part, affect plant stand at flight and can considerably deviate from the intended direction. It results in significant grain losses (fig. 3) *(Aldoshin N.V., 2016).*

The purpose of our investigation was estimation of utilization possibility and operation quality of stripper header “Ozon” at harvesting white lupine of “Dega” variety.

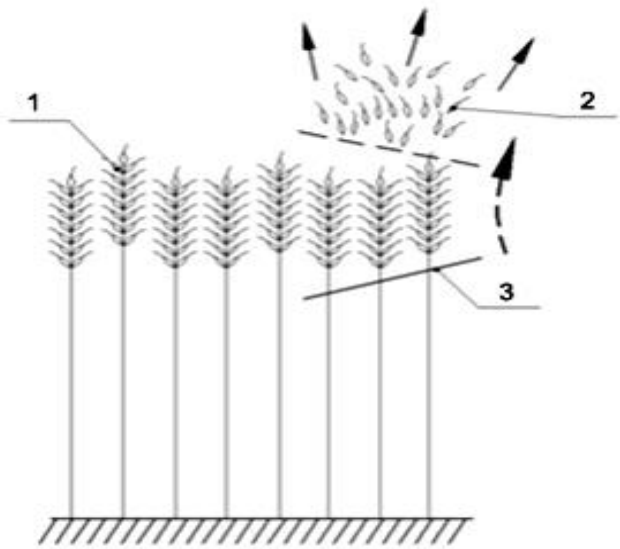

Fig. 2 - Scheme of stripping of cereals and headings crops
1 – inflorescences; 2 – stripped grains; 3 – finger

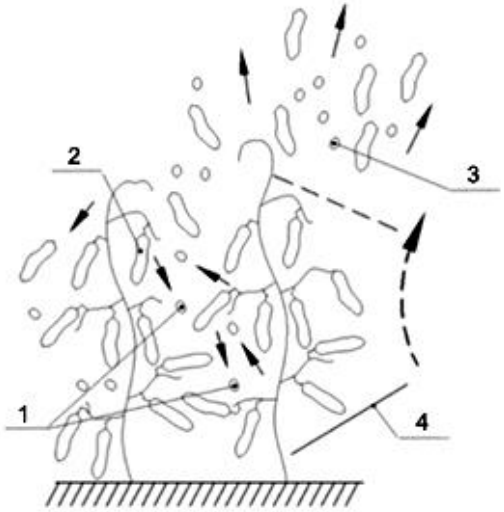

Fig. 3 - Scheme of leguminous crops stripping
1 – grains flying incorrectly; 2 – beans; 3 – stripped grains; 4 – finger

MATERIALS AND METHODS

White lupine "Dega" beans are located mostly in one upper layer. This allows using ultimately the technology of stripping at its harvesting *(Mosyakov M.A., 2016; Sergeeva V.A. et al, 2016).* Nevertheless, for harvesting leguminous crops with rather large bean size the stripper header of type "Ozon" in the conventional design has sufficiently small spacing between tines of the beater stripping fingers. In this case, bigger beans of white lupine do not fit in spacing between finger tines and the stripping process runs inefficiently. Therefore, to harvest white lupine sowings, we use modernized fingers with large spacing between tines *(Lukomets V.V. et al, 2016)* together with conventional ones. Different variants of stripping fingers are shown in figure 4.

Finger of stripper beater performs plane-parallel motion relative to ground surface composed from combine harvester forward speed and beater rotating motion. Each point of stripper beater in this case travels along a cycloid. In this regard, the stripping efficiency will depend on correlation of combine harvester forward speed and linear speed of stripper beater finger, determined with angular speed of beater and its geometrical dimensions, i.e. kinematic parameter λ.

The formula to determine kinematic parameter λ appears as follows:

$$\lambda = \frac{V_n}{V_p} = \frac{\omega r}{V_p} = \frac{\pi n r}{30 V_p}, \quad (1)$$

where:

V_n – linear speed of stripper beater finger, [m/s];
V_p – operation speed of combine harvester, [m/s];
ω – angular speed of stripper beater, [s^{-1}];
r – beater radius, [m];
n – beater rotational frequency, [min^{-1}].

The stripper beater drive provides three angular speeds: 485, 580 and 662 min^{-1}.

Fig. 4 - Stripping fingers of the "OZON" header (Russia):
left – conventional; right – modernized with large spacing between tines

RESULTS

According to testing data (fig. 5-8), efficient operation of stripper header at white lupine harvesting can be realized at the following correlations of combine harvester operation speeds and stripper beater rotation frequency:

a) at a stripper beater rotation frequency of 485 min^{-1} the operation speeds of combine harvester should be ≤ 4.3 km/h;

b) at a stripper beater rotation frequency of 580 min^{-1} the operation speeds of combine harvester should be ≤ 5.3 km/h;

c) at a stripper beater rotation frequency of 662 min^{-1} the operation speeds of combine harvester should be ≤ 6.0 km/h.

This limits the combine harvester operation at rather high operation speeds. According to the energy data it can be considered as the advantage over crop harvesting by the conventional method with the threshing of all straw-grain mass. In this regard, in the header design, it is reasonable to provide the possibility of further increase the rotation speed of the stripper beater.

From figure 5 follows that reduction of white lupine losses due to incomplete stripping decreases with reduction of plant mass supply for every finger, i.e. increase of linear speed of the stripping beater fingers in relation to combine harvester forward speed.

According to dependency, presented in figure 6, it follows that with the decrease of mass supply for every finger, shatter losses increase. It is the result of the construction fault of conventional stripping finger of beater for harvesting leguminous crops, particularly white lupine. Because of too small spacing between conventional finger tines, the sufficiently big beans of white lupine cannot get through the space between tines. In this case, in a greater degree the wearing out of legumes takes place and, as a result, great shatter losses occur. Since kinematic parameter increases, mainly because of the increase of the stripper beater rotation speed in relation to the combine harvester speed, the "effect" of legumes wearing out increases and shatter losses grow.

According to the data in figure 5, the results presented in figure 7 demonstrate that reduction of white lupine losses, because of incomplete stripping with the modernized header, is reducing with respect to the reduction of plant mass supply for every finger. There is the increase of linear speed of the stripper beater fingers in relation to forward speed of the combine harvester.

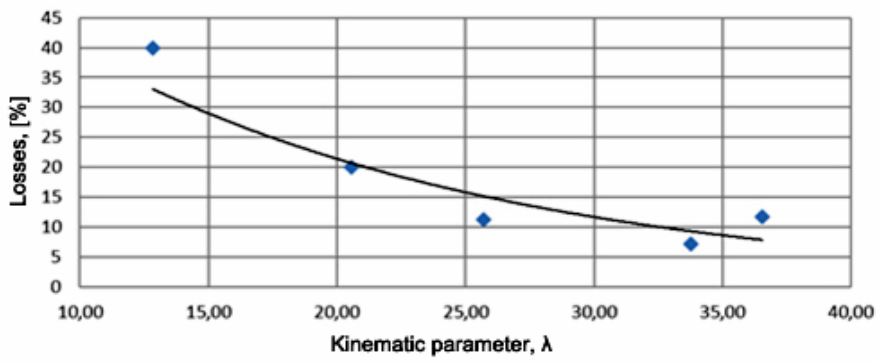

Fig. 5 - Dependence of white lupine losses due to incomplete stripping on λ, when using conventional design of stripper header fingers

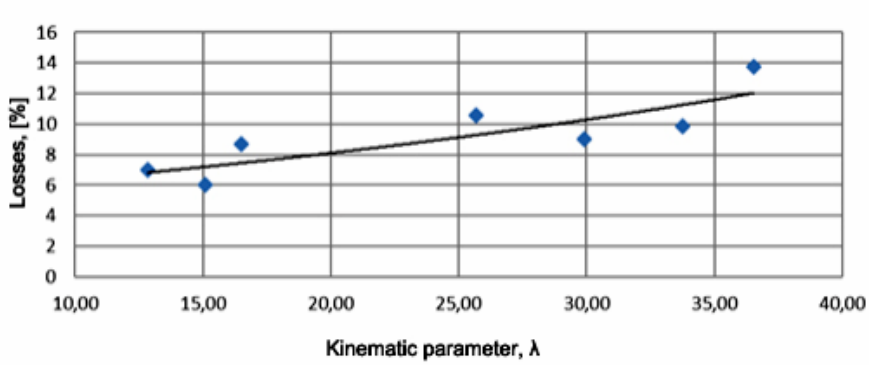

Fig. 6 - Dependence of white lupine shatter losses on λ, when using conventional design of stripper header fingers

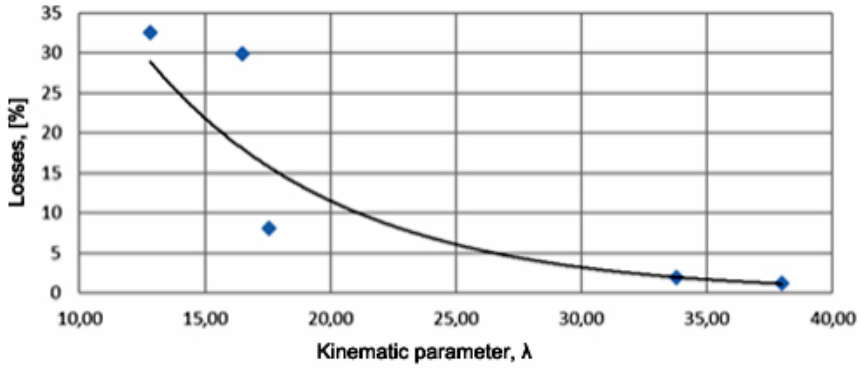

Fig. 7 - Dependence of white lupine losses due to incomplete stripping on λ, when using modernized fingers of the stripper header

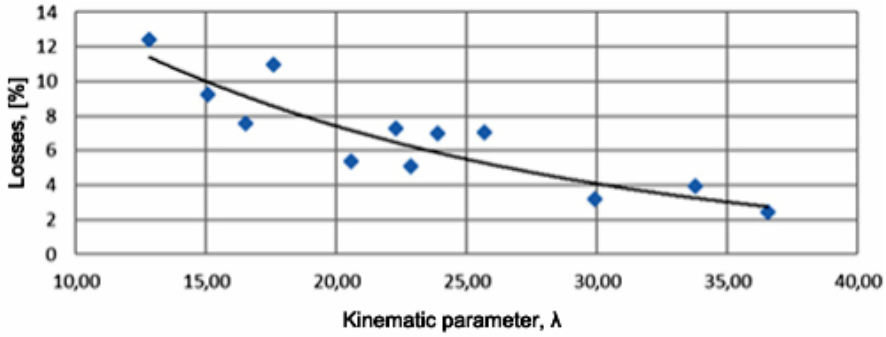

Fig. 8 - Dependence of white lupine shatter losses on λ, when using modernized fingers of the stripper header

The dependence presented in figure 6 demonstrates that the utilization of the modernized stripping fingers allows changing the white lupine grain losses behaviour due to the mass supply for every finger (kinematic parameter increase). Modification of the stripping finger construction due to the increase of the tines spacing provides more efficient stripping of white lupine.

According to the data presented in figures 7 and 8, it is possible to stress that utilization of the modernized fingers of the stripper beater can provide decrease of total losses of white lupine grain from incomplete stripping and loose grain up to 5% and lower. Herewith the operation speed of the combine harvester does not exceed 4.0 km/h at the stripper beater rotation frequency of 662 min^{-1}; 3.6 km/h – at 580 min^{-1}; 3.0 km/h – at 485 min^{-1}.

CONCLUSIONS

The "Ozon" stripper header of the OJSC "Penzmash" (Russia) production can be successfully utilized at harvesting white lupine of the "Dega" variety. In this regard, we recommend using the modernized fingers of the stripper beater with the increased spacing between tines. Herewith total losses of white lupine grain from incomplete stripping and loose grain can be up to 5% and lower.

The existing rotation speeds of the stripper header do not allow harvesting at combine harvester speeds of more than 6.0 km/h. To increase operation speeds of the combine harvester is necessary to foresee the possibility of rotation speed growth of the stripper header beater.

REFERENCES

[1] Aladyev N.A., (2015), Influence of tool-point velocity on grain damage of white lupine (Влияние скорости рабочих органов на повреждение зерна белого люпина), *Innovations in agriculture (Инновации в сельском хозяйстве),* Issue number 4 (14), pp. 97-102, Moscow/Russia;

[2] Aldoshin N., (2016), Methods of harvesting of mixed crops. (Методы уборки смешанных культур), *Proceeding of 6th International Conference on Trends in Agricultural Engineering 2016*, *Part 1, Czech University of Life Sciences Prague, Faculty of Engineering*, pp. 26-32, Prague/ Czech Republic;

[3] Chegini G., Mirnezami S.V., (2016), Experimental comparison of combine performance with two harvesting methods: Stripper header and conventional header, *Agricultural Engineering International: GIGR Journal*, Vol. 18, Issue 1, ISSN:1682-1130, pp. 192-200, Beijing/China;

[4] Henry W.B., Nielsen D.C., Vigil M.V., Calderon F.J., West M.S., (2008), Proso millet yield and residue mass following direct harvest with a stripper-header, *Agronomy journal*, Vol. 100, Issue 3, ISSN:0002-1962, pp. 580-584, Madison/USA;

[5] Ince A., Say M.S., Kara O., Bilgili E., (2011), Comparing of Different Harvesting Systems in Wheat Harvesting, *Tarim Makinalari Bilimi Dergisi (Journal of Agricultural Machinery Science)*, Vol. 7, Issue 1, ISSN:1306-0007, pp. 89-93, Alsancak-Izmir/Turkey;

[6] Lukomets V.V., Aldoshin N.V., Zolotov A.A., (2016*), Stripper beater.* Russia, Patent RU, No. 164619, МПК A01D 41/08;

[7] Mkrtchyan S.R., Ignatov V.D., Zhalnin E.V., Struzhkin N.I., (2013), Stripper headers: state and development perspectives (Очесывающие жатки: состояние и перспективы развития), *Agricultural Machinery and Technologies (Сельскохозяйственные машины и технологии),* Issue 4, ISSN:2073-7599, pp. 18-21, Moscow/Russia;

[8] Mosyakov M.A., (2016), Comparative evaluation of combine harvesters for white lupine harvesting (Сравнительная оценка комбайнов для уборки белого люпина), *Horticulture and berry culture of Russia (Плодоводство и ягодоводство России),* Vol. XXXXVI, pp. 246-250, Moscow/Russia;

[9] Sergeeva V.A., Nuravyev A.A., Naumkin V.N., (2016), Agricultural methods of obtaining high yield of white lupine (Агротехнические приемы получения высокого урожая люпина белого), *Agrarian science (Аграрная наука),* Issue 7, ISSN:0869-8115, pp. 4-7, Moscow/Russia;

[10] Stagnari F., Maggio A., Galieni A., Pisante M., (2017), Multiple benefits of legumes for agriculture sustainability: an overview, *Chemical and Biological Technologies in Agriculture*, Vol. 4:2, Issue 1, ISSN:2196-5641 (Online), Heidelberg: Springer/Germany;

[11] Zotikov V.I., (2017), Leguminous and cereal crops – acute direction of production quality growth (Зернобобовые и крупяные культуры – актуальное направление повышения качества), *Leguminous and cereal crops (Зернобобовые и крупяные культуры),* Issue 3(23), ISSN:2309-348X, pp. 23-28, Orel/Russia.

SOIL COMPRESSION DEGREE BY USING THE VIBRO-COMBINATOR
/
GRADUL DE COMPACTARE A SOLULUI LA UTILIZAREA VIBRO-COMBINATORULUI

Assoc. Prof. Ph.D. Eng. Boja N.*[1)], Lect. Ph.D. Eng. Boja F.[1)], Stud. Ph.D.Eng. Vidrean D.[1)], Lect. Ph.D. Eng. Teusdea A.[2)], Assoc. Prof. Ph.D. Eng. Bungescu S.[3)], Prof. Ph.D. Eng. Borz SA.[4)]

[1)] "Vasile Goldiş" Western University of Arad, Faculty of Economics, Informatics and Engineering / Romania;

[2)]University of Oradea, Faculty of Environmental Protection / Romania

[3)]University of Agricultural Sciences and Veterinary Medicine of Banat Timişoara, Faculty of Agriculture, Timişoara, Romania

[4)] Transilvania University of Brasov, Faculty of Silviculture and Forest Engineering, Brasov, Romania

Tel: 0733021750; E-mail: bojanicu@yahoo.com

Keywords: *vibro-combinator, bulk density, total porosity, compression degree*

ABSTRACT

Seedbed preparation for crop establishment (sowing) is one of the most important agricultural works, as it is done with high energy consumption and high costs. The quality of this work influences to a large extent crop germination and the productivity that can be obtained per hectare. Therefore, at present, there is different equipment from the one found in classical cultivation technologies, which by single pass can achieve tillage with minimum energy consumption, thus creating optimal conditions for sowing and for obtaining higher yield without soil degradation. These devices are called combinators. Of all the existing combinators, the most performant are the vibro-combinators. In order to carry out the research, we settled in six parcels in the plains of the West of Romania so that we could have three different types of soils which are representative for that specific area. From each profile soil samples were collected in three steps of 6, 12 and 18 cm. For each sample six repetitions were performed (N = 6). We started by measuring the particle size distribution (granulometric composition) and the main physical properties of the soil (moisture, bulk density, total porosity and soil compression degree).

REZUMAT

Pregătirea patului germinativ (însămânțarea) este una dintre cele mai importante lucrări agricole, ce implica un consumul ridicat de energie și costurile ridicate. Calitatea acestei lucrări influențează în mare măsură germinarea culturii și productivitatea care poate fi obținută pe hectar. De aceea, în prezent există echipamente diferite de cele din tehnologiile clasice de cultivare, care pot realiza pregătirea patului germinativ la o singură trecere, cu un consum minim de energie, creând astfel condiții optime pentru însămânțare și pentru obținerea unui randament mai ridicat fără degradarea solului. Aceste echipamente tehnice sunt numite combinatoare. Dintre toate variantele existente, cel mai performant este vibrocombinatorul. Pentru realizarea cercetării, am ales șase parcele din câmpiile din vestul României, astfel încât să putem avea trei tipuri diferite de soluri reprezentative pentru acea zonă. Din fiecare profil s-au colectat probe de sol în trei trepte de adâncime de la 6, 12 și 18 cm. Pentru fiecare probă s-au efectuat șase repetiții (N = 6). S-a realizat măsurarea distribuției dimensiunii particulelor (compoziția granulometrică) și a principalelor proprietăți fizice ale solului (umiditate, densitate aparentă, porozitate totală și grad de tasare a solului).

INTRODUCTION

Compaction of agricultural soils below the cultivated layer commonly results from the passage of vehicular traffic. Compaction causes a rearrangement of the soil particles and many properties of the soil are influenced as a result. Pore size distribution is altered, total porosity is decreased, and there are changes in the movement and content of heat, air, water and nutrients in the soil. The restricted growth of roots commonly observed in compacted soil has been variously attributed to all of these properties, and to the high mechanical resistance which compacted soil present at plant roots. *(Shierlaw J. and Alston A.M., 1984)*

Soil compaction, as a consequence of frequent cultivation with heavy machinery, is one of the most important problems that modern mechanized agriculture is facing. Although the negative effects of heavy farm machinery on the physical characteristics of soil fertility, e.g. decreased aggregate stability, soil

crusting, and formation of traffic pans and plough-pans, is well documented, much less is known about how soil compaction affects soil biological fertility. *(Neve S.D. and Hofman G.; 2000)*

The mechanization technologies of soil works have a major impact on soil physical state. This situation is generated by the mechanical action of working parts which are involved in soil works and by the traffic of running systems of tractors and agricultural machines.

These mechanization technologies have been tested to determine which of them correspond to the highest degree of sustainable agriculture concept and ensure protection, preservation and improvement of agricultural lands. The testing results of mechanization technologies for soil works variants which include a wide spectrum of conservative and unconventional works, performed with appropriate equipment, were compared both between them and also with witness variant which involved the classical and conventional technologies for soil processing. *(Ţenu I., et al, 2009)*

The structure is a distinctive characteristic, appropriate to soil, being of great importance for physical, chemical and biological processes which are developed in soil and in the soil-plant-atmosphere system. Many authors consider the structure as a basic characteristic, on which depends the soil fertility (mainly water and air regime, thermal and nutrient regime).

The degradation of the structure is determined by two groups of causes:

- changing the chemistry of the soil by decreasing soil humus content, and sometimes, especially as a result of unbalanced fertilization or irrigation with poor quality water by alkalization or acidification of soil;
- the direct destruction actions of structural elements, including soil dusting due to excessive work, or inadequate humidity, compaction due to exaggerated traffic especially when it is performed on wet ground, formation of crust under rain drops action or sprinkling-irrigations, etc. *(Ţenu I., et al, 2009)*

The reduction of soil volume (a simple reduction in pore space) due to external factors is called soil compaction. Soil compaction is defined as increase in soil bulk density or decrease in soil volume and porosity (Fig. 1) due to mechanical stress on soil (e.g., from traffic of farm machinery). It can also occur due to natural reconsolidation of soil. There are two types of compaction, namely, surface compaction and subsoil compaction. The compaction that occurs in the surface “plow layer” is called surface compaction, while the compaction that occurs as a result of a surface load below the plow layer is called subsoil compaction.

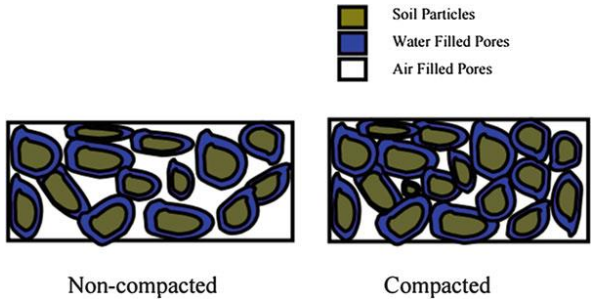

Fig. 1 - Effect of soil compaction on pore space *(Neve S.D. and Hofman G.; 2000)*

Nowadays, humanity is facing a major controversy over the choice of appropriate technology of soil tillage. It is the time that is required an intelligent choice between conventional technologies (classical) for seedbed preparation, assuming an intense mechanical processing of soil, which affects soil structure and soil organic matter, and the conservative tillage technologies for seedbed preparation which remove these disadvantages in terms of an accepted decrease of the production. *(Benites J., 2000)*

At present, increase in the size of farm equipment used to carry out various farm operations increases the risk of soil compaction. The agricultural soil compaction can take place due to frequent movement of farm machinery. Factors responsible for compaction due to vehicular traffic include weak soil (soil density and moisture content effect) and excessive loads (size of vehicles, tire size, and number of passes are directly related to compaction). Soil tillage operations are also responsible for soil compaction. *(Pisante et al, 2010)*

The advantages of using vibro-combinators are: required preparation of seedbed in difficult working conditions and preservation of moisture and total porosity and the reduction of soil compression degree. Such important factors can ensure fast, uniform and early germination of seeds, these requirements standing at the basis of abundant harvests.

The paper presents a study on the optimization of working regime of vibro-cultivators based on environmental impact assessment for use in seedbed processing. Study presents a method to determinate some physical and mechanical proprieties before and after soil tillage works of aggregates consisting of tractor and vibro-cultivators, on three parcels in the plains of the West of Romania.

Vibro-cultivators are machines for seedbed preparation. They are equipped with tools sustained by elastic suspension. The elasticity of supports facilitates the oscillations of working tool – elastic support assembly. This set has a natural mode shape which corresponds to a natural frequency of vibration *(Cardei P. et al, 2015).*

Modern agricultural operations now demand the utilization of a wide variety of equipment and specialist machinery systems, with many having rotary elements such as axles, gears, pulleys etc. With these agricultural machinery systems which have rotary elements, uncontrolled vibrations may become an important problem to consider. When the initial 'switch-on' frequency meets with the natural frequency of a machine element in the system, undesired noise, high levels of vibration and mechanical failures may occur during operation *(Celik H et al, 2010; Petrescu H.A. el al, 2015).*

Generally, combinators consist of a vibro-cultivator A (cultivator for total processing of soil), composed of: frame *1*, coupling device at the power source *2*, wheels for limiting the working depth *3*, soil loosening bodies *4*, and a helix harrow B, which consists of frame *5*, two rod rotors *6*, and horizontality adjustment system *7* (Fig. 2). Worldwide, more and more prestigious companies have incorporated such vibro-combinators into the range of products.

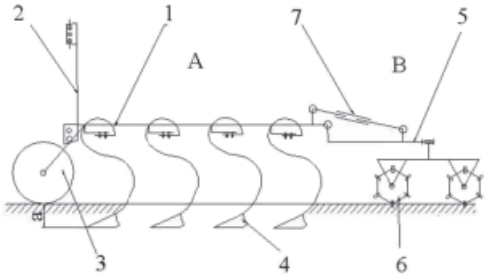

Fig. 2 - General scheme of a vibro-combinator
(Caproiu St. et al, 1982; Biris S.St. et al,2015)

Deep tillage tools are one of the primary components of agricultural equipment which experience high level soil reaction forces during tillage operations. These forces may cause plastic deformation or failure which is undesirable for tillage machines/tools. The active tillage elements of agricultural machineries require extensive studies in order to obtain a proper soil fragmentation and displacement *(Petrescu H.A. el al, 2015).*

MATERIALS AND METHODS

In order to obtain a global image on the impact of the new vibro-combinator (the prototype SANDOKAN 2) (table 1) in terms of physical-mechanical properties of the soil, it was necessary to determine its properties before the passage of the equipment (in the state of the soil), and after its passage on all the three parcels and trials. These parcels will be suggestively named: soil 1, soil 2 and soil 3; and the three types of active parts (Gamma, Delta1 and Delta2) (fig. 3-4).

Table 1

Main characteristics of the prototype vibro-combinator SANDOKAN 2

No.	Characteristics	MU	Values
1	Mass	kg	5670
2	Length in transport	m	6.6
3	Height in transport	m	3.95
4	Width in transport	m	2.93
5	Width of the gamma active parts, reversible chipper type	mm	35
6	Width of the delta 1 active parts, arrow type	mm	150
7	Width of the delta 2 active parts, arrow type	mm	250

The physical properties were determined by using the method of the cylinders with a constant volume of 100 cm^3, carrying out six repetitions at different depth, namely 6, 12 and 18 cm. The methods of analysis and interpretation of the results as well as the work procedure for the determination of the physical – mechanical properties are those indicated in the specialized literature (*Boja et al, 2012; Boja et al, 2013*).

Fig. 3 - The prototype vibro-combinator SANDOKAN 2 equipped with the three types of active parts (GAMMA, DELTA1, DELTA2)

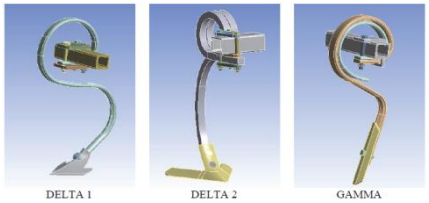

Fig. 4 - Geometrical models for the three active parts *(Petrescu H.A. el al, 2015)*

Statistical analysis. All data were subjected to univariate three-way analysis of variance (ANOVA, P = 0.05) and done with KyPlot (Kyplot Version 5.0.2, http://www.kyplot.software.informer.com). The ANOVA factors were: Soil (soil type), h (depth), Device (active part) and their three order interaction. The means pairwise comparisons were investigated by Tukey's post-hoc test (P =0.05). Multivariate analysis: principal component analysis (PCA) was performed with P.A.S.T. version 3.04 statistical software, (Palaeontology Statistics, Copyright Oyvind Hammer and D.A.T. Harper (November 2014), http://folk.uio.no/ohammer/ past/) *(Hammer et al, 2001).*

RESULTS

When analysing the granulometric curves presented in figure 5 and table 2, one can notice the fact that there was a sandy-clay-dusty texture in soil 2 and 3 encompassed in the experiment at a participation quota that scarcely varies, with the exception of the 1st soil where the particle size distribution is different: clay-dusty-sandy texture.

Table 2

Average values of the granulometric analysis at different depths of prelevation

Type of soil			SOIL 1 (S1)			SOIL 2 (S2)			SOIL 3 (S3)		
Depth of prelevation,		(cm)	6	12	18	6	12	18	6	12	18
Values of the granulometric analysis	Sand,	%	26.2	26.8	27.4	35.7	35.1	35.1	43.4	43.2	43.2
	Dust,	%	28.6	28.7	28.7	30.2	30.2	30.1	27.8	28.1	28.5
	Clay,	%	44.8	44.3	44.4	34.5	34.8	34.7	28.5	28.7	25.9

From the analysis of the values gathered for the participation quotas of the granulometric fractions, we could infer some interesting differentiations among the three types of soil in which we tried the vibro-combinator, as follows: All the three types of soil that we tried the vibro-combinator on are a relatively close mix, but in different proportions among the three granulometric fractions; The sand fraction (gravel + fine) is predominant in the soil 3 (43,2 %); For the dust fraction (I + II), the differences among the three types range only for 2%, the highest value being registered on the soil 2 (30,1 %); The participation quotas of the clay granulometric fraction are among the biggest, varying between 28,7 % (soil 3) and 34,7 % (soil 2), and reaching 44,5 % for soil 1; The dust granulometric fraction is almost constant for all the three types of soil.

To synthesise more efficiently the data taken and to be able to describe completely the intrinsic characteristics of the sample, it was chosen a statistic processing with the aid of the program KyPlot. The results obtained are given in Table 3, having as a purpose to underline the variance of apparent density, soil moisture, total porosity and soil compression degree, and to compare each type of soils and three active

parts (Gama, Delta 1, Delta 2). Thus, for each type of soils included in the experiment eight statistical indicators resulted, for each technical work using a new vibro-combinator, but also witness sample. The mechanical processing of the soil through traditional and modern methods is currently put under question due to the high energy consumption and the continuous degradation of the arable horizon through erosion and excessive compaction.

It is known that the bulk density varies between 1-2 g/cm^3, according to the type soil and horizon, being generally lower in the case of the soils rich in humus and in the structured soils as compared to the unstructured soils. The values of the bulk density are in tight correlation with the degree of soil settlement. The high bulk density means a decrease of the capacity to retain water, of the permeability, of aeration and an increase of the mechanical resistance opposed by the soil during its sampling. On the contrary, low bulk densities can reduce the bearing of the soil, making difficult the mechanized execution of the works, even the driving of the operation machinery *(Spoljar et al, 2009; Spoljar et al, 2011; Boyraz D. and Atilgan M.C., 2014; Boja et al, 2016; Calistru et al, 2016; Vidrean et al, 2018).*

By analyzing the values of total porosity, we can say that for the 1st type of soil we noticed an increase of the total porosity from 40.19%, which represents the initial state of the soil, to 44.36% (value obtained after the working of the soil with the vibro-combinator equipped with Gamma elements), 45.64% (with Delta 1 elements) and 45.71% (with Delta 2 elements).

The degree of settlement for the first type of soil presents values > 18%, which means that the soil is strongly settled for all levels of depth and after the passage with the three types of active parts of the cultivator.

The values gathered for the second type of soil varies from weakly settled (1…10%) to moderately settled (11…18%). However, it is important to specify the fact that the lowest values of the degree of settlement appeared after preparing the germination bed with the aid of the active parts Delta 2.

In the case of the third type of soil, we had negative values for this mechanical index of the soil at all depths, especially for the types of active parts, which means there is a soil moderately loose (-17…-10%) - fact that can be explained by the fact that this parcel has been annually worked.

Analyzing the influence of the active parts on the different types of soils, some conclusions can be drawn (Table 3 and Fig. 5-9): in terms of apparent density values (Da), the lowest value is found on all soil types (S1, S2, S3) when working with the active parts Delta2; the total soil porosity has maximum values when the vibro-combinator is equipped with the Delta2 active parts, logical situation due to the existing relation to density and porosity; soil moisture values reach peak values after processing with Delta2 to S1 and S2, and in S3 the maximum value of soil moisture is reached after processing with Delta1; the soil compaction degree has a similar humidity variation, namely: minimum values for S1 and S2 using Delta2 and for S3 following the use of Delta1.

Analyzing the impact of active parts on soil depth, some conclusions can be drawn (Table 3 and Figure 5-9): apparent density (Da) records minimum values when using Delta2 for all three depths (6 cm, 12 cm, 18 cm); total porosity has an inverse variation such as that of apparent density: the highest values are found for all three depths when working with Delta2; and soil moisture values respect the same law that: for all three depths the maximum value occurs after processing with Delta2; the soil compaction degree has a similar variation, that is, the smallest values are recorded at all depths when working with Delta2; when working with Delta2 active parts, all physico-mechanical soil indicators have optimal values regardless of the working depth; the same legality is preserved (with few exceptions) and when analyzing the impacts of the vibro-combinator active part on the soil types contained in the experimental field.

Table 3

Results for the soil physical and mechanical properties (values are expressed as mean ± standard deviation) for the interaction factor Soil*h*Device (CTRL, Gama, Delta1, Delta2)

Device*h*Soil	Soil moisture (%)	Bulk Density (g/cm^3)	Total Porosity (%)	Soil compression (%)	Water retention (m^3/ha)
CTRL.06.S1	16.18j±0.09	1.50cde±0.02	42.18hij±0.63	19.23cdef±1.20	361.69ef±4.29
CTRL.12.S1	20.25r±0.09	1.56ab±0.01	40.19kl±0.40	23.16a±0.77	150.91k±1.61
CTRL.18.S1	22.25t±0.09	1.41bc±0.03	45.71jk±1.32	12.62bc±2.52	186.58m±6.33
CTRL.06.S2	22.36s±0.16	1.46ab±0.01	43.91kl±0.29	15.92defg±0.55	404.69h±5.18
CTRL.12.S2	29.86r±0.16	1.45def±0.06	44.36ghi±2.22	15.19ab±4.25	141.00lm±4.31
CTRL.18.S2	33.93mn±0.15	1.74a±0.01	33.27l±0.40	36.29cd±0.77	421.44f±3.84
CTRL.06.S3	20.93u±0.28	1.75cd±0.01	32.89ij±0.40	37.05defgh±0.77	698.62op±6.12
CTRL.12.S3	28.23l±0.28	1.41defgh±0.02	45.64efghi±0.63	12.74ab±1.20	86.92k±1.59

Device*h*Soil	Soil moisture (%)	Bulk Density (g/cm³)	Total Porosity (%)	Soil compression (%)	Water retention (m³/ha)
CTRL.18.S3	35.03mn±0.28	1.63cdef±0.19	37.31ghij±7.27	28.56cde ±13.92	343.31g ±40.44
Delta1.06.S1	10.25f±0.19	1.31defgh±0.06	49.81efghi±2.16	1.61fghi±4.27	186.63hi±10.22
Delta1.12.S1	20.05v±0.19	1.69fghi±0.17	34.87defg±6.51	33.24defgh±12.47	568.50q±57.85
Delta1.18.S1	22.15g±0.19	1.44defg±0.02	44.71fghi±0.80	11.68efgh±1.59	192.88ij±2.54
Delta1.06.S2	21.75e±0.19	1.48defg±0.02	43.17fghi±0.80	14.80fghi±1.59	529.47b±6.80
Delta1.12.S2	28.75mno±0.19	1.52fghi±0.02	41.41defg±0.63	20.73defgh±1.20	607.34no±6.89
Delta1.18.S2	31.25h±0.19	1.39defgh±0.01	46.54efghi±0.34	8.07fgh±0.68	179.45j±1.41
Delta1.06.S3	21.03f±0.28	1.46defgh±0.03	44.04fghi±1.11	13.09ghi±2.19	548.55c±11.79
Delta1.12.S3	28.43u±0.28	1.54defgh±0.03	40.83efghi±1.12	21.83efgh±2.16	717.94p±19.57
Delta1.18.S3	35.33g±0.28	1.35efgh±0.03	48.17efgh±1.24	4.84fghi±2.46	175.88j±5.73
Delta2.06.S1	22.03i±0.28	1.19kl±0.01	54.17ab±0.38	-9.11kl±0.76	149.62k±2.42
Delta2.12.S1	23.13de±0.28	1.45defgh±0.04	44.42efghi±1.47	12.33ghi±2.90	498.59b±16.30
Delta2.18.S1	25.93no±0.28	1.48hij±0.02	43.27cde±0.72	14.58hij±1.42	961.56nop±13.47
Delta2.06.S2	23.83hi±0.28	1.18l±0.01	54.68a±0.40	-10.14l±0.80	144.60k±2.36
Delta2.12.S2	29.43a±0.28	1.44defg±0.06	44.81fghi±2.16	11.58ghi±4.26	506.86a±24.65
Delta2.18.S2	34.33k±0.28	1.46ijk±0.04	43.85bcd±1.36	13.44ij±2.68	821.35no±24.74
Delta2.06.S3	20.83i±0.28	1.16l±0.01	55.42a±0.37	-11.62l±0.75	146.23kl±2.60
Delta2.12.S3	28.03m±0.28	1.49efgh±0.02	42.79efgh±0.81	15.53ghi±1.59	908.47n±11.63
Delta2.18.S3	34.73op±0.28	1.45ghi±0.06	44.42def±2.16	12.31jk±4.26	893.03nop±41.97
Gama.06.S1	16.25pq±0.19	1.22l±0.02	53.05a±0.70	-7.77l±1.43	755.55p±13.88
Gama.12.S1	17.55i±0.19	1.15kl±0.01	56.00ab±0.41	-12.79l±0.83	142.96kl±2.15
Gama.18.S1	18.65cd±0.19	1.19kl±0.02	54.33a±0.65	-9.36l±1.31	405.10de±9.42
Gama.06.S2	21.52q±0.15	1.21l±0.02	53.62a±0.70	-8.94l±1.43	766.76p±15.14
Gama.12.S2	31.42bc±0.15	1.22jkl±0.02	53.08abc±0.60	-6.84l±1.20	413.25d±8.82
Gama.18.S2	36.22bc±0.15	1.18kl±0.01	54.90ab±0.55	-10.52l±1.12	394.34de±8.03
Gama.06.S3	20.93q±0.28	1.19l±0.02	54.20a±0.64	-10.11l±1.30	744.34p±12.74
Gama.12.S3	28.23b±0.28	1.21kl±0.02	53.75ab±0.65	-8.20l±1.31	399.72d±8.70
Gama.18.S3	35.03q±0.28	1.24l±0.02	52.37a±0.66	-6.40l±1.34	780.73op±14.00

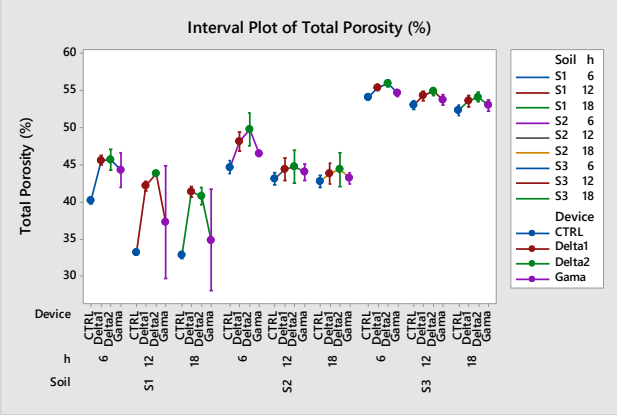

Fig. 5 - Interval plot for total porosity (from three-way ANOVA) for soil types (factor Soil), depth (factor h) and active parts (factor Device)

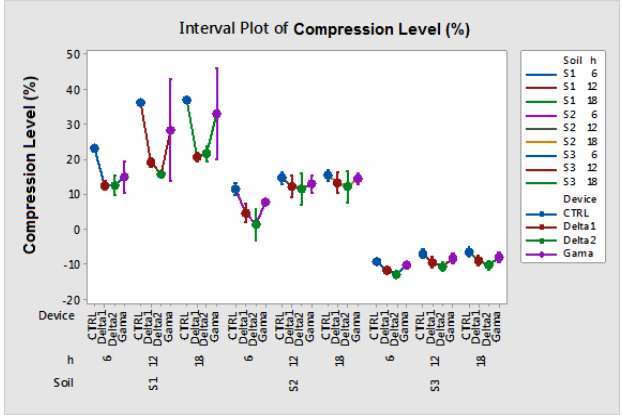

Fig. 6 - Interval plot for compression level (from three-way ANOVA) for soil types (factor Soil), depth (factor h) and active parts (factor Device)

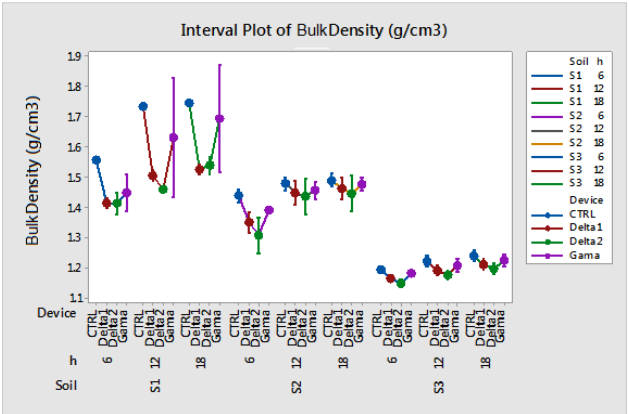

Fig. 7 - Interval plot for bulk density (from three-way ANOVA) for soil types (factor Soil), depth (factor h) and active parts (factor Device)

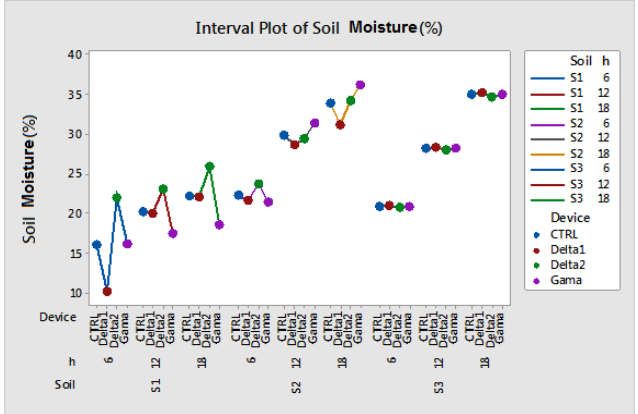

Fig. 8 - Interval plot for soil moisture (from three-way ANOVA) for soil types (factor Soil), depth (factor h) and active parts (factor Device)

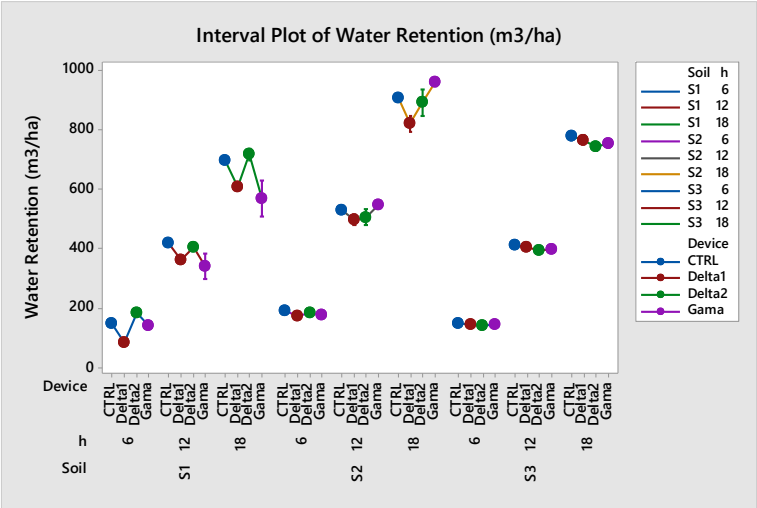

Fig. 9 - Interval plot for water retention (from three-way ANOVA) for soil types (factor Soil), depth (factor h) and active parts (factor Device)

Multivariate analysis

To evaluate the vibro-combinators soil tillage performances were studied the variables: apparent density (g/cm^3), total porosity (%) and soil compression (%). To evaluate the soil environmental impact of the vibro-combinators were considered the variables: soil moisture (%) and water retention (m^3/ha). In order to assess simultaneously the vibro-combinators soil tillage performances and environmental impact, was involved the multivariate analysis: principal component analysis (PCA) and multivariate analysis of variance (MANOVA, P = 0.05). The PCA and MANOVA were done separately for each soil type S1, S2 and S3. The PCA method involved as input data the variables correlation matrix and between sample groups algorithm. The MANOVA algorithm used as input data the first two principal components (PCs) coordinates of the group samples. The group samples were described by the interaction factor Device*h (i.e. active parts*depth).

For all soil types the first two PCs present eigenvalues greater than unity and a cumulative percentage of explained variance greater than 95.0%. Due to this reason these PCs are sufficient to describe the experiment with statistical significance.

The PCAs biplots gathers in the same graphical representation the samples scores and variable loadings (Fig. 10-12). The sample groups are marked by points inside a convex hull and the variables are represented by vectors with the staring points in the coordinate system origin. The variable vectors end points show the direction that describes the highest abundance (or levels) of the corresponding variables. This means that the group samples placed in the one vector direction (marked by its end point), have high abundance/level of that variable. When the sample groups are placed in the opposite direction, they have lowest abundance/levels for that variable. Analysing Fig. 10-13, for the soil type S1, the PCA biplot prescribes (table 4-6).

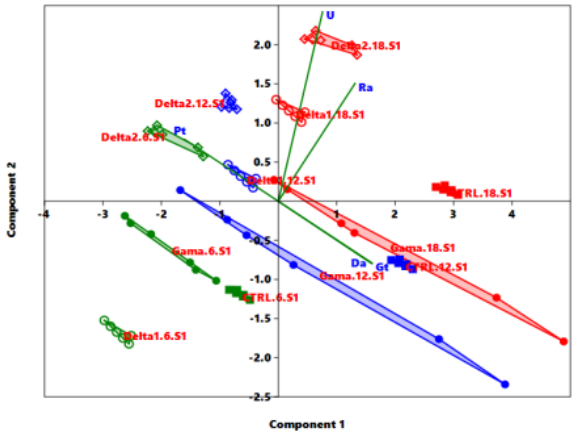

Fig. 10 - Principal component analysis (PCA) biplot for different depths (factor h) and for the three active parts (factor Device) for soil type S1

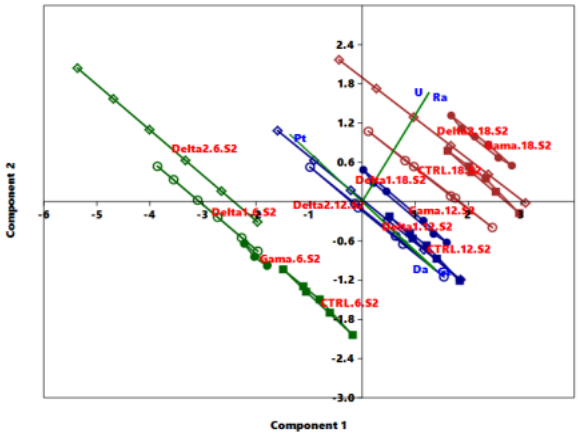

Fig. 11 - Principal component analysis (PCA) biplot for different depths (factor h) and for the three active parts (factor Device) for soil type S2

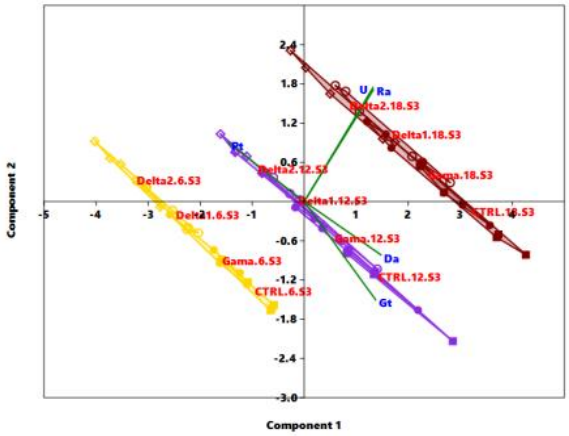

Fig. 12 - Principal component analysis (PCA) biplot for different depths (factor h) and for the three active parts (factor Device) for soil type S3

Table 4

Statistical significance values of multivariate analysis of variance (MANOVA, P = 0.05) for the soil type S1.

MANOVA	CTRL.6.S1	Delta1.6.S1	Delta2.6.S1	Gama.6.S1	CTRL.12.S1	Delta1.12.S1	Delta2.12.S1	Gama.12.S1	CTRL.18.S1	Delta1.18.S1	Delta2.18.S1	Gama.18.S1
CTRL.6.S1		0.000	0.000	2.239	0.000	0.000	0.000	0.000	0.000	0.000	0.000	0.000
Delta1.6.S1	0.000		0.000	0.000	0.000	0.000	0.000	0.000	0.000	0.000	0.000	0.000
Delta2.6.S1	0.000	0.000		0.000	0.000	0.000	0.000	0.000	0.000	0.000	0.000	0.000
Gama.6.S1	2.239	0.000	0.000		0.000	0.000	0.000	0.000	0.000	0.000	0.000	0.000
CTRL.12.S1	0.000	0.000	0.000	0.000		3.940	0.001	0.002	0.000	0.000	0.000	0.000
Delta1.12.S1	0.000	0.000	0.000	0.000	3.940		0.001	0.003	0.000	0.000	0.000	0.000
Delta2.12.S1	0.000	0.000	0.000	0.000	0.001	0.001		0.000	0.000	0.000	0.000	0.000
Gama.12.S1	0.000	0.000	0.000	0.000	0.002	0.003	0.000		0.000	0.000	0.000	0.000
CTRL.18.S1	0.000	0.000	0.000	0.000	0.000	0.000	0.000	0.000		0.241	0.000	0.000
Delta1.18.S1	0.000	0.000	0.000	0.000	0.000	0.000	0.000	0.000	0.241		0.000	0.000
Delta2.18.S1	0.000	0.000	0.000	0.000	0.000	0.000	0.000	0.000	0.000	0.000		0.000
Gama.18.S1	0.000	0.000	0.000	0.000	0.000	0.000	0.000	0.000	0.000	0.000	0.000	

Table 5

Statistical significance values of multivariate analysis of variance (MANOVA, P = 0.05) for the soil type S2.

MANOVA	CTRL.6.S2	Delta1.6.S2	Delta2.6.S2	Gama.6.S2	CTRL.12.S2	Delta1.12.S2	Delta2.12.S2	Gama.12.S2	CTRL.18.S2	Delta1.18.S2	Delta2.18.S2	Gama.18.S2
CTRL.6.S2		0.793	0.001	0.352	0.000	0.000	0.000	0.000	0.000	0.000	0.000	0.000
Delta1.6.S2	0.793		0.001	2.592	0.000	0.000	0.000	0.000	0.000	0.000	0.000	0.000
Delta2.6.S2	0.001	0.001		0.000	0.000	0.000	0.000	0.000	0.000	0.000	0.000	0.000
Gama.6.S2	0.352	2.592	0.000		0.000	0.000	0.000	0.000	0.000	0.000	0.000	0.000
CTRL.12.S2	0.000	0.000	0.000	0.000		0.069	13.997	0.004	0.000	0.000	0.000	0.000
Delta1.12.S2	0.000	0.000	0.000	0.000	0.069		0.327	0.000	0.000	0.000	0.000	0.000
Delta2.12.S2	0.000	0.000	0.000	0.000	13.997	0.327		0.002	0.000	0.000	0.000	0.000
Gama.12.S2	0.000	0.000	0.000	0.000	0.004	0.000	0.002		0.000	0.000	0.000	0.000
CTRL.18.S2	0.000	0.000	0.000	0.000	0.000	0.000	0.000	0.000		0.000	0.938	0.000
Delta1.18.S2	0.000	0.000	0.000	0.000	0.000	0.000	0.000	0.000	0.000		0.000	0.000
Delta2.18.S2	0.000	0.000	0.000	0.000	0.000	0.000	0.000	0.000	0.938	0.000		0.002
Gama.18.S2	0.000	0.000	0.000	0.000	0.000	0.000	0.000	0.000	0.000	0.000	0.002	

Table 6

Statistical significance values of multivariate analysis of variance (MANOVA, P = 0.05) for the soil type S3.

MANOVA	CTRL.6.S3	Delta1.6.S3	Delta2.6.S3	Gama.6.S3	CTRL.12.S3	Delta1.12.S3	Delta2.12.S3	Gama.12.S3	CTRL.18.S3	Delta1.18.S3	Delta2.18.S3	Gama.18.S3
CTRL.6.S3		0.957	0.210	42.092	0.000	0.000	0.000	0.000	0.000	0.000	0.000	0.000
Delta1.6.S3	0.957		21.324	3.674	0.000	0.000	0.000	0.000	0.000	0.000	0.000	0.000
Delta2.6.S3	0.210	21.324		0.564	0.000	0.000	0.000	0.000	0.000	0.000	0.000	0.000
Gama.6.S3	42.092	3.674	0.564		0.000	0.000	0.000	0.000	0.000	0.000	0.000	0.000
CTRL.12.S3	0.000	0.000	0.000	0.000		1.358	1.110	2.199	0.000	0.000	0.000	0.000
Delta1.12.S3	0.000	0.000	0.000	0.000	1.358		36.244	3.884	0.000	0.000	0.000	0.000
Delta2.12.S3	0.000	0.000	0.000	0.000	1.110	36.244		2.363	0.000	0.000	0.000	0.000
Gama.12.S3	0.000	0.000	0.000	0.000	2.199	3.884	2.363		0.000	0.000	0.000	0.000
CTRL.18.S3	0.000	0.000	0.000	0.000	0.000	0.000	0.000	0.000		2.540	1.089	0.278
Delta1.18.S3	0.000	0.000	0.000	0.000	0.000	0.000	0.000	0.000	2.540		4.215	0.228
Delta2.18.S3	0.000	0.000	0.000	0.000	0.000	0.000	0.000	0.000	1.089	4.215		1.277
Gama.18.S3	0.000	0.000	0.000	0.000	0.000	0.000	0.000	0.000	0.278	0.228	1.277	

CONCLUSIONS

The advantages of using vibro-combinators are: perfect preparation of seedbed in difficult working conditions and preservation of soil moisture. Such important factors can ensure fast, uniform and early germination of seeds, these requirements standing at the basis of abundant harvests. The research investigated the soil tillage performances and the environmental impact of several active parts of the vibro-combinators, at certain soil depths and soil types.

The multivariate analysis allowed assessing for each soil type which active part performs both best soil tillage and environmental protection of the soils. From the technical point of view, the 6 cm depth is the most important to soil tillage for crop production. For this depth the active parts of the vibro-combinator: Delta2 and Delta1 are those that perform both best soil tillage and environmental protection of the studied soils.

ACKNOWLEDGEMENTS

This work was supported by POSCCE based on 1CLT/800.024/21.05.2014 financing program.

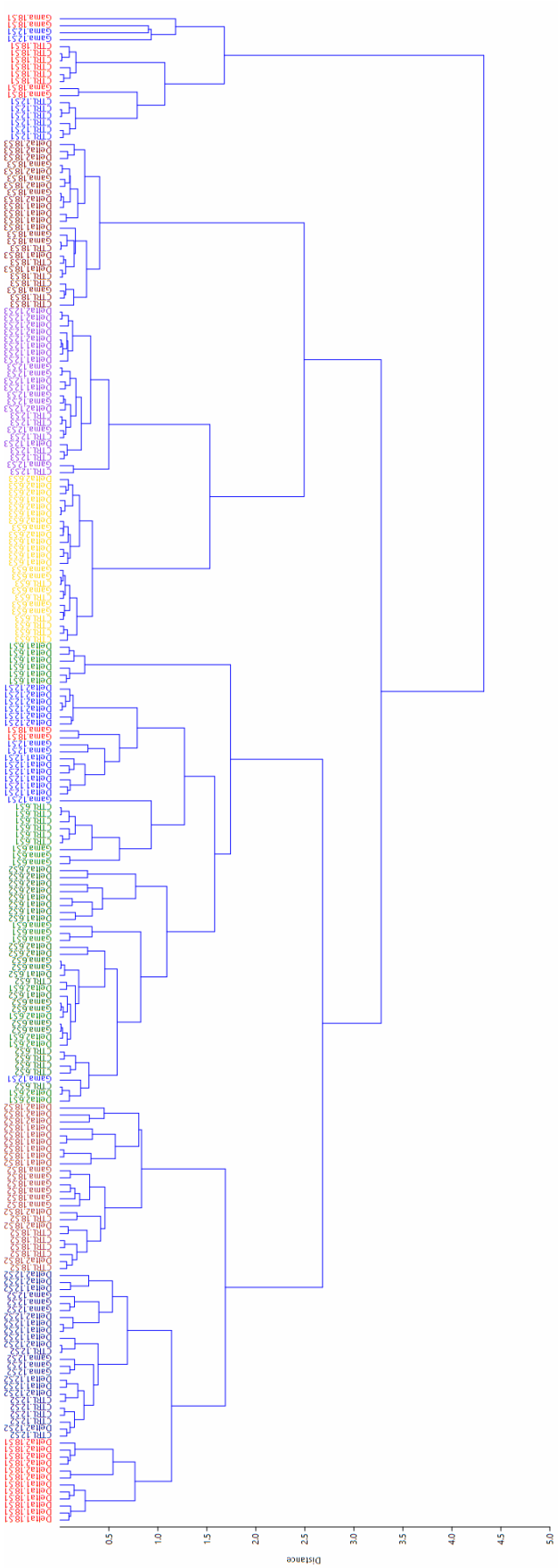

Fig. 13 - Hierarchical cluster analysis (HCA) dendrogram with the clustering information for different types of soils, different depth 6, 12 and 18 cm and for the three active parts: Gama, Delta1, Delta2

REFERENCES

[1] Benites J., (2000), Manual on integrated soil management and conservation practices The Challenge of Agricultural Sustainability for Asia and Europe. *FAO Land and Water Bulletin*, No.8, pp. 1-4;

[2] Biriş S.Şt., Bungescu S.T., Manea D., Boja N., Cilan T.F., Martin R., (2015), State of art approach to vibro-combinators soil tillage implements construction, *Proceedings of 43. International Symposium Agricultural Engineering, Actual Tasks on Agricultural Engineering*, vol. 43, pp. 177-188;

[3] Boja N., Boja F., Teuşdea A., Carţiş M., Puşcaş S., (2012), Study on the Impact of Soil Processing on Some Physico-mechanical Properties, *Journal of Environmental Protection and Ecology (JEPE)*, vol. 13, no.2A/2012, pp. 941-950;

[4] Boja N., Boja F., Teusdea A., Dărău P. A., Maior C., (2013), Research regarding the uniformity of sprinkler irrigation, *Journal of Environmental Protection and Ecology (JEPE)*, vol.14, no.4 / 2013, pp. 1661-1672;

[5] Boja N., Boja F., Teusdea A., Dărău P.A., Maior C., (2016), Soil porosity and compaction as influenced by tillage methods, *Journal of Environmental Protection and Ecology (JEPE)*, vol. 17, no.4 / 2016, pp. 1315–1323;

[6] Boyraz D., Atilgan M. C., (2014), Use of Mechanical Properties for Evaluating Engineering Behaviour of Soils with Different Textural Classes, *Journal of Environmental Protection and Ecology (JEPE)*, Vol. 15, No 1, pp. 78–84;

[7] Calistru A. E., Topa D., Rostek J., Puschmann D. U., Peth S., Horn R., Jitareanu G., (2016), Soil Physical Properties and Winter Wheat Yield as Affected by Different Tillage Systems, *Journal of Environmental Protection and Ecology (JEPE)*, Vol. 17, No 3, p. 978–989;

[8] Căproiu Şt. et al, (1982), *Agricultural machinery for soil tillage, seeding and crop maintenance*. Didactic and Pedagogic Publishing House, Bucharest;

[9] Cardei P., Rigon L., Muraru V.M., Muraru-Ionel C., Constantin N., David A., (2015), A method of calculating the optimal speed of operation for vibro-cultivators, *Proceedings of 43. International Symposium Agricultural Engineering, Actual Tasks on Agricultural Engineering*, vol. 43, p 211-221;

[10] Celik H., Kursat et al, (2010), Modal analysis of agricultural machineries using finite element method: a case study for a V-belt pulley of a fodder crushing machine, *Journal of Food*, Agriculture & Environment (JFAE), 8 (3-4). pp. 439-446;

[11] Hammer O., Harper D. A. T., Ryan P. D. Past, (2001), Paleontological Statistics Software Package for Education and Data Analysis. *Palaeontologia Electronica*, vol.4 (1), 9;

[12] Neve S.D. and Hofman G.; (2000), Influence of soil compaction on carbon and nitrogen mineralization of soil organic matter and crop residues, *Biol Fertil Soils,* vol. 30, pp. 544–549;

[13] Petrescu H. A., Martin R., Vlasceanu D., Hadar A., Parausanu I., Dan R., (2015), Modal analysis using fem of three active parts for an agricultural machine, *Proceedings of 43. International Symposium Agricultural Engineering, Actual Tasks on Agricultural Engineering*, vol.43, pp. 201-209;

[14] Pisante M., Corsi S., Kassam A., (2010), The Challenge of Agricultural Sustainability for Asia and Europe. *Transist. Stud. Rev.*, Springer, Vol. 17, No.4, pp. 662-667;

[15] Shierlaw J. and Alston A.M., (1984), Effect of soil compaction on root growth and uptake of phosphorus, *Plant and soil*, vol.77, pp.15-28;

[16] Spoljar A., Kisic I., Birkas M., Gunjaca J., Kvaternjak I., (2011), Influence of Crop Rotation, Liming and Green Manuring on Soil Properties and Yields. *Journal of Environmental Protection and Ecology (JEPE)*, Vol. 12, No 1, p. 54–69;

[17] Spoljar A., Kisic I., Birkas M., Kvaternjak I., Marencic D., Orehovacki V., (2009), Influence of tillage on soil properties, yield and protein content in maize and soybean grain, *Journal of Environmental Protection and Ecology (JEPE)*, Vol. 10, No 4, p. 1013–1031;

[18] Ţenu I., Jităreanu G., Muraru-Ionel C., Cojocariu P., Muraru V.M., (2009), The impact of mechanization technologies on soil, *Environmental Engineering and Management Journal*, Vol. 8, No.5, p. 1263-1267;

[19] Vidrean D., Boja F., Teuşdea A., Dragomir C., Boja N., (2018), Assessment of soil impact after using a vibro-combinator, *Proceedings of 46. International Symposium Agricultural Engineering*, Actual Tasks on Agricultural Engineering, Opatija, Croatia, 27 February - 01 March 2018, vol. 46, p 169-179;

[20] ***http://www.kyplot.software.informer.com.

THE NUMERICAL SIMULATION OF HEAT AND MASS TRANSFER PROCESSES IN TUNNELING AIR VENTILATION SYSTEM IN POULTRY HOUSES
/
ЧИСЕЛЬНЕ МОДЕЛЮВАННЯ ПРОЦЕСІВ ТЕПЛО- І МАСООБМІНУ ПРИ ТУНЕЛЬНІЙ СИСТЕМІ ВЕНТИЛЯЦІЇ ПОВІТРЯ У ПТАШНИКАХ

Prof. Ph.D. Eng. Gorobets V.G.[1)], Senior lecturer Ph.D. Eng. Trokhaniak V.I.[1)], Senior lecturer Ph.D. Eng. Antypov I.O.[1)], Assoc. Prof. Ph.D. Eng. Bohdan Yu.O.[2)]
[1)] National University of Life and Environmental Sciences of Ukraine;
[2)] Kherson State Maritime Academy
E-mail: Trohaniak.v@gmail.com

Keywords: *numerical simulation, heat and mass transfer processes, velocity field, poultry house, cooling system*

ABSTRACT

The mathematical modeling was provided for heat and mass transfer during the air ventilation in poultry houses. Air ventilation systems based on the injectors or moisture pads is well known. Our system is different from the existing ones by using special construction heat exchangers. The cooling medium in heat exchangers special construction is the water from the underground wells. The ANSYS Fluent software is used for receiving numerical simulation velocity fields, temperature and pressure in poultry house. The recommendations are made for the choice of poultry house's air ventilating system.

РЕЗЮМЕ

Проведено математичне моделювання процесів тепло- і масопереносу при вентиляції повітря в птахівничих приміщеннях. На відміну від існуючих систем охолодження припливного повітря, що базуються на використанні форсунок або зволожуючих касет, запропоновано нову систему охолодження з використанням теплообмінних апаратів спеціальної конструкції, в яких в якості охолоджувача використовується вода підземних свердловин. В результаті чисельного моделювання отримані поля швидкостей, температур і тисків у пташнику використовуючи програмний продукт ANSYS Fluent. Дано рекомендації по вибору конструкції систем вентиляції в пташниках.

INTRODUCTION

The modern cooling systems for supplying air in poultry houses *(Donald O.J., 2012; Czarick M. and Fairchild B., 2014; Hui, X., 2018)* are based on the usage of spraying or evaporating systems. The principle of adiabatic cooling is a base for both systems *(Kim K. et.al., 2008)*, when water transfers from liquid into gaseous state through the free evaporating. This process allows decreasing the external heated air temperature in poultry house.

The aerosol or spray appears in systems with injectors or disc sprayers. This spray consists of water drops of small diameter (*Vyshnevskyi E.P., 2004*). The injectors may be of two types: lower or high pressure. When used for air cooling, the injectors' method requires the presence of a special system of water treatment – cleaning, filtering, etc., because contamination of nozzles quickly disables the operation of injectors. Besides, the operation of such system needs high power consumption.

The pad usage is necessary for steam forced cooling. The air enters through the channels system with humid walls. Such pad's working principles were described in detail *(Hulzebosch J., 2005)*. The cooling pads are used in the terms of high temperature for external air, which increases +37°C. The pad method is the most effective in the modern time. The cooling process for supplied air in the moisture pads was described in detail in *Campbell J. et.al. (2007)* works. The aerodynamic resistance and the high price of the units are the main lacks for this method. The contamination of pad's channel by dusts during the operation process is one of the lacks for the present method. It is necessary to talk about the mould formation on the contaminated surfaces. This mould adds components into supplied air. These components favour the poultry diseases at the high temperature. The algae may appear on the pad's surface in the case of non-time cleaning. The indicated factors encourage the frequent replacement of pads in the first year of operation. The maximum life

of the pads does not exceed 10 years and depends on the quality of water, preventive work and special operating conditions. The effectiveness of pad cooling to a large extent also depends on the tightness of the poultry house.

There are some systems for air ventilating equipment. It depends upon the location of vent door and air exhauster *(Donald O.J., 2012)*. The tunnel ventilation is the most energetically effective as per analysis among the existing systems. The tunnel system was chosen as the basic during the modeling and providing the numerical simulation process for heat exchanging and mass transfer in the poultry houses *(Chui E.H. and Raithby G.D. 2013)*.

The CFD simulation was provided in the works *(Blanes-Vidal V. et. al., 2008; Bustamante E., et. al., 2008)* about the poultry houses with the side ventilation system. The authors *(Blanes-Vidal V., et. al., 2008; Bustamante E., et.al., 2008)* considered the method of side mechanical ventilation system as the most effective in comparison with other methods. It allows decreasing the heat stress and increasing poultry productivity during the summer period. The velocities distribution pressures and temperature for air flow for side ventilating systems were obtained from the results of numerical simulation. The results of numerical simulation were compared with the data of experimental researches, with a difference of 12 %.

The conclusion was drawn in the results of authors' researches *(Blanes-Vidal V. et. al., 2008; Bustamante E. et.al., 2008)* namely that the lack of air and the absence of cooling system generate the poultry's heat stress. It is accompanied by the productivity decrease during the poultry growing. The air-flow non-homogeneity and stagnation zone existence in the areas with poultries decrease the terms of poultry's thermal regulation.

The influence of maximal air exchange and intensity for poultry cooling through the air high velocities in the poultry houses during the summer period of the year was researched in the paper *(Zajicek M. and Kic P., 2013).* The Ansys Fluent software was used for the numerical simulation in poultry house in different configurations of air ventilating system's inlet and outlet holes. The dimensions and forms of inlet holes and their locations on poultry houses wall were changed during the simulation. The influence of these factors on the basic data of air exchange was analyzed. The data were put as per technical standards for keeping poultry. The recommendations were proposed for the choice of the most effective configuration of inlet velocity profile form and optimal temperature for internal area of poultry house by the researches results.

The analysis of the existing researches for numerical simulation of heat and mass transfer during the ventilation of poultry houses in the summer period have showed the direction for improving the existing ventilation system. It is necessary to develop new air ventilating systems. These systems differ from the traditional system of air supply with injectors and moisture pads usage.

MATERIALS AND METHODS

The new technique for the cooling of external air in poultry houses' ventilating system was proposed in this paper. This technique is based on the water usage from the underground well with use of heat exchangers - recuperators. Heat exchangers, smooth-tube or finned shell-and-tube heat exchangers, as well as plate heat exchangers with water-air heat carriers, can be used, taking into account the conditions under which they operate *(Gorobets, V.G., 2006)*. This technique makes it possible to reduce the temperature of the outside air without increasing its relative humidity, in contrast, for example, with cooling systems with water spraying. The aim of this paper is to propose theoretical researches on the heat and mass transfer in poultry houses. These processes run inside the accommodation and run through the external barrier. The proposed system can be used to keep a normalized microclimate in a poultry house and, for example, to grow broiler chickens with floor-keeping (10 thousand heads).

The poultry house of standard type has the following main characteristics:

- Building data- 90x20x5m
- External barriers are made of claydite-concrete with 0.2 m thickness.
- External air temperature in summer period +40^{o}C.
- Building volume 7200 m^{3}.
- Internal air temperature as per norm +17^{o}C

The schematic top view is shown in Fig. 1 a, Fig. 1 b side view by shown stall space of poultry house with ventilating equipment. The proposed air ventilating system works in the following way. The heated air runs from the external medium into the house *1* through heat exchangers *4*. They are installed on the vent holes *2*. Air runs through all heat exchangers sections *4*; after that, cooled air enters into the house. The waste air removes through the individual ventilating units *3*. The movement of air in the accommodation *1* is

due to the difference in atmospheric pressure at the inlet to the heat exchanger *4* and the ventilation units *3* at the outlet of them. The cold water runs from the well *5* through pipeline *7* by the pump *6* to heat exchanger *4*. The heated water is removed through the outlet nozzle *8*. The heated water can be used for the internal needs.

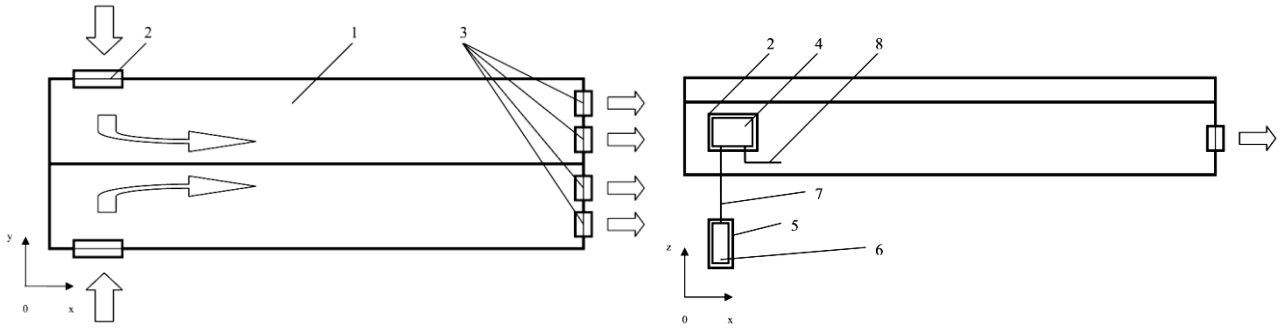

a) ***b)***

Fig. 1 - Scheme of air-running in poultry house

a) top view; b) side view

1 – poultry house building; 2 – vent doors; 3 – air exhausters; 4 – heat exchanger recuperator; 5 – well; 6 – pump; 7 – pipeline; 8 – outlet nozzle

Numerical mathematical simulation of hydrodynamic and heat and mass transfer processes in an industrial greenhouse was conducted. For this purpose, computer-generated simulation method based on ANSYS Fluent software was used. Navier-Stokes equations *(Khmelnik S.I., 2018)* and energy-transfer equations for convective currents are the basis for this mathematical model. Spalarta-Allmarasa turbulence model *(Spalart P.R. and Rumsey C.L., 2007; Allmaras S.R. et.al., 2012; Bailly C. and Comte-Bello G., 2015)* and Discrete Ordinates (DO) radiation model *(ANSYS, 2011)* were used for the calculations. The computation was conducted using heating and ventilating systems in buildings during winter time, taking into account solar radiation.

Navier-Stokes equation:

$$\left.\begin{aligned}
\rho\left(\frac{\partial u}{\partial t}+u\frac{\partial u}{\partial x}+v\frac{\partial u}{\partial y}+w\frac{\partial u}{\partial z}\right)&=-\frac{\partial p}{\partial x}+\mu\left(\frac{\partial^2 u}{\partial x^2}+\frac{\partial^2 u}{\partial y^2}+\frac{\partial^2 u}{\partial z^2}\right),\\
\rho\left(\frac{\partial u}{\partial t}+u\frac{\partial u}{\partial x}+v\frac{\partial u}{\partial y}+w\frac{\partial u}{\partial z}\right)&=-\frac{\partial p}{\partial y}+\mu\left(\frac{\partial^2 u}{\partial x^2}+\frac{\partial^2 u}{\partial y^2}+\frac{\partial^2 u}{\partial z^2}\right),\\
\rho\left(\frac{\partial u}{\partial t}+u\frac{\partial u}{\partial x}+v\frac{\partial u}{\partial y}+w\frac{\partial u}{\partial z}\right)&=-\frac{\partial p}{\partial z}+\mu\left(\frac{\partial^2 u}{\partial x^2}+\frac{\partial^2 u}{\partial y^2}+\frac{\partial^2 u}{\partial z^2}\right),
\end{aligned}\right\} \quad (1)$$

where ρ – medium density, kg/m^3; μ – medium dynamic viscosity, Pa•s; p - pressure, Pa; u, v, w – velocity field of vectors; t – time, s.

A continuity equation:

$$\frac{\partial u}{\partial x}+\frac{\partial v}{\partial y}+\frac{\partial w}{\partial z}=0, \quad (2)$$

An energy-conservation equation:

$$\rho C_p\left(V_x\frac{\partial T}{\partial x}+V_y\frac{\partial T}{\partial y}+V_z\frac{\partial T}{\partial z}\right)=\frac{\partial}{\partial x}\left(\lambda\frac{\partial T}{\partial x}\right)+\frac{\partial}{\partial y}\left(\lambda\frac{\partial T}{\partial y}\right)+\frac{\partial}{\partial z}\left(\lambda\frac{\partial T}{\partial z}\right) \quad (3)$$

where T – point temperature, °K; λ – coefficient of medium heat transfer capacity, W / m • °K; C_p – specific heat capacity of a medium, J/kg • °K.

Boundary Conditions

Let us set boundary conditions (see Fig. 2 a) for ventilation openings on the front end wall:

$$\left.\begin{aligned}
&y'_{Si}\le y\le y''_{Si};\ z'_{Si}\le z\le z''_{Si};\ i=1,2...6;\ S_i\left(y=\pm M/2,x,z\right);\\
&W=W_{inlet};\ T=T_{env.}.
\end{aligned}\right\} \quad (4)$$

For ventilation openings on the sidewalls (see Fig. 2 b):

$$y'_{\varphi i}(z) \le y \le y''_{\varphi i}(z);\ z'_{\varphi i}(y) \le z \le z''_{\varphi i}(y);\ i = 1,2...7;\ \varphi_i(x = L, y, z);$$
$$W = W_{outlet};\ \left.\frac{\partial T}{\partial x}\right|_{x=L} = 0. \quad (5)$$

For ventilation openings on the back end wall, where fans are located (see Fig. 2 c):

$$x'_{Si} \le x \le x''_{Si};\ z'_{Si} \le z \le z''_{Si};\ i = 7,8...10;\ S_i(y = \pm M/2, x, z);$$
$$W = W_{inlet};\ T = T_{env.}. \quad (6)$$

Attachment conditions for heat carrying air on the front end wall (see Fig. 2 a):

$$-M/2 \le y \le M/2;\ 0 \le z \le H + h(y);\ 0 \le h(y) \le h_{max};$$
$$y \notin S_i(x = 0, y, z);\ i = 1,2...6;\ W = 0;\ T = T_{wall}. \quad (7)$$

Attachment conditions on the back end wall (see Fig. 2 b):

$$-M/2 \le y \le M/2;\ 0 \le z \le H + h(y);\ 0 \le h(y) \le h_{max};$$
$$y \notin \varphi_i(x = L, y, z);\ i = 1,2...7;\ W = 0;\ T = T_{wall}. \quad (8)$$

Attachment conditions on the sidewalls and the roof wall (see Fig. 2 c):

$$y = \pm M/2;\ 0 \le x \le L;\ 0 \le z \le H + h(y);\ y \notin S_i(y = \pm M/2, x, z);$$
$$z \notin S_i(y = \pm M/2, x, z);\ i = 7,8...10;\ W = 0;\ T = T_{wall}. \quad (9)$$

where $S_i(x \le 0, y, z)$ − the function that describes the boundaries of air inlet openings; $\varphi_i(x = L, y, z)$ − the function that describes the boundaries of air outlet openings; L – the length of greenhouse sidewalls, m; M – the width of the front and the back end wall, m; H – the height of the greenhouse, m; $h(y)$ – the function of roof wall height in section 0y, m; T_{wall} – wall temperature, °C; $T_{env.}$ – environment temperature, °C; W_{inlet} – inlet air velocity when entering the greenhouse, m/s; W_{outlet} – outlet air velocity when leaving the greenhouse, m/s.

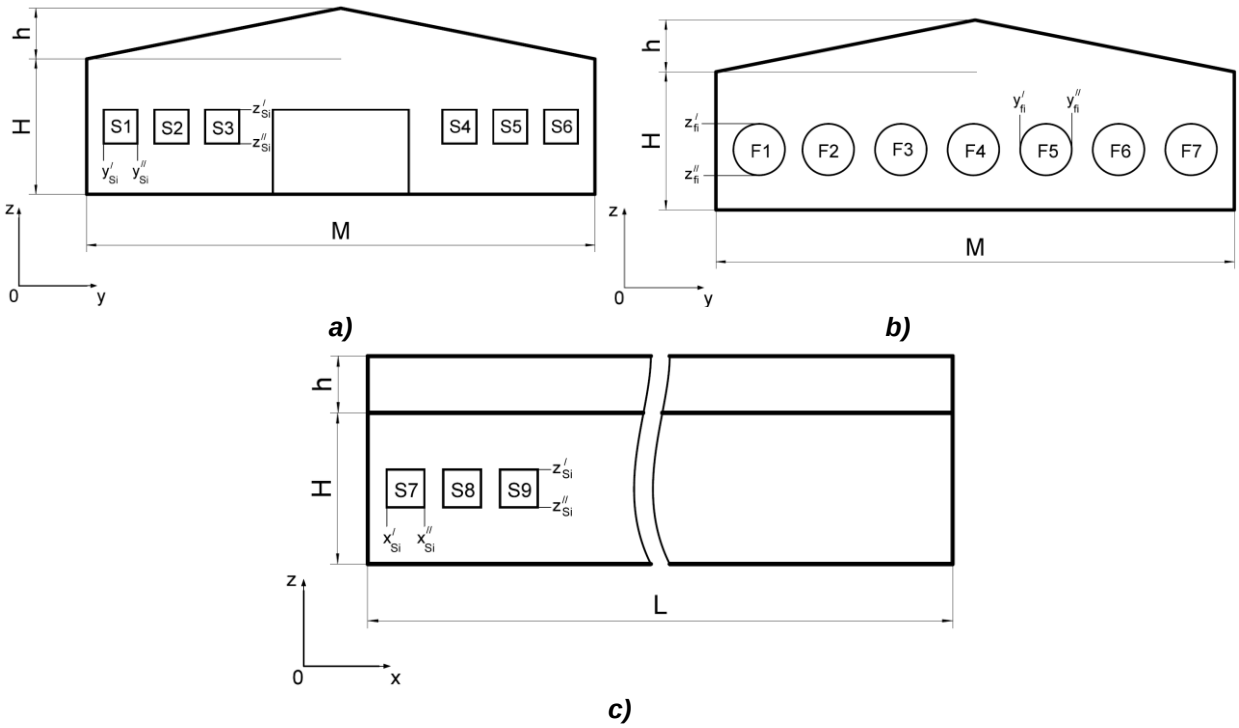

Fig. 2 - General view of poultry houses walls projection

a – front end wall; b – back end wall; c – side wall

Spalarta-Allmarasa turbulence model:

The transported variable in the Spalart-Allmaras model, ṽ, is identical to the turbulent kinematic viscosity except in the near-wall (viscosity-affected) region. The transport equation for the modified turbulent viscosity ṽ is:

$$\frac{\partial}{\partial t}(\rho\tilde{\nu})+\frac{\partial}{\partial x_i}(\rho\tilde{\nu}u_i)=G_\nu+\frac{1}{\sigma_{\tilde{\nu}}}\left[\frac{\partial}{\partial x_i}\left\{(\mu+\rho\tilde{\nu})\frac{\partial\tilde{\nu}}{\partial x_i}\right\}+C_{b2\rho}\left(\frac{\partial\tilde{\nu}}{\partial x_i}\right)^2\right]-Y_\nu+S_{\tilde{\nu}} \quad (10)$$

where G_v is the production of turbulent viscosity and Y_v is the destruction of turbulent viscosity that occurs in the near-wall region due to wall blocking and viscous damping. $\sigma_{\tilde{\nu}}$ and C_{b2} are the constants and v is the molecular kinematic viscosity. $S_{\tilde{\nu}}$ is a user-defined source term.

Discrete Ordinates radiation model:

The radiative transfer equation for an absorbing, emitting, and scattering medium at position $\vec{r}$ in the direction $\vec{s}$ is:

$$\frac{dI(\vec{r},\vec{s})}{ds}+(a+\sigma_s)I(\vec{r},\vec{s})=an^2\frac{\sigma T^4}{\pi}+\frac{\sigma_s}{4\pi}\int_0^{4\pi}I(\vec{r},\vec{s}')\Phi(\vec{s}\cdot\vec{s}')d\Omega' \quad (11)$$

where $\vec{r}$ – position vector, $\vec{s}$ – direction vector, $\vec{s}'$ – scattering direction vector, s – path length, α – absorption coefficient, n – refractive index, σ_s – scattering coefficient, σ – Stefan-Boltzmann constant (5,669·10^{-8} W/m^2·K^4), I – radiation intensity, which depends on position $(\vec{r})$ and direction $(\vec{s})$, Φ – phase function, Ω' – solid angle, $(\alpha+\sigma_s)s$ is the optical thickness or opacity of the medium. The refractive index n is important when considering radiation in semi-transparent media.

The discrete ordinates radiation model solves the radiative transfer equation (RTE) for a finite number of discrete solid angles, each associated with a vector direction fixed in the global Cartesian system *(x, y, z)*. The uncoupled implementation is sequential in nature and uses a conservative variant of the DO model called the finite-volume scheme *(Chui E.H. and Raithby G.D., 2013; Hassanzadeh P. et.al., 2008)*, and its extension to unstructured meshes *(Murthy J.Y. and Mathur S.R., 1998)*. In the uncoupled case, the equations for the energy and radiation intensities are solved one by one, assuming prevailing values for other variables.

The discrete ordinates model considers the radiative transfer equation in the direction $\vec{s}$ as a field equation.

Thus, equation 11 is written as:

$$\nabla\cdot(I(\vec{r},\vec{s})\vec{s})+(a+\sigma_s)I(\vec{r},\vec{s})=an^2\frac{\sigma T^4}{\pi}+\frac{\sigma_s}{4\pi}\int_0^{4\pi}I(\vec{r},\vec{s}')\Phi(\vec{s}\cdot\vec{s}')d\Omega' \quad (12)$$

ANSYS Fluent also allows the modeling of non-gray radiation using a gray-band model. The RTE for the spectral intensity $I_\lambda(\vec{r},\vec{s})$ can be written as *(Modest M.F., 2013)*

$$\nabla\cdot(I_\lambda(\vec{r},\vec{s})\vec{s})+(a_\lambda+\sigma_s)I_\lambda(\vec{r},\vec{s})=a_\lambda I_{b\lambda}+\frac{\sigma_s}{4\pi}\int_0^{4\pi}I_\lambda(\vec{r},\vec{s}')\Phi(\vec{s}\cdot\vec{s}')d\Omega' \quad (13)$$

Here λ is the wavelength, α_λ is the spectral absorption coefficient, and $I_{b\lambda}$ is the black body intensity given by the Planck function. The scattering coefficient, the scattering phase function, and the refractive index n are assumed independent of wavelength.

The non-gray DO implementation divides the radiation spectrum into N wavelength bands, which need not be contiguous or equal in extent. The wavelength intervals are supplied by you and correspond to values in vacuum (n=1). The RTE is integrated over each wavelength interval, resulting in transport equations for the quantity $I_\lambda\Delta\lambda$, the radiant energy contained in the wavelength band $\Delta\lambda$.

The behaviour in each band is assumed gray. The black body emission in the wavelength band per unit solid angle is written as:

$$\left[F(0\rightarrow n\lambda_2 T)-F(0\rightarrow n\lambda_1 T)\right]n^2\frac{\sigma T^4}{\pi} \quad (14)$$

where $F(0\rightarrow n\lambda T)$ is the fraction of radiant energy emitted by a black body *(Modest M.F., 2013)* in the wavelength interval from 0 to λ at temperature T in a medium of refractive index $n.\lambda_2$. and λ_1 are the wavelength boundaries of the band.

The total intensity $I(\vec{r},\vec{s})$ in each direction $\vec{s}$ at position $\vec{r}$ is computed using:

$$I(\vec{r},\vec{s}) = \sum_{k} I_{\lambda_k}(\vec{r},\vec{s})\Delta\lambda_k , \quad (15)$$

where the summation is over the wavelength bands.

Boundary conditions for the non-gray DO model are applied on a band basis.

The treatment within a band is the same as that for the gray DO model.

RESULTS

The finite element method is used for the numerical simulation of hydrodynamics and heat and mass transfer. The principle of this method is based on the approximate method for solving definition of a variational task. The notional of functional is used for the formulation of this task. The operator *I[f (x)]* is called a functional which was given on some set of functions f(x), if for each function *f(x)* it corresponds to a certain rule or law a certain numerical value *I=I[f (x)] (Dulnev G.N., 1990).*

The mesh building is made in the ANSYS Meshing mesh generator on the base platform Workbench. The method of local mesh control was used for the mesh building. The index of Orthogonal Quality *(Trokhanyak V.I. and Bogdan Yu.O., 2015)* equalled nearly 0.45. Minimum dimension of bound was 2.3×10^{-2} m.

The data of heat and mass transfer in the mesh of ANSYS Meshing were put in Table 1. They will be needed for the further calculation of heat exchange and mass transfer. The geometry was built in real dimensions. The quantity of elements and bounds are rather big during the mesh building. Considering big dimensions of the building, element's dimensions and bounds are not much increased through the limits of productive and design computer's capacity.

Table 1

The data for the building mesh of poultry house

Setting data	Poultry house
Indexes for mesh orthogonal quality	0.45
Element's quantity, [pcs]	1628712
Joints number, [pcs]	9303422
Angles curvature, [grad]	45
Method	Triangle
Element's maximum dimension, [m]	2.3
Bound's maximum dimension, [m]	4.6
Bound's minimal dimension, [m]	2.3×10^{-2}

Fig. 3 shows a constructed poultry house mesh from the frontal side. The mesh is slightly reduced (concentrated) near the holes of the inflow air relative to the rest of the wall area. These measures are applied for the improved calculation of hydrodynamics. In the section (Fig. 4), a mesh is clearly visible, so you can better assess the quality and disadvantages of the mesh itself. We also notice concentration of the mesh near the floor due to the location of the poultry on it.

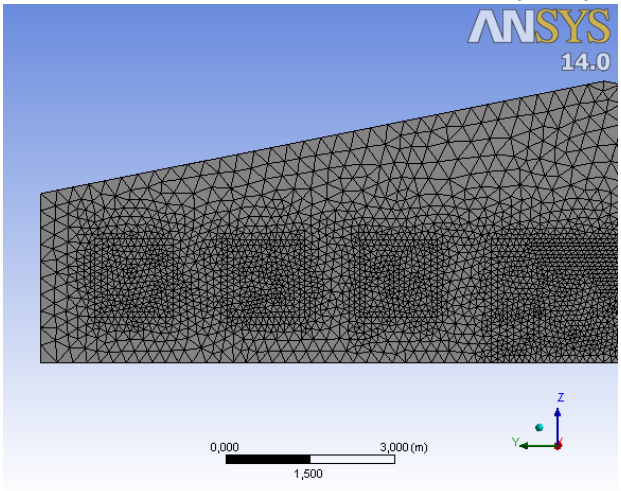

Fig. 3 - Front end wall

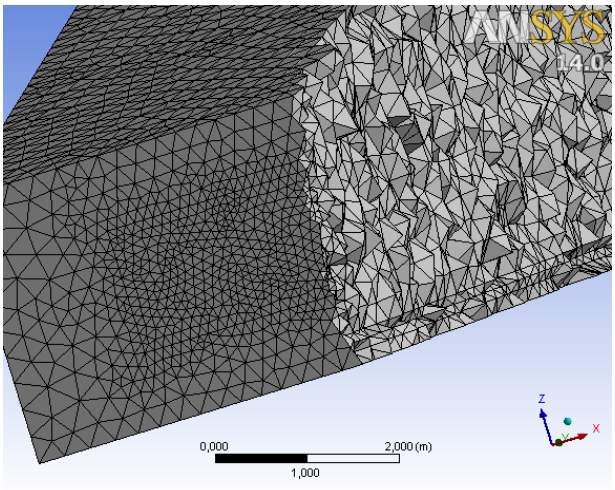

Fig. 4 - Back end wall's poultry house in section

The calculations' results of computer mathematic simulation for poultry house were given in Fig. 5-11.

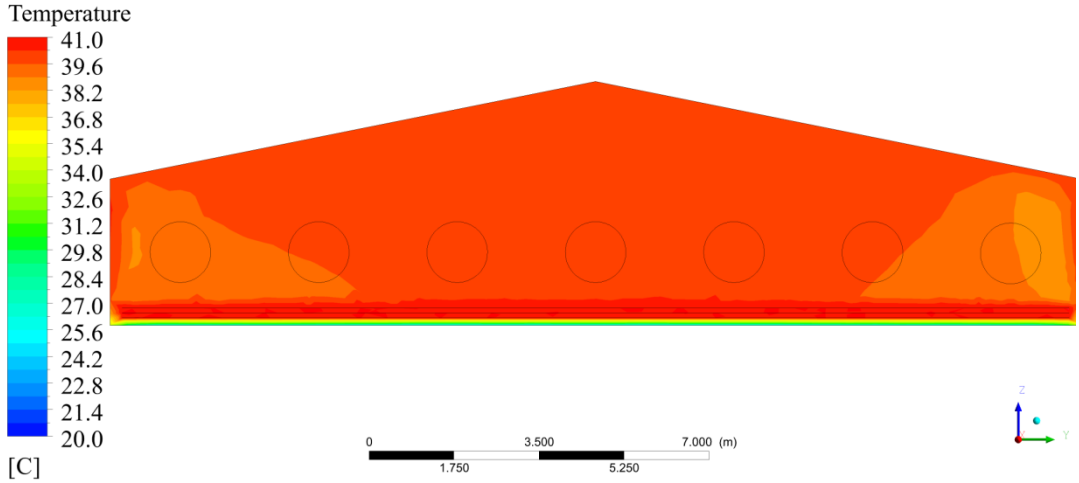

Fig. 5 - Temperature field in poultry houses of transverse section by centreline Oy on the distance 30 m from inlet, ºC

All calculations were made on the mass rate of 170 kg/s. Walls and floor are produced from claydite-concrete with 0.2 m thickness. The calculation was made twice without or with air cooling systems usage of water from the underground cells in heat exchangers recuperators. The external air and water are chosen as a medium in heat exchanger recuperator The temperature of the external air at the inlet to the heat exchanger is +40°C. Heat capacity of the heat exchanger is selected in such a way that at the outlet the temperature of the air is + 20°C. The cooling water coming from underground wells has a temperature of +10°C. The poultry locates in floor holding. It is a source for the heat output with the temperature +41ºC.

The high temperature without air cooling system has negative influence on poultry holding. You may decrease the temperature by ±2ºC using the high productive vents in the poultry houses. These terms cannot reach the standard microclimate in poultry-farm. The temperature field distribution with inlet external air temperature +40ºC is shown in Fig. 3, without heat exchanger recuperators' usage as air cooling system elements. The maximum temperature area is in the place of poultry floor holding as shown in Fig. 5.

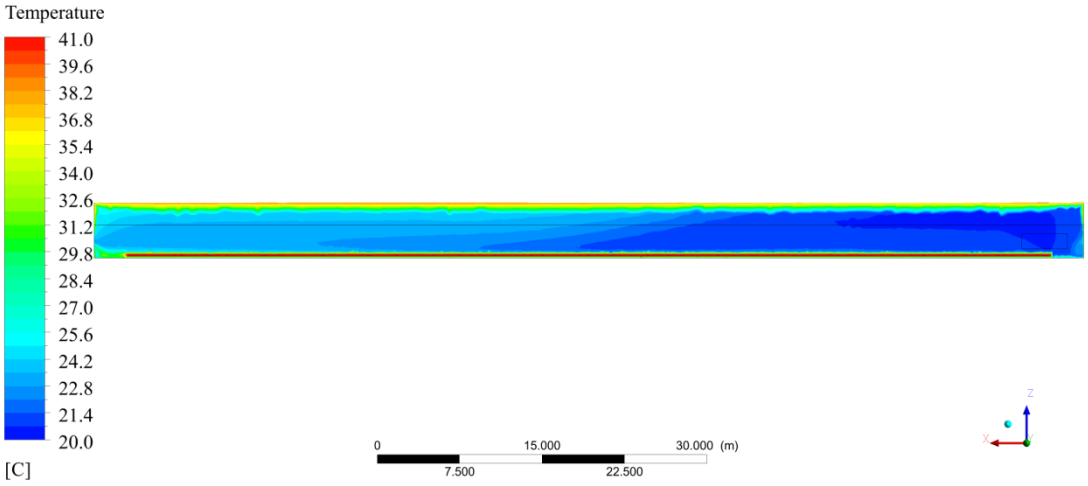

Fig. 6 - The change of temperature fields in longitudinal section of the building by centreline on the 6 m distance from the wall, ºC

The temperature distribution was shown in Fig. 6-9 in the service area of cooling water usage from underground walls. The internal temperature was considered +20ºC during the heat exchanger recuperator usage. The air temperature growing through the whole house was clearly observed in Fig. 7-8. The outlet temperature of cooled air was nearly +27ºC. It is caused by poultry's heat output and the external poultry houses' walls by external air. So, the air supply did not increase the allowable norms in the present air ventilating system. The poultry house's temperature field has not homogenous character and oscillates in the

range from +20 to +40ºC. The highest temperature was observed near the wall. It was caused by the heat exchange between the external and internal air cooling through barriers system considered the convective and radioactive components of heat exchanging. The heating air areas locate far from poultry floor holding. It did not affect the cooling.

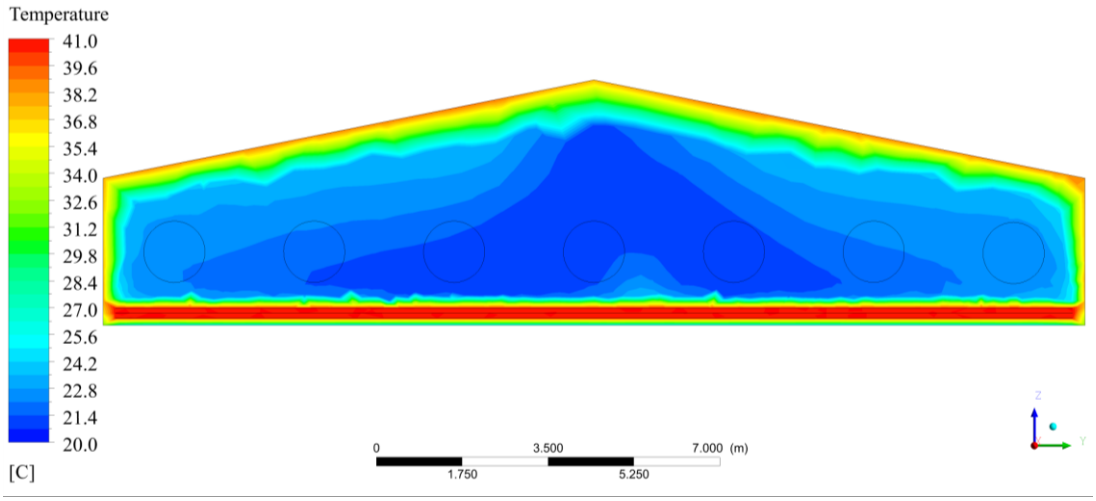

Fig. 7 - The temperature fields in the transverse section by axis 0y on the 30 m distance from inlet, ºC

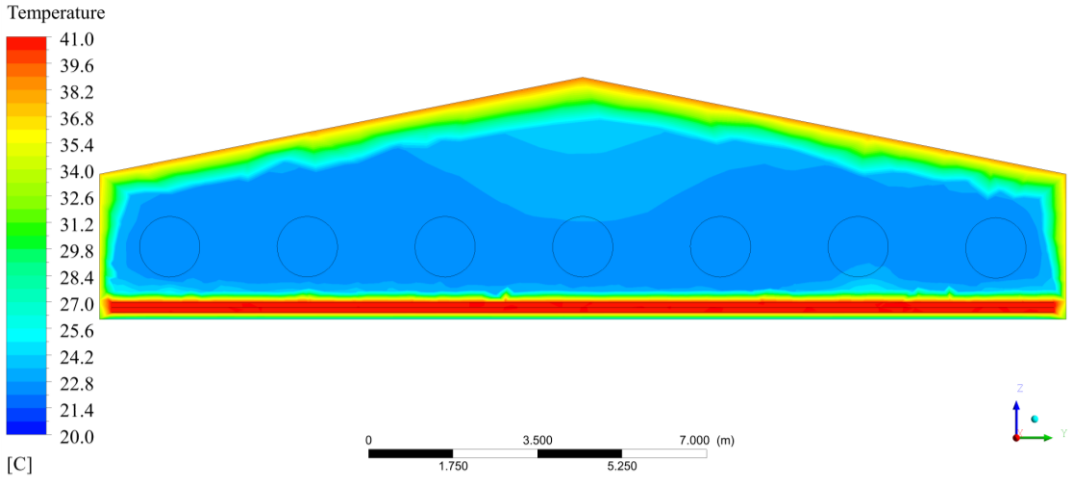

Fig. 8 - Temperature fields in poultry house in transversal section by axis 0y on the 60 m distance from inlet, ºC

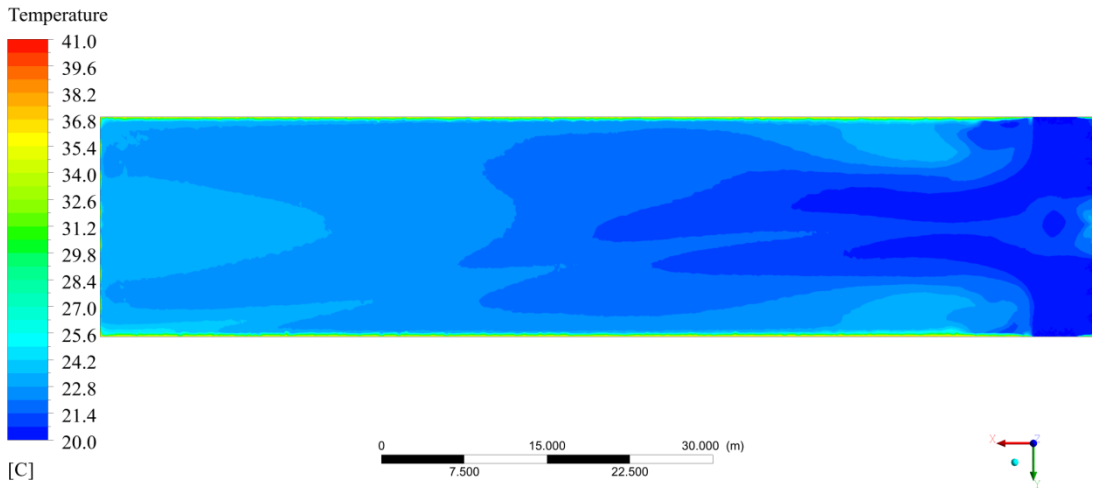

Fig. 9 - Temperature fields in poultry house in transversal section by axis *0z* on the 1.3 m height from the floor ºC

The air velocity of the poultry houses is the most important data for the poultry holding, especially near the poultry. The poultry houses velocity field is on the 0.5 height from the floor as shown in Fig. 10. The maximum velocity is not increased at 2.5 m/s. It is observed near the inlet and outlet parts of the poultry house. The air velocity reaches zero in the stagnation area. The average air velocity at the 0.5 m height is 1.97 m/s in spite of the high turbulence and non-homogenous flow. The air streamlines are shown in 3D image. The building's internal air motion has rectilinear character. As we have mentioned before, the stream non-uniformity and the stagnation area presence is near the side walls.

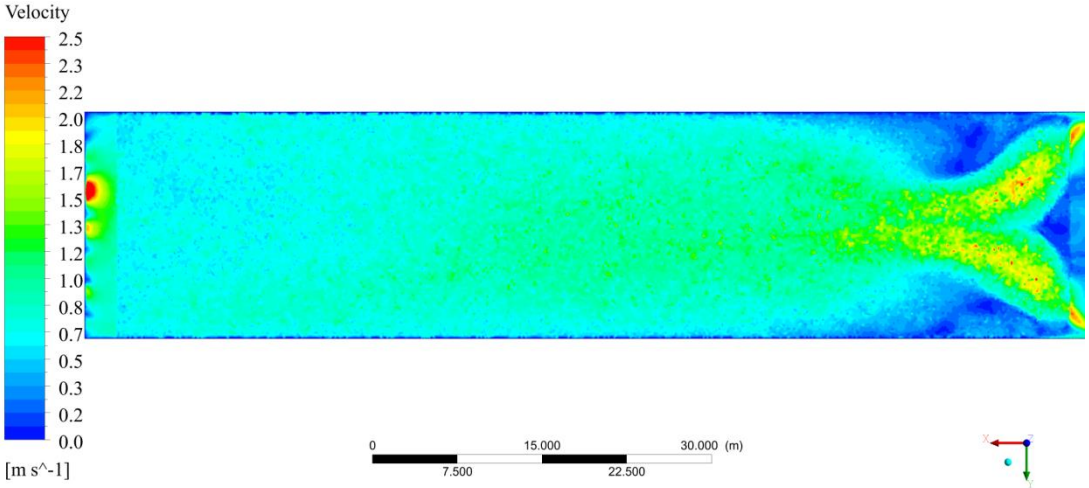

Fig. 10 - The velocity fields in poultry house in transverse section by axis *Oz* at 0.5 m height from the floor, m/s

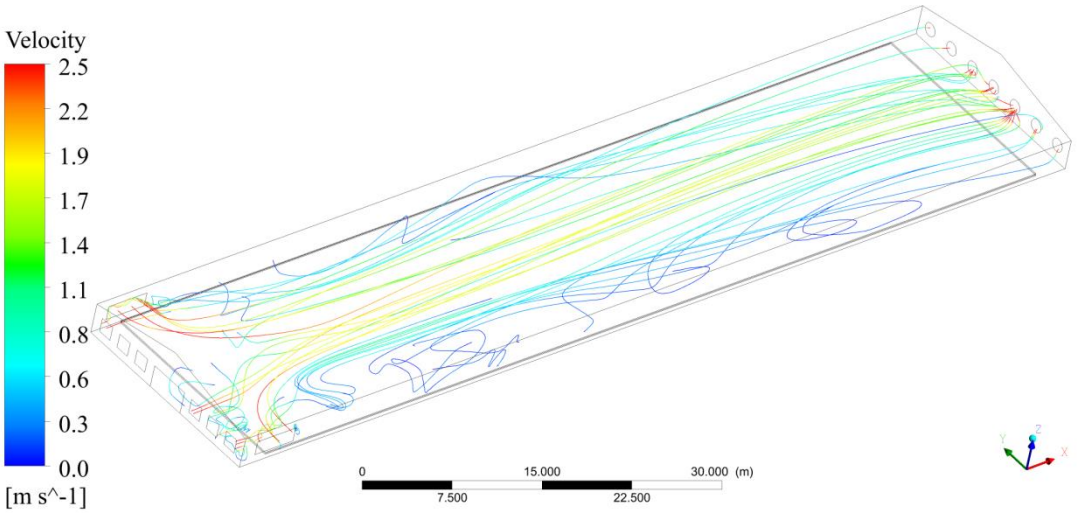

Fig. 11 - The air streamlines of poultry house in 3D image, m/s

CONCLUSIONS

The new air cooling system with heat exchangers recuperators was proposed. Heat exchangers were used for the water cooling from underground wells. It allows decreasing the poultry houses temperature to +20°C without increasing its relative humidity. The numerical simulation for the heat and mass transfer of ventilating air in poultry houses with or without cooling heat exchangers for air supply was provided. The velocity field, temperature and pressure were received using ANSYS Fluent software.

REFERENCES

[1] Allmaras S.R., Johnson F.T., Spalart P.R., (2012), Modifications and Clarifications for the Implementation of the Spalart-Allmaras Turbulence Model, *7th International Conference on Computational Fluid Dynamics*, pp. 9-13, Big Island/Hawaii;

[2] ANSYS (2011), ANSYS Fluent Theory Guide. Release, *Published in the USA*, 794 p.;

[3] Bailly C., Comte-Bello G., (2015), Turbulence. Series: Experimental Fluid Mechanics, *Springer International Publishing*, 360 p., Heidelberg/Germany;

[4] Blanes-Vidal V., Guijarro E., Balasch S., Torres A.G., (2008), Application of computational fluid dynamics to the prediction of airflow in a mechanically ventilated commercial poultry building. *Biosystems Engineering,* vol.100, no.1, pp. 105-116, San Diego/USA;
[5] Bustamante E., Calvet S., Estelles F., Torres A.G., Hospitaler A., (2017), Measurement and numerical simulation of single-sided mechanical ventilation in broiler houses, *Biosystems Engineering,* vol.160, pp. 55-68, San Diego/USA;
[6] Campbell J., Donald J., Simpson G. and other, (2007), Keeping birds cool costs down in summertime heat, *Auburn University in association with the US poultry and egg association*, no.48, pp. 12-15;
[7] Chui E.H., Raithby G.D., (2013), Computation of radiant heat transfer on a non-orthogonal mesh using the finite-volume method, *Numerical Heat Transfer*, vol.23, part B, pp. 269–288;
[8] Curi T., de Moura D.J., Massari J.M., Mesquita M., Pereira D.F., (2017), Computational fluid dynamics (CFD) application for ventilation studies in broiler houses, *Engenharia Agricola,* vol.37, no.1, pp. 1-12, Jaboticabal/Spain;
[9] Czarick M., Fairchild B., (2014), Plastic cooling pads are found to be less efficient comparing to paper cool pads, *Poultry Housing Tips. College of Agricultural and Environmental Sciences. The University of Georgia*, vol. 24, no.8, pp. 64-69, Georgia/USA;
[10] Dulnev G.N., Parfenov V.H., Sihalov A.V., (1990), Application of an EC for solving heat exchange problems (Применение ЭВМ для решения задач теплообмена), *by publishing in "High school" (опубліковано у видавництві «Вища школа»)*, 207 p., Moscow/Russia;
[11] Gorobets, V.G., (2006), Influence of nonisothermicity on the heat transfer from a bank of finned tubes in the presence of coating on the outside surface. *Heat Transfer Research,* vol. 37, no 2, pp. 93-102, Redding/USA;
[12] Hassanzadeh P., Raithby G.D., Chui E.H., (2008), Efficient calculation of radiation heat transfer in participating media, *Journal of Thermophysics and Heat Transfer,* vol. *22*, no 2, pp. 129-139, doi:10.2514/1.33271, Reston/USA;
[13] Hui X., Li B.M., Xin H.W., Zheng W.C., Shi Z.X., Yang X., Zhao S.M., (2018), New control strategy against temperature sudden-drop in the initial stage of pad cooling process in poultry houses, *International Journal of Agricultural and Biological Engineering,* vol. 11, no 1, pp. 66-73, doi:10.25165/j.ijabe.20181101.2479, Beijing/China;
[14] Hulzebosch J., (2005), How to keep your birds cool, *World Poultry Climate*, vol.21, no.6, pp. 32-34;
[15] Donald O.James, (2012), Technology of microclimate of broiler house, *by publishing in Aviagen Brands*, 44 p., Huntsville/USA;
[16] Khmelnik S.I., (2018), Navier-Stokes equations. On the existence and the search method for global solutions, Mathematics in Computers – MiC, 134 p., Bene-Ayish/Israel;
[17] Kim K., Yoon J. Y. Kwon H.J., Han J.H., Son J.E., Nam S.W., Lee I.B., (2008), 3-D CFD analysis of relative humidity distribution in greenhouse with a fog cooling system and refrigerative dehumidifiers, *Biosystems Engineering,* vol.100, no.2, pp. 245-255, San Diego/USA;
[18] Modest M.F., (2013), Radiative Heat Transfer (Third Edition), *Publishing in: Academic Press*, 897 p.;
[19] Murthy J.Y., Mathur S.R., (1998), Finite volume method for radiative heat transfer using unstructured meshes, *Journal of Thermophysics and Heat Transfer*, vol.12, no.3, pp. 313-321;
[20] Seo I.H., Lee I.B., Moon O.K., Kim H.T., Hwang H.S., Hong S.W., Han J.W., (2009), Improvement of the ventilation system of a naturally ventilated broiler house in the cold season using computational simulations, *Biosystems Engineering,* vol.104, no.1, pp. 106-117, San Diego/USA;
[21] Spalart P.R., Rumsey C.L., (2007), Effective inflow conditions for turbulence models in aerodynamic calculations, *Aiaa Journal,* vol. 45*,* no. 10, pp. 2544-2553 doi:10.2514/1.29373, Reston/USA;
[22] Trokhanyak V.I., Bogdan Yu.O., (2015), The finite element method in making up meshes in ANSYS Meshing for CFD models (Застосування методу кінцевих елементів при побудові сітки в Ansys Meshing для CFD моделей), *Bulletin of Pryazovslyi State Technical University*, vol. 30, no. 2, pp. 181–189., Mariupol/Ukraine;
[23] Vyshnevskyi E.P., (2004), Comparative analysis of adiabatic humidification systems (Сравнительный анализ систем адиабатического увлажнения воздуха), *Plumbing, Heating, Air conditioning (*Сантехника, Отопление, Кондиционирование*)*, no. 8, pp. 76-83, Moscow/Russia;
[24] Zajicek M., Kic P., (2013), Longitudinal ventilation of broiler house – sumulation of variants, *12th International Scientific Conference Engineering for Rural Development*, pp. 198-202, Jelgava/Latvia.

DETERMINATION OF THE PARAMETERS OF TRANSPORTING AND MIXING FEED MIXTURES ALONG THE CURVILINEAR PATHS OF TUBULAR CONVEYORS

/

ВИЗНАЧЕННЯ ПАРАМЕТРІВ ПРОЦЕСУ ТРАНСПОРТУВАННЯ ТА ЗМІШУВАННЯ КОРМОВИХ СУМІШЕЙ НА КРИВОЛІНІЙНИХ ТРАСАХ ТРУБЧАТИХ КОНВЕЄРІВ

Prof. Ph.D. Eng. Hevko R.B.[1)], Assoc. Prof. Ph.D. Eng. Liubin M.V.[2)], Assoc. Prof. Ph.D. Eng. Tokarchuk O.A.[2)], Prof. Ph.D. Eng. Lyashuk O.L.[3)], Prof. Ph.D. Eng. Pohrishchuk B.V.[1)], Assoc. Prof. Ph.D. Eng. Klendii O.M.[4)]

[1)]Ternopil National Economical University / Ukraine; [2)] Vinnytsia National Agrarian University / Ukraine; [3)]Ternopil Ivan Puluj National Technical University; [4)]Separated Subdivision of National University of Life and Environmental Sciences of Ukraine Berezhany Agrotechnical Institute / Ukraine

E-mail: klendii_o@ukr.net

Keywords: *curvilinear path; tubular conveyor; feed mixture; transporting; mixing; scraper.*

ABSTRACT

The results of theoretical and experimental studies of simultaneous transporting and mixing the components of feed mixtures along the curvilinear paths of tubular conveyors are presented in this article. A mathematical model of the dependence of the change of elementary work performed while transporting the bulk material elementary mass along the curvilinear section is developed. Based on experimental researches, the technique of determining the technological parameters, which ensure the reduction of energy consumption while mixing bulk materials with the given quality of feed mixtures, is proposed. When considering the range of changes in the inner holes of the washers d_h *= 14…25 mm* and the angles of their position to the horizon α *= 30˚…75˚*, the intensity of the material components passing-through and their consequent mixing increases with the increase of the value of the parameter d_h and the reduction of the angle α.

РЕЗЮМЕ

У статті представлено результати теоретичних і експериментальних досліджень одночасного транспортування та змішування компонентів кормових сумішей на криволінійних трасах трубчатих конвеєрів. Побудована математична модель, яка характеризує залежність зміни елементарної роботи, що виконується під час переміщення елементарної маси сипкого матеріалу по криволінійній ділянці. Запропонована методика та проведені експериментальні дослідження з визначення параметрів виконання технологічного процесу, які забезпечать зниження енерговитрат при змішуванні сипких тіл та задану якість кормових сумішей. Встановлено, що для діапазону зміни внутрішніх отворів шайб d_h *= 14…25 мм і кутів їх розташування до горизонту* α *= 30˚…75˚ інтенсивність пересипання компонентів матеріалів та відповідно їх змішування зростає при збільшенні значення параметр* d_h *і зменшенні величини кута* α.

INTRODUCTION

Based on the analysis of literature sources and experimental results of studying the processes of bulk materials transportation in closed jackets *(Loveikin V. et al., 2010; Lyashuk O.L. et al., 2015; Owen Philip J. and Cleary Paul W., 2010; Rogatynska O. et. al., 2015; Rohatynskyi R. M. et al., 2016; Roberts Alan W. and Bulk Solids, 2015)* the vast majority of screw conveyors are found to possess the limited functionality; therefore, they can be used only on short paths of material movement. The challenge is to minimize the degree of damage to agricultural materials by applying the elastic working bodies *(Loveikin V. and Rogatynska L., 2011; Rogatynska L.R., 2010)* or by combining the processes of shredding and transporting lump materials (e.g., root crops) for feed preparation *(Pankiv V.R. and Tokarchuk O.A, 2017)*. Due to such minimization of damages, the functional performance of transporters can be significantly improved. To increase the conveyors' performance, the material flow movement should be intensified by means of pneumatic devices *(Manjula E.V.P.J. et al., 2017; Naveen Tripathi et al., 2015; Baranovsky V.M. et al., 2018; Hevko R.B. et al., 2018)* and screw and tubular conveyors *(Haydl H.M., 1986;* Yao Y.P., et.al., 2014*)*. Many scientists have studied the methods of improving the operational and functional performance of screw and tubular conveyors, and the ways of reliable protecting their drive elements *(Hevko B.M. et al., 2017; Hevko R.B. et al., 2016; Hevko R.B. et al., 2017)* The objective of the present research is to ensure the reduction of energy consumption during simultaneous transporting and mixing bulk components of feed mixtures along the curvilinear paths of tubular conveyors.

MATERIALS AND METHODS

The material movement along the curvilinear section of the conveyor *(Hevko R.B. et al., 2017*, Fig. c) is considered as a case of the plane motion of the elementary mass dm_c (Fig.1a); the mass is located between the scraper spaces of the working body moving uniformly at the initial average velocity ϑ_c. The movement of the elementary volume dV_m along the curvilinear section of the path is considered in polar coordinates; the path's axis is at point *O* (Fig.1b). The scraper moves along the trajectory of the fourth section of the ring with an average diameter D_c, transporting the average elementary mass of the bulk material dm_c.

The position of the elementary mass centre of the bulk material dm_c in the vector form is determined by the polar coordinates $\vec{R}_c$ (radius-vector of the mass center movement dm_c) and φ_c (polar angle).

The elementary mass center of the material dm_{Ac} (Fig.1b) at the initial moment of motion at the rate ϑ_A (at t = 0) is at point *A*. Its position is determined by the radius-vector $\vec{R}_A$, where φ_A = 0. In time $t = t_B$, the elementary mass center of the material $dm_{Ac,}$ moves to point B under the action of centrifugal forces. The elementary mass center of the material dm_{Bc} is determined by the radius-vector and the polar angle φ_B.

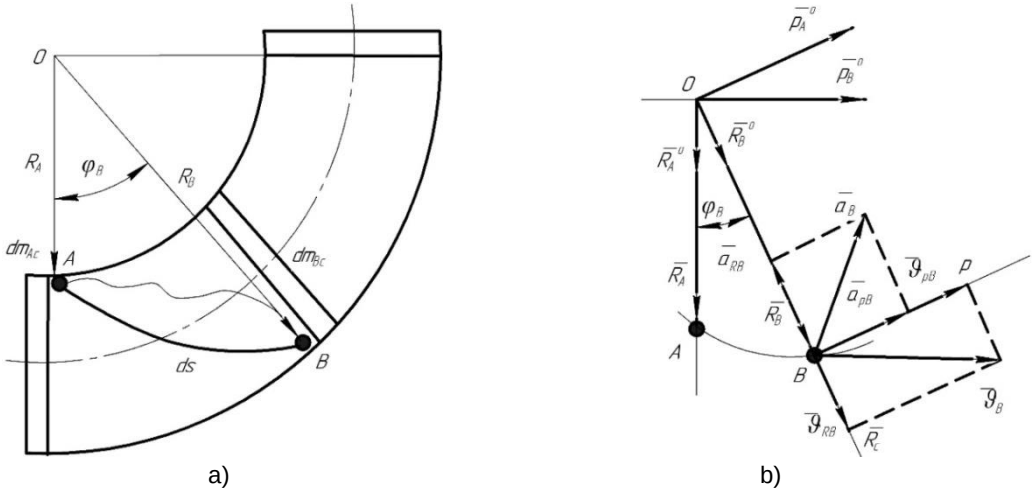

Fig. 1 - Analytical models: a - for determining the movement of the elementary mass center of the material along the curvilinear path; b - for determining the kinematic parameters of the bulk material movement

The motion equations of the elementary mass center of the bulk material dm_c in the polar coordinates for the case of the plane motion of the material body are deduced

$$\vec{R}_c = f_1(t); \quad \varphi_c = f_2(t) \tag{1}$$

For further analysis, the single vectors $\vec{R}_A^0$ and $\vec{R}_B^0$ are introduced (Fig. 1b); the vectors are directed in corresponding radii-vectors of corresponding points that characterize the corresponding elementary mass centres of the bulk material dm_{Ac} and dm_{Bc}, as well as the vectors $\vec{p}_A^0$ and $\vec{p}_B^0$, which are perpendicular to the corresponding radii-vectors $\vec{R}_A$ and $\vec{R}_B$ and directed towards the increase of the polar angle φ_B.

Applying the radial ϑ_{RB} and tangential ϑ_{pB} velocities, the magnitude and direction of the scalar velocity ϑ_B of the elementary mass center of the bulk material dm_{Bc} are determined

$$\vartheta_B = \sqrt{\left(\vartheta_{R_B}\right)^2 + \left(\vartheta_{p_B}\right)^2} = \sqrt{\left(\dot{R}_B\right)^2 + \left(R_B\dot{\varphi}\right)^2} = \sqrt{\left(\frac{dR_B}{dt}\right)^2 + R_B^2\left(\frac{d\varphi_B}{dt}\right)^2} \tag{2}$$

Directional cosines are defined by formulas

- between the directions of the vectors $\vec{\vartheta}_B$ and $\vec{R}_B^0$

$$\cos\left(\vec{\vartheta}_B, \hat{\vec{R}}_B^0\right) = \frac{\frac{d\vec{R}_B}{dt}}{\vec{\vartheta}_B} = \frac{\dot{R}_B}{\vartheta_B} = \frac{\dot{R}_B}{\sqrt{\left(\dot{R}_B\right)^2 + \left(R_B\dot{\varphi}\right)^2}} \tag{3}$$

- between the directions of the vectors $\vec{\vartheta}_B$ and $\vec{p}_B^0$

$$cos\left(\vec{\vartheta}_B, \vec{p}_B\right) = \frac{\vec{R}_B \frac{d\varphi_B}{dt}}{\vec{\vartheta}_B} = \frac{R_B\dot{\varphi}_B}{\vartheta_B} = \frac{R_B\dot{\varphi}_B}{\sqrt{\left(\dot{R}_B\right)^2 + \left(R_B\dot{\varphi}\right)^2}} \tag{4}$$

Differential equation for determining the vector acceleration $\vec{a}_B$ of point *B*, which specifies the position of the elementary mass center of the bulk material dm_{Bc} in time $t = t_B$, is deduced

$$\begin{aligned} \vec{a}_B &= \frac{d^2R_B}{dt^2}\vec{R}_B^0 + \frac{dR_B}{dt}\frac{d\varphi_B}{dt}\vec{p}_B^0 + \frac{dR_B}{dt}\frac{d\varphi_B}{dt}\vec{p}_B^0 + R_B\frac{d^2\varphi_B}{dt^2}\vec{p}_B^0 - R_B\frac{d\varphi_B}{dt}\frac{d\varphi_B}{dt}\vec{R}_B^0 = \\ &= \ddot{R}_B\vec{R}_B^0 + \dot{R}_B\dot{\varphi}_B\vec{p}_B^0 + \dot{R}_B\dot{\varphi}_B\vec{p}_B^0 + R_B\ddot{\varphi}_B\vec{p}_B^0 - R_B\left(\dot{\varphi}_B\right)^2\vec{R}_B^0 = \\ &= \left[\ddot{R}_B - R_B\left(\dot{\varphi}_B\right)^2\right]\vec{R}_B^0 + \left(R_B\ddot{\varphi}_B + 2\dot{R}_B\dot{\varphi}_B\right)\vec{p}_B^0 \end{aligned} \tag{5}$$

Similar to the velocity vector $\vec{\vartheta}_B$, the acceleration vector $\vec{a}_B$ of point *B* is equal to the geometric sum of two vectors, in particular the first vector, which is located on the radius-vector of point *B* $\vec{R}_B = \overrightarrow{OB}$ and directed along it, and the second vector, which is perpendicular to this radius-vector.

The scalar value of the projection of the acceleration vector $\vec{a}_{R_B}$ directed along the radius-vector $\vec{R}_B$ of point *B*, or the scalar value of the projection of the radial acceleration of point *B* are determined by the formula

$$a_{R_B} = \frac{d^2R_B}{dt^2} - R_B\left(\frac{d\varphi_B}{dt}\right)^2 = \ddot{R}_B - R_B\left(\dot{\varphi}_B\right)^2 \tag{6}$$

and the scalar value of the acceleration vector $\vec{a}_{p_B}$ projection, which is perpendicular to the radius-vector $\vec{R}_B$ of point *B*, or the scalar value of the projection of the tangential acceleration of point *B* are equal to

$$a_{p_B} = R_B\frac{d^2\varphi_B}{dt^2} + 2\frac{dR_B}{dt}\frac{d\varphi_B}{dt} = R_B\ddot{\varphi}_B + 2\dot{R}_B\dot{\varphi}_B \tag{7}$$

Applying the radial a_{R_B} and tangential a_{p_B} accelerations, the magnitude and direction of the scalar acceleration of motion a_B of the elementary mass center of the bulk material dm_{Bc} are determined.

$$a_B = \sqrt{\left(a_{R_B}\right)^2 + \left(a_{p_B}\right)^2} = \sqrt{\left(\ddot{R}_B - R_B\dot{\varphi}_B^2\right)^2 + \left(R_B\ddot{\varphi}_B + 2\dot{R}_B\dot{\varphi}_B\right)^2} \tag{8}$$

To operationalize the above provisions, the technological process of moving the elementary mass center *A* of the bulk material dm_c is formalized as follows. The uniformly variable motion of the elementary mass center *A* of the bulk material dm_c is supposed to be set by parametric equations with consideration of aerodynamic forces of air resistance, which is assumed as a quadratic dependence of the resistance forces on the motion velocity.

At the first stage of the research, the force analysis of moving the elementary mass center *A* of the bulk material dm_c along the curvilinear trajectory from point *A* to point *B* is considered.

In Fig. 2, an equivalent model of forces arising during the movement of the elementary mass center *A* of the bulk material dm_c along the curvilinear trajectory of the plane curve without the rolling friction action is shown. To find the total generalized force Q_c acting on the elementary mass center *B* of the bulk material dm_{Bc}, a differential equation of particle motion is deduced

$$dm_{B_c}\frac{d\vartheta_B}{dt} = Q_c = dm_{B_c}d\vartheta_B = Q_c dt = 0 \tag{9}$$

where Q_c is the total generalized force acting on the elementary mass center *B* of the bulk material dm_c during its motion along the curvilinear trajectory from the initial position with the coordinates *A{0, 0}* to position *B* $\{x_B, y_B\}$. Taking into account the components of the forces acting on the elementary mass center *B* of the bulk material dm_{Bc}, the dependence is developed

$$dm_{B_c}\left\{p\left[\left(\frac{dR_B}{dt}\right)^2 + R_B^2\left(\frac{d\varphi_B}{dt}\right)^2\right] + \left[\frac{f}{R_B}\frac{d\vartheta_B}{dt} + g\left(f\,cos\left(arctg\frac{dy}{dx}\right) - sin\left(arctg\frac{dy}{dx}\right)\right)\right]\right\} = 0 \tag{10}$$

where *f* – friction coefficient; *g* – free fall acceleration.

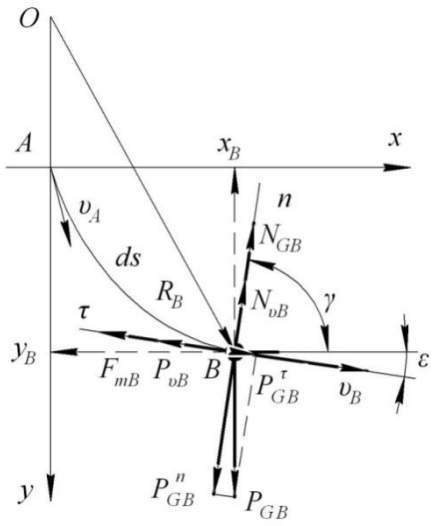

Fig. 2 - Analytical model for determining the dynamic parameters of the bulk cargo movement

The formula of an elementary work δA_{dm_c} that is consumed during the motion of the elementary mass of the bulk material dm_c along the curvilinear trajectory from the initial position with coordinates *A {0, 0}* to position *B* $\{x_B, y_B\}$ is deduced

$$\delta A_{dm_{B_c}} = dV_{B_c}\psi \int_o^{x_B} \begin{matrix} p\left[\left(\frac{dR_B}{dt}\right)^2 + R_B^2\left(\frac{d\varphi_B}{dt}\right)^2\right] + \\ + \left[\begin{matrix} \frac{f}{R_B}\sqrt{\left(\ddot{R}_B - R_B\dot{\varphi}_B^2\right)^2 + \left(R_B\ddot{\varphi}_B + 2\dot{R}_B\dot{\varphi}_B\right)^2} + \\ + g\left[f\cos\left(arctg\left(\dot{y}_x\right)\right) - \sin\left(arctg\left(\dot{y}_x\right)\right)\right] \end{matrix}\right]\sqrt{1+\dot{y}_x} \end{matrix} dx, \quad (11)$$

where dV_{Bc} - elementary volume of the material at point *B*, м^3; ψ - specific mass of the bulk material, kg/m^3.

The deduced equation (Eq.11) is a deterministic mathematical model of the dependence of the change of the elementary work $\delta A dm_c$ performed during the motion of the elementary mass of the bulk material dm_c along the *dc* arc in time t_B on the structural and kinematic parameters of the working body path, or the parameters of material movement with consideration of air resistance forces.

To minimize the elementary work performance during the motion of the bulk material along the curvilinear section of the working body path, the trajectory of the bulk material motion should be determined and optimized by integrating the above analyzed mathematical model (Eq.11). Furthermore, the minimum time of moving the bulk material along the curvilinear section of the working body path can be substantiated.

For experimental research, the working body of the scraper conveyor-mixer is design in the form of separate hinged sections (Fig.3). The design consists of a guiding jacket *1*. In the jacket, there are hinged scraper sections arranged in the form of a ring *2*, and hooks *3* and *7*. The ring part of the sections is covered by a disc *4* with a central inner opening *5*. The working body is driven by a gear wheel, which contacts with the conical surface of the disc. The components of the bulk material *6* are captured by disks and partially passed through the central openings; then, they are mixed into a solid mixture, which is transported to the unloading zone.

To determine the degree of passing the bulk agricultural materials through the washer holes at their various angular positions along the curvilinear sections of the conveyor-mixer, an experimental stand with a working body is developed in the form of washer scrapers with different inner holes of various diameters (Fig. 4). The stand was located vertically; its overall dimensions were horizontally - 500mm; vertically - 650 mm. Radius of knee position - 400 mm; its inner radius - 46 mm; the washer outer diameter - 45mm.

The method for determining the time of the bulk material passing through the washer scrapers is as follows. In the curved knee, which consists of five sections, the bulk cargo weighing from 100 to 150 g was delivered; the coefficient of the space between scrapers is ψ = 0.6 ... 0.9. After opening the damper valve, the pressure of the cargo flow pushed the lever pedal, activating an electric timing device. When the flow stopped moving, the electric timing device was disconnected. The amount of cargo was weighed on electronic weighting machines.

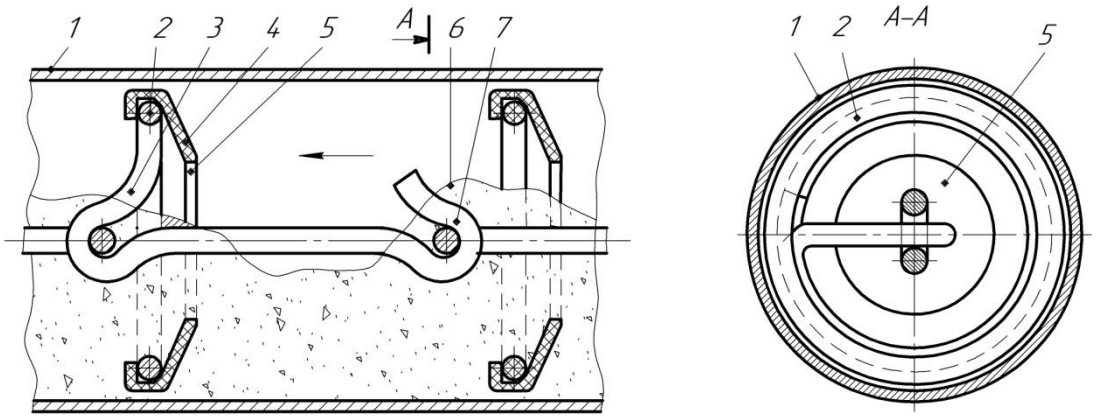

Fig. 3 - Working body of the scraper conveyor-mixer

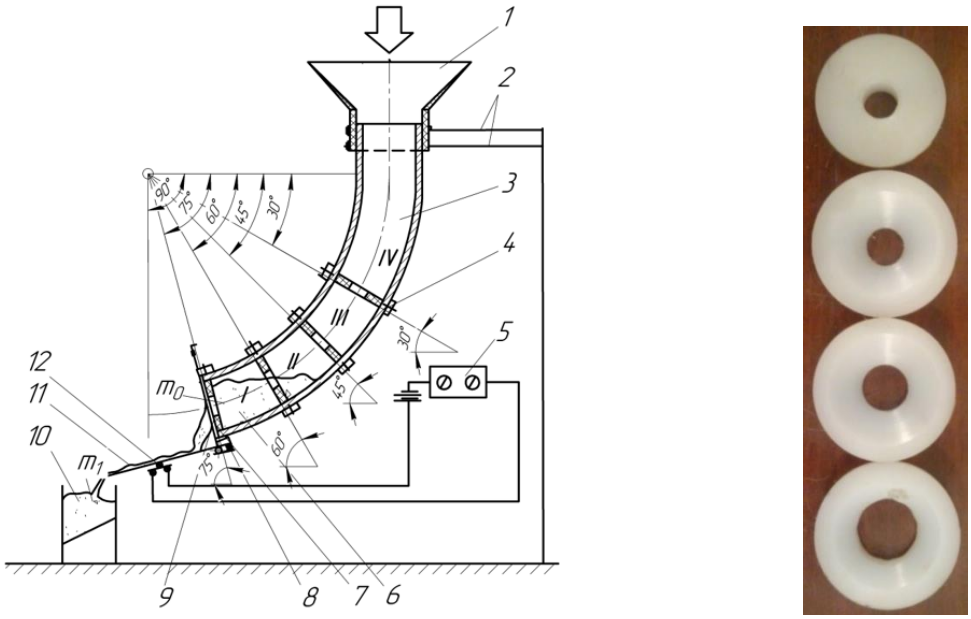

Fig. 4 - General view of the experimental stand (a) and washer scrapers with different inner holes (b)

1 - neck; 2 - stand; 3 - knee; 4 - a clamp; 5 - electric timing device; 6 - bulk material; 7 - scraper; 8 - spring of a lever; 9 - damper valve, 10 - capacity; 11 - lever pedal; 12 - contacts

In the knee sections, the washer scrapers were arranged at the angles: $\alpha_1 = 75°$; $\alpha_1 = 60°$; $\alpha_1 = 45°$; $\alpha_1 = 30°$. The inner holes in the washers varied within the range from 14 to 25 mm.

To provide the process of agricultural product transporting, a passing of the bulk material through the washer scrapers per second was calculated at their various angles of inclination to the horizon: $Q = m / t$, where m – cargo weight; t - time of passing.

RESULTS

The research results are presented on the graphic dependences shown in Fig. 5-6.

Experimental studies were conducted to define the maximum possible loading coefficient between the scraper spaces $\psi = 0.95$.

The graphic dependences of the mass m of the combined feed passed through the washer holes with diameters d_h = 20...25 mm on the moment of time t are shown in Fig. 5 a. The change in the hole diameter from 20 to 25 mm is found to cut time for the combined feed passing-through from 3.5 s to 2.25 s, providing the washer location angle to the horizon is $\alpha = 30°$. At the same time, respectively 84.6% and 96.1% of the combined feed are passed through in the space between the scrapers.

Providing the washer location angle $\alpha = 75$ °,

The time of passing-through the combined feed is t = 4.9 s, provided d_h = 20 mm and α = 75 °. The time of passing-through the combined feed is t = 5.2 s, provided d_h = 25 mm α = 75°. At the same time, respectively, only 17.3% and 30.8% of the combined feed is passed through.

Thus, the angle of the washers' arrangement dominantly influences the process of the combined feed passing-through. Therefore, with the approach to the vertical section, the process of passing-through and consequent mixing the feed components significantly intensifies.

The wheat grain is passed through the washer hole of the diameter d_h = 18 mm (Fig. 5 b).

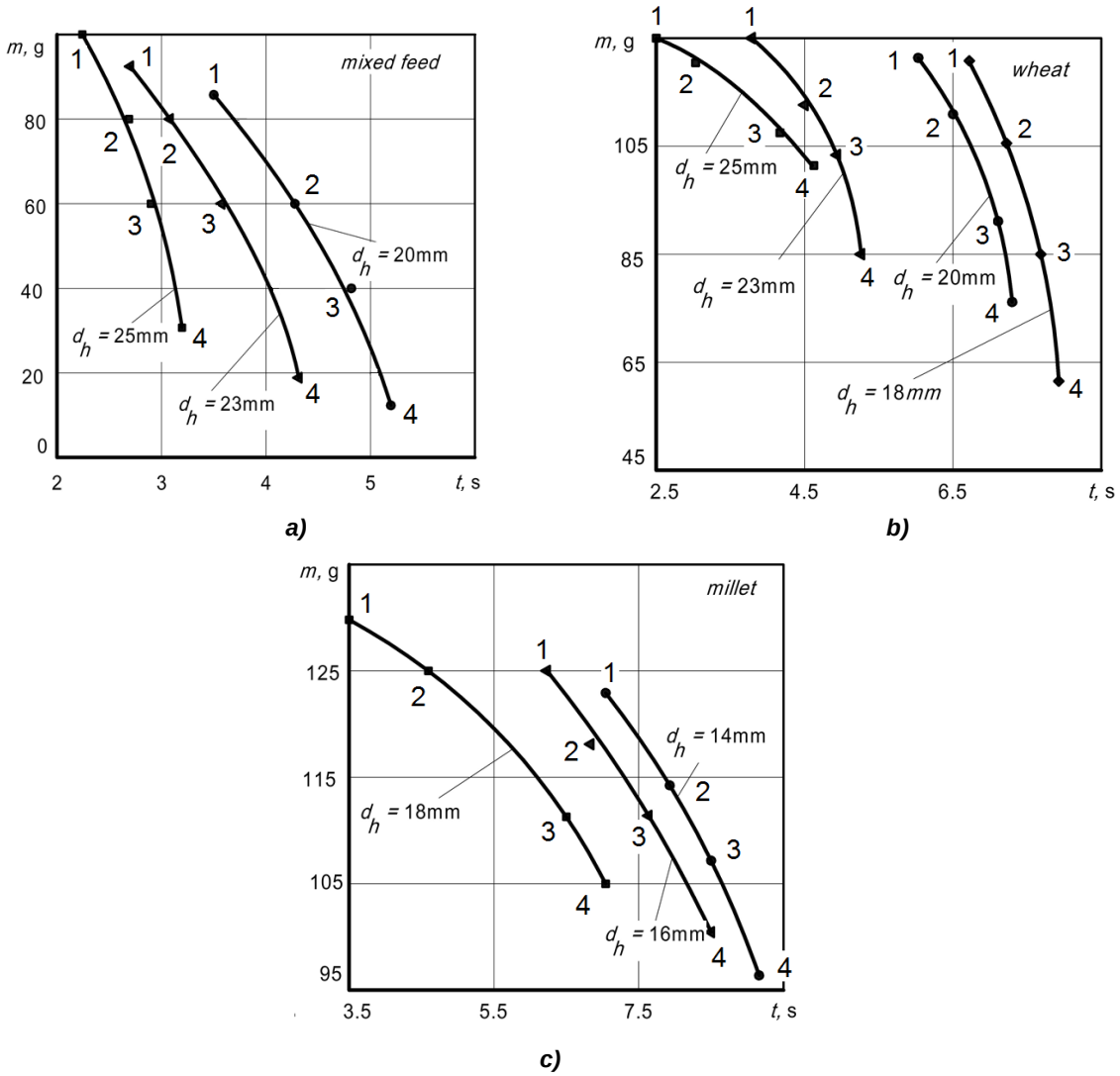

Fig. 5 - Graphic dependences of the mass *m* of the mixed feed (a), wheat (b), and millet (c) passed through washer holes with different diameters d_h and their location angles to the horizon on the moment (1 – α=30°, 2 – α=45°, 3 – α=60°, 4 – α=75°) of time *t*

Thus, providing d_h = 18 mm, α = 30 °, and t = 6.8 s, 96% of wheat is passed-through. Providing d_h = 20 mm, α = 30 °, and 96% of passed-through wheat, the process takes 6 s.

The diameter of the washer hole d_h increases from 23 to 25 mm, the time of wheat passing-through sharply decreases (if α = 30 °), respectively, from 3.7 s to 2.5 s. In both cases, the percentage of passed-through wheat is 98.4%.

At the same time, providing α = 75 ° and d_h = 18 mm, 47% of wheat is passed-through in time t = 8 s; and, respectively, providing α = 75 ° and d_h = 25 mm, 80% of wheat is passed-through in time t = 4.6 s.

Based on the analysis of the graphic dependencies shown in Fig. 5c, the scrapers with the diameter of the inner openings d_h = 14 and 18 mm are found more effective for transporting the millet and its further mixing with the appropriate concentrated additives. Such diameter values are proved to ensure the implementation of the technological process with the corresponding indicators, similar to the above considered cases.

The dependence of passing the combined feed and millet through different holes of scraper washers per second *g* (g/s) on their location angle to the horizon was experimentally developed.

The research results are presented in the form of graphical dependencies shown in Fig. 6.

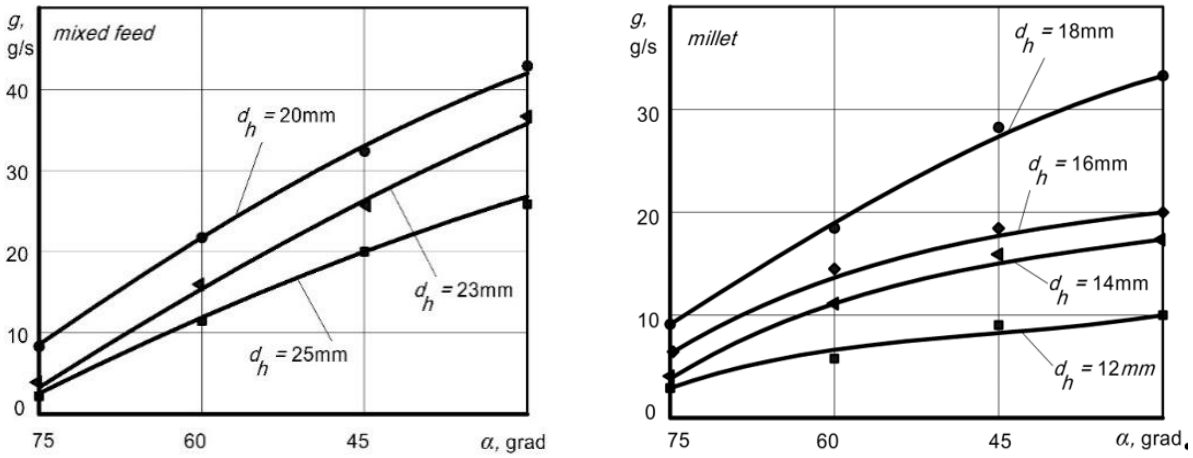

Fig. 6 - Graphical dependencies of passing *g* the combined feed (a) and millet (b) on the inclination angle α of the washer scrapers to the horizon per second

Based on the developed dependencies, the necessary structural parameters of the working bodies of the washer conveyor-mixer can be defined. To provide a certain degree of mixing feed mixtures, their main components should be considered.

CONCLUSIONS

Based on the known research results, a new technological model of simultaneous transporting and mixing the components of bulk cargo along curvilinear paths is proposed.

The process of moving the bulk material by scraper and washer working bodies along the curvilinear section of the technological path is simulated; the dynamic parameters of the bulk cargo movement are determined. The developed equation is a deterministic mathematical model of the dependence of the change of elementary work performed during the movement of the bulk material elementary mass. The model allows determining the minimum time of moving the bulk material along the curvilinear section of the working body path.

The dependences of the mass *m* of the combined feed passed through the holes of diameter d_h = 20 ... 25 mm on time *t* were analyzed. The change in the washer hole' diameter was found to cut time for passing the combined feed in time from 3.5 s to 2.25 s, providing the angle of washer location is $\alpha = 30^{\circ}$. Correspondently, the amount of passed combined feed in the space between scrapers is 84.6% and 96.1% of its total mass. In the range of changing in the holes and angles parameters, the washer location angle is considered to influence dominantly the process of the combined feed passing-through. Therefore, with the approach to the vertical section, the process of passing and mixing the components of feeds significantly intensifies.

The washer hole diameter d_h = 18 mm is found more applicable for transporting the wheat grain. Thus, providing d_h = 18 mm, α = 30°, and *t* = 6.8 s, 96% of wheat is passed-through; providing d_h = 20 mm, α = 30°, and 96% of passed-through wheat, the process takes 6 s. Then, providing α = 75°, d_h = 18 and 25 mm, the percentages of the passed wheat are, respectively, 47% at *t* = 8 s and 80% at *t* = 4.6 s.

The scrapers with the diameter of the inner holes d_h = 14 and 18 mm are found more applicable for transporting the millet and its further mixing with the appropriate concentrated additives. Such diameter values are proved to ensure the implementation of the technological process with the corresponding indicators, similar to the above considered cases.

REFERENCES

[1] Baranovsky V.M., Hevko R.B., Dzyura V.O., Klendii O.M., Klendii M.B., Romanovsky R.M., (2018), Justification of rational parameters of a pneumoconveyor screw feeder, *INMATEH: Agricultural Engineering*, vol.54, no.1, pp. 15-24, Bucharest/Romania;

[2] Haydl H.M., (1986), Design aspects of large-diameter tubular conveyor galleries, *Proceedings of the institution of civil engineers, Part 1 – Design and construction,* Vol. 80, pp. 633-639, London/England;
[3] Hevko B.M., Hevko R.B., Klendii O.M., Buriak M.V., Dzyadykevych Y.V., Rozum R.I., (2018), Improvement of machine safety devices. *Acta Polytechnica, Journal of Advanced Engineering*, Vol.58, no.1, pp.17-25, Prague/Czech Republic;
[4] Hevko R.B., Klendii M.B., Klendii O.M., (2016), Investigation of a transfer branch of a flexible screw conveyer, *INMATEH: Agricultural Engineering*, vol.48. no.1, pp.29-34, Bucharest/Romania;
[5] Hevko R.B., Rozum R.I., Klendiy O.M., (2016), Development of design and investigation of operation processes of loading pipes of screw conveyors, *INMATEH: Agricultural engineering*, vol.50, no.3, pp.89-94, Bucharest/Romania;
[6] Hevko R.B., Yazlyuk B.O., Liubin M.V., Tokarchuk O.A., Klendii O.M., Pankiv V.R., (2017), Feasibility study of mixture transportation and stirring process in continuous-flow conveyors, *INMATEH: Agricultural Engineering*, vol.51, no.1, pp.49-59, Bucharest/Romania;
[7] Hevko R.B., Strishenets O.M., Lyashuk O.L., Tkachenko I.G., Klendii O.M., Dzyura V.O., (2018), Development of a pneumatic screw conveyor design and substantiation of its parameters, *INMATEH: Agricultural Engineering*, vol.54, no.1, pp.153-160, Bucharest/Romania.
[8] Loveikin V., Rogatynska O., Rogatynska L., Dudun Y., (2010), Dynamics of Screw Conveyers (Динаміка гвинтових конвеєрів*), Bulletin of I.Pyliui Ternopil National Technical University (Вісник ТНТУ ім. І.Пулюя)*, Vol.15, pp.100-105, Ternopil/Ukraine;
[9] Loveikin V., Rogatynska L., (2011), A Model of Loose Material Transportation by Means of High-Speed Conveyers with Elastic Operating Devices (Модель транспортування сипкого вантажу швидкохідними гвинтовими конвеєрами з еластичними робочими органами*)*. *Bulletin of I.Pyliui Ternopil National Technical University (Вісник ТНТУ ім. І.Пулюя)*, Vol.16, pp.66-70, Ternopil/Ukraine;
[10] Lyashuk O.L., Rogatynska O.R., Serilko D.L., (2015), Modelling of the vertical screw conveyer loading*, INMATEH Agricultural Engineering*, vol. 45, no. 1, pp. 87-94, Bucharest/Romania;
[11] Manjula E.V.P.J., Hiromi W.K. Ariyaratne, Ratnayake Chandana, Morten C. Melaaen, (2017), A review of CFD modelling studies on pneumatic conveying and challenges in modelling offshore drill cuttings transport, *Powder Technology*, Vol.305, pp.782-793;
[12] Naveen Tripathi, Atul Sharma, S.S. Mallick, Wypych P.W., (2015), Energy loss at bends in the pneumatic conveying of fly ash, *Particuology*, vol.21, pp. 65-73;
[13] Owen Philip J., Cleary Paul W., (2010), Screw conveyor performance: comparison of discrete element modelling with laboratory experiments. *Progress in computational fluid dynamics*, Vol. 10, Issue 5-6, pp.327-333, Geneva/ Switzerland;
[14] Pankiv V.R., Tokarchuk O.A., (2017), Investigation of constructive geometrical and filling coefficients of combined grinding screw conveyor. *INMATEH Agricultural Engineering*, vol.51, no.1, pp.59-68, Bucharest/Romania;
[15] Rogatynska L.R., (2010), Evaluation of Stress-Strained State of Elastic Helixes of Screw Conveyers when Loading (Оцінювання напружено-деформованого стану еластичних спіралей гвинтових конвеєрів при навантаженні), *Bulletin of I. Pyliui Ternopil National Technical University (Вісник ТНТУ ім. І.Пулюя)*, Vol.15, pp.131-137. Ternopil/Ukraine;
[16] Rogatynska O., Liashuk O., Peleshok T., Liubachivskyi R., (2015), Investigation of the Process of Loose Material Transportation by Means of Inclined Screw Conveyers (Дослідження процесу транспортування сипкого вантажу похилими гвинтовими конвеєрами), *Bulletin of I.Pyliui Ternopil National Technical University (Вісник ТНТУ ім. І.Пулюя*), Vol.79, pp.137-143, Ternopil/Ukraine;
[17] Rohatynskyi R.M., Diachun A.I., Varian A.R., (2016), Investigation of Kinematics of Grain Material in a Screw Conveyor with a Rotating Casing (Дослідження кінематики зернового матеріалу у гвинтовому конвеєрі із обертовим кожухом*), Bulletin of Kharkiv Petro Vasylenko National Technical Univarsity of Agriculture (Вісник ХНТУСГ імю Петра Василенка №168)*. Vol. 168, pp.24-31. Kharkiv/Ukraine;
[18] Roberts Alan W., Bulk Solids, (2015), Optimizing Screw Conveyors. *Chemical engineering*. Vol.122 (2), pp.62-67, New York/USA;
[19] Yao Y.P., Kou Z.M., Meng W.J., Han G., (2014), Overall Performance Evaluation of Tubular Scraper Conveyors Using a TOPSIS-Based Multi-attribute Decision-Making Method, *Scientific World Journal*, New York/USA.

EFFECTS OF STEM REGION, MOISTURE CONTENT AND BLADE OBLIQUE ANGLE ON MECHANICAL CUTTING OF MILLET STEMS

/

秸秆部位、含水率和刀片倾斜角对谷子秸秆切割力学性质的影响

As. Ph.D. Stud. Eng. Yanqing Zhang, Prof. Ph.D. Eng. Qingliang Cui*, Prof. Ph.D. Eng. Hongbo Li, M.S. Stud. Eng. Deng Sun, Ph.D. Stud. Eng. Huaming Hou
College of Engineering, Shanxi Agriculture University, Taigu/China
Tel: +86-0354-6289253; E-mail: qlcui@126.com

Keywords: *millet stem, mechanical cutting properties, moisture content; blade oblique angle, stem region*

ABSTRACT

Research has reported that the efficient cutting can improve stem utilisation and lead to energy conservation. In this study, the mechanical cutting properties of millet stems at different stem regions, moisture content and blade oblique angle were investigated. Results showed that cutting stress decreased from stem lower region to upper region, and cutting force and energy were greatly higher in the lower region than in the other areas due to the parameters of the cross section ($p<0.05$). The cutting force and energy of the nodes were significantly larger than those of the internodes ($p<0.05$), whereas the cutting stress of the nodes was significantly smaller than that of the internodes due to structural differences （$p<0.05$）. The cutting stress and specific cutting energy initially increased and then gradually decreased as moisture content increased (10.14% –72.59% [w.b.]). Processing millet stems at high or low moisture content can lead to energy saving. Cutting stress decreased as blade oblique angle was increased. However, specific cutting energy initially decreased and then gradually increased as blade oblique angle was increased. The minimum specific cutting energy values of the internodes and the nodes were reduced by 28.99% and 25.97%, respectively, when 18.8º and 0º blade oblique angles were compared. These findings are useful for further studies on effective stem forage utilisation and mechanical harvesting, deep stem processing.

摘要

切割是秸秆收获加工的主要工序，切割力是衡量秸秆饲料价值的主要指标之一。为高效利用谷子秸秆资源，节省切割能耗，本文对其切割力学性质进行深入研究，分析了茎秆位置、含水率、刀片倾斜角对谷子秸秆切割强度和切割比功的影响。研究结果表明：底部茎秆的切割强度大于顶部秸秆的切割强度；由于秸秆横截面参数的影响，底部秸秆切割力、切割功耗大于顶部茎秆切割力，且差异显著（$p<0.05$）；茎节切割力、切割功耗远大于秸秆节间切割力、切割比功（$p<0.05$）；由于结构差异，茎节的切割强度小于秸秆节间的切割强度，且差异显著（$p<0.05$）。切割强度和切割比功随秸秆含水率的增大先增大后减小（10.14％–72.59％[湿基]），切割过高或过低含水率秸秆可一定程度地减小切割比功。秸秆切割强度随着刀片倾斜角的增大而减小，但切割比功随刀片倾斜角的增大先减小后增大；选用刀片倾斜角 18.8º 切割谷子秸秆时，秸秆节间、茎节切割比功分别减小了28.99％、25.97％。该研究为谷子秸秆资源的高效利用及其收获、加工机械的设计提供理论指导

INTRODUCTION

Millet, a multi-grain crop, is widely grown in the temperate and tropical regions of Eurasia *(Annor et al., 2017).* It has the characteristics of drought resistance, high water use efficiency, wide adaptability and rich nutrition and is considered an ecological crop for sustainable agriculture and human dietary needs *(Devi et al., 2014; Liang et al., 2018)*. Millet stems are rich in fibre, protein and other organic matter, thereby becoming a renewable multi-purpose biological resource *(Zhang, 2012)*. Crushed millet can be used to increase soil fertility in fields, produce forage for ruminants and manufacture fibreboard and other biological building materials through deep stem processing technology.

Cutting is an indispensable step in mechanical harvesting technology and deep stem processing. Meanwhile, cutting force is an index of the chewiness of forage for ruminants *(Chen et al., 2007; Zhou et al. 2012)*. The mechanical cutting properties of millet stems should be researched to improve the utilisation of such stems. Limited research on the mechanical cutting properties of millet stems has been conducted in recent years, whereas the mechanical cutting properties of wheat stems, corn stalks and rice straws have been studied. The mechanical cutting properties of stems vary depending on stem region, moisture content

and cutting form. A study on sunflower stalks showed that the cutting stress and specific cutting energy are higher in the lower region than in other areas *(İnce et al., 2005)*. A study on corn stalks reported that the cutting force and the total cutting energy of internodes and nodes vary significantly due to structural heterogeneity *(Igathinathane et al., 2010)*. Moisture content affects the mechanical properties of stalks. Researches about barley and safflower stalks were carried out to determine the effects of moisture content and stalk position on mechanical properties *(Özbek O. et al., 2009; Tavakoli H., 2009)*. For kenaf stalk cutting, the maximum cutting force and cutting energy were 1584.55 N and 8.75 J, respectively, at 35% moisture content and 694.86 N and 3.50 J, respectively, at 72% moisture content *(Dauda et al., 2014)*. In addition to these factors, the blade oblique angle also affects the mechanical cutting properties of stems. *Mathanker et al. (2015)* found that choosing an optimised blade oblique angle can result in significant savings in cutting energy and improvement of cutting quality for energycane stems. Results from a study of *Miscanthus x giganteus* stems revealed that the cutting energy at 60º blade oblique cutting angle is lower than that at 0º blade oblique cutting angle *(Johnson et al., 2012)*. *Zuoli Fu et al.* (2011) found that the best blade oblique angle to cut alfalfa stems was 10° for energy saving.

Considering the above points, this study focuses on discovering the variations in cutting stress and specific cutting energy with changes in stem regions, moisture content and blade oblique cutting angles. Results can provide basic data for the study of mechanical harvesting and processing of millet stems.

MATERIALS AND METHODS

Millet variety and sample preparation

Zhangza 10 is a fine-grained millet variety. It was planted in Taigu County, Shanxi Province in China (112º55′ E, 37º43′ N), and the sampling date was October 20, 2017.

Stems without lodging, pests and diseases were randomly selected. The average height of the millet stems was 110.9 cm. Leaf sheaths were removed, and the samples were divided into three millet stem height regions, namely, upper (S1), middle (S2) and lower regions (S3) (Fig.1). To prepare stem samples with different moisture content, the millet stems were naturally dried at an average room temperature of 25°C and moisture content was measured using a standard method (ASABE, 2008). Tests were conducted at five moisture content levels of 10.14%, 24.60%, 41.33%, 55.27% and 72.59% (w.b.).

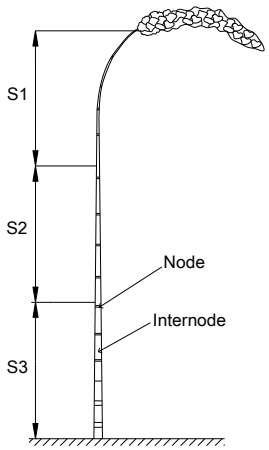

Fig.1 - The millet stem regions evaluated in the cutting test: (S1) upper region, (S2) middle region, (S3) lower region

Testing instrument

The test device used to measure the cutting force was a 5544 universal material testing machine (Instron, United States) with a maximum load of 2 kN. The instrument used to measure moisture content was a DHG-9023A drying oven (*Wuxi Three Xin Seiko Test Equipment Co. Ltd., China*) with a temperature adjustment range of 50°C–200°C. Other instruments utilised included an electronic analytical balance (0.001 g accuracy), a vernier calliper and a custom-made cutting test apparatus.

The custom test apparatus, which includes a fixed blade assembly and a movable blade assembly, can conduct cutting tests with different blade oblique angles (Fig.2a). The movable blade assembly primarily includes an upper joint, an upper joint nut and a moving blade. The fixed blade assembly mainly includes a fixed blade, an adjustment plate for the blade oblique angle, a protractor, a sample plate, a screw, a limiting nut, a sliding rail and a base (Fig.2b). Before the test, the upper joint was fastened on the material testing machine through the upper joint nut. The adjustment plate of the blade oblique angle has a central hole and

a 90° arc hole. Rotating the position of the bolt in the arc hole with the centre hole bolt can change the angle between the moving and fixed blades. To ensure that the sample is placed at the moving blade edge line, the position of the sample plate can be adjusted by the limiting nut. During the test, the material testing machine drove the movable blade assembly to move vertically and cut the stem samples.

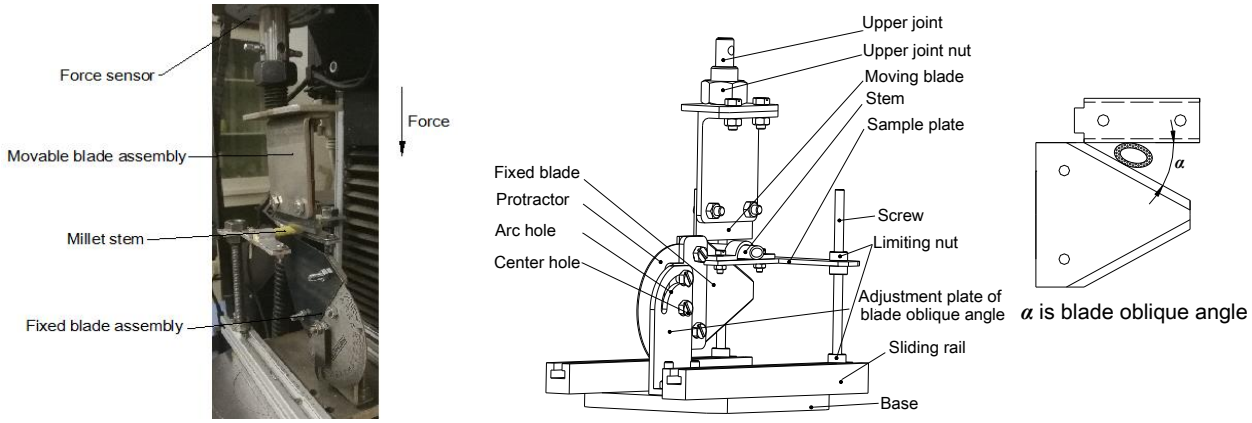

a. Physical map of test apparatus *b. Structure diagram of test apparatus* *c. Cutting diagram*

Fig. 2 - The cutting test

Cutting test

The mechanical cutting properties of the internodes and the nodes were measured due to structural heterogeneity. Before the test, the long and short axes of each sample were measured with the vernier calliper. Then, each sample was placed on the sample plate, with the midpoint of the sample positioned in the blade edge line. Millet stems are viscoelastic materials thus, the blade velocity was maintained at 300 mm·min^{-1} for all cutting tests *(Zhou et al., 2012)*. Each sample was cut, and its wall thickness was measured. Each treatment had six stems. After the tests, the cutting force and cutting energy were recorded by the testing machine at a certain frequency, and the cross-sectional areas, cutting stress and specific cutting energy were calculated as follows:

$$A = \frac{\pi}{4}\left[D_1 x D_2 - \left(D_1 - 2T\right) x \left(D_2 - 2T\right)\right] \quad (1)$$

$$E_t = \int_0^S F(s)ds \quad (2)$$

$$\tau = \frac{F}{A} \quad (3)$$

$$E_{ts} = \frac{1000 \cdot E_t}{A} \quad (4)$$

where: D_1 is the long axis of the stem cross section, [mm];
D_2 is the short axis of the stem cross section, [mm];
T is wall thickness of the stem cross section, [mm];
A is the area of the stem cross section, [mm^2];
E_t is the cutting energy, [J];
s is the cutting displacement of millet stem, [mm];
F is the cutting force, [N];
τ is the cutting stress, [MPa];
E_{ts} is the specific cutting energy, [mJ·mm^{-2}].

Data analysis

Data analysis was conducted using SAS 9.2. ANOVA test and Duncan's multiple comparison test were used to analyse the effect of the stem region on the mechanical cutting parameters, and $p<0.05$ represents that a factor (stem region) of a certain level is significantly different at the 5% levels of significance using the Duncan's multiple comparison test. Polynomial regression analysis was adopted to create a correlation model among the mechanical cutting properties, moisture content and blade oblique cutting angle.

RESULTS

Cutting force–deformation characteristics of millet stem

Millet stems are composite materials composed of multiple tissues, and the laws of deformation and failure are determined by their structure. The overall structure of the internodes and the nodes in this work was similar (Fig.3). The force–deformation curve was divided into two processes, namely, extrusion and cutting (Fig.4). During the extrusion process, the cutting force increased with an increase in displacement. The rate of change in the cutting force was initially slow in the extrusion process and then accelerated, followed by a high peak. The blade had a squeezing effect on the stem due to the stem's hollow core structure. Afterwards, the cutting force dropped abruptly, followed by a second low peak during the cutting process. Experimental observation showed that the blade cut into the stem, and the thick wall mechanical tissue, the fundamental soft tissue and medullary cavity tissue were destroyed in turn. Finally, the cutting force was gradually reduced to 0 N, and the cutting was completed. The blade squeezed the stem during the cutting process.

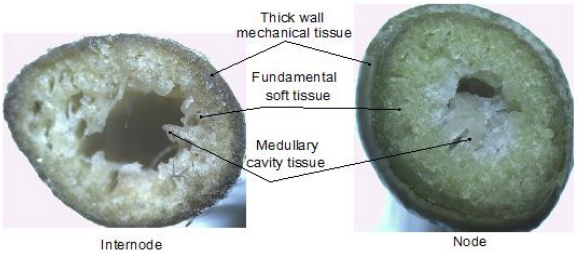

Fig. 3 - The cross-sectional stem structure

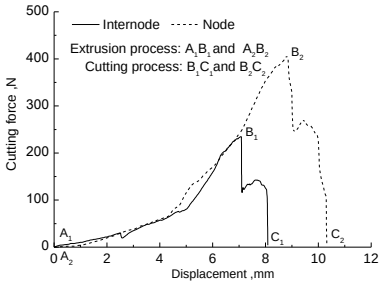

Fig. 4 - The cutting force–displacement curve of the millet stem internodes and nodes

Effects of stem region and material variation on mechanical cutting properties

The mechanical cutting properties between internodes and nodes among different stem regions are shown in Table 1. With internodes, the cutting stress decreased from stem lower region to upper region probably because the accumulation of more mature fibres in the lower region *(İnce et al., 2005)*. The cutting force and energy were higher in the lower region than in the upper region and significantly differed, and *p* value of cutting force and cutting energy were 0.0021 and 0.0029, respectively ($p<0.05$). The main reason was that the long axis, short axis and cross-sectional area decreased from the lower region to the upper region, and the reduced size parameters of the cross section decreased the cutting force and energy of the millet stem. These results were similar to those of cotton stalks in a previous work *(Aydın et al., 2018)*. The pattern of the mechanical cutting properties of nodes between stem regions was similar to that of the internodes.

Table 1

Effect of stem region on the mechanical cutting parameters during millet stem cutting

Physical properties		Stem region					
		Internodes			Nodes		
		S1	S2	S3	S1	S2	S3
Size parameters	D_1 [mm]	6.22cA	7.43bB	9.14aB	7.93bA	10.23aA	11.56aA
	D_2 [mm]	5.13bA	5.49bB	6.692aB	5.98bA	7.96aA	9.34aA
	A [mm^2]	17.50bB	27.69bB	35.54aB	43.47bA	64.72bA	88.490aA
Cutting force [N]		248.41bA	386.64aB	451.30aB	395.86bA	497.47bA	679.94aA
Cutting energy [J]		0.45bB	0.64bB	0.79aB	1.35bA	1.78abA	2.27aA
Cutting stress [MPa]		12.16aA	14.07aA	14.89aA	7.63aB	8.09aB	9.91aB
Specific cutting energy [mJ·mm^{-2}]		23.61aA	23.24aA	24.16aA	30.55aA	28.80aA	30.18aA

Note: moisture content of stem was 72.59%; blade oblique angle was 0°; values presented are mean from the original data; different letters (a, b, c) in the same line represent significant differences among stem region (p<0.05); and different letters (A, B) represent significant differences between internodes and nodes (p<0.05).

The cutting force and energy of the nodes and the internodes were significantly different, and p value of cutting force and cutting energy were 0.0022 and 0.0001, respectively (p<0.05), because the cross-sectional parameters of the nodes were larger than those of the internodes. Although the cutting force,

cutting energy and specific cutting energy of the nodes were larger than those of the internodes, the cutting stress of the nodes was significantly smaller than that of the internodes ($p<0.05$). The thick-walled mechanical tissue and fundamental soft tissue could be the main factor that determined its mechanical properties *(Zhao et al., 2011)*. Since the nodes also had more fundamental soft tissue than did the internodes, the more fundamental soft tissue resulted in a reduced cutting stress for the whole structural organisation of the nodes.

Effect of moisture content of millet stems on mechanical cutting properties

Moisture content is an important factor that affects the mechanical properties of crop stems. In this study, the cutting stress of the upper, middle and lower regions were 10.31–16.97, 12.66–18.17 and 13.57–27.32 MPa, respectively, at 10.14%–72.59% moisture content for the stem internodes.

The cutting stress values of the stem nodes were 7.1–14.67, 9.04–15.5 and 10.43–26.09 MPa, respectively. Fig.5a–5b presents the polynomial relationship between cutting stress and moisture content for the internodes and the nodes, whose r^2 values were larger than 0.82 and 0.73, respectively. The millet stem cutting stress increased with the moisture content when the latter was 10.14%–41.33%. However, the cutting stress of the stem decreased with the increase of the moisture content when the moisture content was higher than 41.33%. This finding could be attributed to the change in density at different moisture content levels *(Dauda et al., 2014)*. Results from the sunflower stalk study were consistent with ours *(Kocabıyık et al., 2004)*. During harvest period, the range of moisture content of millet stems was 45%–73%. Millet stems of lower cutting stress should be harvested at high moisture content to improve the utilisation rate of stem forage.

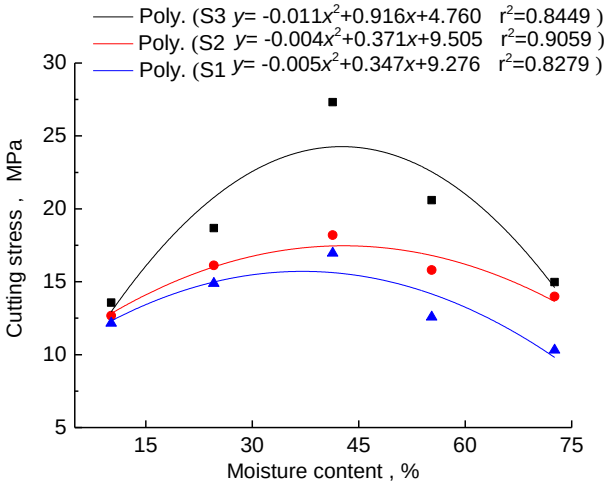

a. The cutting stress of internodes

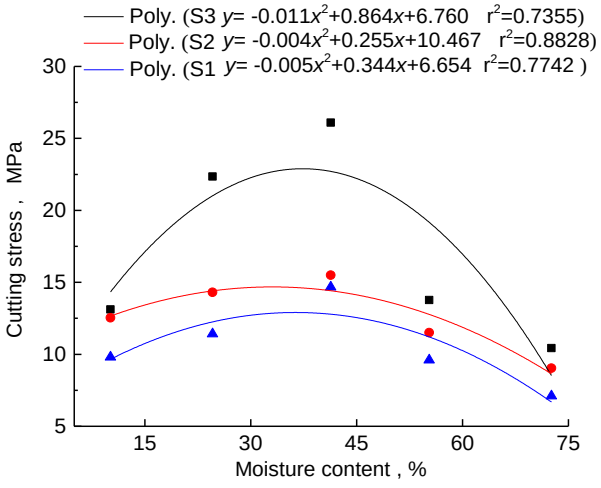

b. The cutting stress of nodes

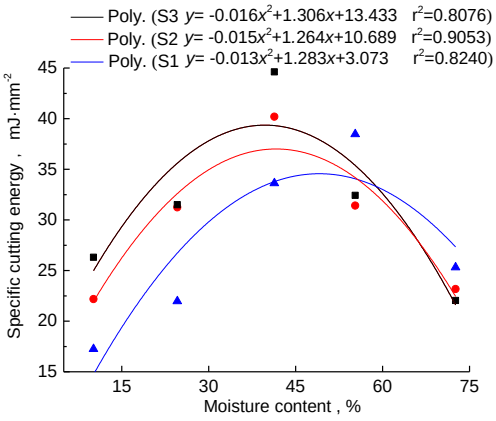

c. The specific cutting energy of internodes

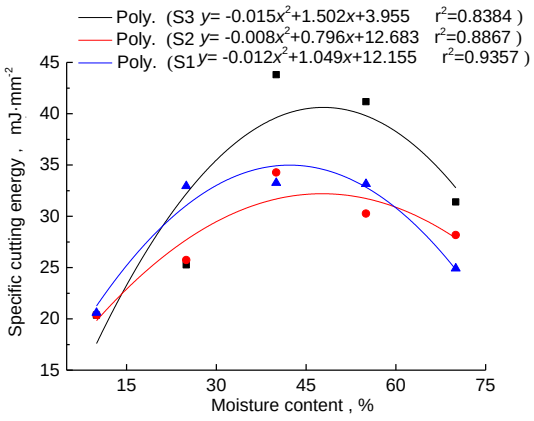

d. The specific cutting energy of nodes

■ Lower region ● Middle region ▲ upper region

Fig. 5 - The relationship between mechanical cutting properties and moisture content

The specific cutting energy values of the upper, middle and lower regions were 17.25–38.47, 22.17–40.20 and 22.04–44.61 mJ·mm^{-2}, respectively, at 10.14%–72.59% moisture content for the stem internodes, and those of the stem nodes were 20.36–43.80, 20.38–34.27 and 20.59–33.26 mJ·mm^{-2}, respectively. Fig.5c–5d shows the polynomial relationship between specific cutting energy and moisture content, whose r^2 values were larger than 0.80 and 0.83, respectively.

The specific cutting energy initially increased and then gradually reduced with the increase in moisture content. These results differed from those of other stem materials, such as sunflower stems (*İnce et al., 2005*). The reason may be that cutting energy is related to maximum cutting force *(Zhou et al., 2012)*, and high-cutting-stress stems require additional energy to be cut. To save energy, millet stems with approximately 41.33% moisture content should not be cut during mechanical harvesting and deep stem processing.

Effect of blade oblique angle on mechanical cutting parameters of millet stems

Tests were conducted at five blade oblique angles of 0º, 12º, 24º, 36º and 48º. The cutting stress of stems decreased as blade oblique angle was increased (Fig.6a–6b). The cutting stress of upper, middle and lower region for internodes were reduced 49.51%, 47.82% and 46.01% respectively compared 48º to 0º blade oblique angle, and those of nodes were reduced 38.32%, 39.37% and 23.82% respectively. These findings were consistent with those for legume forage in a previous work *(Zhao et al., 2009)*. In conclusion, the blade oblique angle has a strong influence on millet stem cutting stress and selecting the suitable blade oblique angle can reduce the cutting stress.

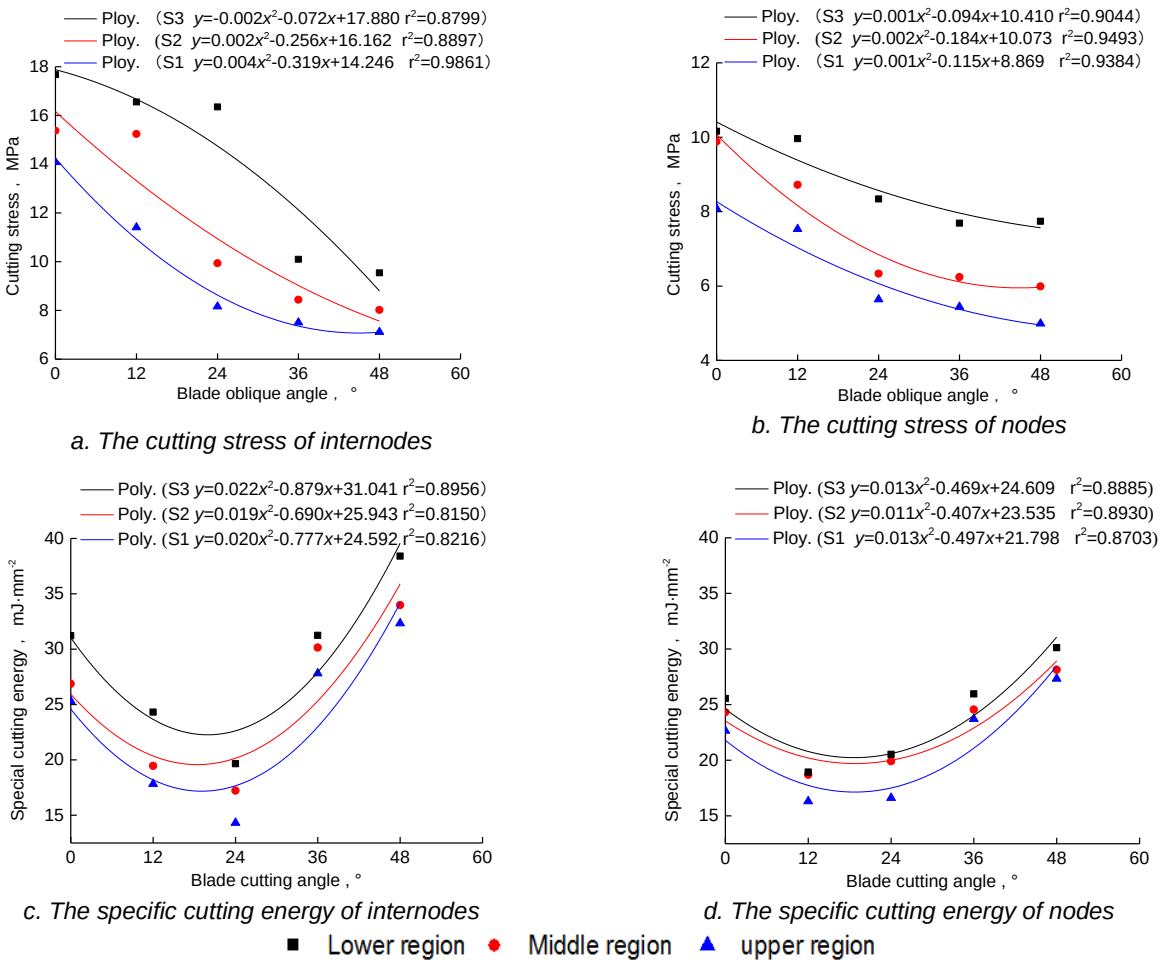

a. The cutting stress of internodes

b. The cutting stress of nodes

c. The specific cutting energy of internodes

d. The specific cutting energy of nodes

Fig. 6 - The relationship between mechanical cutting properties and blade oblique angle

The specific cutting energy of the millet stem initially decreased and then gradually increased as blade oblique angle was increased (Fig.6c–6d). These findings agreed with those for *Atriplex* and corn stems and indicated that the minimum specific cutting energy was at a blade oblique angle of 24º. The reason was that

cutting energy is used not only to cut stems but also for friction between stem and blade when the blade oblique angle is excessively large. Although the cutting force decreased, the frictional force increased rapidly *(Pang, 1982)*. However, these results differed from those for energycane and Miscanthus x giganteus stems *(Johnson et al., 2012; Mathanker et al., 2015)*.

Fig.6 presents the relationship between the mechanical cutting parameters and blade oblique angle for the internodes and the nodes, where the fitting equation accuracy was larger than 0.81. Fitting of the test data revealed that the minimum specific cutting energy of the upper, middle and lower regions of the internodes were 17.05, 19.68 and 22.26 mJ·mm^{-2}, respectively, at blade oblique angles of 19.68º, 18.16º and 19.43º, respectively. Meanwhile, the minimum specific cutting energy for nodes in the upper, middle and lower regions were 17.05, 19.77 and 20.38 mJ·mm^{-2}, respectively, at blade oblique angles of 18.04º, 18.50º and 19.12º, respectively. Overall, the average and optimised blade oblique angle was 18.8º for all regions of the millet stems. Through the verification test, the specific cutting energy was reduced by 28.99% and 25.97% for internodes and nodes, respectively when 18.8º and 0º blade oblique angles were compared (Table 2).

Table 2

Comparison of specific cutting energy for millet stem internodes and nodes

Blade oblique angle [°]	Moisture content [%]	Specific cutting energy [mJ·mm^{-2}]					
		Internodes			Nodes		
		S1	S2	S3	S1	S2	S3
0	10.07	19.63±5.48	22.65±4.96	25.35±5.24	22.80±2.55	23.55±3.36	21.54±6.22
	71.32	25.34±3.08	26.87±4.55	29.21±4.64	22.63±4.55	24.31±2.49	27.55±5.42
18.8	10.07	14.56±1.90	17.11±2.29	17.24±1.76	15.94±3.43	17.24±1.76	17.72±2.04
	71.32	17.90±3.77	18.46±3.75	20.15±3.82	16.11±2.96	17.91±3.95	20.37±2.40
Saving energy ratio [%]		27.59	27.88	31.50	29.45	26.56	21.90
Average [%]		28.99			25.97		

Note: values presented are mean ± standard deviation from the original data.

CONCLUSIONS

Cutting tests were conducted to investigate the mechanical cutting properties of the internodes and nodes of millet stems. This research revealed the effects of stem region, moisture content and blade oblique angle on mechanical cutting parameters. The main conclusions of this study are as follows.

(1) The force–displacement curves in the cutting experiments indicated that the cutting process must be divided into the extrusion and cutting processes due to the hollow core structure of millet stems.

(2) The cutting force and energy of the internodes were 248.41–451.30 N and 0.45–0.79 J at 0° blade oblique angle（72.59% [w.b.]), respectively, and those of the nodes were 395.86–679.94 N and 1.35–2.27 J at 0° blade oblique angle（72.59% [w.b.]), respectively. The cutting force and energy of the nodes were significantly larger than those of the internodes (p<0.05), but the cutting stress of the nodes was greatly smaller than that of the internodes (p<0.05).

(3) The cutting stress was decreased from lower region to upper region of millet stems, and the parameters of cross section, cutting force and cutting energy of the lower stem region were significantly larger than those of the upper region (p<0.05).

(4) The cutting stress and specific cutting energy initially increased and then reduced with increasing moisture content. Cutting millet stems with moisture content of approximately 41.33% should be avoided during mechanical harvesting and deep stem processing to save energy.

(5) The blade oblique angle has a strong influence on the mechanical cutting properties of millet stems. Cutting stress was reduced with the increase in blade oblique angle. However, the specific cutting energy was initially reduced and then increased with the increase in blade oblique angle. Specific cutting energy was reduced by 28.99% and 25.97% for internodes and nodes, respectively when 18.8º and 0º blade oblique angles were compared.

ACKNOWLEDGEMENTS

This research, titled ‘Effects of stem region, moisture content and blade oblique angle on mechanical cutting of millet stems’, was funded by the National Key Research and Development Plan of China (2016YFD0701801). The authors are grateful and honoured to have obtained support from the Key Laboratory of Biomechanics.

REFERENCES

[1] Annor G. A., (2017), Why do millets have slower starch and protein digestibility than other cereals ?. *Trends in Food Science & Technology*, Vol. 2017, Issue 66, pp. 73-83, Ed. Elsevier, London/England;

[2] Aydın İ., (2018), Mechanical properties of cotton shoots for topping. *Industrial Crops & Products,* Vol. 2018, Issue 112, pp. 396-401, Ed. Elsevier, Amsterdam/Netherlands;

[3] Chen Y., (2007), Effect of harvest date on shearing force of maize straws. *Livestock Science*, Vol.2007, Issue 111, pp. 33-44, Ed. Elsevier, Amsterdam/Netherlands;

[4] Dauda S. M., (2014), Physical and mechanical properties of kenaf stems at varying moisture contents. *Agriculture & Agricultural Science Procedia*, Vol. 2, Issue 2, pp. 370-374;

[5] Devi P. B., (2014), Health benefits of finger millet (eleusine coracanal) polyphenols and dietary fibre: a review. *Journal of Food Science & Technology*, Vol. 51, Issue 6, pp. 1021-1040, New Delhi/India;

[6] Igathinathane C., (2010), Corn stalk orientation effect on mechanical cutting. *Biosystems Engineering*, Vol. 107, Issue 2, pp. 97-106, Ed. Elsevier, San Diego/USA;

[7] Ince A., (2005), Bending and shearing characteristics of sunflower stalk residue. *Biosystems Engineering*, Vol. 92, Issue 2, pp. 175-181, Ed. Elsevier, San Diego/USA;

[8] Johnson P. C., (2012), Cutting energy characteristics of miscanthus x giganteus stems with varying oblique angle and cutting speed. *Biosystems Engineering*, Vol. 112; Issue 1; pp. 42-48, Ed. Elsevier, San Diego/USA;

[9] Kocabıyık H., (2004), Determination of cutting properties of sunflower stalk. *Journal of Agriculture. Mach. Science*，Vol. 10, Issue 3, pp. 263–267;

[10] Liang K., (2018), Metabolic variation and cooking qualities of millet cultivars grown both organically and conventionally. *Food Research International*, Vol. 2018, Issue 106, pp. 825, Ed. Elsevier, Amsterdam/Netherlands;

[11] Mathanker S.K., (2015), Effect of blade oblique angle and cutting speed on cutting energy for energycane stems. *Biosystems Engineering*, Vol. 2015, Issue 133, pp. 64-70, Ed. Elsevier, San Diego/USA;

[12] Özbek O., (2009), Some mechanical properties of safflower stalk. *Applied Engineering in Agriculture*, Vol. 25, Issue 4, pp. 619-625, Spokane/U.S.A.;

[13] Pang S.H., (1982), Theory of sliding cutting and the choice of its angle. *Journal of Huazhong Agricultural College*, Vol. 1982, pp. 64-69, Wuhan/P.R.C.;

[14] Tavakoli H., (2009), Some engineering properties of barley straw. *Applied Engineering in Agriculture*, Vol. 25, Issue 4, pp. 627-633, Spokane/U.S.A.;

[15] Zhao C.H., (2009), Experiment on stalk mechanical properties of legume forage and grasses. *Transactions of the Chinese Society of Agricultural Engineering*, Vol. 25, Issue 9, pp. 122－126, Beijing/P.R.C;

[16] Zhao C.H., (2011), Mechanical properties and microstructure of new species forage stems in harvesting period. *Transactions of the Chinese Society of Agricultural Engineering*, Vol. 27, Issue 7, pp. 179－183, Beijing/P.R.C.;

[17] Zhang X.W., (2012), Current situation and problems of millet harvesting machinery. *Agricultural Technology & Equipment*, Vol. 2012, Issue 20, pp. 32-34, Beijing/P.R.C.;

[18] Zhou D., (2012), Temporal dynamics of shearing force of rice stem. *Biomass & Bioenergy*, Vol. 47, Issue 4, pp. 109-114, Ed. Elsevier, London/ England;

[19] ZuoLi Fu., (2011), Experiment for alfalfa stem-cutting and study for mechanical properties, *2011 ASABE Annual International Meeting*, pp.1-8, Spokane/U.S.A.

[20] ***ASABE Standards, 2008. S358.2. Moisture Measurement – Forages. *American Society of Agricultural and Biological Engineers*, St. Joseph, MI, Spokane/U.S.A.;

VERIFICATION OF THE MATHEMATICAL MODEL OF THE ENERGY CONSUMPTION DRIVE FOR VIBRATING DISC CRUSHER
/
ВЕРИФІКАЦІЯ МАТЕМАТИЧНОЇ МОДЕЛІ СПОЖИВАНИХ ЕНЕРГОВИТРАТ ПРИВОДА ВІБРАЦІЙНОЇ ДИСКОВОЇ ДРОБАРКИ

Ph.D. Eng. Kupchuk I.M., Ph.D. Eng. Solona O.V., Ph.D. Eng. Derevenko I.A., Ph.D. Eng. Tverdokhlib I.V.
Vinnytsia National Agrarian University / Ukraine
Tel: +380978173992; E-mail: kupchuk.igor@i.ua

Keywords: *vibrating disc crusher, energy consumption, grinding, cutting, impact*

ABSTRACT

One of the most energy-intensive operations used in feed technology for livestock is grinding. Therefore, scientific research aimed at minimizing the consumption of energy resources by technological machines – crushers and increasing the energy efficiency of the process in general is an important task. When grinding grain with a moisture content index above the basic condition, there is a low efficiency of the method of crushing by impact due to the increased plasticity of the material and an increase in the value of the marginal deformation that the grain can perceive before fracture. Partial solution of this problem is possible by combining the method of cutting and impact, which formed the basis of a technical solution implemented in the scientific laboratory of the Vinnytsia National Agrarian University. In previous scientific research, the authors developed and analyzed a mathematical model of energy consumption by a crusher drive. As a result of theoretical studies, the analytical and graphical dependence of the energy consumption by the drive from the angular velocity of the crusher rotor shaft was obtained. The aim of this article is to verify the reliability of a mathematical model by conducting experimental tests and comparing the results of experimental researches with theoretical researches. The experimental part of the work was performed in the laboratories of the department of processes and processing equipment and food industries of the Vinnytsia National Agrarian University and the specialized laboratory of «Ovchatsky» MPD, SE «Ukrspirt», using the experimental-industrial model of the vibration disc-type crusher. The EMF-1:1 electronic wattmeter recorded energy consumption, as well as wireless tachometer UNI-T UT372 the rotation frequency of the drive shaft (rotor). Verification of the mathematical model has shown a high level of its adequacy, and it can be used in the designing of a vibrating disc crusher of this type.

РЕЗЮМЕ

Однією із найбільш енергоємних операцій, що застосовуються в технології приготування кормів для тваринництва є подрібнення. Тому, наукові дослідження спрямовані на мінімізацію споживання енергетичних ресурсів технологічними машинами – дробарками та підвищення енергоефективності процесу в цілому є актуальною задачею. При подрібненні зерна із показником вологовмісту вище базисної кондиції спостерігається низька ефективність способу подрібнення ударом, що зумовлено підвищеною пластичністю матеріалу та збільшенням значення граничної деформації, яку зерно може сприймати до руйнування. Часткове вирішення даної проблеми можливе при комбінуванні способу різання та удару, що і лягло в основу технічного рішення реалізованого у науковій лабораторії Вінницького національного аграрного університету. В попередніх дослідженнях авторами було розроблено та проаналізовано математичну модель споживання енергії приводом дробарки. В результаті теоретичних досліджень було отримано аналітичну та графічну залежність споживання енергії приводом від кутової швидкості валу ротора дробарки. Метою даної статті є перевірка достовірності математичної моделі шляхом проведення експериментальних випробовувань та порівняння результатів експериментальних досліджень із теоретичними. Експериментальну частину роботи виконано на базі лабораторій кафедри процесів та обладнання переробних та харчових виробництв Вінницького національного аграрного університету і спеціалізованої лабораторії «Овечацького МПД» ДП «Укрспирт» з використанням експериментально-промислового зразка вібродискової дробарки. Електронним ватметром EMF-1:1 фіксували показники споживання енергії, а безпровідним тахометром UNI-T UT372 частоту обертання приводного вала (ротора). Верифікація математичної моделі показала високий рівень її адекватності, та вона може бути використана при проектуванні вібраційної дискової дробарки даного типу.

INTRODUCTION

Today the hammer crushers *(Yanovych V.P., Honcharuk T.V., Honcharuk I.V., Kovalova K.V., 2018)* are usually used in livestock farms and feed mills for grain grinding. In this technological machines, the destruction of the material occurs as a result of the successive stages of the process: applying a distributed load to the area of the hinged-hanging hammer (*Kudinov Ye.S., Bojko I.G., 2010*), the appearance of deformations in the material and the internal tension, the achievement of the limit values of internal tension and deformations, the breaking of the bonds of atoms and molecules among themselves *(Toneva P., Epple P., Breuer M., 2011; Nanka O.V., 2015)*.

In the process of crushing mainly fragile and plastic fractures occur. For a fragile fracture, a slight deformation of the material is characteristic, and after the destruction there is no residual deformation. The impact energy is used to overcome the forces of adhesion of body particles, that is, the formation of a new surface. During the destruction of plastic materials energy is spent on the break of structural bonds and on significant plastic deformation. The energy expended on deformation turns into heat.

The material strength and its extreme deformation is determined by the structural and mechanical characteristics of the grain and depends on the variety, size, density, moisture content, temperature, etc. *(Hvozdiev O.V., Shpyhanovych T.O., Yalpachyk O.V., 2011)*. If moisture content of the material increases, then the fragility and strength of the material decrease, while the plasticity and absolute deformation, which the grain can withstand before the beginning of destruction, increase.

Grinding brittle materials requires significantly less energy than plastic. The fragility and plasticity of a material depends on its physical condition, therefore it is advisable to grind the material in a fragile state.

As experience shows, fodder grain with moisture content, which exceeds the basic conditions, is used mainly for the production of feed. This is due to the material aspects (market value of raw grain is much lower) and the production capacity of a particular enterprise.

It therefore becomes apparent that the profitability and competitiveness of the livestock sector depend on the energy-efficient nature of this technological operation implementation, and the reduction of energy costs in the process is an important task.

In order to reduce costs, it is very promising to use machines for grinding grain proposed by Sergeev N.S. *(Sergeev S.N., 2008)*, Yanovych V.P. *(Yanovych V.P., 2017),* Nanka O.V. *(Nanka O.V, Boyko I.G., 2012)*. The principle of these machines is based on the combination of cutting and impact action on the material. The advantage of such a combination is the local excessive stress of the surface microwaves in the places of loads application. In the cutting process, the knife blade is wedged into the product and at the contact surface a specific pressure is created that is sufficient for the destruction of the body.

Using the infrastructure of the laboratory of the process and processing equipment and food industry of Vinnytsia National Agrarian University, a vibration disc crusher was developed (Fig. 1) *(Palamarchuk I.P., Yanovych V.P., Kupchuk I.M., Solomko I.V., 2013)*. In this crusher, the electric motor *5* transmits to the eccentric shaft *7* (through the coupling *6*) a rotary movement. The counterweight *8* is set to the eccentric shaft *7*. The eccentric shaft *7* is equipped with a rotor *9* with discs *10*.

The rotational movement of the eccentric shaft and counterweight leads to the imbalance of the rotor *9* and the discs *10 (Palamarchuk I.P., Yanovych V.P., Kupchuk I.M., Solomko I.V., 2013; Palamarchuk I.P., Yanovych V.P., Kupchuk I.M., 2015)*.

The material is continuously fed through the feeding throat *2* and is crushed as a result of the rotating and oscillating motion of the discs *10*. With reduced particle size, the crushed material under the action of centrifugal forces and oscillatory movement of the screen is sieved. The particles equal to or smaller than the diameter of the sieve holes *4* are discharged through the neck for unloading *3*; the residue should be re-grinded *(Palamarchuk I.P., Yanovych V.P., Kupchuk I.M., Solomko I.V., 2013; Palamarchuk I.P., Yanovych V.P., Kupchuk I.M., 2015)*.

This combination of methods of action (impact and cutting) makes it possible to grind raw materials with high moisture content and reduce energy costs for this technological operation *(Palamarchuk I.P., Yanovych V.P., Kupchuk I.M., 2015; Yanovych V.P., Kupchuk I.M., Kovalchuk O.S., 2016)*.

The results of theoretical research of energy consumption on the crusher drive showed a reduction in consumption compared to existing crushers *(Yanovych V.P., Kupchuk I.M., Kovalchuk O.S., 2016)*. However, the use of these mathematical models for the design of crushers requires their verification.

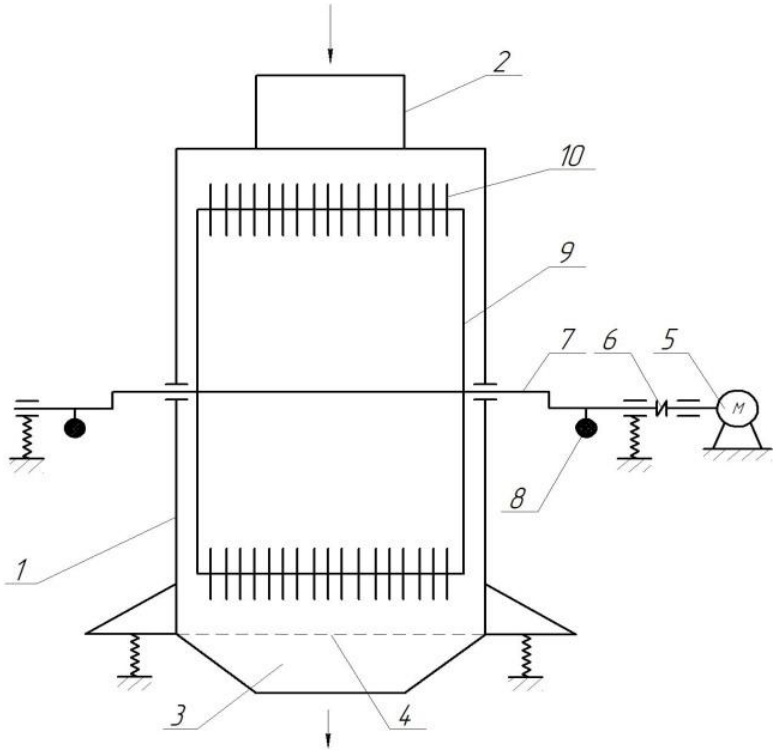

Fig 1 - Vibration disc crusher (kinematic scheme):
1 – frame; 2, 3 - neck for loading and unloading; 4 - sieve; 5 – electric motor; 6 – coupling; 7 – eccentric shaft; 8 - counterweight; 9 - rotor; 10 – discs.

The aim of the article is to check the adequacy of the mathematical model of energy consumption for driving a crusher by comparing the results of theoretical and experimental research.

MATERIALS AND METHODS

The results of theoretical research on energy consumption by crusher drive are presented in the previous article *(Yanovych V.P., Kupchuk I.M., Kovalchuk O.S., 2016)* in the form of analytical (1) and graphical dependence (Fig. 2).

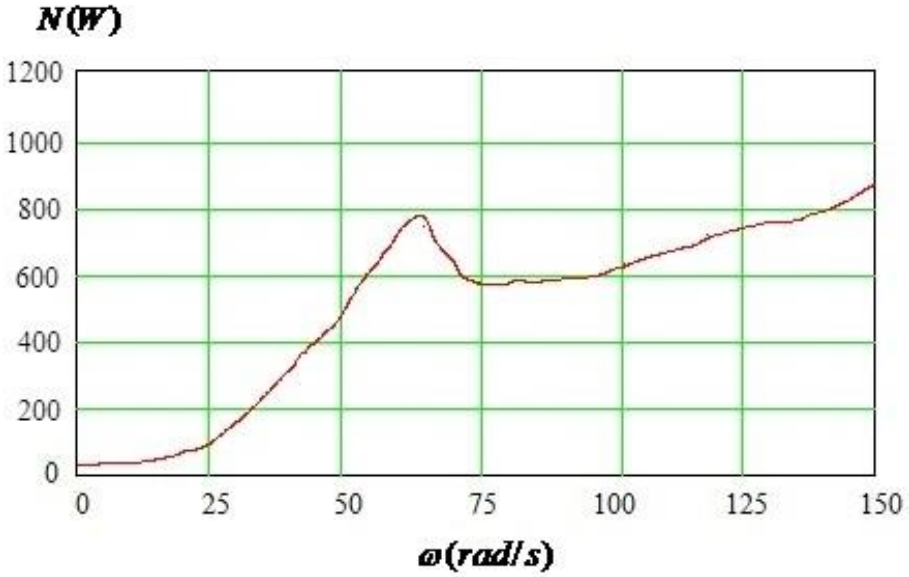

Fig. 2 - Energy consumption by crusher drive (theoretical study)

$$N = \left[\left[\sqrt{\left(\left(\frac{(m_2+m_3)\omega_{rotor}^{\ 2} e - m_4 \omega_{rotor}^{\ 2} l}{m_1} \right) + \left(\frac{m_2 \cdot \omega_{rotor} \cdot \mathrm{e} + m_3 \cdot r \cdot \omega_{rotor} - m_3 \cdot 2ku \cdot r_{disk} \cdot \omega_{disk} + m_4 \cdot \omega_{rotor} \cdot l}{\cos(\omega_{rotor} \cdot t) m_1} \right)^2 + \left(\frac{(m_2+m_3)\omega_{rotor}^{\ 2} e - m_4 \omega_{rotor}^{\ 2} l}{m_1} - \frac{(m_1+m_2+m_3+m_4)g}{\sin(\omega_{rotor} \cdot t) \cdot m_1} \right)^2} \times \right. \right.$$

$$\left. \left. \sqrt{\left(\frac{\left(\frac{(m_2+m_3)\omega_{rotor}^{\ 2} e - m_4 \omega_{rotor}^{\ 2} l}{m_1} + \frac{m_2 \cdot \omega_{rotor} \cdot \mathrm{e} + m_3 \cdot r \cdot \omega_{rotor} - m_3 \cdot 2ku \cdot r_{disk} \cdot \omega_{disk} + m_4 \cdot \omega_{rotor} \cdot l}{\cos(\omega_{rotor} \cdot t) m_1} \right) \cdot \alpha_x \omega_{rotor}}{\left(k_x^2 - \omega^2_{\ rotor}\right)^2 + \alpha_x^2 \omega^2_{\ rotor}} \cdot \left(\alpha_x \omega_{rotor} \cos \omega_{rotor} t - \left(k_x^2 - \omega^2_{\ rotor}\right) \sin \omega_{rotor} t \right) \right)^2 + \left(\frac{\left(\frac{(m_2+m_3)\omega^2_{\ rotor} e - m_4 \omega^2_{\ rotor} l}{m_1} - \frac{(m_1+m_2+m_3+m_4)g}{\sin(\omega_{rotor} \cdot t) \cdot m_1} \right) \cdot \alpha_z \omega_{rotor}}{\left(k_z^2 - \omega^2_{\ rotor}\right)^2 + \alpha_z^2 \omega^2_{\ rotor}} \cdot \left(k_z^2 - \omega^2_{\ rotor}\right) \cos \omega_{rotor} t + \alpha_z \omega_{rotor} \sin \omega_{rotor} t \right)^2} \right] + \right.$$

$$\left. \left[0{,}5 \cdot \mu \cdot d_{bearing} \cdot \omega_{rotor}^{\ 2} \cdot \sqrt{\left(\left(\frac{(m_2+m_3)\omega_{rotor}^{\ 2} e - m_4 \omega_{rotor}^{\ 2} l}{m_1} \right) + \left(\frac{m_2 \cdot \omega_{rotor} \cdot \mathrm{e} + m_3 \cdot r \cdot \omega_{rotor} - m_3 \cdot 2ku \cdot r_{disk} \cdot \omega_{disk} + m_4 \cdot \omega_{rotor} \cdot l}{\cos(\omega_{rotor} \cdot t) m_1} \right)^2 + \left(\frac{(m_2+m_3)\omega_{rotor}^{\ 2} e - m_4 \omega_{rotor}^{\ 2} l}{m_1} - \frac{(m_1+m_2+m_3+m_4)g}{\sin(\omega_{rotor} \cdot t) \cdot m_1} \right)^2} \right] \right] \times \gamma_{eem}^{-1} \quad (1)$$

$$m_1 = m_\kappa + m_m + m_{sf} + m_b \quad (2)$$

$$m_2 = m_r + m_c \quad (3)$$

$$m_3 = m_{id} \quad (4)$$

$$m_4 = m_{cw} \quad (5)$$

$$m_r = m_{esh} + m_{cd} + m_{var} + m_{sup} + m_{axles} \quad (6)$$

where m_κ – mass of frame, kg; m_m – mass of material, kg; m_{sf} – mass of support frame, kg; m_b – mass of bearing units, kg; m_r – rotor weight, kg; m_c – mass of couplings, kg; m_{id} – mass of impact discs, kg;

m_{cw} – weight of counterweight, kg; m_{esh} – mass of eccentric shaft, kg; m_{cd} – mass of intermediate discs, kg; m_{var} – a mass of eccentric variation mechanisms, kg; m_{sup} – mass of support discs, kg; m_{axles} – mass of disc axles, kg; $d_{bearing}$ – bearing diameter, m; γ_{eem} – efficiency of the electric motor; ω_{rotor} – rotor angular velocity, s^{-1}; ω_{disk} – discs angular velocity, s^{-1}; ku – torque transmission ratio; e – eccentricity of the shaft, m; l – length from the counterweight mass centre to the rotation axis of the rotor, m; r – length from disc to rotor, m; r_{disk} – disc radius, m; g – acceleration of gravity, m/s^2; α_x, α_z – dissipation coefficients relative to the axes OX and OZ; k_x^2, k_z^2 – frequency of system free oscillations relative to the axis OX and OZ, *Hz*; t – time, s; μ – coefficient of friction in bearings.

Taking into account the permissible errors of the measuring equipment, a critical value of the discrepancy between the experimental and theoretical research was taken by 15% *(Yanovych V.P., Kupchuk I.M., 2017)*. Exceeding this boundary indicates the unreliability of the mathematical model and the inability to use it when designing a crusher of this type. Processing and analysis of the research results were carried out in the Microsoft Excel software environment *(Kupchuk I.M., 2017)*.

The experimental research was carried out in the laboratories of the department of processes and equipment for the processing and production of food products in Vinnytsia National Agrarian University and the specialized laboratory "OVECHATSKY MTD" of the SE «Ukrspirt» *(Yanovych V.P., Kupchuk I.M., 2017)* using the experimental model of a vibrating disc crusher *(Palamarchuk I.P., Yanovych V.P., Kupchuk I.M., Solomko I.V., 2013)* (Fig. 3).

To manage and change rotation frequencies of the motor shaft, the AOSN-20-220-75 autotransformer was used (Figure 4) *(Kupchuk I.M., 2017; Yanovych V.P., Kupchuk I.M., 2017)*. It contains mobile current-collecting contact in the form of graphite roller and allows you to smoothly change voltage from zero to maximum. Also, the winding of the above mentioned autotransformer has several terminals, which can generate various characteristics of the current at the output.

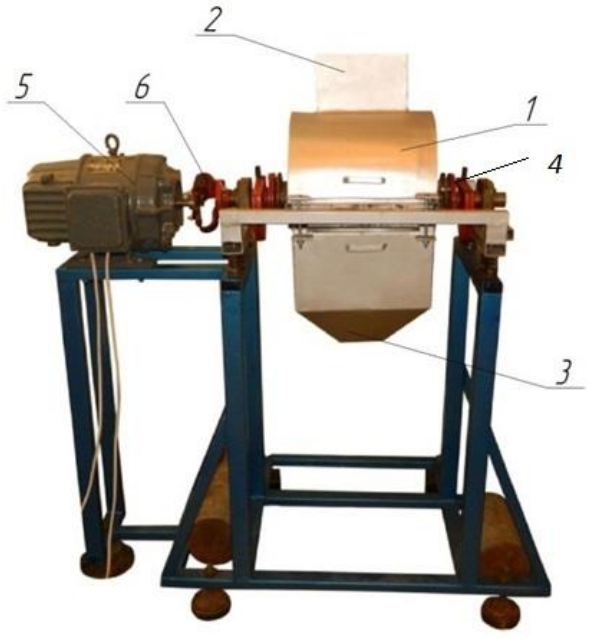

Fig. 3 - Vibrating disc crusher (experimental model)
1 – frame; 2, 3 – neck for loading and unloading; 4 – rotor; 5 – electric motor; 6 – coupling

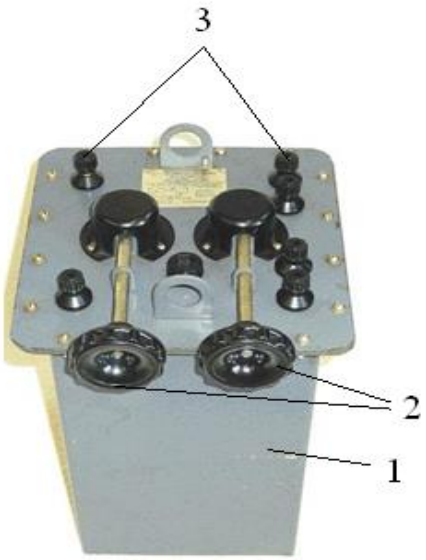

Fig. 4 - Laboratory autotransformer AOSN-20-220-75
1 - external casing; 2 - voltage regulators; 3 -cells

To record the angular velocity values of the drive shaft, the UNI-T UT372 wireless tachometer was used (Fig. 5). The operating principle and operating rules for the tachometer are described in the technical documentation *(Kupchuk I.M., 2017; Yanovych V.P., Kupchuk I.M., 2017)*.

Fig. 5 - Tachometer UNI-TUT372:
1 - laser indication; 2 - digital indicator; 3 - control panel

Fig.6 - Electronic wattmeter EMF-1
1 - wattmeter housing; 2 - control panel; 3 - display

To determine the energy consumption to drive the crusher, the EMF-1 electronic wattmeter was used (Figure 6).

RESULTS

Given the technological condition of material destruction by crusher discs (linear velocity of the edge of the impact disc) *(Yanovych V.P., Honcharuk T.V., Honcharuk I.V., Kovalova K.V., 2018; Sergeev S.N., 2008)*, the experiment was carried out at an angular velocity of the rotor ω = 100...150 s^{-1}.

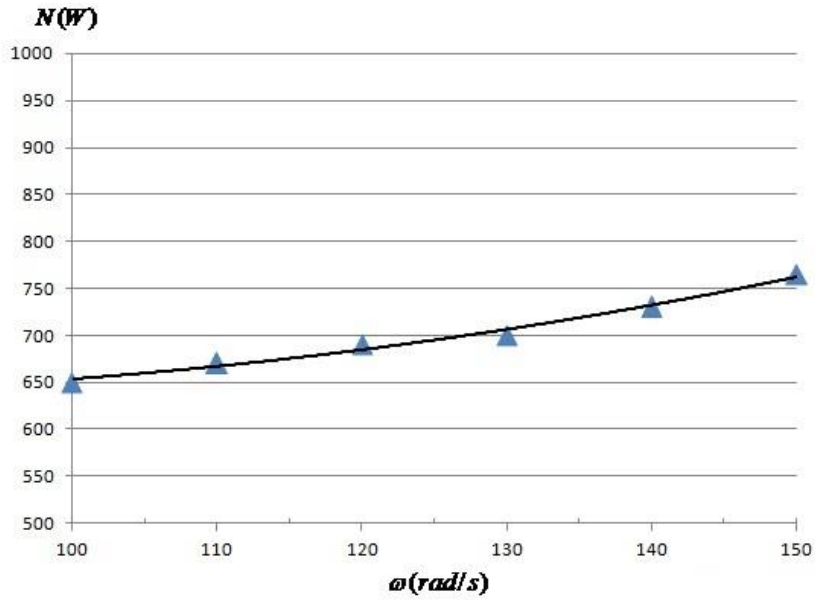

Fig. 7 - Energy consumption by crusher drive (experimental research)

As it can be seen from the results of experimental studies of electric motor consumed power (Fig. 7), with increasing rotor angular velocity ω=100...150 rad/s, power consumption N increases almost proportionally N= 650...765 W. To compare the results of experimental and theoretical research (Table 1), we show them in the form of graphical dependencies (Fig. 8).

Table 1

Energy consumption by crusher drive (experimental and theoretical research results)

ω [s^{-1}]	N_T [W]	N_E [W]	Divergence	
			+/-	%
100	635	650	15	2,31
110	685	670	-15	-2,24
120	710	690	-20	-2,90
130	780	700	-80	-11,43
140	800	730	-70	-9,59
150	840	765	-75	-9,80

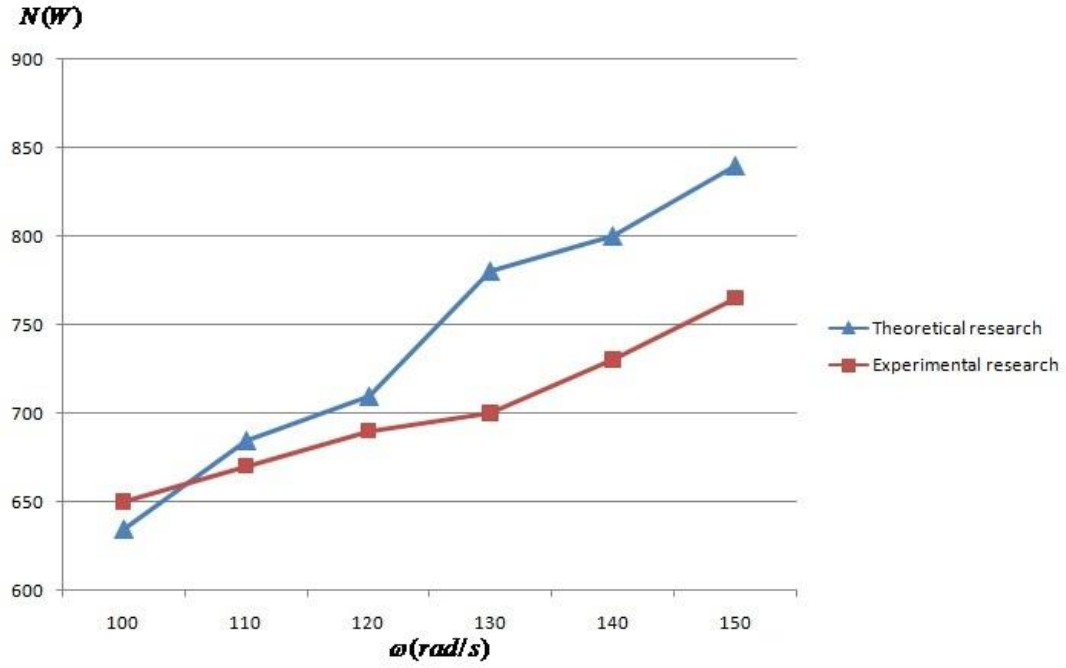

Fig. 8 - Comparison of theoretical and experimental research results

CONCLUSIONS

Comparing the theoretical and experimental research revealed a discrepancy, which is 2.24...11.43 % for the operational regime. Since this discrepancy is lower than the critical one (15%), the mathematical model (1) can be considered verified and it can be used in the construction of vibrating disc crushers of this type.

REFERENCES

[1] Hvozdiev O.V., Shpyhanovych T.O., Yalpachyk O.V., (2011), Improvement of the grain grinding process, *Collection of scientific works of Vinnytsia National Agrarian University. Series: Engineering*, № 11, pp. 143-150;

[2] Kudinov Ye.S., Bojko I.G., (2010), Analysis of methods for grinding grain feeds in relation to their energy intensit, *Bulletin of the Kharkov National Technical University of Agriculture named after Petr Vasilenko. Series: Engineering*, № 95, pp. 5;

[3] Kupchuk I.M., (2017), The compromise optimization of regime parameters for process of grain grinding in the ethanol production, *Vibration in engineering and technology*, № 4(87), pp. 91-100;

[4] Nanka O.V, Boyko I.G., (2012), Ways of reducing the energy intensity of grain milling and improving the quality of grinding, *Technology of production and processing of livestock products. Collection of scientific works of BNAU, №* 7, pp. 55-58;

[5] Nanka O.V., (2015), Areas of increasing the efficiency of the grain milling process, *Construction, production, operation of agricultural machines*, № 45, pp. 152-157;

[6] Palamarchuk I.P., Yanovych V.P., Kupchuk I.M., (2015), The analysis of the mathematical model of the vibrating crusher of grain raw materials of alcohol production, *Motrol. Commission of motorization and energetics in agriculture, №* 17(4), pp. 139-144;

[7] Palamarchuk I.P., Yanovych V.P., Kupchuk I.M., Solomko I.V., (2013), Development of the structural technological scheme of vibrating rotor crusher, *Vibration in engineering and technology*, №1(69), pp.125-129;

[8] Sergeev S.N., (2008), *Centrifugal rotary shredders of feed grain*, PhD dissertation, Chelyabinsk State Agroengineering University, Chelyabinsk/Russian Federation;

[9] Toneva P., Epple P., Breuer M., (2011), Grinding in an air classifier mill, *Powder Technology,* № 211, pp.19–27;

[10] Yanovych V.P., (2017), *Scientific and technical bases of mechanical processing of agricultural raw materials under the condition of vibrational influence*, Dr.Eng dissertation, National Science Centre "Institute of Mechanization and Electrification of Agriculture", Glevaha / Ukraine;

[11] Yanovych V.P., Honcharuk T.V., Honcharuk I.V., Kovalova K.V., (2018), Engineering management of vibrating machines for targeted mechanical activation of premix components, *INMATEH – Agricultural Engineering,* № 54(1), pp. 25–32.

[12] Yanovych V.P., Kupchuk I.M., (2017), Determination of rational operating parameters for a vibrating disk-type grinder used in ethanol industry, *INMATEH – Agricultural engineering,* № 52(2), pp. 143–148;

[13] Yanovych V.P., Kupchuk I.M., Kovalchuk O.S., (2016), The theoretical studies of energy parameters of vibration-disc crusher starch containing substance. *SWorld journal: Technical sciences.* № 11, pp. 17-24.

EVALUATION INDEX SYSTEM OF MECHANIZED MAIZE PRODUCTION
/
玉米生产全程机械化水平评价指标体系的研究与应用

Lecturer Li Xin*[1)]
[1)] College of Electrical and Mechanical Engineering, Agricultural University of Hebei, Baoding / China
Tel: +15930761572; E-mail: lixin20131113@163.com

Keywords: *mechanized maize production, index system, gray correlation analysis, gray analytic hierarchy*

ABSTRACT
Agricultural mechanization plays a positive role in accelerating agricultural modernization and increasing farmers' income. Maize lags far behind in terms of mechanization among three major crops. This study established an evaluation index system based on gray correlation analysis and gray analytic hierarchy process to accurately evaluate mechanized maize production. Correlation analysis was employed to classify the roles of various evaluation indexes for mechanized maize production. A total of 12 indexes were selected by gray correlation analysis, and an index system was established for evaluating mechanized maize production in a case study on Hebei Province in China. Gray analytic hierarchy process was used to determine the weight coefficient of each index, and a comprehensive evaluation value of mechanized maize production was obtained. DPS7.05 data processing software was utilized to calculate the correlation between each index and comprehensive level value. Results demonstrate that the optimal factors in improving the mechanized maize production are as follows: the original value of machine on average (with the evaluation value of 0.9107), mechanized maize plant protection (0.7846), annual output value of maize (0.7718), the degree of mechanized maize sowing (0.7190), and mechanized maize plowing land degree (0.7026). The study shows that the mechanized maize farming, planting, and plant protection can be improved by increasing the capital investment in maize production and by improving technology and application in future mechanized maize production.

摘要
农业机械化的发展水平对引领农业现代化发展，促进农民增收发挥着积极作用。作为三大农作物之一的玉米，在机械化作业方面远远滞后于其它两类作物。为了准确、科学地评价玉米生产全程机械化发展的综合水平，合理制定玉米生产全程机械化发展政策，本文基于灰色关联分析和灰色层次分析方法，构建了玉米生产全程机械化水平评价指标体系，通过关联分析，将各项评价指标对于玉米生产机械化发展的作用进行了排序。最后，以中国河北省为例，运用灰色关联法精选了十二项指标，建立了河北省玉米生产全程机械化发展综合水平评价的指标体系，并运用灰色层次分析法确定了各指标的权重系数，得出了玉米生产机械化水平的综合评价值。借助 DPS7.05 数据处理软件，计算了各项指标与综合水平值之间的关联度。研究结果表明：提高玉米生产全程机械化水平的最优因素是玉米生产劳动平均机械原值，评价值为 0.9107；其次是玉米植保机械化程度，评价值为0.7846；再次，评价值大于0.7 的指标依次为玉米生产年产值、玉米播种机械化程度、玉米耕整地机械化程度，评价值分别为 0.7718、0.7190、0.7026。该研究成果表明，在今后玉米生产机械化工作中，应该加大玉米生产机械装备资金投入力度，加快技术推广应用的步伐，努力提高玉米耕、种、植保的机械化作业水平。

INTRODUCTION

Agricultural mechanization, which is an important technology that supports agriculture modernization, is one of the main symbols of agricultural modernization and an important measure to strengthen agriculture in national economic development. Agricultural mechanization has become increasingly important in many aspects, such as the adjustment of the agricultural industrial structure, the transfer of rural labour force, the construction of rural ecological environment and culture, and the development of a well-to-do rural society. Maize lags far behind rice and wheat in terms of mechanization. In maize production, considerable investments are allocated to human labour with an unbalanced development of each link. Specifically, the serious lag in machine revenue has become a bottleneck that restricts the development of maize production in China. A suitable, objective, and comprehensive index system that evaluates mechanized maize production should be established.

Currently, agricultural mechanization or mechanized agricultural crops generally use analytic hierarchy process and fuzzy comprehensive evaluation (FCE) methods with many qualitative analyses and few quantitative analyses. Certain limitations are observed when the weights of the evaluation indexes are calculated, which give rise to a certain error in the results. Mechanized maize production cannot be evaluated without using a scientific and practical evaluation index system *(Wei Li and Wenqing Yin, 2006; Xiaoyang Li, 2005; Xiaogang Zheng and Hongxing Chen, 2005)*.

Many studies have been conducted on the proper evaluation of agricultural mechanization and standardization of its evaluation index system in China. Tao *(Juchun Tao and Jianmin Wu, 2001)* adopted a weighted scoring method. Tang *(Chunmei Tang, et al, 2010)* used an expert rating method to determine the weight of agricultural mechanization evaluation indexes in Hebei Province. However, this method is subjective because it is only applied to the evaluation and comparison of several slightly complex objects. Fan *(Guoqi Fan, et al, 2016)* established an index system for evaluating mechanized tobacco leaf production and used analytic hierarchy process to determine the weight of each evaluation factor by gradually combining quantitative and qualitative analyses. However, the final calculation result of the analytic hierarchy process depended on the construction of a judgment matrix *(Guangqun Huang, et al, 2012)*, and human subjective factors had a significant influence on the results. The process cannot be used for decision problems with high precision requirements. Many scholars have improved the limitations of the analytic hierarchy process by formulating several new theories and methods. In recent years, the analytic hierarchy process has attracted significant attention in this field. Li *(Meie Li, et al, 2011)* adopted an improved analytic hierarchy process to sort various indexes of agricultural mechanization. A three-scale method to construct the judgment matrix did not require a consistency check in the general analytic hierarchy process, which reduced the blindness of the judgment matrix. The analytic network process (ANP) is a decision method that adjusts to non-independent hierarchies. Ma *(Yanjun Ma, et al, 2007)* applied ANP to obtain the weight of each index in an agricultural mechanization level index system. Ran *(Ran Bi, et al, 2008)* used ANP to establish a metropolitan evaluation index system for agriculture mechanization by analyzing the interdependencies and feedback relationships among indexes. Dantsis *(Theodoros Dantsis, et al, 2010)* adopted a composite index method that used the analytic hierarchy process to determine the weight coefficient of each evaluation factor. Then, the resultant value (obtained by the ratio of the actual and standard values times the weight coefficient) was utilized as the evaluation value of agricultural mechanization. However, the improved AHP still unavoidably influenced the subjectivity of the evaluation results. FCE builds the evaluation process on the expression of fuzzy mathematics. FCE solves the fuzzification of evaluation factors and evaluation criteria, which enhances the persuasiveness and accuracy of evaluation results. Lak *(Lak et al, 2011)* applied fuzzy logic to define the parameters and indexes of agricultural mechanization. Li *(Junhua Li, 2012)* employed fuzzy analytic hierarchy process to design an agricultural mechanization evaluation method based on fuzzy triangles. Dong *(Xiaoyan Dong et al, 2016)* used triangular distribution and semi-trapezoidal distribution membership functions. An evaluation model was constructed to determine agricultural mechanization in the development stage by using an average-weighted fuzzy composition operator based on FCE. However, this model cannot solve the evaluation information duplication on evaluation indexes. No systematic method was reported for determining the membership function. Moreover, the factor weight sets and fuzzy synthesis of evaluation matrix should be investigated.

In summary, considerable local and global studies have been conducted on agricultural mechanization. However, research on the evaluation of mechanized maize production has not been reported. A study on mechanized maize production in Hebei Province used correlation analysis to select indexes that avoided the evaluation information redundancy in evaluation indexes. Then, the analytic hierarchy process and gray system theory were combined to establish a gray hierarchy analysis method. Compared with previous evaluation methods, the gray hierarchy analysis method handled the incomplete index system and rough evaluation model better, which made the evaluation result more comprehensive, complete, and accurate.

MATERIALS AND METHODS

The gray scale of a colour is utilized to represent the information in control theory, in which “black” indicates lack of information, “white” indicates sufficient information, and “gray” is between “white” and “black,” that is, with several known/unknown information in the system. For completeness of information, gray system theory combines system theory, information theory, control theory, and applied mathematical

methods to develop a set of theories and methods for solving incomplete information systems. The basic points of gray system theory are expressed as follows: A random quantity is regarded as a gray quantity that changes in a certain range, and mathematical methods are used to determine the law from the featured data of the research object. Gray system theory can be used to study a complex mechanism with many layers and a precise model system that are difficult to establish from a quantitative perspective. Gray hierarchy analysis process and gray correlation analysis in gray system theory are the basic theories and methods used to establish the evaluation index system for mechanized maize production.

Gray Correlation Analysis

Gray correlation analysis is used to measure the relevance between the factors of two systems based on the similarity or dissimilarity of the development trend between the factors. In the system development process, the trend of two factors is consistent (that is, the synchronization is relatively high) when they have high correlation. The importance of evaluation factors can be analyzed by using gray correlation analysis. The importance order of the relevant evaluation factors can be sorted based on the close order of each relevant evaluation factor to the main evaluation factors. The most important factor is the evaluation factor with the highest gray correlation, and the least important factor is that with the lowest gray correlation *(Dongfeng Wang, 2015; Theodoros Li, 2015)*. The calculation process is expressed as follows:

(1) Set main and correlation sequences

The main sequence, known as the parent sequence, is set as $\{Z_0(k)\},(k=1,2,3,\cdots,n)$.

The correlation sequence, called a subsequence, is set as $\{X_i(k)\},(i=1,2,3,\cdots,m;k=1,2,3,\cdots,n)$.

(2) Make dimensionless data

To construct a gray correlation analysis of data with different unit dimensions, the data should be made dimensionless before the calculation. Data averaging is a common method used for nondimensionalization. The average value of each sequence is obtained by using it to remove the original data in the corresponding sequence. Then, a new data column is obtained, which is the averaged sequence.

$$x_i'(k)=\frac{x_i(k)}{\overline{x_i}} \tag{1}$$

Where $x_i(k)$ is the *i-th* sequence, $x_i'(k)$ is the averaged sequence formed after the *i-th* sequence is averaged, and $\overline{x_i}$ is the average of the *i-th* sequence data.

(3) Calculation of the correlation coefficient

$$\xi_i(k)=\frac{\min\limits_i\min\limits_k\left|z_0'(k)-x_i'(k)\right|+\rho\max\limits_i\max\limits_k\left|z_0'(k)-x_i'(k)\right|}{\left|z_0'(k)-x_i'(k)\right|+\rho\max\limits_i\max\limits_k\left|z_0'(k)-x_i'(k)\right|} \tag{2}$$

Where $\xi_i(k)$ is the correlation coefficient between relevant sequence $X_i(k)$ and main sequence $Z_0(k)$ at point k; ρ is the resolution coefficient, and its value is between 0 and 1 with a general value of 0.5; $\min\limits_i\min\limits_k\left|z_0'(k)-x_i'(k)\right|$ is the minimum difference of two levels; and $\max\limits_i\max\limits_k\left|z_0'(k)-x_i'(k)\right|$ is the maximum difference of two levels.

(4) Calculation of the correlation coefficient

The correlation coefficient for each point is averaged to obtain the correlation as follows:

$$Y_i=\frac{1}{n}\sum_{k=1}^{n}\xi_i(k) \tag{3}$$

Where γ_i is the correlation between relevant sequence $X_i(k)$ and main sequence $Z_0(k)$. Comparing the correlation degree of each factor can determine the closeness between each relevant factor and main factor. A great correlation corresponds to a close proximity.

(5) Sorting of related sequences

The correlation of each subsequence to the parent sequence is sorted to clarify the “primary and subordinate” and “good and poor” relationships of each subsequence to the parent sequence.

If $\gamma_{0a} \succ \gamma_{0b}$, then $X_a(k)$ is better than $X_b(k)$ compared with parent sequence $Z_0(k)$.

If $\gamma_{0a} \prec \gamma_{0b}$, then $X_a(k)$ is worse than $X_b(k)$ compared with parent sequence $Z_0(k)$.

If $\gamma_{0a} \prec \gamma_{0b}$, then $X_a(k)$ is equivalent to $X_b(k)$ compared with parent sequence $Z_0(k)$.

Where γ_{0a} is the correlation value of subsequence $X_a(k)$ relative to parent sequence $Z_0(k)$, and γ_{0b} is the correlation of subsequence relative $X_b(k)$ to parent sequence $Z_0(k)$.

Gray Analytic Hierarchy Analysis

In the traditional analytic hierarchy process, experts cannot provide a definite number when making a pairwise judgment due to insufficient information for a short time. Experts can provide a definite mathematical judgment when the information is complete. Therefore, each judgement element in this case is considered a gray element. The information is a white number when it is complete, and a gray analytic hierarchy process is obtained. The process of determining the weight coefficient is expressed as follows *(Theodoros Dantsis, et al, 2010; Yong Geng and Jun Wang, 2010; Yue Ge, et al,2014)*:

(1) Establishment of a judgment matrix

Let $X = \{x_1, x_2, \cdots, x_n\}$ be the factor set in the same level of the evaluation index system. The judgment scale for the importance of factors x_i and x_j is expressed as follows:

Table 1

Judgment scale and definition

Judgment scale	Meaning of the judgment scale for comparing the importance of factors x_i and x_j
$\otimes_1$	Equal importance
$\otimes_3$	The former is slightly more important than the latter
$\otimes_5$	The former is obviously more important than the latter
$\otimes_7$	The former is intensively more important than the latter
$\otimes_9$	The former is extremely more important than the latter
$\otimes_2, \otimes_4, \otimes_6, \otimes_8$	The median values of the above adjacent judgments
Reciprocal	If the importance ratio of factors x_i to x_j is a_{ij}, then the importance ratio of x_j to x_i is $a_{ji} = 1/a_{ij}$

The pairwise comparison results are written in matrix to obtain the expert judgment matrix:

$$\otimes(A) = \begin{pmatrix} \otimes(a_{11}) & \otimes(a_{12}) & \cdots & \otimes(a_{1n}) \\ \otimes(a_{21}) & \otimes(a_{22}) & \cdots & \otimes(a_{2n}) \\ \vdots & \vdots & \vdots & \vdots \\ \otimes(a_{n1}) & \otimes(a_{n2}) & \cdots & \otimes(a_{n3}) \end{pmatrix} \quad (4)$$

Where $\otimes(A)$ is a gray reciprocal matrix that satisfies $\otimes(a_{ij}) = 1/\otimes(a_{ji})(i, j = 1,2,3\cdots,n)$

(2) Using a sum and product method to determine the eigenvector of matrix $\otimes(A)$.

$\otimes(A)$ is normalized by row.

$$\overline{\otimes}(a_{ij}) = \frac{\otimes(a_{ij})}{\sum_{i=1}^{n} \otimes(a_{ij})}(i, j = 1,2,3\cdots,n) \quad (5)$$

The normalized matrix is added by row to obtain the sum.

$$\overline{\otimes}(W_i) = \sum_{i=1}^{n} \overline{\otimes}(a_{ij})(i, j = 1,2,3\cdots,n) \quad (6)$$

After renormalization, the weight coefficient vector is obtained.

$$\otimes(W_i) = \frac{\overline{\otimes}(W_i)}{\sum_{i=1}^{n} \overline{\otimes}(W_i)}(i, j = 1,2,3\cdots,n) \quad (7)$$

(3) Consistency check

The definition of consistency indexes is expressed as follows:

$$C \cdot I = \frac{\lambda_{max} - n}{n - 1} \quad (8)$$

Where λ_{max} is the greatest eigenvalue, and the formula is expressed as follows:

$$\lambda_{max} = \frac{1}{n}\sum_{i=1}^{n}\frac{\sum_{j=1}^{n}\overline{\otimes}(a_{ij})\overline{\otimes}(W_j)}{\overline{\otimes}(W_i)}(i,j=1,2,3\cdots,n) \quad (9)$$

The random consistency index $R \cdot I$ is defined (Table 2).

Table 2

Random consistency indexes

Matrix order	1	2	3	4	5	6	7	8	9	10	11
$R \cdot I$	0	0	0.58	0.90	1.12	1.24	1.32	1.41	1.45	1.49	1.53

The consistency ratio is defined as follows:

$$C \cdot R = \frac{C \cdot I}{R \cdot I} \quad (10)$$

The consistency is satisfied when $C \cdot R$ <0.1 and the judgment matrix should be properly modified until satisfactory consistency is achieved.

Setting the principles of evaluation indexes

The actual effect of mechanization was utilized as the basis for evaluation and the economic effect was considered the core of the evaluation when mechanized maize production was evaluated. The study established an evaluation index system by using mechanization as basis, capacity as protection, and efficiency as core. On the basis of mechanized maize production in practice, the basic framework of the evaluation index system was determined for mechanized maize production.

(1) Operation of mechanized maize production (B1): Mechanized maize production refers to the use of mechanical operations, such as tillage, planting, fertilizing, plant protection, cultivating, harvesting, and threshing, in maize production. On the basis of the characteristics of Hebei Province, the operations mainly include mechanized tillage, mechanized precision seeding, mechanized cultivator, mechanized plant protection, and mechanized harvesting. Mechanized maize production is comprehensively calculated by focusing on tillage, sowing, and harvesting operations. The following seven secondary indexes are initially set as follows: mechanized maize tillage (B11), mechanized maize sowing (B12), mechanized maize harvest (B13), mechanized maize threshing (B14), mechanized maize irrigation (B15), mechanized plant protection of maize (B16), and mechanized maize processing (B17).

(2) Integrated supportability for mechanized maize production (B2): The machinery and equipment that reflect maize production, the operators of maize production machinery, and the supportability for mechanized maize production from a socialized service system. The following four secondary indexes are initially set as follows: average original value of mechanized maize production (B21), agricultural machinery power of maize planting area (B22), proportion of operators trained in maize production machinery (B23), and social service system construction of maize production machinery (B24).

(3) Comprehensive benefit of mechanized maize production (B3): The economic benefits of mechanized maize production are investigated. The labour results and the labour consumption of mechanized maize production should be considered. The following four secondary indexes are initially set as follows: annual output value of maize production (B31), average planting area of maize production (B32), original profit rate of maize production machinery (B33), and proportion of labour force of maize production accounting for agricultural labour (B34).

The calculation formula of each evaluation index is expressed as follows:

$$Mechanized\ maize\ tillage(B11) = \frac{Mechanized\ tillage\ area\ of\ maize}{Total\ maize-sowing\ area} \times 100\% \quad (11)$$

$$Mechanized\ maize\ sowing(B12) = \frac{Mechanized\ maize-sowing\ area}{Total\ maize-sowing\ area} \times 100\% \quad (12)$$

$$Mechanized\ maize\ harvest(B13) = \frac{Mechanized\ harvest\ area\ of\ maize}{Harvest\ area\ of\ maize} \times 100\% \quad (13)$$

$$Mechanized\ maize\ threshing(B14) = \frac{Mechanized\ maize-threshing\ quantity}{Total\ maize\ production} \times 100\% \quad (14)$$

$$Mechanized\ maize\ irrigation(B15) = \frac{Mechanized\ irrigation\ area\ of\ maize}{Effective\ irrigation\ area} \times 100\% \quad (15)$$

$$\text{Mechanized plant protection of maize}(B16) = \frac{\text{Mechanized plant protection area of maize}}{\text{Total maize} - \text{sowing area}} \times 100\% \quad (16)$$

$$\text{Mechanized maize processing}(B17) = \frac{\text{Mechanized maize processing capacity}}{\text{Total maize harves}} \times 100\% \quad (17)$$

$$\text{Average original value of mechanized maize production}(B21) = \frac{\text{Original value of mechanized maize production}}{\text{Labor force of maize production}} (\text{Yuan / person}) \quad (18)$$

$$\text{Agricultural machinery power of maize planting area}(B22) = \frac{\text{Total power of mechanized maize sowing}}{\text{Total maize sowing area}} (kw \cdot h/m^2) \quad (19)$$

$$\text{Proportion of operators trained in maize production machinery}(B23) = \frac{\text{Professionally} - \text{trained operators of mechanized maize production}}{\text{Total operators of mechanized maize production}} \times 100\% \quad (20)$$

$$\text{Social service system construction of maize production machinery}(B24) = \frac{\text{Machinery management service stations of maize production in township}}{\text{Total township}} \times 100\% \quad (21)$$

$$\text{Annual output value of maize production}(B31) = \frac{\text{Gross output value of maize}}{\text{Labor force of maize production}} (\text{Yuan / person}) \quad (22)$$

$$\text{Average planting area of maize production}(B32) = \frac{\text{Total maize} - \text{sowing area}}{\text{Labor force of maize production}} (m^2 \text{ / person}) \quad (23)$$

$$\text{Original profit rate of maize production machinery}(B33) = \frac{\text{Maize} - \text{operating net income}}{\text{Original value of mechanized maize production}} \times 100\% \quad (24)$$

$$\text{Proportion of labor force of maize production accounting for agricultural labor}(B34) = \frac{\text{Number of labor force of maize production}}{\text{Number of labor force engaged in agriculture}} \times 100\% \quad (25)$$

RESULTS

Establishment of Evaluation Index System

Determination of evaluation indexes

Hebei Province, which is one of the major provinces for maize production in China, is dominated by hills and has a cold climate. Constant drought is observed, and mechanized maize production slowly develops in several areas of Hebei Province. Hebei Province was used as an example to investigate the evaluation system of mechanized maize production. The basic data of each evaluation index were obtained from the statistical data of mechanized maize production in Hebei Province from 2012 to 2016 (Table 3).

Table 3

Data on mechanized maize production in Hebei Province from 2012 to 2016

Indexes	B11	B12	B13	B14	B15	B16	B17	B21	B22	B23	B24	B31	B32	B33	B34
2012	51	1.7	31	99	48	9.0	93	1048	5.6	86	80	0.54	0.4	18	50
2013	52	1.8	34	98	49	9.2	95	1093	5.9	88	82	0.56	0.4	20	51
2014	52	1.9	37	99	49	9.3	96	1137	6.1	88	82	0.57	0.4	22	50
2015	55	2.0	39	99	50	9.8	96	1182	6.4	90	85	0.59	0.4	22	52
2016	56	2.0	41	99	50	10.3	97	1227	6.6	92	88	0.60	0.4	23	52

On the basis of the above statistical data, the following correlation analysis was performed on the evaluation indexes of mechanized maize production by using the gray correlation analysis method.

(1) The correlation was obtained with DPS7.05 data processing system by using the first three basic operations of mechanized maize production (B11, B12, B13) as parent sequences (Z_1, Z_2, Z_3) and additional four indexes (B14, B15, B16, B17) as subsequence (X_1, X_2, X_3, X_4).

Table 4

Correlation of mechanized maize production indexes

Sequences	X_1	X_2	X_3	X_4
Z_1	0.4577	0.5509	0.7290	0.5098
Z_2	0.5307	0.5497	0.6593	0.5713
Z_3	0.5268	0.5388	0.6139	0.5503
Comprehensive correlation （γ_i）	1.5152	1.6394	2.0023	1.6314

As shown in Table 4, the sorting of comprehensive correlation of all the parent sequences for each subsequence was obtained.

$$\gamma_1 (1.5152) < \gamma_4 (1.6314) < \gamma_2 (1.6394) < \gamma_3 (2.0023)$$

Therefore, mechanized maize threshing (B14) was deleted from the evaluation index system due to its minimal impact in four additional indexes for mechanized maize production in Hebei Province.

(2) The correlation was obtained with DPS7.05 data processing system by using the selected indexes of the mechanized operation level of maize production (B11, B12, B13, B15, B16, B17) as the parent sequences $(Z_1, Z_2, Z_3, Z_4, Z_5, Z_6)$ and four indexes of integrated supportability of mechanized maize production (B21, B22, B23, B24) as subsequence (X_1, X_2, X_3, X_4).

Table 5

Correlation of the integrated supportability indexes of mechanized maize production

Sequences	X_1	X_2	X_3	X_4
Z_1	0.5383	0.5176	0.6017	0.8100
Z_2	0.7093	0.7206	0.4737	0.5337
Z_3	0.6225	0.6263	0.4862	0.5021
Z_4	0.5283	0.5319	0.8145	0.6875
Z_5	0.6760	0.6653	0.5049	0.6276
Z_6	0.4960	0.4749	0.7585	0.6205
comprehensive correlation （γ_i）	3.5702	3.5366	3.6394	3.7813

As shown in Table 5, the comprehensive correlation of all the parent sequences was sorted for each subsequence.

$$\gamma_2\,(3.5366) < \gamma_1\,(3.5702) < \gamma_3\,(3.6394) < \gamma_4\,(3.7813)$$

Therefore, the influence of the united area of maize on agricultural machinery (B22) was the least and was deleted from the four indicators of integrated supportability of mechanized maize production to the correlation of mechanized maize production.

(3) The correlation was obtained with the DPS7.05 data processing system by using the selected indexes of operation of mechanized maize production (B11, B12, B13, B15, B16, B17) as parent sequences $(Z_1, Z_2, Z_3, Z_4, Z_5, Z_6)$ and four indexes of comprehensive benefit of mechanized maize (B31, B32, B33, B34) production as subsequence (X_1, X_2, X_3, X_4).

Table 6

Correlation of comprehensive benefit indexes of mechanized maize production

Sequences	X_1	X_2	X_3	X_4
Z_1	0.8723	0.6053	0.5505	0.7449
Z_2	0.6734	0.5076	0.6647	0.5136
Z_3	0.5990	0.5120	0.7797	0.5133
Z_4	0.7722	0.8298	0.5052	0.9093
Z_5	0.7936	0.5241	0.5905	0.6568
Z_6	0.7278	0.8438	0.5024	0.8622
comprehensive correlation （γ_i）	4.4382	3.8227	3.5931	4.2000

As shown in Table 6, comprehensive correlation was sorted from all the parent sequences for each subsequence.

$$\gamma_3\,(3.5931) < \gamma_2\ (3.8227) < \gamma_4\,(4.2000) < \gamma_1\,(4.4382)$$

Therefore, the profitability of original value of maize production machinery (B33) was deleted due to its minimal impact from the correlation of four indexes of comprehensive benefit of mechanized maize production to mechanized operation.

Determination of index weight coefficients

The weight of each evaluation index was calculated based on the gray analytic hierarchy process. The first-layer evaluation factors were determined by five experts. Let the judgment of the $k\text{-}th\ (k=1,2,3,4,5)$ expert be the weight coefficient vector $\otimes(W^{(K)})$, the method of mean is utilized to synthesize the results, and the weight coefficients of the first-layer factors are obtained as follows:

$$\otimes(W) = \frac{1}{5}\sum_{K=1}^{5}\otimes(W^{(K)}) = (0.52, 0.30, 0.18) \tag{26}$$

The proportion of consistency on multiple experts is expressed as follows:

$$C \cdot R = \frac{1}{R \cdot I} = \frac{C \cdot I}{R \cdot I} \cdot \frac{1}{5}\sum_{K=1}^{5}(C \cdot I)^K \prec 0.1 \otimes (W^{(K)}) \tag{27}$$

Similarly, the weight factors for the second-level evaluation factors are expressed as $\otimes(W_{B1}) = (\otimes(W_{B11}) \otimes(W_{B12}) \otimes(W_{B13}) \otimes(W_{B14}) \otimes(W_{B15}) \otimes(W_{B16})) = (0.16,0.05,0.1,0.06,0.09,0.06)$,

$\otimes(W_{B2}) = (\otimes(W_{B21}) \otimes(W_{B23}) \otimes(W_{B23})) = (0.15,0.08,0.07)$, .

$\otimes(W_{B3}) = (\otimes(W_{B31}) \otimes(W_{B33}) \otimes(W_{B33})) = (0.09,0.06,0.03)$.

On the basis of the analysis on the evaluation indexes and the determination of weight coefficients, the evaluation index system for mechanized maize production in Hebei Province was established as follows:

Table 7

Evaluation indexes and weights of mechanized maize production in Hebei Province

First-level evaluation indexes and weights		Second-level evaluation indexes and weights	
Operation of mechanized maize production (B1)	0.52	Mechanized maize tillage (B11)	0.16
		Mechanized maize sowing (B12)	0.05
		Mechanized maize harvest (B13)	0.1
		Mechanized maize threshing (B14)	0.06
		Mechanized maize irrigation (B15)	0.09
		Mechanized plant protection of maize (B16)	0.06
Integrated supportability for mechanized maize production (B2)	0.30	Average original value of mechanized maize production (B21)	0.15
		Agricultural machinery power of maize planting area (B22)	0.08
		Proportion of operators trained in maize production machinery (B23)	0.07
Comprehensive benefit of mechanized maize production (B3)	0.18	Annual output value of maize production (B31)	0.09
		Average planting area of maize production (B32)	0.06
		Original profit rate of maize production machinery (B33)	0.03

Determination of Comprehensive Evaluation Model for Mechanized Maize Production

A weight is given to the evaluation index of mechanized maize production, and a comprehensive evaluation method is employed to obtain a comprehensive evaluation value. The evaluation model is expressed as follows:

$$A = \sum_{i=1}^{n} W_i P_i \tag{28}$$

Where A is the comprehensive evaluation value of mechanized maize production, W is the weight of the evaluation index, and P is the calculation data of each evaluation index.

Therefore, the comprehensive mechanization values of maize production in Hebei Province during 2012–2016 are 191.8676, 199.6124, 206.5573, 214.5291, and 222.115, respectively, based on Tables 3 and 7.

Correlation analysis on the development of mechanized maize production

The comprehensive level of mechanized maize production in Hebei Province from 2012 to 2016 is used as the parent sequence and is denoted as $Z_0 = \{191.8676, 199.6124, 206.5573, 214.5291, 222.115\}$.

The data in Table 3 are selected, and 12 evaluation factors are used as subsequence $\{Xi(k)\}$ $(I = 1,2,3...12;\ k = 1,2,3,4,5)$. The following results are obtained using the DPS7.05 data processing system for correlation analysis and sorting.

Table 8

Correlation sorting of mechanized maize production indexes

Sorting	Index	Correlation value
1	B21	0.9107
2	B15	0.7846
3	B31	0.7718
4	B12	0.7190
5	B11	0.7026
6	B23	0.6571
7	B22	0.6059
8	B14	0.5952
9	B16	0.5534
10	B33	0.5425
11	B32	0.5317
12	B13	0.4993

CONCLUSIONS

To evaluate the development of mechanized maize production, this study considered the actual development situation of mechanized maize production in Hebei Province in the past five years as the research object. On the basis of the gray hierarchy analysis process and gray correlation analysis in gray system theory, the evaluation indexes were selected by determining the weights of indexes. The index system was established for mechanized maize production in Hebei Province by calculating the mechanized maize production during 2012–2016. Correlation analysis on mechanized maize production was performed with the evaluation indexes over the past five years. The correlation sorting of various evaluation indexes was obtained with the following conclusions:

(1) Mechanized maize production increased year by year in 2012–2016.

(2) The greatest correlation value of the average original value of mechanized maize production indicated that the investment in maize production gradually increased in Hebei Province in the past five years. The development of mechanized maize production must be based on integrated supportability. In the future, capital investments in agricultural equipment should be increased. At the same time, the transfer of agricultural labour force should be accelerated by small-town development in Hebei Province and the employment channels of the rural labour force, which increase the average original value of mechanized maize production labour.

(3) Mechanized maize plant protection has advantages, such as mechanized maize plowing and mechanized maize sowing. However, mechanized maize harvesting still has disadvantages. Therefore, mechanized maize production in Hebei Province should focus on mechanized maize plant protection, mechanized maize planting, and mechanized maize plowing in the future. Scientific and technological innovations as the driving force should accelerate the upgrading of maize production machinery and equipment.

The study used the evaluation system established by gray system theory to evaluate mechanized maize production in Hebei Province from the quantitative point of view and to provide guidance. However, the proposed method cannot be used for periodic evaluation. In future research, a staged evaluation and calculation model will be established for mechanized maize production.

ACKNOWLEDGEMENTS

This work was supported by natural science foundation of agricultural university of Hebei (Grant No. LG201625).

REFERENCES

[1] Chunmei Tang, Shuqing Niu, Shufei Tian, Zhenhua Qu, Jing Wang, (2010), The agricultural mechanization evaluation system of Hebei province and its' application in Shijiazhuang (河北省农业机械化评价体系及其在石家庄地区的应用), *Animal Husbandry and Veterinary Medicine in Heilongjiang*, Vol.16, Issue 8, Agency of Animal Husbandry and Veterinary Medicine in Heilongjiang, Shijiazhuang/China, pp.13-15;

[2] Dongfeng Wang, (2015), Analysis of the factors influencing the scale of mobile electronic commerce transaction based on grey correlation degree (基于灰色关联度的移动电子商务交易规模影响因素分析), *Journal of Nanyang Institute of Technology,* Vol. 7, Issue 3, Agency of Nanyang Institute of Technology, Nanyang /China, pp. 39- 41;

[3] Guangqun Huang, Lujia Han , Xian Liu, Zengling Yang, (2012), Establishment of evaluation system for integrated agricultural mechanization engineering technology (农业机械化工程集成技术评价体系的建立), *Transactions of the Chinese Society of Agricultural Engineering*, Vol.28, Issue 16, Agency of Transactions of the Chinese Society of Agricultural Engineering, Beijing /China, pp.74-79;

[4] Guoqi Fan, Fugui Zhang, Yuanming Qi, Xiaoliu Han, Houlong He, Yuan Fang, (2016), Study on the evaluation index system of mechanization of tobacco leaf production in mountain area (山区烟叶生产机械化水平评价指标体系研究), *Journal of Chinese Agricultural Mechanization*, Vol.37, Issue 1, Agency of Chinese Agricultural Mechanization, Nanjing/China, pp.268-271;

[5] Juchun Tao, Jianmin Wu, (2001), Study on determining the weight of index in synthetic weighted mark method(综合加权评分法的综合权重确定新探), *Systems Engineering Theory and Practice*, Vol.26, Issue 8, Agency of Systems Engineering Theory and Practice, Beijing/China, pp.43-48;

[6] Junhua Li, (2012), Evaluation of agricultural mechanization level based on triangular fuzzy number (基于模糊三角数的农业机械化水平评价), *Anhui Agricultural Sciences,* Vol. 40, Issue 7, Agency of Anhui Agricultural Sciences, Hehui/China, pp. 4426- 4428;

[7] Lak, Mohammad Bagher, Almassi, Morteza, (2011), An analytical review of parameters and indices affecting decision making in agricultural mechanization, *Australian Journal of Agricultural Engineering*, Vol.5, Issue 2, Springer, Canberra / Australian, pp.140-146;

[8] Meie Li, Shirui Dan, (2011), Application of improved AHP method in the evaluation of agricultural mechanization development level (改进的 AHP 法在评价农业机械化发展水平中的应用), *Agricultural Mechanization Research,* Vol.35, Issue 5, Agency of Agricultural Mechanization Research, Haerbing /China, pp.56-59;

[9] Ran Bi, Jinyu Wei, Rui Chen, (2008), The application of ANP in evaluation index system of urban agriculture (ANP 方法在都市型农业评价指标体系中的应用), *Journal of Chinese Agricultural Mechanization,* Vol.38, Issue 6, Agency of Chinese Agricultural Mechanization, Nanjing/China, pp.30-34;

[10] Shangyuan Yu, Xiaobing Liu, Fanghong Xue, (2016), Evaluation of ship repair project priority based on gray analytic hierarchy analysis (基于灰色层次分析法的船舶修理项目优先级评价研究), *Project Management Technology,* Vol. 7, Issue 14, Agency of Project Management Technology, Beijing /China, pp. 122- 128;

[11] Theodoros Dantsis, Caterina Douma, Christina Giourga, Aggeliki Loumou, Eleni A.Polychronaki, (2010), A methodological approach to assess and compare the sustainability level of agricultural plant production systems, *Ecological Indicators,* Vol.10, Issue 2, Elsevier, Amsterdam/Netherlands, pp.256-263;

[12] Wei Li, Wenqing Yin, (2006), Research on comprehensive evaluation index system of agricultural mechanization (农业机械化综合评价指标体系的研究), *Anhui Agricultural Sciences*, Vol. 34, Issue 22, Agency of Anhui Agricultural Sciences, Hehui/China, pp.5937- 5938;

[13] Xiaogang Zheng, Hongxing Chen, (2005), Discussion on research methods of agricultural mechanization evaluation index system (关于农业机械化评价指标体系的研究方法探讨), *Agricultural Equipment & Technology*, Vol.31, Issue 1, Agency of Agricultural Equipment & Technology, Nanjing/China, pp.9-12;

[14] Xiaoyan Dong, Pei Yang, Rongjie Song, Mei Li, (2016), Evaluation study on Shanxi province agricultural mechanization development stage - Based on fuzzy comprehensive evaluation (陕西省农机化发展阶段评价研究-基于模糊综合评判), *Agricultural Mechanization Research,* Vol. 10, Issue.6, Agency of Agricultural Mechanization Research, Haerbing /China, pp. 27- 31;

[15] Xiaoyang Li, (2005), *Study on the evaluation method of agricultural mechanization development level in Hunan province (湖南省农业机械化发展综合水平评价方法的研究),* Master dissertation, Hunan Agricultural University, Changsha/China;

[16] Yanjun Ma, Junhui Zhang, Haiyan Zhang, (2007), The optimization of agricultural machinery level evaluation index weight based on ANP (基于 ANP 的农业机械化水平评价指标权重优化), *Agricultural Mechanization Research,* Vol.28, Issue 5, Agency of Agricultural Mechanization Research, Haerbing / China, pp.55-57;

[17] Yong Geng, Jun Wang, (2010), Comprehensive assessment of ecosystem of cities, integrative industries based on grey hierarchy analysis (基于灰色层次分析法的城市复合产业生态系统综合评价), *China Population, Resources and Environment,* Vol. 1, Issue 20, Agency of China Population, Resources and Environment, Beijing / China, pp. 112- 117;

[18] Yue Ge, Hao Wang, Yabo Xu, (2014), Evaluation of emergent emergency management capability based on grey level analytic method (基于灰色层次分析法的突发事件应急管理能力评价), *Journal of Safety Science and Technology,* Vol.10, Issue 12, Agency of Safety Science and Technology, Beijing /China, pp. 80- 86;

[19] Zhiguo Li, (2015), Application of grey relational analysis in the analysis of casualties in machinery factories (灰色关联分析法在机械工厂伤亡事故分析中的应用), *Journal of Inner Mongolia Agricultural University,* Vol. 10, Issue 6, Agency of Inner Mongolia Agricultural University, Huhhot / China, pp. 82-85.

PERFORMANCE AND KINETIC STUDY OF THE ANAEROBIC CO-DIGESTION OF COCOA HUSK AND DIGESTED COW MANURE WITH HIGH ORGANIC LOADING RATE

PERFORMANSI DAN STUDI KINETIKA PADA PROSES ANAEROBIK CO-DIGESI KULIT KAKAO DAN LIMBAH MANURE SAPI DENGAN LAJU PEMASUKAN BAHAN ORGANIK YANG TINGGI

Darwin, Muhammad Ilham, Afrizal Fazil
Department of Agricultural Engineering, Syiah Kuala University, Darussalam, Banda Aceh 23111, Indonesia
Email: darwin_ae@unsyiah.ac.id; Tel: +62 853 6142 3969

Keywords: *Anaerobic co-digestion, cocoa husk, Short HRT, Biogas Production*

ABSTRACT
Biogas is a clean and cheap renewable energy that can be used for generating electricity. One of the current methods applied to enhance biogas production was through anaerobic co-digestion. The current study revealed that anaerobic digestion of cow manure co-digested with cocoa husk produced higher biogas production (348.3 mL/day) than anaerobic digestion of cow manure alone (26.5 mL/day). Even if a high organic loading rate (OLR) (4.173 kg VS/m³.day) was applied to the reactor of anaerobic co-digestion, no inhibition was found at which pH was stable at 7.08. The results suggested that high OLR and short HRT (10 days) did not inhibit biogas production.

ABSTRAK
Biogas adalah energi terbarukan yang bersih dan murah yang dapat digunakan untuk menghasilkan listrik. Salah satu metode saat ini yang telah diterapkan untuk meningkatkan produksi biogas adalah melalui anaerobic co-digesi. Penelitian saat ini mengungkapkan bahwa pencernaan anaerobik dari kotoran sapi yang dicerna bersama dengan kulit coklat dapat menghasilkan produksi biogas yang lebih tinggi (348,3 mL / hari) dibandingkan dengan pencernaan anaerobik dari kotoran sapi saja (26,5 mL / hari). Meskipun OLR yang tinggi (4,173 kg VS / m3.day) diaplikasikan pada reaktor anaerobic codigesi, tidak ada hambatan yang ditemukan di mana pada penelitian ini pH tetap stabil pada 7,08. Hasil penelitian ini menunjukkan bahwa OLR tinggi dan HRT singkat (10 hari) tidak menghambat produksi biogas.

INTRODUCTION

Anaerobic digestion is an established technology that has been widely used as well as applied for biologically treating wastewater in the wastewater treatment plants *(Monroy et al, 2000; Gomec C.Y., 2010).* The application of anaerobic digestion process is not only used for treating and/or managing the organic liquid and solid wastes but also can be used for generating renewable energy (i.e. biogas) *(Lastella et al, 2002; Gontupil et al, 2012).* In the process of anaerobic digestion, complex organic materials are biologically decomposed and converted into biogas (methane) as the end-product. The process involves different types of microbial consortia *(Narihiro et al, 2007; Riviere et al, 2009; Barta et al., 2010).*

In order to achieve the complete conversion of the organic materials into biogas, the process of anaerobic digestion should be controlled and maintained in accordance to the optimal operating conditions. Some parameters that highly affected the process of anaerobic digestion to generate biogas include pH, alkalinity and/or buffer capacity, temperature, hydraulic retention time (HRT) and organic loading rate (OLR) *(Maharaj et al., 2001; El-Mashad et al., 2004; Gustin et al., 2011; Liu et al., 2012).* As the application of anaerobic digestion for the purpose of generating renewable energy and converting organic wastes becomes more attractive to the researchers, current study would be more focused on finding out the significant approaches and better strategies for preventing the process failure of anaerobic digestion, and/or optimizing the production of biogas as the end-product.

Some studies had revealed that anaerobic digestion process operated in the continuous as well as semi-continuous modes highly depended on the HRT *(Salminen and Rintala, 2002; Dareioti and Kornaros, 2014).* HRT is known as a measure of the average length of time at which the anaerobic culture remains in the reactor. Therefore, the steady state condition of the anaerobic digestion process would be highly dependent on the flow rate of the influent as well as effluent of the anaerobic reactor *(Sialve et al., 2009).*

Further, HRT applied would affect the microbial growth rate in the anaerobic reactor in which insufficient retention time applied to the process of anaerobic digestion would lower the concentration of biomass in the digester *(Zhang et al., 2006).* This suggested that short HRT would slow down the process of anaerobic digestion to form methane due to the biomass washout *(Chen et al., 2008; Sialve et al., 2009).*

Some studies revealing that the optimum HRT for optimizing the process of anaerobic digestion operated in continuous as well as semi-continuous system was in the range 20-25 days *(Bouallagui et al., 2005; Demirer and Chen, 2005; Chandra et al., 2012).* Within those HRT range the production of anaerobic digestion could be optimized due to the fact that the anaerobic microbes would have sufficient time for completely converting the complex organic materials into biogas. The maximum production of methane gas was achieved when the continuous process of anaerobic co-digestion was operated at 20 days of HRT *(Kaosol and Sohgrathok, 2012).* Study conducted by *Onthong and Juntarachat (2017)* revealed that the highest biogas yield obtained from the process of anaerobic co-digestion of cow manure with bagasse and soybean residue, could be reached by applying 25 days of HRT. However, the authors also found that anaerobic co-digestion of cow manure with papaya peels had the highest biogas yield at 15 days of HRT. This suggested that the different types of substrate loaded into the anaerobic digester would have a different optimum HRT for optimizing the production of biogas *(Willeghems and Buysse, 2016).*

Beside the HRT, OLR is also a vital parameter that would affect the performance of anaerobic digestion. The production of biogas as well as biogas yield would significantly decrease once OLR was increased *(Elango et al., 2007).* High OLR could also contribute to the acid accumulation in the reactor which could increase the proton concentration and pH drop. This occurred as high OLR applied would stimulate acidogenic bacteria to consume and convert all soluble organic matters into volatile fatty acids (VFA) *(Elango et al., 2007). Manyi-Loh et al. (2013)* mentioned that the rate of VFA formation is higher than the rate of its conversion into methane gas, and thereby the VFA would be accumulated in the digester and could inhibit the whole process of anaerobic digestion.

To understand the performance of anaerobic digestion process, kinetic model could be used to evaluate the fermentation pathways as well as the behaviour of microorganisms in the anaerobic digester *(Kafle et al., 2014).* Kinetic models are developed to assess whether the process of anaerobic digestion could run properly for generating biogas as the end-product *(Mähnert and Linke, 2009)*. A simple kinetic model that had been developed for assessing the behaviour of microbial activity in the fermentation process was based on the Monod equation *(Fernández et al., 2010).* As the Monod model is only suitable for the single culture, the use of this model on the assessment of anaerobic digestion process would be infeasible *(Momoh et al., 2013).* This is due to the fact that the process of anaerobic digestion is normally inoculated with the mixed microbial consortia.

Study on the kinetic assessment of anaerobic co-digestion of digested cow manure and lignocellulosic biomass (i.e. bagasse), revealed that the specific growth rate obtained was higher than the dilution rate applied representing the presence of cell mass in the reactor (*Darwin et al., 2017*). Some other previous studies also added that some parameters such as, volatile solids (VS) and chemical oxygen demand (COD) could be used as the input parameters on the kinetic models to assess the microbial activity during the process of anaerobic digestion *(Fernández et al., 2010; Momoh et al., 2013)*. Kinetic assessment on the process of anaerobic digestion inoculated with microbial mixed cultures could generate various bioconversion stages which could stimulate the dynamic change of biochemical pathways (*Momoh et al., 2013*). This is due to the fact that the anaerobic digestion inoculated with mixed cultures might have different types of microbial population involved *(Momoh et al., 2013).*

The purpose of the study reported here was to investigate the effects of high organic loading rate and short hydraulic retention time on the biogas production from the single stage anaerobic co-digestion of cocoa husk and digested cow manure. Parameters involved in the process of anaerobic digestion operated in semi-continuous system were also evaluated through kinetic model assessment.

MATERIALS AND METHODS

Preparation of substrates

Cocoa husk used for this experiment was collected from cocoa plantation located in Lamtamot Village, Seulawah Valley-District of Aceh Besar. The cocoa husk obtained was dried to reach moisture content of ± 7 % (wet basis). The dried cocoa husk was milled using a laboratory mill to an average particle size of 35 Mesh. The percentage of total solids of cocoa husk used as a co-substrate was about 93.22 ± 0.08%. The digested cow manure used for the experiment was taken from the anaerobic wastewater

treatment plant located in the Cow Farming at Sibreh, the District of Aceh Besar. The sludge was stored in the fridge at the temperature of ± 5°C prior to using it. For characterization of substrates, cocoa husk and sludge used was analyzed for solid concentration. Samples of cocoa husk and sludge were dried at the temperature of 105°C, and followed with burning the samples at the temperature of 550°C in the furnace for total solid and volatile solid analysis, respectively. Total solids (TS) and volatile solids (VS) analysis was carried out in accordance with the Standard Methods *(APHA, 2012).*

Experimental Procedure

Experiments were carried out in the Laboratory of Bioprocess and Postharvest Technology, Department of Agricultural Engineering, Syiah Kuala University. Some sample analysis measurements were conducted at the Institute for Research and Standardization of Industry, Banda Aceh. An anaerobic semi-continuous reactor was operated at the steady state condition in which the temperature was maintained under the mesophilic condition at the temperature of 34 ± 1°C by using thermostatic water bath. The working volume of the digester was 3000 mL. The short hydraulic retention time applied in this experiment was 10 days. The loading rate applied in this experiment was 300 mL/day. High organic loading rate was applied in this experiment in which 30 g of cocoa husk was mixed with 300 mL of digested cow manure. This indicated that cocoa husk as a co-substrate was added at 10% of the total volume of the daily digested cow manure loaded.

Prior to the start of the anaerobic digestion process, organic loading rate applied was firstly measured. The measurement of organic loading rate was based on the percentage of total solids and volatile solids of the anaerobic digestion culture. Based on the initial analysis, total solids and volatile solids of the culture obtained were 5.28% and 79.034%, respectively. As some parameters including the working volume of the anaerobic digester (3 litters) and loading rate (300 mL/day) had been obtained, organic loading rate (OLR) applied in this current experiment would be 4.173 kg VS/m^3.day.

The anaerobic digesters were equipped with the effluent and influent sample ports. Samples of the effluent were taken from the port for further analysis. To ensure the anaerobic digestion process operated in semi-continuous system running properly, pH of the samples including influent and effluent was measured periodically during the feeding and the discharging periods. No pH control was applied in this system, and thereby no alkaline and acid added to the reactors. Biogas production was measured using a gas meter based on water displacement method. The gas outlet located on the top of each reactor was connected using tubes to the port of the gas meter. The gas meter installed was calibrated periodically. Prior to the start of the feeding substrates, the culture was acclimated with the anaerobic digestion condition in order to avoid the failure of digestion process and to reach a steady state condition at pH between 6.8 and 7.2.

Analytical methods

The influent and effluent samples were analyzed for total solids (TS) and volatile solids (VS) contents, moisture content (MC), total dissolved solids (TDS), chemical oxygen demand (COD) and total kjeldahl nitrogen (TKN). All parameters measured were carried out based on the Standard Methods (APHA2012). To determine the strength and the amount of solid mixed and organic compounds present in the wastewater and sludge, the analysis of solid content and its removal after digestion process should be conducted *(Darwin et al., 2016a)*.VS reduction and COD removal were analyzed in order to know the efficiency of biodegradation during the anaerobic digestion process, which were based on the formula used by previous studies *(Darwin et al., 2016b)*. The rates of biogas production were measured as the volume of biogas produced per day. The biogas yield was measured based on the total biogas produced per gram volatile solids added *(Parawira et al., 2008; Darwin et al., 2016b)*.

RESULTS

The performance of anaerobic co-digestion with high organic loading rate

To evaluate the effects of high organic loading rate on the anaerobic co-digestion of cocoa husk with digested cow manure, the anaerobic reactors were operated under semi-continuous mode. As shown in Table 1, both single substrate digestion and co-digestion reactors had culture with pH neutral (7.0-7.06). The influent of anaerobic co-digestion of cocoa husk with digested cow manure had higher organic contents of COD and VS (11361 mg/l and 79.03%) than the COD and VS of the influent of anaerobic digestion of cow manure alone (1900 mg/l and 67%). This would indicate that the anaerobic digestion of digested cow manure using cocoa husk as a co-substrate would have the potential for enhancing the biogas production rather than the anaerobic digestion of cow manure alone.

Table 1

Influent data of anaerobic digestion process

Analysis	Unit	Cow manure	Cocoa husk co-digested with cow manure
COD	mg/L	1900	11361.08
TS	%	1.3	5.28
VS	%	67	79.03
pH	-	7.0	7.06
TKN	mg/L	321	769.92
TDS	mg/L	1600	1510

Results showed that anaerobic co-digestion of digested cow manure and cocoa husk produced biogas at thirteen times higher than biogas produced from the anaerobic digestion of digested cow manure alone (Fig. 1). High organic loading rate (OLR) and short HRT applied to the anaerobic co-digestion process did not give any significant inhibition to the biogas production. Results also showed that pH culture of anaerobic co-digestion of cocoa husk and digested cow manure were quite stable between 6.92 and 7.23 (Table 2), which was considered as the optimal pH range for biogas and/or methane production via anaerobic digestion *(Rajeshwari et al., 2000)*.

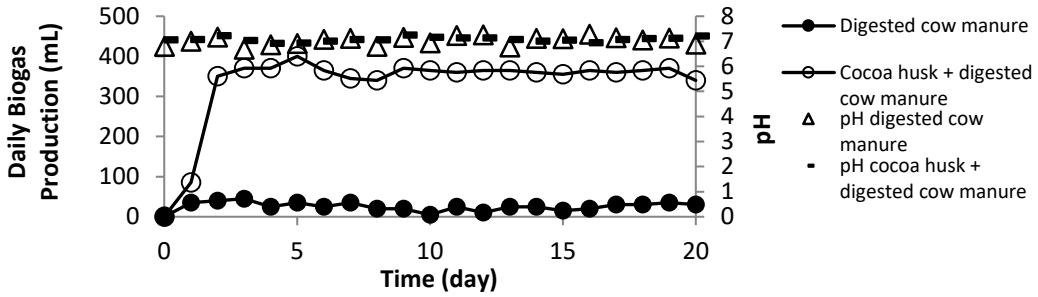

Fig. 1 - Daily biogas production of cocoa husk and digested cow manure under semi-continuous operation

Table 2

Effluent data of anaerobic digestion process

Analysis	Unit	Cow manure	Cocoa husk co-digested with cow manure
COD	mg/L	645	3225.22
TS	%	0.6	5.44
VS	%	40	77.12
pH	-	6.9	7.22
TKN	mg/L	212.2	752.8
TDS	mg/L	1620	3020

The current results were quite different from the previous study carried out by *Darwin et al. (2017)* on the anaerobic co-digestion of bagasse and digested cow manure, which revealed that the acid buildup occurred in the digester in which pH culture dropped from 7.0 to 5.0. The difference occurred as the characteristics of substrate used were quite different. The previous study used bagasse as a co-substrate that may have lower lignin content (≤ 5% lignin) in comparison to cocoa husk (14% lignin) that was used as a co-substrate for this current study *(Alemawor et al., 2009; Paixão et al., 2016).* This suggested that the different types and characteristics of substrate used for anaerobic digestion would affect the rate of hydrolysis as well as conversion of the organic materials into intermediates (e.g. organic acids) and/or end-product (e.g. biogas/methane) during the process of anaerobic digestion *(Taherzadeh and Karimi, 2008; Ge et al., 2010).*

Biodegradation efficiency assessment showed that high OLR (4.173 kg VS/m^3.day) and short HRT (10 day) applied to the process of anaerobic co-digestion of cocoa husk and digested cow manure did not inhibit the degradation process of organic matters to biogas. The degradation of organic materials in the process of anaerobic co-digestion of cocoa husk and digested cow manure was showed in a fairly high percentage of COD removal which was about 72% reduction. High organic conversion showed in COD removal, could lead to an increase of biogas production in the process of anaerobic co-digestion of cocoa husk and digested cow manure.

Results revealed that high OLR and short HRT applied did not affect the performance of anaerobic co-digestion of cocoa husk and digested cow manure to produce biogas. Overall, biogas generated from the anaerobic co-digestion of cocoa husk and digested cow manure was significantly higher than biogas produced from the anaerobic digestion of cow manure alone (Fig.1). As shown in Table 3, the yield and productivity of biogas generated from the anaerobic co-digestion of cocoa husk and digested cow manure were around 56mL/gVS added and 350 mL/day, respectively. Those results were twice than the yield and productivity of biogas generated from the anaerobic digestion of digested cow manure alone, which were 21 mL/gVS added and 27 mL/day, respectively. These results suggested that the short HRT and high OLR applied did not generate acid accumulation in which the proton concentration in the digester was quite low (pH 6.90 - 7.2).

The current results are quite different from the study conducted by *Babaee and Shayegan (2011)* revealing that high organic loading rate applied in the process of anaerobic digestion could lower the production of biogas. The authors also mentioned that an increase of high organic loading rate could lead to the decrease of VS degradation and biogas yield. In their study, they applied a gradual increase of organic loading rate from 1.4 to 2.75 kg VS/m^3.day and resulted in a significant decrease of biogas production even if HRT applied was a normal retention time for operating anaerobic digestion which was 25 days. This is quite different from the current study in which high organic loading rate (4.173 kg VS/m^3.day) and short HRT (10 days) applied did not cause any significant inhibition for biogas production. The difference could be related to the substrate used for the anaerobic digestion in which the previous study (*Babaee and Shayegan, 2011)* used vegetable waste which was more biodegradable than the substrate used in this current study (cocoa husk). This is possible as the more biodegradable substrate loaded the easier the conversion would be *(Schiener et al., 1998)*. Therefore, high organic loading rate applied would generate acid buildup leading to an increase of proton (H^+) concentration in the anaerobic digester, and this condition would screw up the anaerobic digestion process completely *(Rincón et al., 2008; Darwin et al., 2018).*

Table 3

Biodegradation efficiency

Analysis	Unit	Cow manure	Cocoa husk co-digested with cow manure
COD removal	%	66.05	72
VS reduction	%	67.2	10.6
Total biogas accumulated	mL	530	6965
Biogas productivity	mL/day	26.5	348.3
Biogas yield	mL/gVS added	21	55.64

Kinetic assessment of anaerobic co-digestion of cocoa husk and digested cow manure

The process of anaerobic digestion highly depended on the microbial activity for succeeding the production of biogas as the end-product. Understanding the microbial activity during the anaerobic digestion process is essential to minimize the risk of process failure. Microbial activity in anaerobic digestion could be evaluated through the kinetic model analysis *(Linke, 2006).* The assessment included the kinetics on substrate consumption/uptake, the microbial growth and/or death rate.

In the process of anaerobic digestion, the limited substrate uptake could be described by assessing the first order reaction model *(Raj and Anjaneyulu, 2005; Vavilin et al., 2008)* as mentioned in Eq. (1):

$$\frac{-ds}{dt} = K'S \tag{1}$$

As K' is the rate constant, the formula could be considered as the model of microbial exponential growth. The substrate concentration could be described by assessing the exponential growth of the biomass while the substrate is uptake. In this case, the influent substrate concentration (S_o, mg/l) is proportional to the effluent substrate concentration (S, mg/l) and the retention time applied (t, day).

$$S = S_o \exp(-K_s t) \tag{2}$$

To evaluate whether the process of anaerobic co-digestion of cocoa husk with digested cow manure would follow the first order reaction describing the limited substrate uptake, the application of natural logarithm should be given into both sides of Eq. (2).

$$ln\left(\frac{S}{S_0}\right) = -K_s t \tag{3}$$

Based on Eq. (3), the half –velocity constant, K_s(mg/l) would be expressed in Eq. (4).

$$K_s = \frac{-ln\left(\frac{S}{S_o}\right)}{t} \tag{4}$$

Results revealed that a linear relationship between the half velocity constant and retention time was obtained indicating that the kinetics of the process of anaerobic co-digestion of cocoa husk with digested cow manure complied a first order reaction. As depicted in Fig.2, when $-ln\left(\frac{S}{S_o}\right)$ was plotted against the retention time, the linear curve was obtained with the regression coefficient of 0.999.

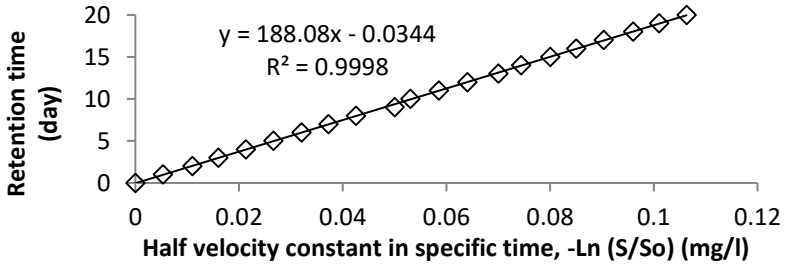

Fig. 2 - Kinetic plot of the first order reaction on the anaerobic co-digestion of cocoa husk with digested cow manure

Some essential kinetic parameters that could be used for describing the performance of anaerobic digestion included the maximum specific growth rate of biomass (μ_{max}) and the maximum substrate uptake rate (*K*). Those parameters could be obtained by plotting the total substrate effluent (*St*) against a retention time (*T*) in which the models were expressed in Eq. (5) and (6) *(Darwin et al., 2017; Zainol, 2012).*

$$S_t = \frac{S_o - S}{S} \quad (5)$$

$$T = \frac{1}{\mu_{max}} + \frac{K}{\mu_{max}}\frac{S_o - S}{S} \quad (6)$$

Based on the data plot depicted in Fig. 3, the value of μ_{max} were an inverse of intercept (1/intercept), and *K* were the division of slope and intercept (slope/intercept) *(Zainol, 2012; Darwin et al., 2017).*

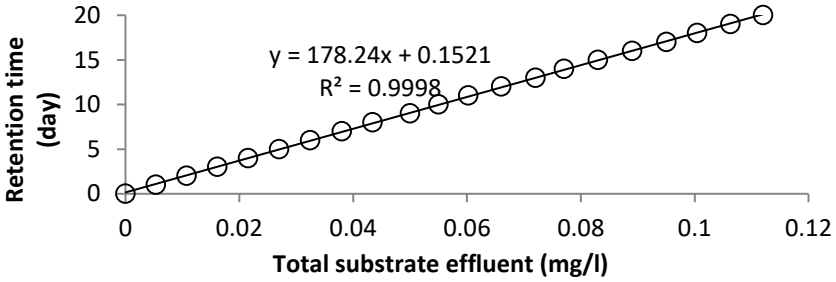

Fig. 3 - Determination of the maximum specific growth rate of biomass and the maximum rate of substrate utilization

Results of the current study revealed that the maximum specific growth rate of biomass (μ_{max}) and the maximum substrate uptake rate (*K*) during the process of anaerobic co-digestion of cocoa husk and digested cow manure obtained were 6.58 day $^{-1}$ and 1172.4 mg/mg, respectively.

As the valued of the maximum specific growth rate of biomass was higher than dilution rate (*D)* applied which was 0.1 day $^{-1}$. This suggested that the cell mass in the reactor still could retain and grow effectively in the anaerobic bioreactor even if short HRT (10 days) and 300 mL/day of flow rate were applied to the process of anaerobic co-digestion of cocoa husk and digested cow manure. This current study was in line with some previous studies *(Wirtz, 2002; Wick et al., 2002; Darwin et al., 2017)* revealing that the dilution rate applied should be lower than the value of μ_{max} in order to sustain the culture and biomass cells in the bioreactor, and also to prevent culture wash out during the process of anaerobic digestion.

Results showed that the value of the maximum specific growth rate in the process of anaerobic co-digestion of cocoa husk and digested cow manure obtained was quite high suggesting that the microbial cell mass present in the reactor was relatively small. This is due to the fact that the specific microbial growth rate was inversely proportional to the concentration of microbial cell mass during the process of anaerobic digestion *(Zainol, 2012; Darwin et al., 2017)*. The results revealed that high OLR and short HRT applied did not cause acid accumulation or drop of pH during the anaerobic co-digestion process, and thereby the production of biogas was still stable at around 348.3 ml/day (Table 2).

In order to evaluate the relationship between the substrate uptake rate (*U*) and the concentration of the substrate after the digestion process (*S*), the kinetic model would be expressed as depicted in Eq. (7) *(Viessman and Hammer, 1993).*

$$\frac{1}{U} = \frac{K_S}{KS} + \frac{1}{K} \quad (7)$$

K_S is the value of the half-velocity constant, which is related to the hydrolysed substrate (mass/volume) during the digestion process *(Faisal and Unno, 2001).* In this current study, K_S obtained was 22.04 mg/L. According to the data of the half-velocity constant K_S and the maximum substrate uptake rate (*K*) obtained, the performance of anaerobic co-digestion of cocoa husk and digested cow manure did not run effectively. This occurred as organic loading rate applied was quite high, which may lead to the inefficient conversion during the anaerobic digestion process.

An inefficient digestion process was also influenced by the short HRT. As some studies had revealed that an optimum HRT for operating anaerobic digestion process was 25 to 30 days *(Bougrier et al., 2008; Juntarachat, 2017).* This suggested that the HRT applied in this current study was about 2.5 times lower than a normal hydraulic retention time of anaerobic digestion process for biogas production, and thereby the anaerobic microbes did not have sufficient time for completely converting organic materials into biogas. As an optimum HRT for operating anaerobic digestion was 25 days, this indicated that the OLR that should be feasible for optimizing the process of anaerobic co-digestion of cocoa husk and digested cow manure to form biogas, was at around 1.67 kg VS/m^3.day.

In anaerobic digestion, the specific substrate uptake rate could be related to some kinetic parameters including the biomass yield, mean cell residence time and the endogenous decay coefficient. The relationship among those parameters could be expressed in kinetic model as shown in Eq. (8).

$$\frac{1}{\theta} = YU - K_d \quad (8)$$

where θ is mean cell residence time (day), *Y* is the biomass yield (mg/mg), and K_d is the endogenous decay coefficient (day^{-1}) *(Taherzadeh M.J.; Karimi K., 2008)*.

By plotting the substrate uptake rate (*U*) against the inverse of cell residence timeθ^{-1}, some kinetic parameters including the biomass yield and the endogenous decay coefficient would be obtained (Fig. 4).

The results of this current study were quite different from the previous study conducted by *Darwin et al. (2017)* in which the biomass yield was quite low, and the endogenous decay coefficient obtained was fairly high indicating the short HRT (10 days) and high OLR (3.47 kg VS/m^3.day) applied were not feasible for the process of anaerobic co-digestion of bagasse and digested cow manure. Short HRT and high OLR applied in the previous study also contributed to the drop of pH during the anaerobic digestion process. An acid accumulation and high proton concentration inhibited the growth as well as the activity of the anaerobic microbes, and thereby lower the biomass yield.

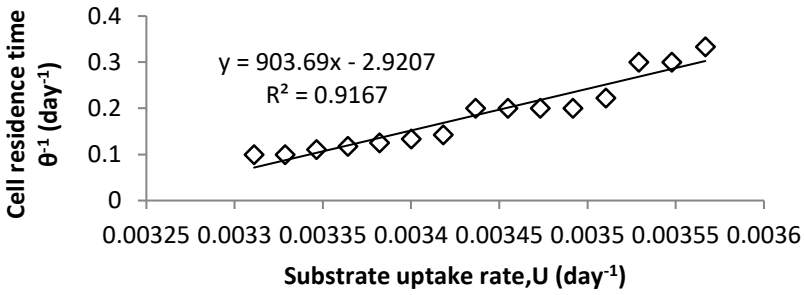

Fig. 4 - Plot for determination of the biomass yield and the endogenous decay coefficient

CONCLUSIONS

High organic loading rate and short HRT applied to the process of anaerobic co-digestion of cocoa husk and digested cow manure did not inhibit the biogas production in which pH was stable at between 6.8 and 7.2 suggesting that acid was not accumulated in the reactor. The production of biogas was stable at around 348.3 mL/day, and the biogas yield obtained was about 55.64 69 mL/gVS added. The kinetic study revealed that the maximum specific growth rate μ_{max}obtained from the anaerobic co-digestion process of cocoa husk and digested cow manure was quite high at about 6.58 day $^{-1}$. Pre-treatment of cocoa husk would be potential to be applied in order to enhance biogas production as well as its yield.

Results showed that the biomass yield and endogenous decay coefficient obtained from the process of anaerobic co-digestion of cocoa husk and digested cow manure were 903.6 mg/mg and 2.92 day^{-1}, respectively. As the yield of biomass was quite high, and the endogenous decay coefficient obtained was fairly low, this suggested that anaerobic microbes still could grow during the anaerobic digestion. This indicated that high OLR and short HRT applied to the anaerobic process did not significantly affect the microbial activity. As depicted in Fig.1, the production of biogas generated from the anaerobic co-digestion of cocoa husk and digested cow manure was still quite high, or about 10 times higher than biogas produced from the anaerobic digestion of cow manure alone.

Further, the reason why the different outcome appeared between the previous and the current studies possibly related to the co-substrate usage. As the current study using cocoa husk as the co-substrate, the hardness of the substrate may lead to the slow hydrolysis process to generate cellulose and release sugar, and thereby acid buildup did not occur during the digestion process. Further, in this current study short HRT and high OLR applied did not significantly affect the pH drop. As pH was stable at 7, the process of anaerobic digestion could run stably, and thereby could optimize biogas production, and enhance the yield of biomass.

ACKNOWLEDGMENTS

The authors would like to record their thanks to the Institute for Research and Community Services, Syiah Kuala University for partly funding this research work.

REFERENCES

[1] Alemawor F., Dzogbefia V.P., Oddoye E.O., Oldham, J.H., (2009), Enzyme cocktail for enhancing poultry utilisation of cocoa pod husk, *Scientific Research and Essay*, Vol. 4, no. 6, pp. 555-559;

[2] APHA, (2012), Standard Methods for the Examination of Water and Wastewater, *American Public Health Association*, Washington, D.C./U.S.A.;

[3] Babaee A., Shayegan, (2011), Effect of organic loading rates (OLR) on production of methane from anaerobic digestion of vegetables waste, *Proceedings of* the *World Renewable Energy Congress,* Sweden;

[4] Barta Z., Reczey K., Zacchi G., (2010), Techno-economic evaluation of stillage treatment with anaerobic digestion in a softwood-to-ethanol process, *Biotechnology for Biofuels*, Vol. 3, no. 1, pp. 1-11;

[5] Bougrier C., Delgenès J.P., Carrère H., (2008), Effects of thermal treatments on five different waste activated sludge samples solubilisation, physical properties and anaerobic digestion, *Chemical Engineering Journal*, Vol. 139, no. 2, pp. 236-244;

[6] Bouallagui H., Touhami Y., Cheikh R.B., Hamdi M., (2005), Bioreactor performance in anaerobic digestion of fruit and vegetable wastes, *Process Biochemistry,* Vol. 40, pp. 989-995;

[7] Chandra R., Takeuchi H., Hasegawa T., Kumar R., (2012), Improving biodegradability and biogas production of wheat straw substrates using sodium hydroxide and hydrothermal pretreatments, *Energy*, Vol. 43, no.1, pp. 273-282;

[8] Chen C.C., Chen H.P., Wu J.H., Lin C.Y., (2008), Fermentative hydrogen production at high sulphate concentration, *International Journal of Hydrogen Energy*, Vol. 33, no. 5, pp. 1573-1578;

[9] Dareioti M.A., Kornaros M., (2014), Effect of hydraulic retention time (HRT) on the anaerobic co-digestion of agro-industrial wastes in a two-stage CSTR system*, Bioresource Technology*, Vol. 167, pp. 407-415;

[10] Darwin Cheng J.J., Gontupil J., Liu Z., (2016a), Influence of total solid concentration for methane production of cocoa husk co-digested with digested swine manure, *International Journal of Environment and Waste Management*, Vol. 17, no.1, pp. 71-90;

[11] Darwin Cheng J.J., Liu Z., Gontupil J., (2016b), Anaerobic co-digestion of cocoa husk with digested swine manure: evaluation of biodegradation efficiency in methane productivity. *Agricultural Engineering International: The CIGR Journal,* Vol. 18, no. 4, pp. 147–156;

[12] Darwin Fazil A., Ilham M., Sarbaini Purwanto S., (2017), Kinetics on anaerobic co-digestion of bagasse and digested cow manure with short hydraulic retention time, *Research in Agricultural Engineering Journal*, Vol. 63, no. 3, pp. 121-127;

[13] Darwin Barnes A., Cord-Ruwisch R., (2018), In vitro rumen fermentation of soluble and non-soluble polymeric carbohydrates in relation to ruminal acidosis, *Annals of Microbiology*, Vol. 68, no. 1, pp. 1-8;
[14] Demirer G.N., Chen S., (2005), Two-phase anaerobic digestion of unscreened dairy manure, *Process biochemistry*, Vol. 40, no. 11, pp. 3542-3549;
[15] Elango D., Pulikesi M., Baskaralingam P., Ramamurthi V., Sivanesan S., (2007), Production of biogas from municipal solid waste with domestic sewage, *Journal of hazardous materials*, Vol. 141, no. 1, pp. 301-304;
[16] El-Mashad H.M., Zeeman G., Van Loon W.K., Bot G.P., (2004), Effect of temperature and temperature fluctuation on thermophilic anaerobic digestion of cattle manure, *Bioresource technology*, Vol. 95, no.2, pp. 191-201;
[17] Faisal M., Unno H., (2001), Kinetic analysis of palm oil mill wastewater treatment by a modified anaerobic baffled reactor, *Biochemical Engineering Journal*, Vol. 9, pp. 25-31;
[18] Fernández J., Pérez M., Romero L.I., (2010), Kinetics of mesophilic anaerobic digestion of the organic fraction of municipal solid waste: influence of initial total solid concentration, *Bioresource Technology*, Vol. 101, no. 16, pp. 6322-6328;
[19] Ge H., Jensen P.D., Batstone D.J., (2010), Pre-treatment mechanisms during thermophilic–mesophilic temperature phased anaerobic digestion of primary sludge, *Water research*, Vol. 44, no. 1, pp. 123-130;
[20] Gomec C.Y., (2010), High-rate anaerobic treatment of domestic wastewater at ambient operating temperatures: A review on benefits and drawbacks, *Journal of Environmental Science and Health Part A*, Vol. 45, no. 10, pp. 1169-1184;
[21] Gontupil J., Darwin M., Liu Z., Cheng J.J., Chen H., (2012), Anaerobic co-digestion of swine manure and corn stover for biogas production, *Annual International Meeting Conference, American Society of Agricultural and Biological Engineers*, Dallas, U.S.A.;
[22] Guštin S., Marinšek-Logar R., (2011), Effect of pH, temperature and air flow rate on the continuous ammonia stripping of the anaerobic digestion effluent, *Process Safety and Environmental Protection*, Vol. 89, no. 1, pp. 61-66;
[23] Juntarachat N., (2017), Evaluation of Biogas Production Potential from Raw and Processed Agricultural Wastes, *Energy Procedia*, Vol. 138, pp. 205-210;
[24] Kaosol T., Sohgrathok N., (2012), Influence of Hydraulic Retention Time on Biogas Production from Frozen Seafood Wastewater Using Decanter Cake as Anaerobic Co-digestion Material, *International Journal of Environmental and Ecological Engineering*, Vol. 6, no. 5, pp. 303-307;
[25] Kafle G.K., Bhattarai S., Kim S.H., Chen L., (2014), Effect of feed to microbe ratios on anaerobic digestion of Chinese cabbage waste under mesophilic and thermophilic conditions: biogas potential and kinetic study, *Journal of environmental management*, Vol. 133, pp. 293-301;
[26] Lastella G., Testa C., Cornacchia G., Notornicola M., Voltasio F., Sharma V.K., (2002), Anaerobic digestion of semi-solid organic waste: biogas production and its purification, *Energy Conversion and Management*, Vol. 43, no.1, pp. 63-75;
[27] Linke B., (2006), Kinetic study of thermophilic anaerobic digestion of solid wastes from potato processing. *Biomass and Bioenergy*, Vol. 30, no. 10, pp. 892-896;
[28] Liu X., Wang W., Shi Y., Zheng L., Gao X., Qiao W., Zhou Y., (2012), Pilot-scale anaerobic co-digestion of municipal biomass waste and waste activated sludge in China: effect of organic loading rate, *Waste Management*, Vol. 32, no. 11, pp. 2056-2060;
[29] Maharaj I., Elefsiniotis P., (2001), The role of HRT and low temperature on the acid-phase anaerobic digestion of municipal and industrial wastewaters, *Bioresource Technology*, Vol. 76, no. 3, pp. 191-197;
[30] Mähnert P., Linke B., (2009), Kinetic study of biogas production from energy crops and animal waste slurry: effect of organic loading rate and reactor size. *Environmental Technology*, vol.30, no. 1, pp. 93-99;
[31] Manyi-Loh C.E., Mamphweli S.N., Meyer E.L., Okoh A.I., Makaka G., Simon M., (2013), Microbial anaerobic digestion (bio-digesters) as an approach to the decontamination of animal wastes in pollution control and the generation of renewable energy, *International Journal of Environmental Research and Public Health*, Vol. 10, no. 9, pp. 4390-4417;

[32] Momoh O.Y., Anyata B.U., Saroj D.P., (2013), Development of simplified anaerobic digestion models (SADM's) for studying anaerobic biodegradability and kinetics of complex biomass, *Biochemical Engineering Journal*, Vol. 79, pp.84-93;
[33] Monroy O., Famá G., Meraz M., Montoya L., Macarie H., (2000), Anaerobic digestion for wastewater treatment in Mexico: state of the technology, *Water Research*, Vol. 34, pp. 1803-1816;
[34] Narihiro T., Sekiguchi Y., (2007), Microbial communities in anaerobic digestion processes for waste and wastewater treatment: a microbiological update, *Current Opinion in Biotechnology*, Vol. 18, no. 3, pp. 273-278;
[35] Onthong U., Juntarachat N., (2017), Evaluation of Biogas Production Potential from Raw and Processed Agricultural Wastes, *Energy Procedia*, Vol. 138, pp. 205-210;
[36] Paixão S.M., Ladeira S.A., Silva T.P., Arez B.F., Roseiro J.C., Martins M.L.L., Alves L., (2016). Sugarcane bagasse delignification with potassium hydroxide for enhanced enzymatic hydrolysis, *RSC Advances*, Vol. 6, no. 2, pp. 1042-1052;
[37] Parawira W., Read J.S., Mattiasson B., Bjornsson L., (2008), Energy production from agricultural residues: high methane yields in pilot-scale two-stage anaerobic digestion, *Biomass and Bioenergy*, Vol. 32, pp. 44–50;
[38] Raj D.S.S., Anjaneyulu Y., (2005), Evaluation of biokinetic parameters for pharmaceutical wastewaters using aerobic oxidation integrated with chemical treatment, *Process Biochemistry*, Vol. 40, pp. 165-175;
[39] Rajeshwari K.V., Balakrishnan M., Kansal A., Lata K., Kishore V.V.N., (2000), State-of-the-art of anaerobic digestion technology for industrial wastewater treatment, *Renewable and Sustainable Energy Reviews*, Vol. 4, no. 2, pp. 135-156;
[40] Rincón B., Borja R., González J.M., Portillo M.C., Sáiz-Jiménez C., (2008), Influence of organic loading rate and hydraulic retention time on the performance, stability and microbial communities of one-stage anaerobic digestion of two-phase olive mill solid residue, *Biochemical Engineering Journal*, Vol. 40, pp. 253–261;
[41] Riviere D., Desvignes V., Pelletier E., Chaussonnerie S., Guermazi S., Weissenbach J., Sghir A., (2009), Towards the definition of a core of microorganisms involved in anaerobic digestion of sludge, *The ISME journal*, Vol. 3, no. 6, pp. 700-714;
[42] Salminen E.A., Rintala J.A., (2002), Semi-continuous anaerobic digestion of solid poultry slaughterhouse waste: effect of hydraulic retention time and loading, *Water research*, Vol. 36, no. 13, pp. 3175-3182;
[43] Schiener P., Nachaiyasit S., Stuckey D.C., (1998), Production of soluble microbial products (SMP) in an anaerobic baffled reactor: composition, biodegradability, and the effect of process parameters, *Environmental Technology*, Vol. 19, no. 4, pp. 391-399;
[44] Sialve B., Bernet N., Bernard O., (2009), Anaerobic digestion of microalgae as a necessary step to make microalgal biodiesel sustainable, *Biotechnology Advances*, Vol. 27, no. 4, pp. 409-416;
[45] Taherzadeh M.J., Karimi K., (2008), Pretreatment of lignocellulosic wastes to improve ethanol and biogas production: a review, International *Journal of Molecular Sciences*, Vol. 9, no. 9, pp. 1621-1651;
[46] Vavilin V.A., Fernandez B., Palatsi, J., Flotats, X., (2008), Hydrolysis kinetics in anaerobic degradation of particulate organic material: an overview. *Waste management*, Vol. 28, no. 6, pp. 939-951;
[47] Viessman W., Hammer M.J., (1993), Waste Supply and Pollution Control, *Harper Collins College Publishers*, New York/U.S.A.;
[48] Wick L.M., Weilenmann H., Egli T., (2002) The apparent clock-like evolution of Escherichia coli in glucose-limited chemostats is reproducible at large but not at small population sizes and can be explained with Monod kinetics, *Microbiology*, Vol. 148, no. 9, pp. 2889-2902;
[49] Willeghems G., Buysse, J., (2016), Changing old habits: The case of feeding patterns in anaerobic digesters, *Renewable Energy*, Vol. 92, pp. 212-221;
[50] Wirtz K.W., (2002), A generic model for changes in microbial kinetic coefficients, *Journal of Biotechnology*, Vol. 97, no. 2, pp. 147-162;
[51] Zainol N., (2012), Kinetics of Biogas Production from Banana Stem Waste, *INTECH Publisher,* London/U.K.;
[52] Zhang Z.P., Show K.Y., Tay J.H., Liang D.T., Lee D.J., Jiang W.J., (2006), Effect of hydraulic retention time on biohydrogen production and anaerobic microbial community, *Process Biochemistry*, Vol. 41, no. 10, pp. 2118-2123.

MEASUREMENT OF DOWNWASH VELOCITY GENERATED BY ROTORS OF AGRICULTURE DRONES
/
植保无人机旋翼下洗气流速度的测量

As. Prof. Ph.D. Tan Feng*[1)], Ph.D. Lian Qi[2)], M.S. Liu Chang-liang[3)], M.S. Jin Bing-kun[4)]

[1)] School of Electrical and Information, Heilongjiang Bayi Agricultural University, Daqing / China; [2)] School of Engineering, Heilongjiang Bayi Agricultural University, Daqing / China; [3)] Key Laboratory of Surface Engineering of Equipment for Hydraulic Engineering of Zhejiang Province, Hangzhou / China; [4)] Faculty of Mechanical and Materials Engineer, Western University, London/Canada

Tel: +8613836962600; E-mail: tf1972@163.com

Keywords: *agriculture drone; downwash velocity; rotors; measurement*

ABSTRACT

With the rapid development of drones in China, the use of multi-rotor drones for spraying chemical pesticide against pests and weeds has recently become common in agriculture. However, the downwash generated by drone rotors considerably influences the droplet deposition process by potentially causing the liquid to drift. A test analysis method was presented and a rotor rotation test bench was designed to simulate the different rotation speed of a six-rotor drone and thus study the characteristics and distribution law of the downwash velocity. An anemometer was used to measure the downwash velocity generated at different radial positions of the rotor. Results show that the downwash velocity generated by each radial position of the rotor is evenly distributed on the rotating loop and the standard deviation of the circumferential downwash velocity is less than 1 m/s. The downwash velocity along each position in the radial direction of the rotor increase first and then decrease and the 1/2 radius position of rotor blade generate the maximum downwash velocity of 10.8 m/s in the test. The downwash velocity does not considerably change with longitude, but decreases at a distance of 10 cm from the ground due to the ground effect. Therefore, the parameters of airfoil profile at each radial position on the rotors have a marked effect on the magnitude of the downwash velocity. This study provides an effective measurement method for the investigation of the downwash velocity distribution of drone rotors. The measurement results can provide a reference for the nozzle distribution under the rotor and the study of droplet movement.

摘要

随着无人机在中国的快速发展，近年来在农业领域使用多旋翼无人机喷洒化学药剂进行病虫草害的防治变得越加普遍。但由于无人机旋翼产生的下洗气流对雾滴沉积过程具有显著影响，极易造成药液的漂移。为了研究旋翼下洗气流的流动特性和分布规律，本文提出了一种旋翼下洗气流速度分布的测试分析方法，设计了一种能够模拟六旋翼无人机不同旋翼转速状态下的旋翼旋转试验台，利用风速仪对旋翼不同径向位置产生的下洗气流进行了风速分布测量研究。研究结果表明旋翼径向各位置产生的下洗风速在旋转环线上分布较均匀，环向风速标准差小于 1m/s；沿旋翼径向各位置产生的下洗风速先增大后减小，1/2 旋翼半径处产生的下洗风速最大，试验中获得的最大下洗风速为 10.8m/s；旋翼产生的下洗风速随纵向变化不大，在距离地面 10cm 处受到地面效应的影响导致该高度下洗风速整体变小。通过以上研究结果可以得出旋翼径向各位置的翼型参数对该位置产生的下洗风速大小有显著影响，该研究成果为无人机旋翼下洗气流风速分布的研究提供了一种有效的测量方法，测量结果可为喷头在旋翼下方的分布及雾滴运动研究提供参考。

INTRODUCTION

In recent years, drones have been widely utilized in many fields, including agriculture (*Xiongkui H. et al., 2017; Veroustraete. F, 2015*) due to the popularity of civilian-grade drones.

Utilizing drones with pesticide spraying systems for crops such as rice, corn, cotton and tea, can effectively avoid the limitation of special field conditions and the state of crop growth on the plant protection machinery with large wheels (*Xue X Y. et al., 2014*), resulting in efficient, safe, and non-destructive plant protection. Numerous advanced technologies such as automatic path planning, unmanned operation and Real - time kinematic (RTK) high-accuracy positioning have been applied to multi-rotor drones (*Lu L, 2017; Wang Y. et al., 2018; Xu B et al., 2015*) to considerably improve their operational stability, efficiency, accuracy and ease of operation. Consequently, multi-rotor drones have become the main models of plant protection drones in China. The most important feature of utilizing multi-rotor drones for pesticide spraying is that it generates a powerful downwash during the flight due to its unique rotor structure and principle of

motion, promoting the disturbance to crops and increasing the penetration of liquid. Therefore, liquid also has a good deposition effect on the lower part of crops (*Yang Y S et al., 2013, Reed W H, 1953*).

However, due to the wide variety of drones that can be used for pesticide spraying, the specifications, numbers, and installation positions of various types of rotors differ. Therefore, large variations in downwash flow field are generated by different rotors. Thus, solving the problem of accurately depicting the overall spatial distribution characteristics of rotor downwash flow field and the distribution of downwash velocity at various locations inside the rotor is urgent.

Therefore, this study designs a test bed that simulates the rotor downwash flow field and measures and analyses the magnitude of the rotor downwash velocity and its distribution on the entire rotor through a uniform distribution point measurement method. This approach provides a basis for studying the spray performance of the nozzle in the downwash airflow field and the droplets settling. Moreover, improving the application effect of the multi-rotor plant protection drones is of considerable importance.

Scholars all over the world have conducted numerous studies to improve the application effect of agriculture drones. For example, Faical B.S. optimized the real-time flight path of the drone, which can independently adjust the flight route according to the changes in meteorological conditions (*Faiçal B.S. et al., 2017*). However, changing the drone's flight route will also affect the deposition on the ground of droplets, which is not conducive to uniform spraying. Kirk studied the effects of boom length and droplet size on effective spray and spray drift, respectively (*Kirk I.W., Hoffmann W.C, 2002*). Their results showed that the effective spray width produced when the boom length is 75% of the rotor diameter is less than the length of the boom equal to the diameter of the rotor. In addition, the droplet diameter of 400 microns has more drift compared with 1000 microns diameter of droplets to explore the effect of spray parameters on the deposition of wheat leaf in wheat disease prevention. However, the preceding studies did not reveal the influence of rotor airflow on the nozzles on different boom lengths. Fritz (*Fritz B.K. et al., 2006*) conducted air spray tests to determine the type of spray head, particle size of spray droplets, and spray flow at the best deposition rate. However, environmental factors and the influence of the rotor airflow on the nozzle were not considered during the test; thus, the optimal parameters obtained were not universal.

The study of rotor downwash starts with helicopters. Quackenbush numerically calculated the flow field distribution of helicopter rotor/fuselage by applying the fuselage cell model and the free-wake method (*Quackenbush T.R. et al.,1994*). Caradonna and Isom used a relatively simple potential flow equation to calculate the rotor flow without lift in the hovering state, but the application of the proposed method was limited for ignoring the lift (*Caradonna F.X., Isom M.P., 1972*). Rajagopalan proposed a momentum source method for the simulation of helicopter flow fields in 1993 (*Rajagopalan R.G. et al., 1993*). Wang Bo employed the momentum source method to investigate the numerical simulation of helicopter rotor and fuselage flow field and verified the effectiveness of the method (*Wang B. et al., 2008*). Ren L.F. studied the influence of helicopter rotor field on the exhausted wake (*Ren L.F. et al., 2015*). Sun Peng examined the influence of the outside wind on the helicopter rotor and the mixed airflow field on the deck (*Sun P. et al., 2015*). Although these scholars mostly focused on aerodynamic characteristics of rotors and fuselage, the numerical simulations and tests extensively applied multi-rotor plant protection drones to crop pesticide spraying and achieved numerous research results (*Xiongkui H. et al., 2017*). The downwash airflow generated by the multi-rotor plant protection drone was studied to investigate its effect on the nozzle spraying characteristics and the deposition law of the droplets in the flow field. In response, Wang C.L. proposed a space mass balance test method (*Wang C.L. et al., 2016*). The effects of 3WQF80-10 single-rotor plant protection drone on the mass balance distribution of the droplets in space and the distribution of the downwash velocity under the different flight modes and flight parameters analysed by outdoor experiments. Although the velocity of downwash generated by the rotors in different modes was measured, analysis of the causes of differences in droplet deposition due to the generated airflow fields with varying flight conditions is absent. Yang conducted a simulation experiment based on the XV-2 single-rotor agriculture drone to study the influence of downwash on the spray amplitude. The results showed that rotor downwash increased the spray amplitude (*Yang Z.L. et al., 2018*). Tang utilized the high-velocity particle image velocity measurement method in the laboratory to obtain the movement of droplets under the rotor downwash (*Tang Q. et al., 2017*). It was concluded that the downwash generated by rotors was the main factor affecting the droplet volume and sedimentation velocity. Yang adopted the CFD method to simulate the downwash air flow generated by the six-rotor drone and obtained the downwash velocity distribution rule of the rotor downwash at different height levels through a series of outdoor experiments (*Fengbo Y. et al., 2017*).

Based on the preceding research literature, the downwash is found to have a considerable influence on the droplet sedimentation process and deposition effect. However, at present, scholars have studied the distribution of the overall downwash flow field generated by all rotors of a multi-rotor drone near the ground through different means. The differences in the downwash velocity distribution at varying positions inside the downwash flow field generated by each rotor due to the differences in rotor airfoil structure are neglected. This will directly affect the initial spray characteristics of the inner sprayer in the airflow field below the rotor. Therefore, a rotor rotation test bench is designed to measure and analyse the velocity distribution at different positions inside the downwash flow field generated during the rotation of any rotor.

The layout of this study is as follows. In Section 3, the structure and working principle of the rotor rotation test bench are introduced. In Section 4, the specific method of the velocity measurement test of rotor downwash airflow field is highlighted and the relative experimental results are analysed. In Section 5, the conclusions of this study are presented based on the experimental results.

MATERIALS AND METHODS

Structure and Principle of Test Bench

The frame of test bench is designed according to the six-rotor drone, with a wheelbase of 130 cm. In addition, the diameter of propeller is 56 cm. The frame is fixed on an aluminium profile support table that can be either raised or lowered (0-4m). The power part consists of brushless motor and electronic speed controller. The power source is the lithium battery (6s 18000mAH). The main structure is presented in fig.1.

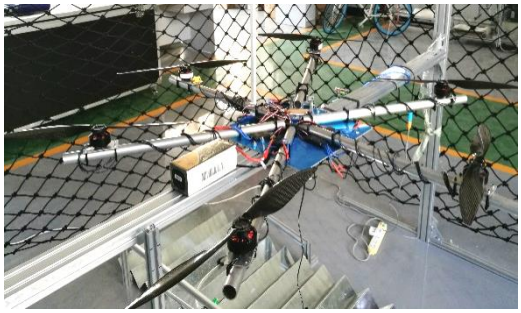

Fig.1 - The main structure of test bench

The control system and data acquisition system of test bench consist of computer, core controller and sensors. The core controller communicates with the computer through USB to TLL port line. With the use of the computer software, the rotation speed of rotor can be controlled remotely, and data, such as rotor tension, rotation speed, system voltage, current, throttle volume and throttle pulse width modulation (PWM) can be collected. The rotation speed measuring device is a photoelectric switch (QS18VN6D) produced by the Bonner Company. By attaching a black and white reflective paper on the wall of the motor, the photoelectric switch directly faces the motor wall to acquire the motor rotation speed signal, thereby obtaining the rotation speed of the rotor. The propeller pull can be measured by a pressure sensor (HX711AD) produced by the Gaoling company and located at the end of the rotor support. The downwash velocity of the rotor is measured by a wireless anemometer (410i) produced by Testo of Germany and data transmission is performed via Bluetooth. The parameters of each sensor are shown in table 1. And the control and data acquisition systems are presented in fig.2.

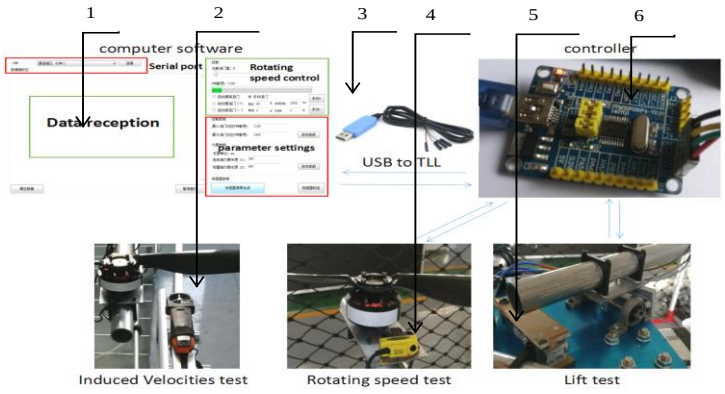

Fig.2 - The System of Control and Data Acquisition

1. Host computer interface 2. Anemometer 3. Serial cable 4. Photoelectric switch 5. Pressure sensor 6. Main controller

Table 1

Sensor Performance Parameters

Range of tension sensor	Parameter value
Accuracy of tension sensor	0-10kg
Acquisition frequency of tensile sensor	1g
Range of velocity test	50hz
Frequency of velocity acquisition	0-10000r/min
Range of downwash velocity test	50hz
Accuracy of downwash velocity test	0.4-30M/s
Range of tension sensor	0.001m/s

Downwash Velocity Measurement Test

Test Conditions

The test is carried out in an airtight laboratory, the average temperature is 23°C indoor, the average humidity is 48%, the air density is 1.29 kg/m^3 and the air pressure is 1 standard atmosphere. To simulate the hovering state of the six-rotor drone under a take-off weight of 10 kg, the rotation speed can be maintained at 2500 r/min during the test.

Measurement Point Arrangement

The purpose of this test is to investigate the distribution law of downwash velocity of rotors in the horizontal cross-section and vertical cross-section of the downwash airflow. Thereby, the layout of the downwash velocity measurement points is as below:

(1) Horizontal Test Point Arrangement

To measure the velocity of the downwash generated at different radial positions of rotor blades, six measurement points (o, a, b, c, d, e) are set at the interval of 6 cm in the direction of the wing tip centring on the rotor rotation axis, and the radial measurement range is 0-30 cm. In the direction of the rotation of the blade, eight measuring points (N1-N8) are respectively arranged at the intervals of 45° on each equal-diameter ring so that the radial and circumferential directions of the blades together constitute the downwash-velocity measurement plane at the same height, for a total of 41 downwash velocity measurement points, as they are indicated in fig. 3(a).

(2) Vertical Test Point Arrangement

To investigate velocity of the downwash at different heights while the rotor is rotating, the rotating surface of the rotor is utilized as a reference plane, a total of 5 measurement planes (H1-H5) are set downward at a height interval of 20 cm and the range of vertical height is 0-100 cm. The layout scheme for each plane is the same as the horizontal layout scheme. The longitudinal distribution of the measurement points in the two directions of the same line is presented in fig. 3(b).

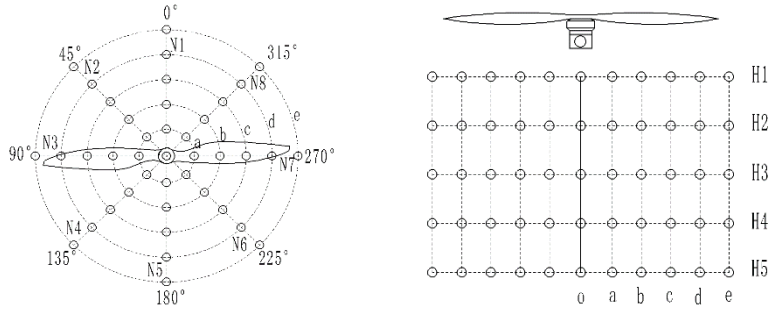

(a) Horizontal section test point layout (b) Vertical section test point layout

Fig. 3 - Below the rotor under the wash air velocity measurement point

RESULTS

Downwash Velocity Results

According to the layout scheme of fig. 3, the downwash velocity at each measurement point is measured. After the downwash is stable, the measured value of velocity can be recorded. Fig. 4 presents the average of the downwash velocity measurements at all the measurement points for each horizontal section height.

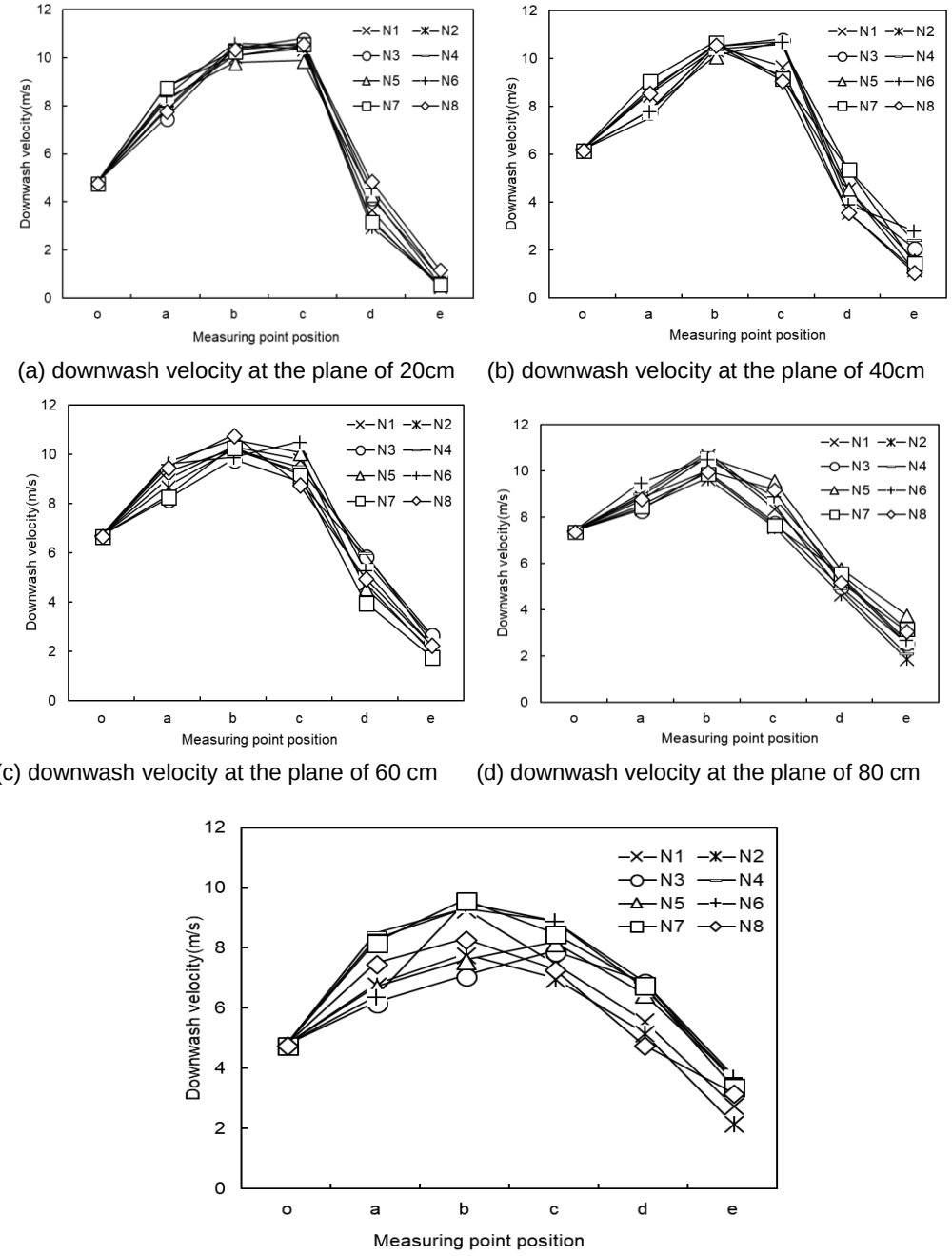

(a) downwash velocity at the plane of 20cm (b) downwash velocity at the plane of 40cm

(c) downwash velocity at the plane of 60 cm (d) downwash velocity at the plane of 80 cm

(e) downwash velocity at the plane of 100 cm

Fig.4 - The measurement results of rotor downwash velocity

Standard Deviation Analysis of Downwash Velocity

The standard deviation of the data reflects the degree of dispersion of a set of data and the average value. The deviation is calculated according to the following equation:

$$\sigma = \sqrt{\frac{1}{N}\sum_{i=1}^{N}(x_i - \mu)^2} \quad (1)$$

Where, σ is standard deviation, [m/s], N is the number of samples, x_i is the sample value, [m/s], μ is sample mean.

This study calculates the standard deviations of eight measurements of downwash air velocity data for each radial position at each measurement height level, the results being presented in fig. 5.

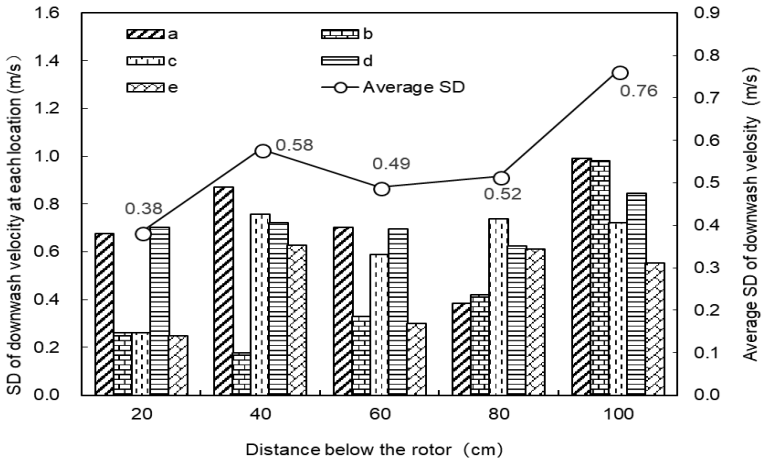

Fig. 5 - The Standard deviation of downwash velocity at each level below the rotor

The histogram in fig. 5 indicates the standard deviation of downwash velocity measurements in eight directions (N1 to N8) while five positions (a to e) rotate in five different height planes (H1 to H5).

In fig. 5 it can be seen that there are certain differences in the standard deviation of downwash velocity measurements at different positions in the same height and the differences in the rules are different at each height. The standard deviation of downwash velocity measurement results of the same radius position within the rotation circle is less than 1 m/s, which indicates that the downwash velocity generated at the same radius position of the rotation circle has no significant difference.

The discounted graph in fig. 5 presents the standard deviation of the average downwash velocity over the rotor radius at all the measurement locations as a function of the test height. It can be seen from the figure that with the increase of the test height, the standard deviation gradually increases, which suggests that the dispersion of the downwash velocity values at each measurement point increases. Nevertheless, the overall standard deviation is less than 1 m/s.

Analysis of the Changing Law of Downwash Velocity

The variation of the average downwash velocity generated by the rotor at each radial position with the radius is presented in fig. 6. The measured values of o~e in these six positions represent the downwash velocity of the downwash airflow generated while the rotor rotates at its centre position with the radius of 6 cm, 12 cm, 18 cm, 24 cm and 30 cm. Fig. 7 shows that the downwash velocity generated from the rotor centre position to the wingtip position suggests a changing trend of increasing first and decreasing later. The downwash velocity generated at the position of the rotor with the radius of 12 cm and 18 cm (b, c) is shown relatively close and is obviously higher than it was generated in other radial positions. The value of the downwash velocity generated at the tip of the rotor is the smallest. In the range of 20 cm-80 cm below the rotor, the variation of the downwash velocity produced by each radius position is basically the same and the change of the rules is slightly different at the height of 100 cm below the rotor due to the ground effect. Nevertheless, it conforms to the overall change trend.

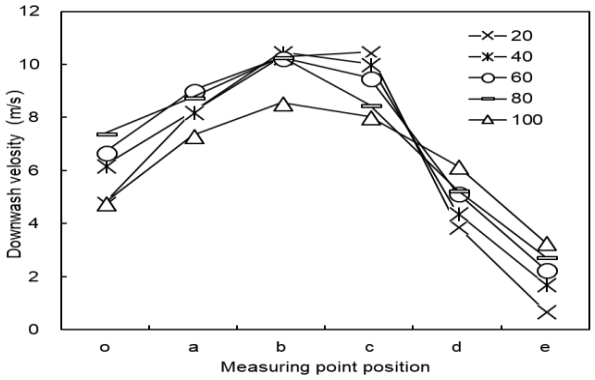

Fig. 6- Changes with the radial of downwash velocity

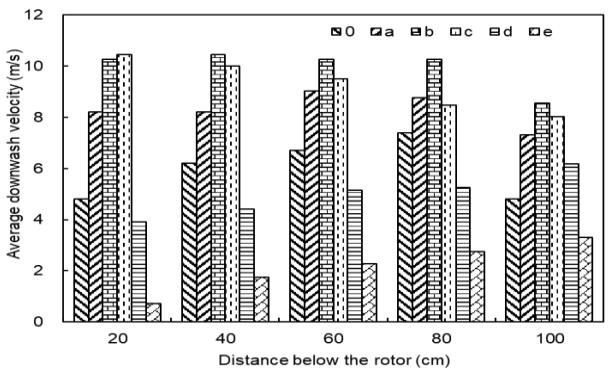

Fig. 7 - Changes with the height of downwash velocity

Fig. 7 presents the fact that downwash velocity varies with the height; it can be seen from the figure that the value of the downwash velocity generated at the centre of the rotor and the wing tip in the height range of 20-80 cm below the rotor increases with the height. The value of the downwash velocity generated at the rotor radius of 12 cm basically remains unchanged. The value of the downwash velocity generated at a rotor radius of 18 cm reduces with the height. Nevertheless, the variation of downwash velocity at 100 cm below the rotor is different from that of other positions since the position is closer to the ground and can be affected by the ground effect of the downwash airflow.

As it is shown in fig. 7, the average downwash velocity at the position of 'o' shows a trend of increasing first and decreasing later with the increasing height. This indicates that the downwash velocity generated by the inner rotor section is first compressed by the outer downwash airflow, leading to an increase in both airflow density and downwash velocity. Afterwards, due to the divergent lateral airflow, the density decreases, resulting in a decrease in downwash velocity. The average downwash velocity values at the positions of 'b' and 'c' decrease gradually with the increase of height, indicating that the downwash airflow generated in the middle of the rotor first compresses inward and then diverges outwards, resulting in a decrease in the vertical airflow density at the position and leading to a decrease in downwash velocity. The downwash velocity generated at the positions of 'd' and 'e' increases with height, which suggests that the airflow generated by the rotor outer segment can be affected by the diffusion from the inside airflow, which strengthens the airflow density at this position as well as increases the downwash velocity. It can be inferred that the overall trend of the airflow field below the rotor is the convergence in the middle and the end diffusion, as presented in fig. 8.

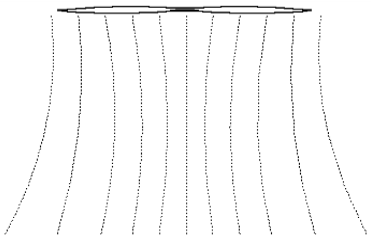

Fig. 8 - Trend of airflow field below the rotor

Horizontal and Vertical Distribution of the Downwash Velocity

To investigate the distribution of downwash velocity in horizontal and vertical sections under the rotor, the central position of the rotor is utilized as the origin of coordinates to establish the plane coordinate system of downwash distribution at each height plane and the spatial coordinate system of downwash velocity distribution below the rotor. Besides, the corresponding coordinates of the measurement point and the space coordinates are calibrated. The distribution of the calibrated measurement points in the coordinates is presented in fig. 9. Fig. 9(a) shows the distribution of 41 measuring points in the plane coordinate system. Fig. 9(b) indicates the distribution of a total of 205 measuring points in spatial coordinate system. According to the data of the known measurement points, the downwash velocity distribution cloud diagram of the lower scrub flow at each height level can be plotted by interpolation with the usage of the Matlab software, as presented in fig. 10. It can be seen from fig. 10 that the downwash velocity generated by the lower scrubbing is higher than the one produced by other positions in the middle section of the rotor (10-20 cm). With the increase of altitude, the boundary of downwash velocity generated at each location is gradually blurred and the distribution of downwash velocity at the section becomes more uniformed.

All the collection points in the space can form vertical downwash velocity distribution planes in four directions of N1N5, N2N6, N3N7 and N4N8 according to fig.3. The interpolation method is utilized to complement the downwash velocity outside the measurement plane in the measurement plane, and the downwash velocity distribution cloud diagram is plotted with the usage of the Matlab software, as shown in fig.11. According to the vertical cross-section downwash velocity distribution cloud diagram of the downwash airflow field as shown in fig.11, the downwash airflow presents a diffusion trend from top to bottom, being consistent with the predicted trend in fig. 8.

The downwash airflow generated in the middle of the rotor has the largest downwash velocity below the rotor. At the near-ground end, the downwash velocity weakens due to the influence of the airflow field ground effect. According to fig. 11, the overall trend of the airflow fields distribution within the cross section of each value is the same, which also corresponds to the results of the standard deviation analysis of fig.5.

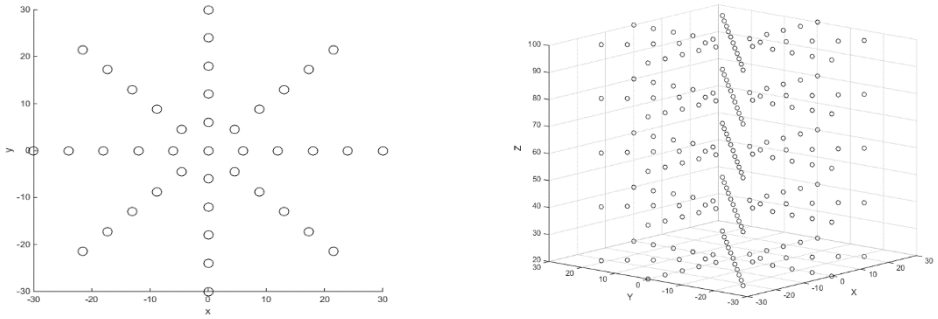

(a) Measurement point of plane calibration (b) Measurement point of space calibration

Fig. 9 - Coordinate calibration of measuring points

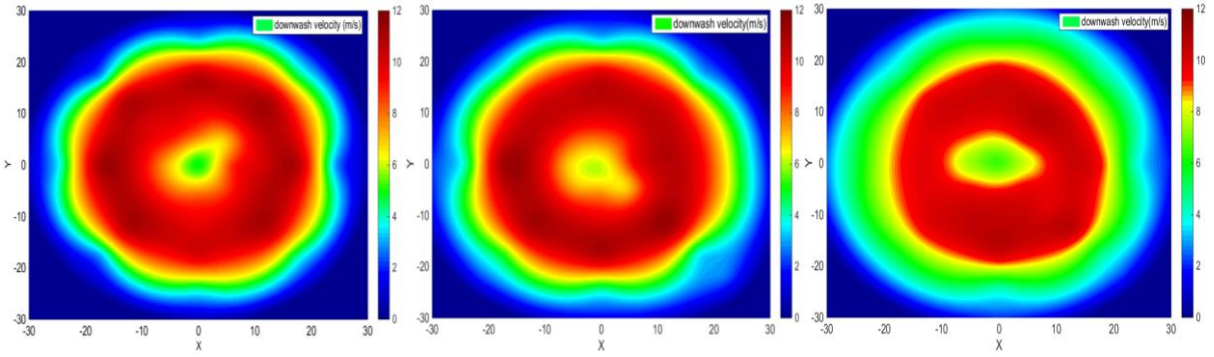

(a) 20 cm below the rotor (b) 40 cm below the rotor (c) 60 cm below the rotor

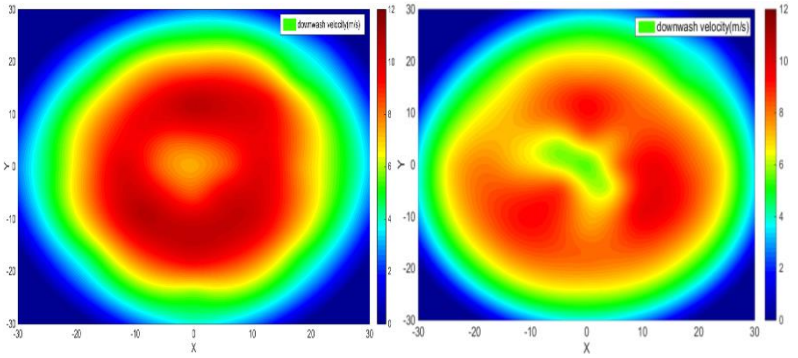

(d) 80 cm below the rotor (e) 100 cm below the rotor

Fig. 10 - The downwash velocity cloud of the horizontal cross-section

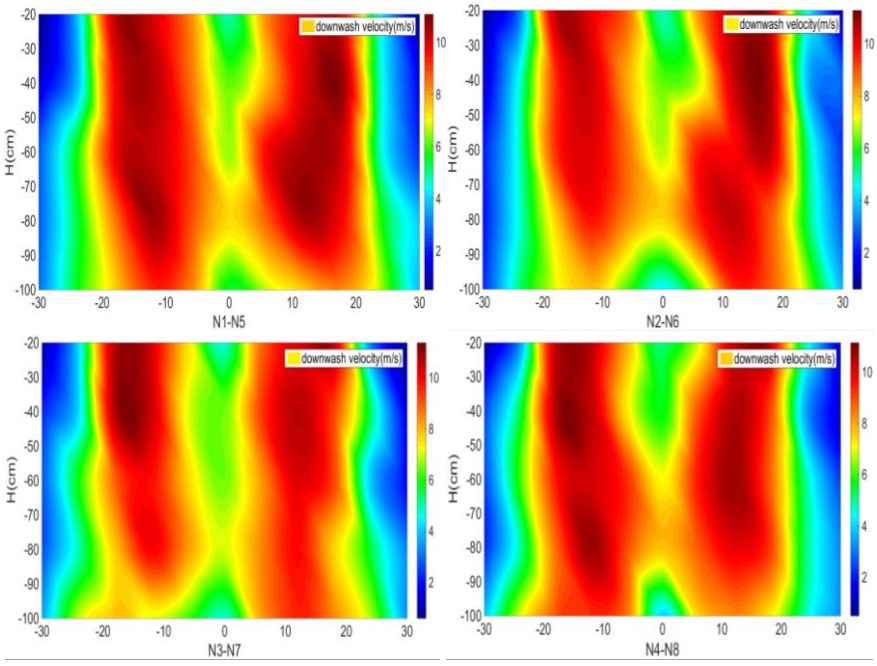

Fig. 11 - Distribution of downwash velocities in different vertical planes under the rotor

CONCLUSIONS

To investigate the downwash velocity distribution of the downwash airflow generated by propellers of multirotor plant protection drone in the rotor diameter, this study designed a test bed for measuring the downwash velocity distribution of the rotor downwash airflow of the plant protection drone and adopted the multi-layer annular uniform distribution method. The downwash velocity distribution in the space below the rotor was measured and the results were analysed. Finally, the following conclusions were obtained:

(1) According to the standard deviation analysis of the airflow field data, at any height level below the rotor, the magnitude of the downwash velocity generated at the same radial position of the rotor has slight differences at each position on the rotation circle. The total standard deviation of data at each point of the wake increases with height but is less than 1 m/s in the range of 1 m below the rotor.

(2) From the centre to the tip of the rotor wing, the downwash velocity generated by each position is different. With the increase in radial distance, the downwash velocity increases first and decreases later. The maximum downwash velocity of 10.8 m/s can be measured on the 80 cm plane below the rotor.

(3) As the height increases below the rotor, the airflow gradually spreads to the surroundings and the area covered by the downwash gradually increases. Nevertheless, the magnitude of the downwash velocity in the high-speed region does not considerably change with the height. In this experiment, the effect of ground on the downwash velocity can be found at the height of 10 cm near the ground.

The results in this study can provide references for the arrangement of nozzles in the airflow field below the rotor and establish a foundation for the spatial motion trend analysis of the droplets in the rotor-downwash airflow field. Nonetheless, establishing an airflow field distribution model along the radial direction of the rotor and the height variation with the change of the rotor's own structural parameters is also necessary to clearly understand the changing law of the airflow under the rotor.

ACKNOWLEDGEMENTS

The work was financially supported by National Key Technology Research and Development Program of the Ministry of Science and Technology of China (2014BAD06B01).

REFERENCES

[1] Bo W., Qi-jun Z., Guo-hua X., (2008), Numerical Simulation for the flow field of helicopter rotor/fuselage based upon Momentum-Source Method. *Helicopter technique*, Vol. 3, Issue. 06, Aviation Industry Corporation of China, Jingdezhen/China;

[2] Caradonna F.X., Isom M. P., (1972), Subsonic and Transonic Potential Glow over Helicopter Rotor Blades. *AIAA Journal*, Vol. 10, Issue. 12, American Institute of Aeronautics and Astronautics, Reston/U.S.A., pp. 1606-1612;

[3] Faical B.S., Freitas H., Gomes P.H., Mano L.Y., Pessin G., de Carvalho A.C., Ueyama J., (2017), An adaptive approach for UAV-based pesticide spraying in dynamic environments. *Computers and Electronics in Agriculture*, Vol. 138, Elsevier, New York/U.S.A., pp. 210-223;

[4] Fengbo Y., Xinyu X., Ling Z., Zhu S., (2017), Numerical simulation and experimental verification on downwash air flow of six-rotor agricultural unmanned aerial vehicle in hover. *International Journal of Agricultural and Biological Engineering*, Vol. 10, Issue. 4, Editorial Office of IJABE, Beijing/China, pp. 41-53;

[5] Fritz B.K, Kirk I.W., Hoffmann W.C., Martin D. E., Hofman V.L., Hollingsworth C., Halley S., (2006). Aerial application methods for increasing spray deposition on wheat heads. *Applied Engineering in Agriculture*, Vol. 22, Issue. 3, American Society of Agricultural and Biological Engineers, St Joseph/U.S.A., pp. 357-364;

[6] Kirk I. W., Hoffmann W.C., (2002), Operational Factors Influence Spray Drift and Deposition from Helicopters. *ASAE Paper*, No. 02-AA06. American Society of Agricultural and Biological Engineers, St. Joseph/U.S.A.;

[7] Lu., (2017), Application of BDS based on RTK in Agricultural Plant Protection Unmanned Helicopter. *Proceedings of the 8th China Satellite Navigation Academic Conference - S01 Satellite Navigation Application Technology*. Academic Communication Centre of China Satellite Navigation System Management Office. Shanghai/China;

[8] Quackenbush T.R., Lam C. M. G, Bliss D. B., (1994), Vortex methods for the computational analysis of rotor/body interaction. *Journal of the American Helicopter Society*, Vol. 39, Issue. 4, American Helicopter Society, Alexandria/U.S.A., pp. 14-24;

[9] Rajagopalan R. G., Mathur S. R. (1993), Three-dimensional analysis of a rotor in forward flight. *Journal of the American Helicopter Society,* Vol. 38, Issue. 3, American Helicopter Society, Alexandria/U.S.A., pp. 14-25;

[10] Reed W. H. (1953), An analytical study of the effect of airplane wake on the lateral dispersion of aerial sprays. National Aeronautics and Space Administration, Washington DC/U.S.A.;

[11] Ren L. F., Zhang J. Z., Shan Y., (2015), Effect of helicopter rotor downwash air flow on exhaust plume flow. *Journal of Aerospace Power*, Vol. 29, Issue. 1, Chinese Society of Aeronautics and Astronautics, Beijing/China, pp. 51–58;

[12] Sun P., Geng X., Zhao X., Zhong J.J., (2015), Influence of wind directions on the flow field structures of helicopter rotor and deck. *Journal of Aerospace Power*, Vol. 30, Issue 08, Chinese Society of Aeronautics and Astronautics, Beijing/China, pp. 1802-1810;

[13] Tang Qing, Zhang Ruirui, Chen Liping, Xu Min, Yi Tongchuan, Zhang Bin, (2017), Droplets movement and deposition of an eight-rotor agricultural UAV in downwash flow field. *International Journal of Agricultural and Biological Engineering*. Vol. 10, Issue. 3, Editorial Office of IJABE, Beijing/China, pp. 47-56;

[14] Veroustraete F., (2015), The rise of the drones in agriculture. *EC agriculture*, E-Cronicon Journals, London /United Kingdom pp. 325–327;

[15] Wang C., He X., Wang X., Wang Z., Wang S., Li L., Mei S., (2016), Distribution characteristics of pesticide application droplets deposition of unmanned aerial vehicle based on testing method of deposition quality balance. *Transactions of the Chinese Society of Agricultural Engineering*, Vol. 32, Issue. 24, Chinese Society of Agricultural Engineering, Beijing/China, pp. 89-97;

[16] Wang Yu, Chen Haitao, Li Haichuan, (2018), A three-dimensional path planning method for plant protection UAV based on gravitational search algorithm. *Transactions of the Chinese Society of Agricultural Machinery*, Vol. 49, Issue. 02, Chinese Society for Agricultural Machinery, Beijing/China, pp. 28-33;

[17] Xinyu X., Kang T., Weicai Q., Yubin L., Huihui Z., (2014). Drift and deposition of ultra-low altitude and low volume application in paddy field. *International Journal of Agricultural and Biological Engineering*, Vol. 7, Issue. 4, Editorial Office of IJABE, Beijing/China, pp. 23-28.

[18] Xiongkui H., Bonds J., Herbst A., Langenakens J., (2017), Recent development of unmanned aerial vehicle for plant protection in East Asia. *International Journal of Agricultural and Biological Engineering*, Vol. 10, Issue. 3, Editorial Office of IJABE, Beijing/China, pp. 18-30;

[19] Xu Bo, Chen Liping, Tan Hao, Xu Wei, (2015), Study on Minimum Energy Consumption Track Planning Algorithm for Multi-platform Operation Plant Protection UAV. *Transactions of the Chinese Society of Agricultural Machinery*, Vol. 46, Issue 11, Chinese Society for Agricultural Machinery, Beijing/China, pp. 36-42;

[20] Yang Zhilun, Ge Luzhen, Zhai Lijun, Cheng Yifan, Wu Yalei, (2018), Study on the Effect of Rotor Washing Airflow on the Spray Rate of Plant Protection UAV[J]. *Transactions of the Chinese Society for Agricultural Machinery*, Vol. 49, Issue 01, Chinese Society for Agricultural Machinery, Beijing/China, pp. 116-122;

[21] Yousheng Y., Jianping Z., Songlin N., (2013), Energy loss of nozzles in water jet system. *Journal of Mechanical Engineering*, Vol. 49, Issue 02, Chinese Mechanical Engineering Society, Beijing/China, pp. 139-145.

DROUGHT MONITORING AND FORECASTING METHOD BASED ON GOOGLE CLOUD COMPUTING SERVICE PLATFORM

/

基于GOOGLE 云计算服务平台的旱情监测预测方法

Kai Zhao[*1),2)], Jingwei Chang[1)], Xinming Ma[2)], Feng Zhao[3)]

[1)]Information Engineering College, North China University of Water Resources and Electric Power, Zhengzhou/China;
[2)] Henan Agricultural University, Zhengzhou/China; [3)]Department of Aerospace Sciences School of Engineering, Cranfield University, Bedfordshire/U.K.
Tel: +8615038365238; E-mail: zhaozhangk@126.com

Keywords: *Drought Monitoring; Cloud Computing; Google App Engine; Back-propagation Neural Network*

ABSTRACT

As a progressively accumulating and dynamically changing process, agricultural drought stress is influenced by various factors, such as atmospheric environment, hydrogeology and vegetation. To master the change laws of soil drought, we proposed a novel soil drought monitoring forecasting method based on Google cloud computing service platform. The Google cloud computing platform Google App Engine was analysed. This computing platform was utilized for drought monitoring. A three-layer back-propagation neural network was used for the forecasting analysis of corresponding soil drought. The accuracy of the method was verified through an experiment. Results demonstrate that all the relative errors of the method were lower than 10% and thus it has a high monitoring precision. These findings can be used as a theoretical basis for formulating strategies for drought resistance. The proposed method provides a good prospect to drought monitoring and forecasting strategies using other cloud computing platforms.

摘要

农业干旱影响是渐进累积、动态变化的过程，它是受大气环境、水文地质、植被等诸多因的素影响，为了了解掌握土壤旱情的变化规律，本文提出了一种基于 Google 云计算服务平台的土壤旱情监测预测方法。首先，对Google 云计算平台Google App Engine 进行了分析。然后，利用Google 云计算平台对旱情进行监测并利用三层 BP 神经网络对相应土壤旱情进行了预测分析，通过实验验证了该方法的正确性。研究结果表明该方法对土壤旱情预测的相对误差均小于 10%，监测精度较高。该研究成果可作为制定抗旱策略的理论依据，对基于其它云计算服务平台的旱情监测与预测的研究提供了一定参考。

INTRODUCTION

With the development of computer technology especially rapid development of the Internet and Geographic Information System (GIS) technology, agricultural information monitoring technology has enjoyed rapid development. As the giant of Internet search, Google has promoted its own cloud computing platforms, the Google App Engine (GAE), which enable developers to run applications on the basis of the Google framework and extend them according to traffic and data storage *(Sadiku M.N.O. et al, 2014; Correa J.D.Y. et al, 2014)*. WebGIS is an important technology realizing mutual operation with GIS and uses the product of GIS and World Wide Web technology. A GIS cloud provides spatial data access and exchange, spatial information inquiry, spatial information analysis, and spatial information application interface services through the Internet in the form of Web service. Drought disaster is one of the natural disasters with high occurrence frequency, broad scope of influence and considerable loss. As an important path of relieving loss and influence caused by agricultural disaster, agricultural drought monitoring and forecasting is one of the weak links of drought study. At present, a series of productive research work has been conducted in various countries (*Sheffield J et al, 2014; Magno R et al, 2014; Yue P et al, 2013*). America founded the National Centre of Drought Reduction and established several drought monitoring and research institutes in local regions in America and within a global scope. Similarly, China established drought monitoring institutes, such as the Meteorological Satellite Centre of State Meteorological Administration, Hydrological Bureau of Ministry of Water Resources, and National Disaster Reduction Centre of China for drought monitoring and forecasting (*Yin Y.P., 2004*). However, agricultural drought involves

numerous fields, such as agriculture, meteorology, hydrology and plant physiology. Meanwhile, agricultural systems are interweaved natural and artificial systems; Therefore, developing agricultural drought monitoring is faced with a large theoretical or technical bottleneck (*Liu X. F et al, 2016*).

Cloud computing applications have recently become a focus of research in the field of the Internet. Google (*Wang D., 2015; Lawton G.,2008; Han W et al, 2012*) was the first to propose the concept of cloud computing. As a cloud computing service promoted by Google Corporation, GAE is a Web application platform integrating development and trust and is the most mature product in the PaaS platform with the most complete functions. Developers can run their compiled online applications on Google resources without worrying about the additional resources used by the running application because Google provides all platform resources needed for application operation and maintenance. "Open for Questions" of the White House in the US has realized processing of approximately million-level traffic within several hours by using GAE. Many foreign libraries have established business services that used GAE to facilitate mutual contact to improve working efficiency and reduce IT cost. For example, Elibrary, which was established by the Western State College of Colorado, can be used by students and teachers as well (*Liu Y.X et al, 2014; Han P et al, 2012*). In May of 2012, China's Ministry of Industry and Information Technology issued "The 12th Five-Year Plan Development Plan in Communications Industry," which positioned cloud computing as a key technology and development orientation for the establishment of a national-level information infrastructure and realization of an integrated innovation. Tsinghua University (*Wang J.J et al, 2010; Liu P, 2017*) is the first university to participate in the Chinese cloud computing plan. It has cooperated with Google to set up a "large-scale data processing" course, which mainly helps researchers learn to create pragmatic Internet-scale application programs under cloud computing environments. Taking GAE as the development platform, Zhenxin Qu and Wenchang Zhu (*Qu Z. X and Zhu W.C., 2013*) effectively solved problems, such as planning task management, multitask trigger, and high concurrency, with the help of multiple cloud services provided by the platform. However, multitask concurrent execution was not realized. Xiaoyu Shi (*Shi X.Y, 2011*) used the infrastructure supplied by GAE to establish and deploy application programs in order to achieve split-type data de-enveloping and storage, mainly implementing applied research on system query speed. Hua Ma (*Ma. H., 2015*) used an Android technology to realize mobile application service at client end based on the cloud service end of GAE. However, he did not study safety in the implementation process of mobile service, namely, evading access of privileged users. Currently, innovative data technologies are used for monitoring soil moisture content, particularly through the use of ZigBee, gathering soil moisture content data into the radio network gateway, and uploading data to Wanwuyun for analysis and processing (http://www.sohu.com/a/208613429610696).

Studies on drought monitoring through GAE are rare. Domestic and foreign drought monitoring research modes remain stand-alone independent operation modes, mainly using computer for data processing, developing databases, and employing various technologies, such as image processing, data analysis, decision-making support, and expert system. Monitoring information related to agricultural condition is of poor openness and transparency; thus, addressing users' diversified and informatization requirements are difficult. For example, America (*Wang Y., 2011; Zhang L et al, 2017*) has built a network system for real-time monitoring, simulation, and evaluation of soil moisture content, soil release, and climatic conditions. Zhang et al. (*Zhang X.F et al,2013)* used the German SIMPEL model to calculate potential evaporation amount, soil water-holding capacity and wilting coefficient in a farmland according to moisture balance principle and forecasted soil moisture content at wheat root in the German Osnabrueck region. However, many input parameters, which were difficult to acquire in reality, were found in the model. Zongzhou Wen (*Wen Zongzhou and Li Ying et al, 2015*) designed a remote metering terminal based on STM32 drought information acquisition and data teletransmission. In this terminal, acquired data were transmitted to junction centre through the GPRS wireless network, the junction centre conducted comprehensive evaluation of the drought through back-propagation (BP) neural network algorithm model, and data processing was implemented on local machine with poor sharing property. Yongxue Huang et al. (*Huang Y. X et al, 2010*) developed a WebGIS-based drought disaster monitoring and analysis system and used GIS technology to conduct fine drought simulation and monitoring through meteorological factors in a station-free region. This system introduced WebGIS technology into drought monitoring and management system, gained access to data in GIS through a browser, and conducted visualization research with low system transmission rate without data processing in a complicated space. Acquiring long-term record of soil moisture content in drought

research is difficult because most data concentrate in a local machine, and this situation considerably restricts information sharing.

Although information acquisition through computer networks has evidently improved and become more time efficient than traditional methods, the workload is still large and mostly single-point test. Therefore, basing on the analysis of the Google cloud platform, we utilized communications network technology, computer technology, sensor technology, GIS technology and data mining technology to establish a drought monitoring and forecasting method. We constructed a forecasting model by designing a three-layer neural network to conduct simulation analysis of soil drought within one year. With the continuous development of technologies, such as IoT, mobile internet, and sensor technologies, addressing the requirement for mass data processing through traditional drought monitoring mode in stand-alone independent operation is difficult. Therefore, a preliminary exploration of drought monitoring and forecasting method based on the Google cloud computing service platform was conducted in this study. Drought information and resources are integrated to improve data processing speed, timely and effectively forecast agricultural drought development, and provide important decision-making basis for relevant departments to formulate drought prevention and resisting measures and organize disaster relief.

The remainder of this study is organized as follows: Section 3 describes the framework of the service platform and establishes a drought monitoring and forecasting model based on Google cloud service platform under GAE framework. Section 4 conducts drought monitoring and networking release through Google cloud service platform and uses a back-propagation (BP) neural network for the forecasting analysis of drought information. The final section summarizes this study and provides relevant conclusions.

MATERIALS AND METHODS

Overall Framework of Drought Monitoring and Forecasting Based on Google Cloud Computing

(1) Design objectives of information management system

On the one hand, complicated changes in soil moisture and climatic environment affect daily life and agricultural production. On the other hand, decision-makers can accurately master drought information by monitoring soil moisture information and determine how to guide agricultural production. Therefore, establishing a drought monitoring information management system is urgent. For a long time, many problems have existed in drought monitoring information systems (soil moisture), such as old monitoring equipment, backward technology, poor real-time property and long monitoring time. The research in this study is implemented on the basis of monitoring equipment selection, data transmission, and software development according to physical truth. A reliable and advanced drought monitoring information management system suitable for local conditions is then designed and developed. This system adopted advanced modern technologies, such as data fusion processing, computer network communication, modern sensor technology and intelligent decision for automatic data acquisition, storage and transmission. Computer is used for the simulation analysis of soil drought information. Data information is calculated on Google cloud platform and released under computer networking condition.

(2) Design principles of information management system

Standardization is the foundation of information system. For the convenience of system extension, upgrading, and optimization, the system design conforms to industry standard and design standardization principle to realize seamless connection to other systems.

According to software engineering theory, system maintenance is the longest process in the entire software life cycle. Therefore, improving system flexibility and extendibility is an important measure of the performance enhancement of the entire system. The development of science and technology and the improvement of management level have results in the changes in the requirements of information management systems. This drought monitoring information system lays a foundation for realizing multi-network integration by designing all kinds of extendible interface, especially interfaces of information system.

This system realizes the comprehensive perception of soil drought through sensor technology, completely develops the effects of already built automatic monitoring stations and future stations, and regards monitoring points as front-end data perception equipment of cloud computing for drought monitoring. An online monitoring system is established for various aspects, such as water resources.

This system conducts the online automatic monitoring and data transmission of rainfall, water level and water quality through wireless transmission to provide a scientific basis for comprehensive decision-making related to soil drought. On the cloud business management platform, alarm information is generated through the analytical computation of automatically monitored data to improve drought monitoring efficiency. The structure of drought monitoring and forecasting based on Google cloud computing is shown in figure 1 and drought monitoring interface is shown in figure 2.

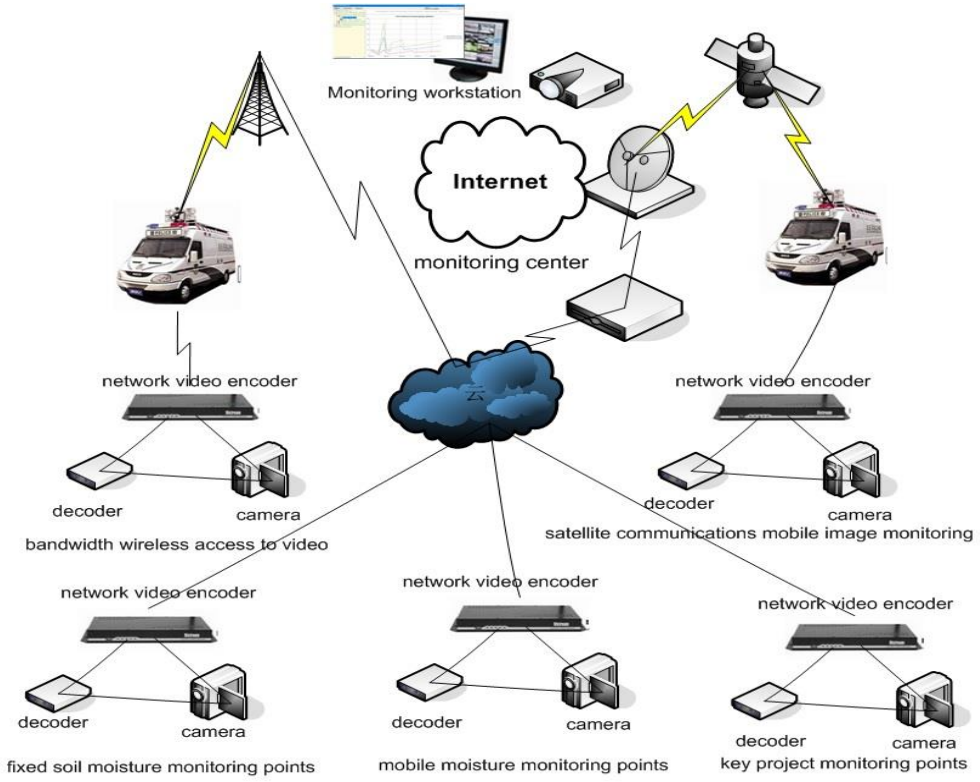

Fig. 1- Illustration of overall monitoring system plan based on Google cloud computing

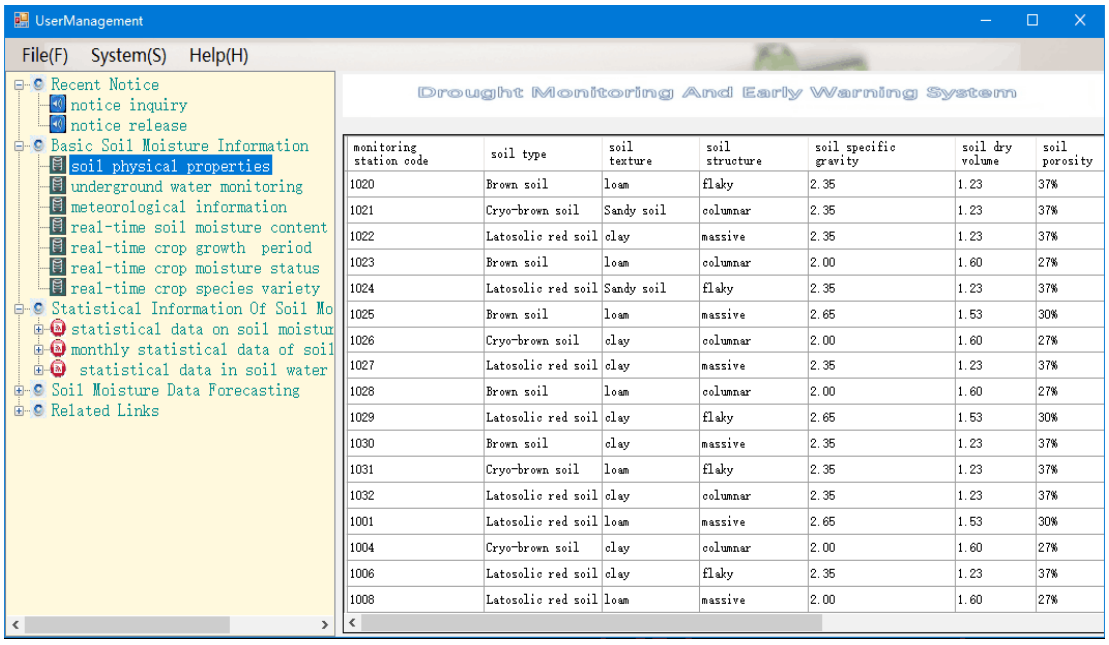

monitoring station code	soil type	soil texture	soil structure	soil specific gravity	soil dry volume	soil porosity
1020	Brown soil	loam	flaky	2.35	1.23	37%
1021	Cryo-brown soil	Sandy soil	columnar	2.35	1.23	37%
1022	Latosolic red soil	clay	massive	2.35	1.23	37%
1023	Brown soil	loam	columnar	2.00	1.60	27%
1024	Latosolic red soil	Sandy soil	flaky	2.35	1.23	37%
1025	Brown soil	loam	massive	2.65	1.53	30%
1026	Cryo-brown soil	clay	columnar	2.00	1.60	27%
1027	Latosolic red soil	clay	massive	2.35	1.23	37%
1028	Brown soil	loam	columnar	2.00	1.60	27%
1029	Latosolic red soil	clay	flaky	2.65	1.53	30%
1030	Brown soil	clay	massive	2.35	1.23	37%
1031	Cryo-brown soil	loam	flaky	2.35	1.23	37%
1032	Latosolic red soil	clay	columnar	2.35	1.23	37%
1001	Latosolic red soil	loam	massive	2.65	1.53	30%
1004	Cryo-brown soil	clay	columnar	2.00	1.60	27%
1006	Latosolic red soil	clay	flaky	2.35	1.23	37%
1008	Latosolic red soil	loam	massive	2.00	1.60	27%

Fig. 2 - Drought monitoring and early warning system

Study of Google Cloud Service Platform Based on GAE Framework

This study is conducted on the basis of the Google cloud computing platform. Cloud application program is developed on a GAE platform. The infrastructure solution of the cloud platform is necessary and GAE includes three main components: runtime environment, data storage and data compression.

(1) Operating environment

To complete an application program in the entire operation procedure, processors handle different requests and do not influence each other while the application program operates in a sealed "sandbox" environment. An application program is prohibited to write data in the file system server during the operating process. A socket cannot open or directly gain access to other hosts and will not be generated into a subprocess or thread and the system is not allowed to deploy other servers. The operating environment is independent from server hardware, operating system and location. This approach ensures the safety and reliability of the operating environment.

After the code and resource file of the application program are loaded, they are stored in the application program memory. This process facilitates direct reading in the memory and improves processor speed.

Although the application program can read its own files through the file system, it cannot write or read other documents from other application programs. The application program can also gain the access to an independent system through API to obtain corresponding service, improve code recycle rate and reduce complexity of developing application programs.

GAE request processing framework is shown in figure 3, where front-end, application and static file servers are all server clusters comprising multiple servers. After the Web sends the request, it passes through the front-end server and is allocated by a load balancer in the optimal form to one of the front-end servers. This server determines the target application program of the request according to domain name of the received request and then confirms the process of the request according to the configuration files of the application program. If a request URL path matches the paths of the static files, such as images of the application program or JavaScript code file, then the request is allocated to a static file server. If the request URL path matches the request processor path of the application program, then the request is allocated to the application program server. If the request URL path cannot be mapped to anything in the application program, then an HTTP 404 (Not Found) error response is returned directly to the client.

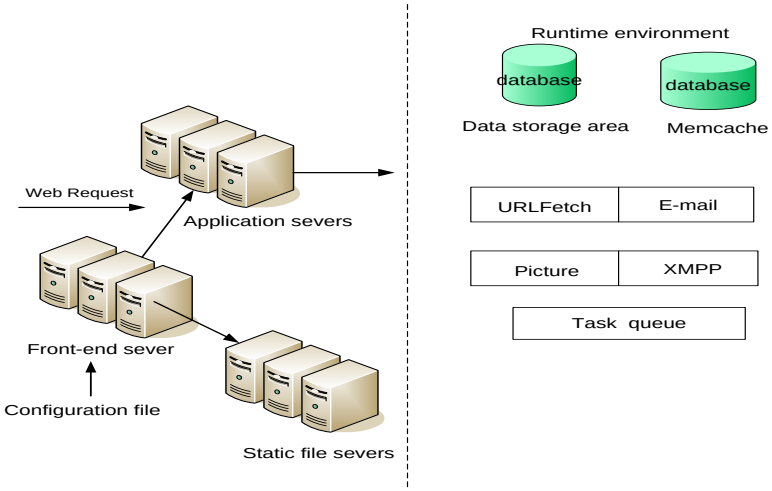

Fig. 3- GAE request processing framework Data storage of GAE

(2) Data storage of GAE

Data storage can save data objects called entities. Each entity has its own key and one or multiple properties. The key of each entity is its unique identification, which can be automatically generated by the application program in data storage area. Properties are used for expressing the properties of data objects, which can be character strings, integers or quotes and one property can have one or multiple different values.

The application program can extract data from data storage in two ways: using key or executing inquiry matches of data properties. Most database systems check records in the database and execute computation for result inquiry through specialized inquiry system. However, the inquiry system of GAE is different. That is, it scans a list of relational databases, also called indexes, and uses these indexes to screen, sort and store results in the query table. Data and indexes are distributed on multiple servers, all of which scan indexes in a parallel way. The GAE does not require the execution of a complicated clustering operation to return the inquiry results of each server to the application program.

(3) Extendible service

GAE provides all kinds of extending services. A standard API and a low-level API application that uses standard API, which can be easily moved in or out of the GAE, are usually established. The application program and GAE server are “separated” and low-level API application program can be directly used in the application program or implemented in a new interface adapter. The GAE service is a kind of application program that uses specific API to gain system access independent of the runtime environment in order to realize common operations, such as data storage, caching and access to network resources.

Data storage service: Data storage service offers reliable and extendible data storage. However, disk addressing is time consuming for high-performance Web application programs. Thus, disk addressing is usually used in caching, and data are kept in a storage unit for high-speed caching. Nevertheless, simple storage and retrieval operation are faster than data storage. Therefore, data storage mode is suitable for frequently read or accessed data.

Caching service: GAE provides a distributed memory cashing service Memcache, which is a keyword storage service that acquires corresponding value through keywords. Multiple values can be set or acquired once through a batch of operations with faster speed than that of the execution of multiple operations. However, total data size cannot exceed one terabyte (TB). The key consists of 250 bytes and the number of its bytes can reach nearly one TB. The Memcache API is allowed to use a large key, which can be converted into 250 bytes with an array algorithm. Data in caching can be saved under general circumstances. If memory cache is insufficient, then the values recently used in caching are cleaned up. Storage time can be set to automatically clean up the value when storage time is exceeded.

Structural Design of Information Management System

According to relevant standard and actual demand, drought information monitoring management system should be able to realize automatic functions, such as drought information statistics, analysis, and inquiry, on a computer platform. Information monitoring management system is designed and established in this study according to actual situations. In this system, a user can rapidly and flexibly view images and changes in monitored drought-stricken regions at client end and browser user interface. The user can also accurately calculate, analyse, and forecast the generation and development of a drought disaster. According to the preceding requirements, system structure is of browser/server (B/S) architecture. The overall framework design is divided into three layers: Web service layer, application layer and data link layer.

The web service layer is the human–machine interface between a user and a software application. Its function is to construct the software application environment of the system. The concrete requirement is application software operation, which includes the parameter inputs and outputs of operation results.

The application layer is the core layer of the system and provides information statistics, analysis and query necessary for all kinds of business analyses, information processing and data management. According to actual requirements for drought monitoring, the system application layer is divided into three functional modules: graphic display, information service and drought forecasting.

The data link layer provides data and data storage functions by using the database on the Google cloud computing platform.

RESULTS

Topsoil moistures at different depths are automatically acquired through the monitoring system, and data are transmitted to the drought information monitoring centre for the observation of drought development in different regions and acquisition of timely and accurate data for drought forecasting.

Change Curves of Soil Moisture Content Within One Year

Changes in soil moisture content in a farmland is caused by the joint effects of multiple complicated factors but can generally be divided into two major types, namely, water consumption and water retention capacity. In this study, a soil drought event in a region in China is used as an example, and soil drought change is explained.

Change of soil moisture content in one year is shown in Fig. 4. Initially, the soil moisture content increases with time, reaching maximum values in July, August and September. Thereafter, the values start to steadily decrease with time. The results show that the change of soil moisture content in one year can be divided into three stages.

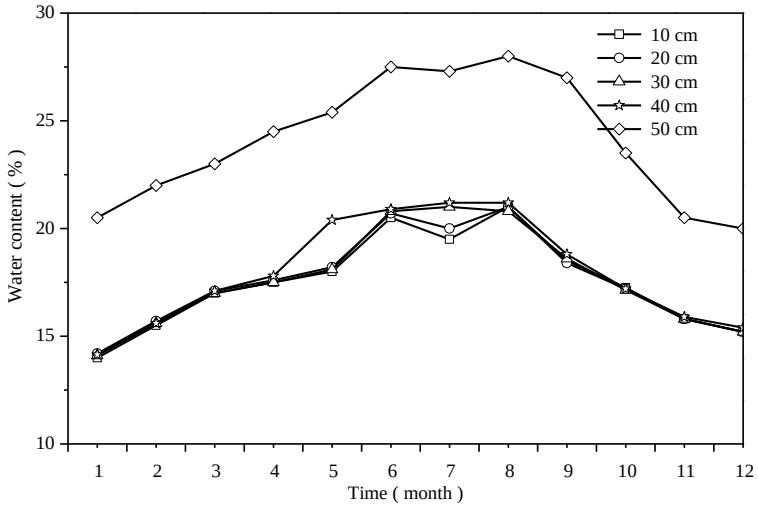

Fig. 4- Change curves of soil moisture content within one year

Large changes in soil moisture content is observed in May and October mainly because of the sufficient rainfall from May to October. As the soil has high moisture content, soil moisture retention capacity rapidly increases. However, given that soil moisture content in this stage is large, water consumption is also large when the temperature rises. Therefore, when water retention capacity is larger than water consumption in this stage, soil moisture content increases; when soil moisture retention capacity is smaller than water consumption, soil moisture content reduces.

Soil moisture content is relatively stable from November to January in the subsequent year. During this stage, air temperature continuously decreases with time while rainfall and evaporation capacity gradually reduce. When the temperature is lower than zero, water turns into ice, the land surface is frozen and soil humidity on the surface is relatively stable.

Soil moisture slowly changes from February to April. During this stage, soil starts thawing as the temperature gradually rises and rainfall slowly permeates the soil, gradually increasing soil moisture content.

Soil Drought Forecasting Model Based on BP Neural Network

The BP neural network algorithm is also called error back-propagation algorithm. Nerve cell transmission conforms to an S-type function and can map the relationship between any nonlinear input and output. BP neural network has been extensively applied to many research fields in recent years. Many researchers have employed this network in soil moisture forecasting and obtained favourable effect. Improved BP neural network is utilized to study data based on drought information management system and its effectiveness is verified through simulation results.

Soil data acquired based on soil moisture sensor data at different soil depths in May of 2017 are selected as study objects. Soil moisture forecasting model of the improved three-layer structure of BP neural network is then established. The moisture contents in daily average layers of 10, 20, 30, 40, and 50 cm selected at the 1st day are used as input variables. Soil moisture contents at 10 and 20 cm forecasted 3 days later are used as output variables. The structure of the BP neural network is shown in Fig. 5. The quantity of nerve cells is calculated according to the empirical formula

$$Z = \sqrt{a + b + c} \tag{1}$$

where Z is the quantity of nerve cells, a is the input of nerve cells, b is the output of nerve cells, and $c \in (1,10)$ is the constant quantity. Number 12 of nerve cells at the hidden layer is optimal through analysis and verification.

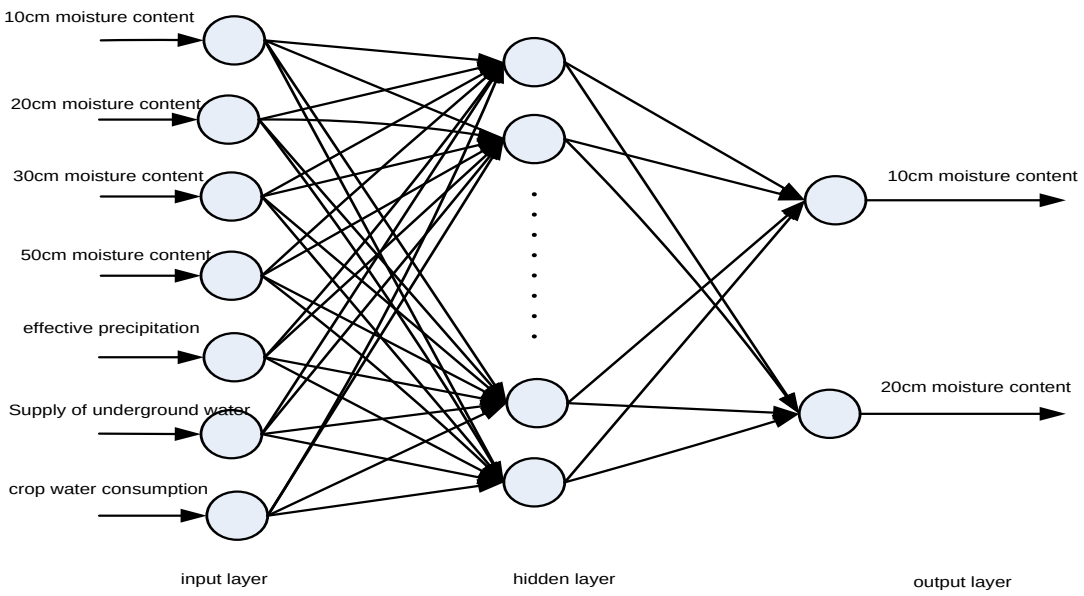

Fig. 5 - Structural model of BP neural network

Soil Moisture Forecasting Based on BP Neural Network

After the weight training of the Google neural network, error definition is shown in Formula (2) to verify the accuracy of the BP neural network.

$$\eta = \left(\frac{predicted}{real}\right) * 100\% \quad (2)$$

where η is relative error, predicted is predicted value, and real is measured value.

Corresponding data are obtained through input training of 15 groups of measured values, which are shown in Tables 1 and 2. Relative errors are obtained through Formula (2).

Corresponding data are obtained through input training of 15 groups of measured values as shown in Tables 1 and 2. Relative errors are obtained through formula (2).

Table 1

Measured and predicted values

Measured and predicted values at 10 cm			Measured and predicted values at 20 cm		
Measured value (%)	Predicted value (%)	Relative error (%)	Measured value (%)	Predicted value (%)	Relative error (%)
17.52	18.06	3.08	17.48	17.65	0.97
17.40	18.83	8.22	17.34	17.01	1.90
17.58	16.67	5.18	17.57	17.94	2.11
17.56	18.53	5.52	17.52	17.29	1.31
17.03	17.81	4.58	16.75	17.03	1.67
16.82	17.64	4.88	16.21	16.88	4.13
16.32	15.76	3.43	15.78	15.04	4.69
18.60	17.32	6.88	18.65	18.84	1.02
18.69	17.76	4.98	18.67	19.87	6.43
18.57	18.02	2.96	18.52	18.84	1.73
17.83	19.65	10.21	17.78	18.80	5.72
17.43	16.32	6.37	17.35	17.79	2.54
17.45	17.24	1.20	17.42	17.84	2.41
17.27	17.96	4.00	17.26	17.35	0.52
17.08	17.68	3.51	17.05	17.26	1.23

Table 1 is transformed into curve forms as shown in Fig. 6(a) and Fig.6(b), respectively, to display errors intuitively.

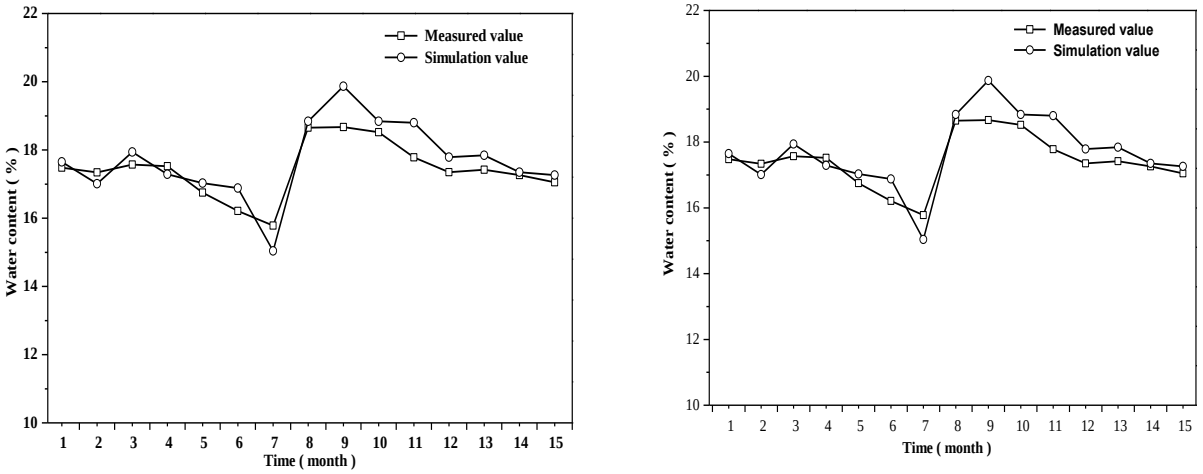

(a) 10 cm (b) 20 cm

Fig. 6 - Curves of measured and predicted values

The simulation result shows that the relative forecasting errors of the improved BP neural network are all smaller than 10%, thereby confirming the feasibility of the BP neural network in soil drought forecasting. This result also indicates that a forecasting analysis study of BP neural network can be implemented by using additional data.

CONCLUSIONS

To improve agricultural drought monitoring and forecasting accuracy, we studied a monitoring and forecasting method for acquiring agricultural drought information on the basis of a Google cloud computing service platform. BP neural network was used for agricultural drought forecasting analysis. The following conclusions were drawn:

(1) Google cloud platform service monitoring components were selected in this study for soil drought monitoring analysis in one region. Data were acquired and integrated under complicated conditions with real-time property, stability, and intelligence.

(2) Drought can be forecasted by using the designed three-layer BP neural network. All the relative errors were smaller than 10%. The simulation verified the effectiveness of BP neural network in soil drought forecasting.

A present hotspot related to agricultural problems was selected. We investigated drought monitoring and forecasting on the basis of the Google cloud computing service platform to provide technical support for the system and deploy other cloud service platforms. Nevertheless, we focused more on the methods for soil drought monitoring and forecasting than on data storage and visualization of agricultural drought data. Therefore, studies considering data storage and agricultural drought data visualization are necessary.

ACKNOWLEDGEMENTS

We would like to thank the support of Henan Department of Education (No.: 15A120011 Drought Monitoring and Forecasting Method Based on Google Cloud Computing Service Platform) in our key research project.

REFERENCES

[1] Correa J.D.Y., Ricaurte J.A.B., (2014), Web Application Development Technologies Using Google Web Toolkit and Google App Engine-Java, *IEEE Latin America Transactions*, vol.12, Issue 2, pp.372-377, IEEE, Piscataway/U.S.A.;

[2] Han P., Shen S., Lu G.F., (2012), Application and Progress of Cloud Computing in Domestic and Foreign Digital Libraries, *Modern Information*, vol.32, Issue 5, pp.67-70, Jilin provincial institute of science and technology information, Changchun/Jilin;

[3] Han W., Yang Z., Di L. et al., (2012), Crop Scape: A Web service-based application for exploring and disseminating US conterminous geospatial cropland data products for decision support, *Computers &*

Electronics in Agriculture, vol. 84, Issue11, Elsevier Sci Ltd, Amsterdam/ Netherlands, pp.111-123;
[4] Huang Y.X, Liu A.G, Yang J. et al., (2010), Design and Application of Hubei Drought Monitoring System based on WebGIS, *Chinese Journal of Agrometeorology*, Vol. 31, Issue 1, pp.112-116, Institute of Agricultural Environment and Sustainable Development in Agriculture, Beijing/China;
[5] Lawton G., (2008), Developing Software Online with Platform-as-a-Service Technology, *IEEE Computer*, vol. 41, Issue 6, pp.13-15, IEEE Computer Society, New York/ U.S.A.;
[6] Liu P., (2017), Development Analysis of Cloud Computing Technology and Discussion about Its Application, *Science and Technology Information*, vol. 15, Issue 9, pp. 21-22, Beijing International Technology Service Centre, Beijing/China;
[7] Liu P., (2017), Introduction to Big Data, *Tsinghua University*, pp. 177-187, Beijing/China;
[8] Liu X.F, Zhu X.F, Pan Y.Z et al., (2016), Research Progress and Expectation of Agricultural Drought Monitoring (English), *Journal of Geographical Sciences*, vol. 26 Issue 6, pp. 750-767, Chinese Academy of Sciences, Beijing/China;
[9] Liu Y.X, Liu S.J, Hu X.W., (2014), Cloud Computing Application Investigation and Analysis of Domestic and Foreign Digital Libraries, *Journal of Library and Information Sciences in Agriculture*, Vol. 26, Issue 12, pp. 90-94, Chinese Academy of Agricultural Sciences, Beijing/China;
[10] Magno R., Angeli L., Chiesi M. et al., (2014), Prototype of a drought monitoring and forecasting system for the Tuscany region, *Advances in Science and Research*, vol. 11, Issue 1, pp. 7-10, Copernicus publications, Leibniz/Germany;
[11] Ma H., (2015), *Applied Study of Mobile Service Implementation Based on GAE Cloud Computing Platform*, MSc dissertation, Ningxia University, Yinchuan/China;
[12] Qu Z.X, Zhu W.C., (2013), Study of Cloud Computing Based Beam Search Monitoring, *Computer Engineering and Scienc*e, vol. 35, Issue 1, pp. 82-87, National University of Defence Technology, Changsha/Hunan;
[13] Sheffield J., Wood E.F., Chaney N. et al., (2014), A drought monitoring and forecasting system for sub-Sahara African water resources and food security, Bulletin of the American Meteorological Society, Vol. 95, Issue 6, pp.861-882, American Meteorological Society, Boston/U.S.A.;
[14] Shi X.Y., (2011), *Study of Google App Engine Based Mobile Information Service*, MSc dissertation, Dalian University of Technology, Dalian /China;
[15] S Sadiku M.N.O., Musa S.M., Momoh O.D., (2014), Cloud computing: opportunities and challenges, *IEEE potentials*, Vol. 33, Issue 1, pp. 34-36, IEEE Press, New York /U.S.A.;
[16] Wang D., (2013), Influences of Cloud Computing on E-Commerce Businesses and Industry, *Journal of Software Engineering & Applications*, vol. 6, Issue 6, pp. 313-318, World Scientific Publication Co. LTD, Singapore / Singapore;
[17] Wang J.J, Lv Z.H, Wu J. et al., (2010), Development Analysis of Cloud Computing Technology and Discussion about Its Application, *Computer Engineering and Design*, vol. 31, Issue 20, pp. 4404-4409, China Aerospace Electromechanical Group 706, Beijing/China;
[18] Wang Y., (2011), *Response of Soil Carbon Nitrogen and Biological Characteristics to Management and Environmen*t., PhD dissertation, Northwest Agriculture & Forestry University, Xian yang/China;
[19] Wen Zongzhou, Li Ying., (2015), Design of soil drought monitoring system, *Application of Electronic Technique*, vol. 41, Issue. 8, Ministry of Information Industry, Sixth Institute of Electronics, Beijing/China, pp. 30-33;
[20] Yin Y.P., (2004), Preliminary Study of Disaster Reduction Strategies of Chinese Geological Disasters, *The Chinese Journal of Geological Hazard and Control*, vol. 15, Issue 2, pp. 1-8, China Geological Environment Monitoring Institute, Beijing/China;
[21] Yue P., Zhou H., Gong J. et al., (2013), Geoprocessing in Cloud Computing platforms–a comparative analysis*, International Journal of Digital Earth*, vol. 6, Issue 4, pp. 404-425, Taylor & Francis, Beijing/China;
[22] Zhang L., Zhang H, Zhang Q. et al., (2017), On the potential application of land surface models for drought monitoring in China. *Theoretical & Applied Climatology*, vol. 128, Issue (3-4), pp. 649-665, Springer Open, Berlin/Germany;
[23] Zhang X.F, Ma Y.H, Rudiger et al., (2013), Forecasting Study of SIMPEL Model Based Soil Moisture Status, *Agricultural Science & Technology*, vol. 14, Issue 3, pp. 490-493, Hunan Academy of Agricultural Sciences, Changsha/Hunan.

THEORETICAL SUBSTANTIATION OF THE SCRAPER INSTALLATION PARAMETERS FOR REMOVING MANURE
/
ТЕОРЕТИЧНЕ ОБҐРУНТУВАННЯ ПАРАМЕТРІВ СКРЕПЕРНОЇ УСТАНОВКИ ДЛЯ ПРИБИРАННЯ ГНОЮ

Prof. Dr. Eng. Sc. Golub G.A.[1)], Ph.D. Eng. Ikalchyk M.I.[2)], Prof., Dr. Eng. Sc. Pilipaka S.F.[1)], Prof., Dr. Agr. Sc. Teslyuk V.V.[1)], Ph.D.Eng. Khmelevskiy V.S.[1)], Eng. Shvets R.L.[1)]
[1)] National University of Life and Environmental Sciences of Ukraine, Kyiv / Ukraine;
[2)] Separated subdivision of the National University of Bioresources and Nature Management of Ukraine "Nizhyn Agrotechnical Institute", Nizhyn / Ukraine
Tel: 097-48-827-89; E-mail: m.ikalchyk@gmail.com

Keywords: *manure, scraper, surface, dump, trajectory, energy intensity*

ABSTRACT

The mathematical model of the interaction of the working surface of the scraper plant scrubber with manure, which determines the trajectory of manure movement on a cylindrical surface with variable radius of curvature under the action of the support forces, is given, and it allows determining the shape of the scrubber surface. The influence of the scrubbers' inclination angle and the scraper movement speed on the power consumption, productivity, specific energy consumption of the advanced scraper plant is investigated. The theoretical calculations of productivity, traction resistance and the choice of electric power of a scraper plant for cleaning manure have been carried out.

РЕЗЮМЕ

Приведено математичну модель взаємодії робочої поверхні скребка скреперної установки з гноєм, яка визначає траєкторію руху гною по циліндричній поверхні зі змінним радіусом кривизни під дією сил підпору і дозволяє визначити форму поверхні скребка. Досліджено вплив кута нахилу скребків та швидкості руху скрепера на споживану потужність, продуктивність, питому енергоємність удосконаленої скреперної установки. Проведено теоретичні розрахунки продуктивності, тягового опору та вибору потужності електродвигуна скреперної установки для прибирання гною.

INTRODUCTION

In the work of scraper plants, there is an inadequate quality of manure removal, which leads to the development of new structures of delta scrapers *(Revenko et al., 2009; Boltianskaia, 2012; Marcussen and Krog Laursen, 2008)*, therefore, the study of the principles of interaction between the scraper plant working bodies and manure, as well as justification of the scraper plant rational parameters are relevant.

Measurements of activity of cows' cardiac function during manure removing with scraper showed that milk cows are experiencing minor stress during manure removal. Cows sometimes perceived negatively manure removal with scrapers during feeding, but they showed an immediate reaction and avoided collisions with scrubbers *(Buck et al., 2013)*. This suggests that manure removal with scrapers, especially considering their simplicity and reliability, is today one of the most effective means of removing manure from livestock houses.

Comparison of manure removal with scraper and manually showed that emissions of ammonia NH_3, methane CH_4 and carbon dioxide CO_2 were significantly lower while removing manure with scraper. This suggests that such systems are more environmentally friendly *(Cai et al., 2015)*.

Modeling of scraper and screw transport systems for manure removal showed that the screw system has no advantages in terms of the rate of manure unloading from the houses *(Landry et al., 2006)*.

Measurement of harmful gas emissions in naturally ventilated rooms for keeping milk cows with different types of floors and manure removing systems showed that scrubbers increase ammonia emissions during manure removal *(Baldini et al., 2016)*.

A model has also been developed to demonstrate that manure acidification is the most effective method for reducing NH_3 emissions, especially when manure removal is combined with its acidification (NH_3 emission reduction efficiency is 44-49%) *(Mendes et al., 2017)*.

There have been also carried out studies showing that manure removed from the houses with scrubber conveyors to the barn storage has higher NH_3 emissions than the manure removed with the help of washing *(Venkata et al., 2011)*. This fact must be taken into account when calculating the standards of the bedding material, as well as its influence on the change of physical and mechanical properties of manure, which is removed from the houses.

It was also established that loss of nitrogen during manure removal was less than half of the losses during the summer *and the frequency of manure removal had little or no effect on nitrogen loss* (Moreira and Satter, 2006).

The efficiency of using the corrugated floor in the manure removal with scrubbers was also proved, which in turn leads to reduction in ammonia emissions *(Dennis et al., 2017)*. This suggests that there is a significant potential for improving the efficiency of manure removal with scrubbers.

It was also established that mechanical scrapers greatly improve the hygiene of keeping cows (evaluated for the cleanliness of the stalls, udder and dugs of cows), especially on the rubberized lattice floor *(Magnusson et al., 2008).*

It is also established that, regardless of the type and purpose, transporting working bodies should be designed in the form of linear surfaces specified by the curvilinear guide *(Tyshchenko, 2010; Tyshchenko, 2012)*. In this case, the law of motion of surface generator is substantiated taking into account the requirements for transportation.

The given data indicate that the substantiation of the parameters of the scraper plant for manure removal from the manure channels of cow barns requires further studying.

MATERIALS AND METHODS

The theoretical trajectory of a particle motion on a sloping plane was studied using the technique of the accompanying Frenet trihedral. The solution of the obtained differential equations is carried out with the help of symbolic mathematics of the software envelope “Mathematica”.

Experimental studies were carried out using a scraper plant (fig. 1) and a frequency converter FR-D700, which changed the speed of the scraper in the range from 0.04 to 0.18 m/sec, kilowatt meter “Lovato elektrik DMK 40” and personal computer HP Pavilion dv6000 with software DMK Remote Control, which fixed the power to move the scraper. The angle of inclination of the scraper scrubbers to the surface of the manure channel was varied from 30 to 90 degrees. The time of each passage of the scraper was fixed by a stopwatch. The quality of manure removal was determined by additional cleaning of the manure channel surface manually and weighing the manure mass on the scales.

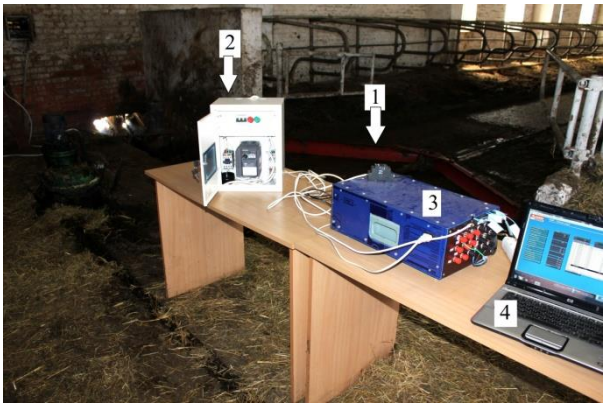

Fig. 1 - Instruments and equipment for scraper plant experimental studying

1 – scraper; 2 – frequency converter FR-D700; 3 – kilowatt meter “Lovato elektrik DMK 40”; 4 – personal computer HP Pavilion dv6000 with a software DMK Remote Control

RESULTS

For efficient operation of scraper plant it is necessary to provide constant pressure of manure, which moves on the working surface of the scraper. To achieve this, the scraper dump should have variable radius

of curvilinear (fig. 2). The working surface of scraper scrubbers in the form of a dump allows the layer of manure to partially accumulate on the surface of the scrubbers and create additional pressure on the scrubber, pushing it to the bottom of the manure channel. Such a design of scraper scrubbers improves the quality of manure removal, and as a result reduces the number of working passages of the scraper.

Manure particles move along the scrubber surface under the action of the support forces with constant speed, so it is necessary to find such a trajectory of the curve as when moving on it, at constant speed, the particles make a constant pressure on the scrubbers working surface.

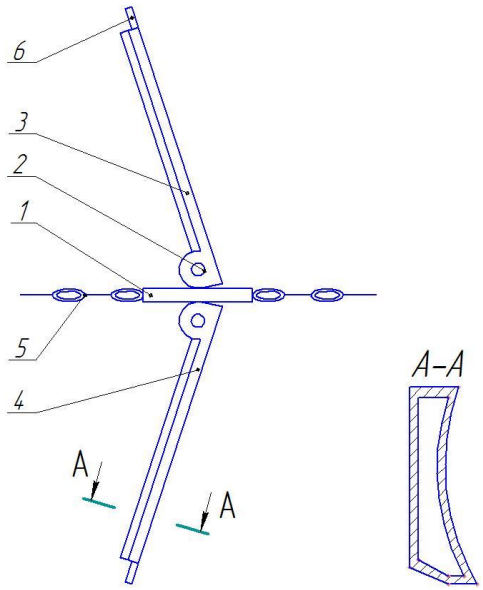

Fig. 2 - Modernized scraper plant for manure removal

1 – ram; 2 – rotary device; 3 – right scrubber; 4 – left scrubber; 5 – chain; 6 – rubber cleanser

Assume that under the action of the support force the manure particle moves upward along the cross-sectional curve of the surface with constant velocity, and also that the velocity of the particle motion along the scrubber is equal to the velocity of the scrubber itself on the manure channel. On the basis of this, a curve (Fig. 3) is constructed, which, at a given speed, will provide a steady surface reaction, and therefore a constant pressure on the entire surface of the scrubber. Such a surface will be less prone to sticking manure and will evenly wear out.

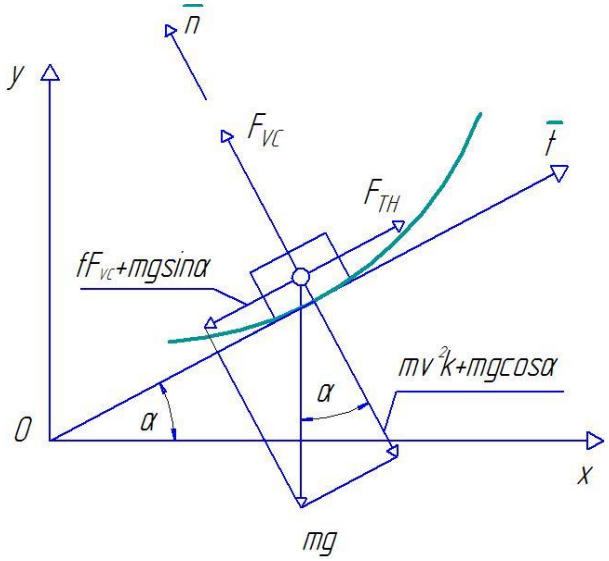

Fig. 3 - Scheme of forces effect on the scrubber

Having designed all the forces acting on the main normal of this curve, we obtain the equation:

$$mg\cos\alpha + mv^2k = F_{VC}, \quad (1)$$

where m – particle mass, [kg];

g – gravitational acceleration $g = 9.81$ [m/sec^2];

α – the angle formed by the unit vector $\bar{t}$ (tangential to the trajectory) with the axis Ox, [grad].

v – speed, [m/sec];

$k = \frac{1}{r}$ – curvature of curve at this point, [m];

r – the radius of curvature, [m];

F_{VC} – stable reaction of the surface, [H].

Divide the left and right sides of the equation (1) by particle weight mg and write the curvature k by the ratio $k = \frac{d\alpha}{ds} = 1 : \frac{ds}{d\alpha} = \frac{1}{s'}$, where s, s' – the length of the arc of the curve and its derivative, we obtain the equation:

$$\cos\alpha + \frac{v^2}{s'g} = \frac{F_{VC}}{mg} \tag{2}$$

Ratio $\frac{F_{VC}}{mg} = a_{VC}$ is a magnitude that shows the fraction of the particle weight in the total force of pressure, when the particles move along the concave side of the surface $a_{VC} > 1$. On the basis of the interconnections of the curve differential characteristics, the transition from equation (2) to parametric equations is carried out:

$$x = \frac{2a_{VC}v^2}{g\sqrt{a_{VC}^2 - 1}} \operatorname{arctg} \sqrt{\frac{\sqrt{a_{VC}^2 + 1}}{\sqrt{a_{VC}^2 - 1}}} \operatorname{tg}\frac{\alpha}{2} - \frac{v^2}{g}\alpha, \qquad y = \frac{v^2}{g}\ln(a_{VC} - \cos\alpha) \tag{3}$$

The cross-sectional curve of the surface, the pressure at which it is larger than particle weight by 1.2 times ($a_{VC} = 1.2$), at a given speed $v = 0.18$ m/sec is shown in Fig. 4. The fragment of the curve AB is taken as a scraper scrubber profile model.

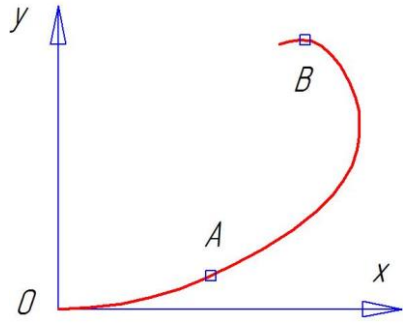

Fig. 4 - The curve providing constant pressure at constant particle velocity

Let's suppose that the lower edge of the scraper is located at a certain angle γ, but not perpendicular to the direction of its displacement. Proceeding from this, when the particle is pushed onto the scrubber (Fig. 5), the direction of its velocity will make an angle γ with the lower surface generator (the straight edge of the scrubber). As the curve of the scrubber cross section we accept a parabola. In projections on a plane xOz, it is written by the equation $z = ax^2$ (a – constant).

At the current point A, the tangent to the parabola with the axis Ox forms an angle ε (Fig. 6). Having switched to a new variable – angle ε, we obtained the parametric equations of the cylindrical surface:

$$X = -\frac{\operatorname{tg}\varepsilon}{2a}; \quad Y = -u; \quad Z = \frac{\operatorname{tg}^2\varepsilon}{4a} \tag{4}$$

In equations (4), the symbol "u" is the length of a straight-line surface generator, the second independent variable. The minus signs provide the required compartment of the surface according to its location on the system $Oxyz$. If two independent variables of the surface ε and u (4) interconnect with each other by certain dependence, then the corresponding line will appear on the surface. We consider it a trajectory of the particle equation that must be found. Between the variables ε and u establish dependence through the third variable – time *t*, i.e. $\varepsilon = \varepsilon(t)$ and $u = u(t)$. Replacing uppercase letters in the equations (4) by lower-case ones, we obtain the equation of the trajectory - the line on the surface with unknown dependencies $\varepsilon = \varepsilon(t)$ and $u = u(t)$, that we need to find.

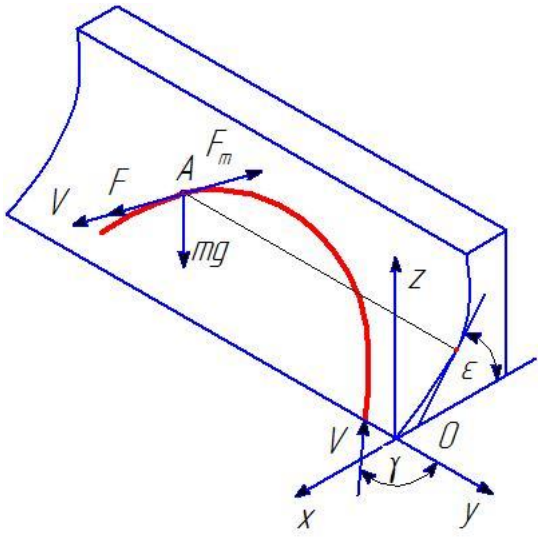

Fig. 5 - The scheme of the effect of forces on a particle at the point and trajectory of its motion on a cylindrical surface

Thanks to the time-differentiation t of the trajectory (4), equations were obtained for determining the acceleration of the particle:

$$x'' = -\frac{\varepsilon'' + 2\varepsilon'^2 \mathrm{tg}\varepsilon}{2a\cos^2\varepsilon}, \qquad y'' = -u'', \qquad z'' = \frac{\varepsilon'' \mathrm{tg}\varepsilon + \varepsilon'^2\left(3\sec^2\varepsilon - 2\right)}{2a\cos^2\varepsilon} \tag{5}$$

where x'', y'', z'' – projections of particle acceleration.

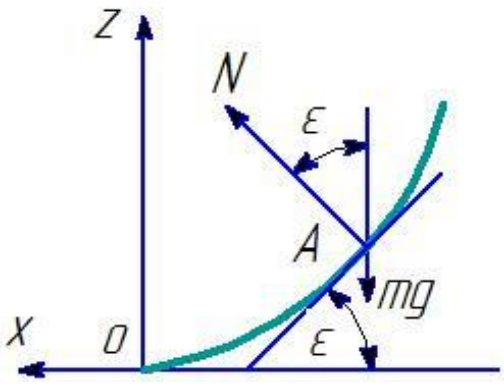

Fig. 6 - The scheme of determining the direction of the normal to the surface at the current point (the axis is projected to the point)

The particle is forced to move along the surface of the scrubber, under the action of the force of the support, F, at a speed v that we will accept equal to the speed of the scrubber movement. The particle is also influenced by other forces, beside force F directed in the direction of speed v; the friction force F_{FR}

directed to the opposite side of the particle velocity v; the force of the surface reaction N, which coincides with the direction of the normal to it, and the weight mg directed vertically downwards.

On the basis of Newton's second law, the differential equations of a particle motion on the scrubber surface were composed and expressions of forces applied to the particle were obtained, i.e., their direction and magnitude, which depend on the point on the trajectory, being functions of the curvilinear coordinates ε and u. In turn, ε and u are connected with each other by the constancy of the particle velocity v. After transforming the system of differential equations, we obtain the following expressions:

$$\varepsilon'' = \frac{\varepsilon'^2 \sin\varepsilon}{2av^2\cos^3\varepsilon}\left(g - 6av^2\cos^2\varepsilon\right) - ag\sin 2\varepsilon\cos^2\varepsilon \tag{6}$$

$$F = m\frac{4g\varepsilon'\sin\varepsilon + Vf\left(4\varepsilon'^2 + 4ag\cos 2\varepsilon + ag\cos 4\varepsilon + 3ag\right)}{8av\cos^3\varepsilon} \tag{7}$$

$$N = m\left(g\cos\varepsilon + \frac{\varepsilon'^2}{2a\cos^3\varepsilon}\right) \tag{8}$$

The differential equation (6) is independent, namely, it can be solved concerning the function $\varepsilon = \varepsilon(t)$. However, it is not possible to do this in an analytical form, therefore, numerous methods have been applied. To construct the trajectory of a manure particle on a scrubber cylindrical surface, it suffices to add the dependence $\varepsilon = \varepsilon(t)$ in equation (4). To the initial conditions of integration refers the angle γ, which is determined by the differential characteristics of the trajectory (Fig. 7).

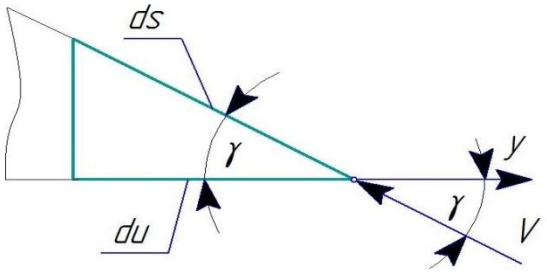

Fig. 7 - To determine the angle γ of particle entering on the surface

Thus, the obtained mathematical model allows us to calculate the optimum working surface of the scraper plant scrubber, in which a layer of manure will press on the scrubber and press it to the bottom of the manure channel, which will improve the quality of manure removal.

The calculation of the scraper plant (fig. 8) is reduced to the definition of the performance, traction resistance and the choice of the electric motor power. Assume that the scrubber is immersed in the manure with maximum effort $(k_{1MAX} = 1)$ at the optimal angle of inclination of the scrubber, and the minimum value (take $k_{1MIN} = 0.75$) at the least effective angle of inclination of scrubbers, namely $90°$ for scraper plant USH-3.

The efficiency of the scraper plant is determined by the formula:

$$Q_{SM} = h_{AV} b \rho v_{SC} k_1 \frac{C_2 + K_{OV} - K_R}{C_2 + K_{OV} + C_{1IV}}, \tag{9}$$

where Q_{SM} – performance of scraper plant, [kg/sec];

h_{AV} – average thickness of manure layer in the manure channel, [m];

b – width of the manure channel, [m]; $b = 3.3$m;

ρ – manure density, [kg/m³]; for the floor manure we accept $\rho = 750$ kg/m³;

v_{SC} – average speed of the scraper movement in one cycle, [m/sec];

k_1 – delivery rate that takes into account the angle of inclination of the scrubber; $k_1 = 0.3...1$ *(Boiko, 2006)*;

C_2 – step between scrapers, [m];

K_{OV} – the distance of the scraper overlaps so that the manure from scraper № 2 (fig. 8) was passed to the scraper № 1, [m]; K_{OV} = 4 m;

K_R – the path needed to open the scrubbers, [m]; K_R = 2 m;

C_{1IV} – total length of motion of the first scraper in reverse, [m].

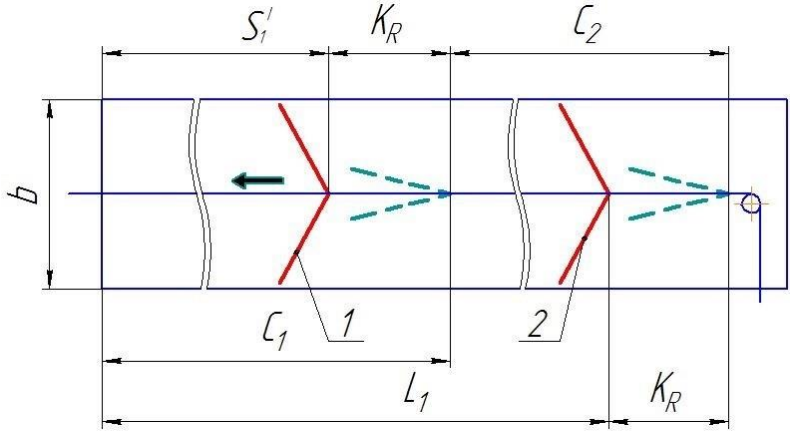

Fig. 8 - Schematic diagram of scraper plant

1 – scraper № 1; 2 – scraper № 2; S_1' *– working length of the motion of the first scraper, m;*

C_1 *– total length of movement of the first scraper,* L_1 *– working length of the manure channel, m*

Fig. 9 shows graph for changing productivity according to equations 9.

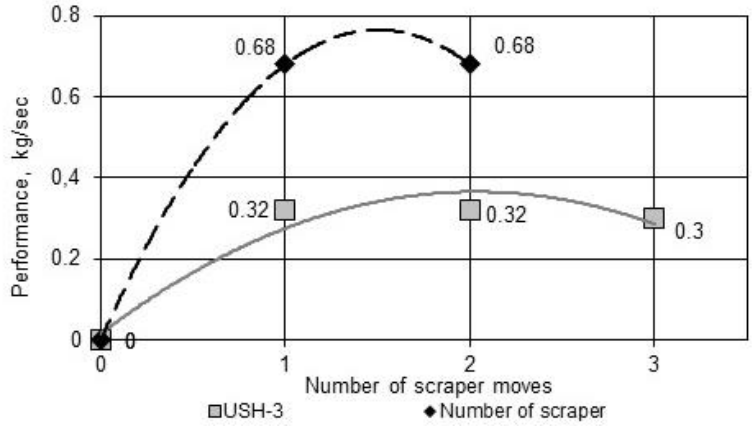

Fig. 9 - Schedule for changing the performance of the scraper plant according to the results of theoretical calculations

The comparison results of the calculated and experimental values of the scraper plant performance showed that the average deviation between them did not exceed 4.4% (Fig. 10).

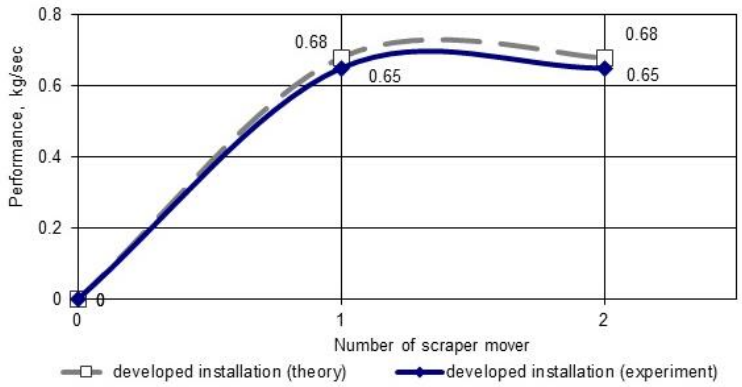

Fig. 10 - Schedule of changes in the productivity of the developed scraper plant according to the comparison of computational and experimental studies

The engine power is determined by the expression:

$$N_{ENG} = kv\frac{(m_1 + m_2) f_{MN} g + \frac{h^2}{2} m_{SCR} l_{AVE} \rho g \xi f_{MN} + Mgf_{ST} + m_{SCR}\rho_{WD}}{1000\eta_{DRI}} \quad (10)$$

Where: N_{ENG} – engine power, [kW];

k – coefficient taking into account the resistance of the tension on the drive sprocket; $k = 1.1$;

v – speed of scraper movement, [m/sec];

m_1 – mass of the manure transported by the first scraper, [kg];

m_2 – mass of the manure transported by the second scraper, [kg];

f_{MN} – coefficient of manure friction along the bottom of the manure channel. For manure friction on concrete at speed 0.085 m/sec, $f_{MN1} = 1.1$, and at speed 0.15 m/sec, $f_{MN2} = 0.9$ *(Tsarenko, 2003);*

h – scraper scrubber height, [m];

m_{SCR} – number of scrubbers, [un.];

l_{AVE} – mean value of the length of traction prism, [m];

ξ – side-thrust coefficient; $\xi = 1.2\ldots1.4$ *(Boiko, 2006)*;

M – mass of moving part of scraper plant (chain, scrapers), [kg];

f_{ST} – coefficient of friction of steel on concrete. At speed 0.085 m/sec $f_{ST1} = 0.8$, and at speed 0.15 m/sec $f_{ST1} = 0.5$ *(Tsarenko, 2003)*;

ρ_{WD} – the effort necessary to overcome the jamming in one scraper, [H]; $\rho_{WD} = 15\ldots30$ H *(Boiko, 2006)*;

η_{DRI} – efficiency factor of transmission and drive $\eta_{DRI} = 0.75\ldots0.85$, for our gearbox $\eta_{DRI} = 0.82$ *(Boiko, 2006)*.

Energy intensity of the full speed of the scraper is:

$$N_{SCR} = \frac{L_{PC}}{vm_{MN}}\left(N_{END.WF} + N_{END.IW}\right) \quad (11)$$

where N_{SCR} – energy intensity of the full speed of the scraper, [kW h./t];

L_{PC} – the length of the manure channel, [m];

v – speed of scraper movement, [m/h];

m_{MN} – mass of the manure removed from the manure channel, [t];

$N_{END.WF}$ – engine power during operating stroke, [kW];

$N_{END.IW}$ – engine power during idle stroke, [kW].

Fig. 11 shows graphs for changing specific energy consumption according to equation 11.

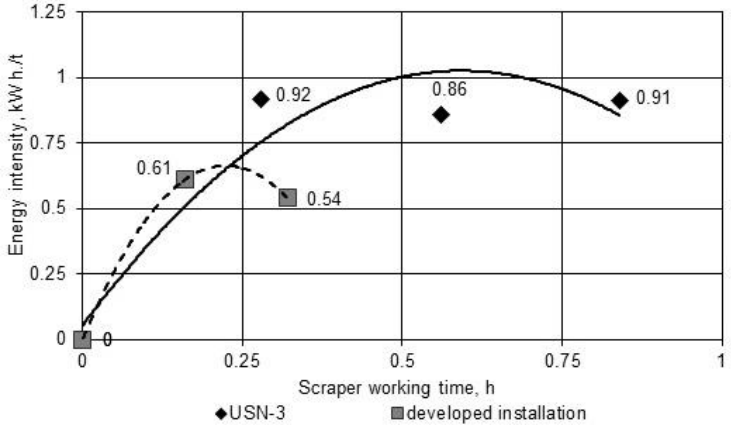

Fig. 11 - Graph of changes in specific energy consumption of a scraper plant based on theoretical calculations (mean values)

Comparison of calculated and experimental values of specific energy consumption showed that the mean value of deviations was 7.4% (Fig. 12).

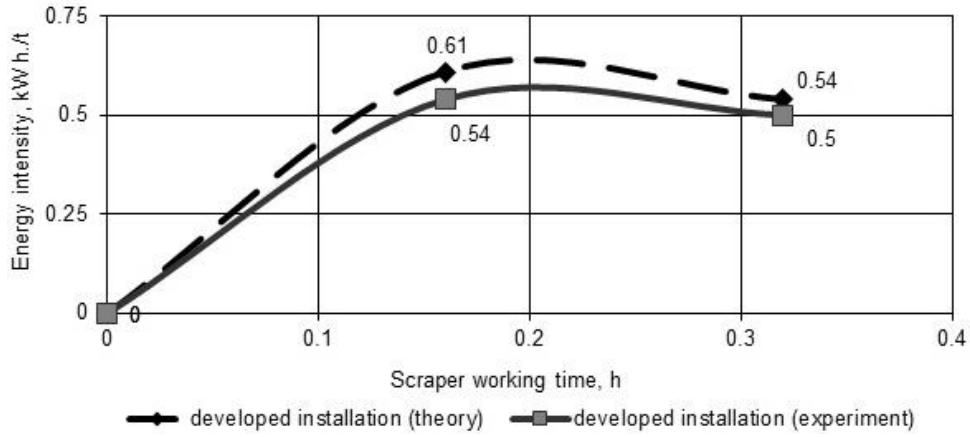

Fig. 12 - Comparison of calculated and experimental values of specific energy consumption for the developed scraper plant

Thus, theoretical and experimental results comparison of the research on productivity and specific energy intensity of the scraper plant indicates the legitimacy of using the obtained analytical expressions in the calculations for scraper plants.

CONCLUSIONS

The conducted researches revealed the possibility of directed adjusting of the energy intensity of the manure removal process by changing the parameters of the scraper plant.

The researches have determined that the performance of the advanced scraper plant when compared to the scraper plant USN-3 increased from 0.3 to 0.68 kg/sec and the specific energy consumption decreased from 0.91 to 0.54 kW h/t.

The results of the calculated and experimental values comparison of the scraper plant performance showed that the average deviation between them did not exceed 4.4%, and the average value of deviations of the calculated and experimental values of specific energy consumption was 7.4%.

REFERENCES

[1] Baldini C., Borgonovo F., Gardoni D. and Guarino M., (2016), Comparison among NH_3 and GHGs emissive patterns from different housing solutions of dairy farms, *Atmospheric Environment,* vol. 141, Supplement C, pp. 60–66, Ed. Elsevier, London/U.K.;

[2] Boltianskaia N., (2012), Ways of the pig industry development and increasing the competitiveness of its products, *Motrol. Commission Of Motorization And Energetics In Agriculture,* vol. 14, 3, pp. 164–175, Lublin-Rzeszow/Poland;

[3] Boiko I. H., (2006), *Livestock Machines and Equipment, Textbook*, Kharkov National Technical University of Agriculture, pp. 84-90, - ISBN 5-7763-0037-1, Kharkiv/Ukraine;

[4] Buck M., Friedli K., Steiner B., Gygax L., Wechsler B. and Steiner A., (2013), Influence of manure scrapers on dairy cows in cubicle housing systems, *Livestock Science*, vol. 158, Issue 1, pp. 129–137, Ed. Elsevier, London/U.K;

[5] Cai L., Yu J., Zhang J. and Qi D., (2015), The effects of slatted floors and manure scraper systems on the concentrations and emission rates of ammonia, methane and carbon dioxide in goat buildings, *Small Ruminant Research,* vol. 132, Supplement C, pp. 103–110, Ed. Elsevier, London/U.K.;

[6] Dennis J. W. Snoek, Johannes D. Stigter, Sam K. Blaauw, Peter W. G. Groot Koerkamp, Nico W. M. Ogink., (2017), Assessing fresh urine puddle physics in commercial dairy cow houses, *Biosystems Engineering,* vol. 159, pp. 133-142, Ed. Elsevier, London/U.K.;

[7] Revenko I. I., Brahinets M. V., Rebenko V. I., (2009), *Livestock Machines and Equipment*, Textbook, Kondor, pp. 486-496, - ISBN 978-966-351-189-4, Kiev/Ukraine;

[8] Landry H., Laguë C. and Roberge M., (2006), Discrete element modeling of machine–manure interactions, *Computers and Electronics in Agriculture,* vol. 52, Issue 1, pp. 90–106, Ed. Elsevier, London/U.K.;

[9] Magnusson M., Herlin A., Ventorp M., (2008), Effect of Alley Floor Cleanliness on Free-Stall and Udder Hygiene, *Journal of Dairy Science*, vol. 91, Issue 10, pp. 3927-3930, Ed. Elsevier, London/U.K.;

[10] Marcussen D., Krog Laursen A., (2008), The basics of dairy cattle production, *Aarhus: Agricultural Agency: Danish Agricultural Advisory Center, National Center,* pp. 175-176, - ISBN 978-87-7470-972-5, Landbrugsforlaget;

[11] Mendes L.B., Pieters J.G., Snoek D., Ogink N.W.M., Brusselman E., Demeyer P., (2017), Reduction of ammonia emissions from dairy cattle cubicle houses via improved management or design-based strategies: A modeling approach, *Science of The Total Environment,* vol. 574, January 1, pp. 520-531, Ed. Elsevier, London/U.K.;

[12] Moreira V., Satter L., (2006), Effect of Scraping Frequency in a Free-stall Barn on Volatile Nitrogen Loss from Dairy Manure1, *Journal of Dairy Science,* vol. 89, Issue 7, pp. 2579-2587, Ed. Elsevier, London/U.K.;

[13] Tsarenko O. M., Voitiuk D. H., Shvaiko V. M., (2003), Mechanical and technological properties of agricultural materials, Textbook, *Meta,* pp. 171-185, - ISBN 966-7947-06-8, Kiev/Ukraine;

[14] Tyshchenko S. S., (2010), Designing of guide curves of surfaces of soil cultivating working bodies with given curvature, *Scientific booklet of National University of Life and Environmental Sciences of Ukraine*, Vol. 144, T. 3, pp. 243-252, Kiev/Ukraine;

[15] Tyshchenko S.S., (2012), Justification of the guiding curves of adaptive surfaces of soil working machinery, *Proceedings of the Tavria State Agrotechnological University, Applied geometry and engineering graphics,* Vol. 4, T. 55, pp. 208-213, Melitopol / Ukraine;

[16] Venkata K. Vaddella, Pius M. Ndegwa, Hung Soo Joo., (2011), Ammonia loss from simulated post-collection storage of scraped and flushed dairy-cattle manure, *Biosystems Engineering,* vol. 110, Issue 3, November, pp. 291-296, Ed. Elsevier, London/U.K.

ANALYTICAL INVESTIGATION OF THE INTERACTION OF THE SUNFLOWER STEM WITH THE LATERAL SURFACE OF THE REAPER LIFTER
/
АНАЛІТИЧНЕ ДОСЛІДЖЕННЯ ВЗАЄМОДІЇ СТЕБЛА СОНЯШНИКУ ІЗ БІЧНОЮ ГРАННЮ ЛІФТЕРА ЖАТКИ

Prof. Ph.D. Eng. Nalobina O.O. [1)], Ph.D. Eng. Gerasymchuk O.P. [2)], Ph.D. Eng. Puts V.S.[2)], Ph.D. Eng. Martyniuk V.L. [2)], Ph.D. Eng. Shovkomyd O.V. [2)], Vasylchuk N.V. [2)], Ph.D. Eng. Bundza O.Z. [1)], Ph.D. Eng. Holotiuk M.V. [1)], Ph.D. Eng. Serilko D.L. [1)]

[1)]National University of Water and Environmental Engineering / Ukraine

[2)]Lutsk National Technical University / Lvivska str., 75, Lutsk, Ukraine;

E-mail: o.z.bundza@nuwm.edu.ua

Keywords: *reaper, sunflower, stem, lift, lifting stem, slip, bend*

ABSTRACT

The design of a reaper that provides grinding of stems, which eliminates the need for mulcher application, offers the conditions for introducing a new technology of growing No-Till crops in agrarian enterprises. The substantiation method of the analytical model is proposed, which allows to determine the nature of the stem movement on the side surface of the sunflower header elevator in the process of their interaction.

РЕЗЮМЕ

Запропоновано конструкцію жатки, яка забезпечує подрібнення стебел, що усуває необхідність застосування мульчера, створює умови для запровадження нової технології вирощування сільськогосподарських культур No-Till в аграрних підприємствах. Запропоновано методику обґрунтування аналітичної моделі, яка дозволяє встановити характер руху стебла по бічній поверхні ліфтера соняшникової жатки в процесі їхньої взаємодії.

INTRODUCTION

One of the profitable crops in the European Union countries *(Martinez-Force E., 2015)* is sunflower. The trend of increasing sown areas for this culture is also observed in Ukraine, where over the past ten years the crop area has grown by 60% *(Statistical bulletin, 2018)*. The rapid growth of sunflower production has led to the need to solve the following problems:

- technological: reduction of losses, which are explained by the peculiarities of the structures of the reaper, passing through the threshing apparatus of baskets with long remains of the stems, which leads to the clogging of the deck, reducing its passage section, and as a result, leads to seed damage *(Kapustyn, S.A., Kunakov V.P., 2004)*.

- ecological: loss of microbial activity of the soil, decrease of fertility and accumulation of pathogens due to the fact that there are left rough stems remaining in the fields that do not have time to rot *(Lyon D., 1998; Pacini C., Wossink A., Giesen G., Huirne R., 2004)*.

- Operating: With the introduction of the new No-Till technology, which is gaining in popularity, the life of the tires and caterpillars of agricultural machines is significantly reduced.

Considering the foregoing development of a reaper's design for sunflower harvesting, the need for solving the above-mentioned problems and the analytical methods of research of its individual working bodies represent an important scientific and practical problem.

The traditional oilseed is sunflower, the cultivation of which is characterized by relatively high profitability, export attractiveness. Sunflower plays an important role in the rotation of cereals and is one of the most common crops in the European Union *(Martinez-Force E., 2015)*. In Ukraine, in 2017, sunflower crop area reached 5779 thousand hectares *(Statistical bulletin, 2018)*.

The final harvesting process *(Anwar M. T., Gupta C. P., 1990; Burianov M. A., 2011; Kapustyn, S.A., Kunakov V.P., 2004; Kepner R.A., 1978; Klenyn N. Y., Sakun V. A., 1980; Maksoud A., El-Sayed M.A.F., Shalaby G.H., 2009)* has a significant impact on the actual yield of sunflower. Indicators that assess the process of harvesting sunflower depend on the technical and constructive parameters of the machines. In

particular, the authors *Kapustyn, S.A., Kunakov V.P., (2004)* established a list of causes of losses during harvesting under the influence of the working bodies of the reaper. In particular, it is established that under the influence of lifters of sunflower reaper there are losses of free grains, which are explained by the impact on the sunflower stem.

It has been established that the effect of the shield causes the seed of the baskets to be pulled out. Losses in cut-out baskets come from the action of lifters and a reel. When driving a combine, the lifters drove the stems, which leads to the loss of uncut baskets. As field studies have shown, this type of loss is most characteristic of sloping plants.

The research of constructions and basic parameters of sunflower header in order to reduce seed losses is presented in some papers *(Kukhmazov K.Z., Fedorov V.V., 2013; Shaforostov V.D., Makarov S.S., Pohorelov V.N., 2015)*.

One of this paper *(Kukhmazov K.Z., Fedorov V.V., 2013)* describes the results of laboratory-field studies of a developed and produced pilot plant for sunflower harvesting, equipped with elastic seed traps. The authors investigate the influence of the angle of inclination of elastic traps and their diameter on the loss of sunflower seeds.

The rational value of the combine working speed is established, provided high productivity and reduction of yield losses are ensured. Advice is given on the rational speed of the combine, which must be within 2 ... 2.5 m/s. It has been established that further increase in speed leads to an increase in sunflower seeds losses.

The results of field trials of the experimental sample of a two-row reaper to the Wintersteiger breeding combine are presented in *(Shaforostov V.D., Makarov S.S., Pohorelov V.N., 2015)*. The description of the proposed construction with the description of the basic parameters is given. This design is recommended for use in multi-leaf forms of plants.

A number of valid studies are devoted to the improvement of structures and the establishment of patterns of interaction between a reaper and sunflower harvesters *(Popov M., 2013; Startsev A. S., 2017)*.

Popov M. (2013) proposed a design-technological scheme of a screw-shaft, which contains a tubular shaft with two-sided winding. Theoretical studies allowed the author to obtain analytical expressions describing the technological process of interaction of sunflower stems and sunflower baskets with a winding and cutter screw-rotor. The influence of constructive and regime parameters on crop losses is established. On the basis of experimental data, the author obtained regression models that reveal the dependence of seed losses on the winding width, the cutter length provided different angles of inclination of the cutter working part to its base.

Experimental dependence of sunflower seeds losses on the acceleration of the sunflower baskets movement was determined by *Startsev A.S. (2017)*, provided that they hit the tube shaft of the rotor. The author obtained equations that reveal the dependence of seed loss on the acceleration of the baskets due to interaction with the reel without winding and with waving. It has been established that the presence of screw-on screw can reduce the speed of the baskets movement, mitigate the impact and reduce losses.

Makarov S.S. (2007) developed a method for determining the optimal parameters for the process of harvesting sunflower with a combine harvester with screw feed. The basis of the methodology is based on the calculation models of the theory of oscillations. In this work, an estimation of the effect of the screw speed and the size of its step on the intensity of the forced oscillations of sunflower during its interaction with the screw is given.

In order to solve the second and third problems outlined in the introduction, the authors *Dalmist I.S. and others (2013)* investigated the possibility of installing additional cutting devices in sunflower harvesters.

These authors *(Dalmist I.S., Kayisoglu B., Bayhan Y., Ulger P., Toruk F. and Durgut F., 2013),* in order to solve the problem of improving the physico-microbiological structure of the soil, proposed to grind the remains of sunflower plants, remaining in the field, and then to mix them with the soil. In this study, a shredding device that is placed under a combine has been developed. The developed crushing device was tested using three different grinding methods, provided that the speed of the knives was 2443 min^{-1}. The author evaluated the fuel consumption of the machine with different types of chopper. According to the results of experimental researches, recommendations were given regarding the design of the crushing device.

The performed analysis of current research has shown that the development of working bodies of reapers for sunflower harvesting, which ensure the reduction of seed loss and the reduction of the height of

the longitudinal stem in the field that remains after the harvesting, is an actual task that has an important scientific and applied value.

The purpose of the work is to establish an analytical link between the parameters of the lifters of the proposed reaper for harvesting sunflower and the nature of the stalk movement.

To achieve the goal, you need to solve the following tasks:

- to carry out an analytical substantiation of the stem movement under the influence of the lateral surface of the header lift;
- to substantiate the mathematical model, which reveals the relationship between the parameters of the elevator and the location of the stem in the field.

MATERIALS AND METHODS

Theoretical studies that reveal the influence of the lateral surface of the lifters of the sunflower harvesters, which are authored and subject to research *(Nalobina O.O., 2017, 2018)* (Fig. 1), on the stems, are based on the theory of agricultural machines, developed by academician M.N. Letoshnev *(Letoshnev M. N., 1934)* and the theoretical foundations of analytic geometry *(Efymov N.V., 1975)*.

Analytical studies were carried out on the assumption that the sunflower stems are located on an equal surface and not bent, that is, they have a vertical initial position.

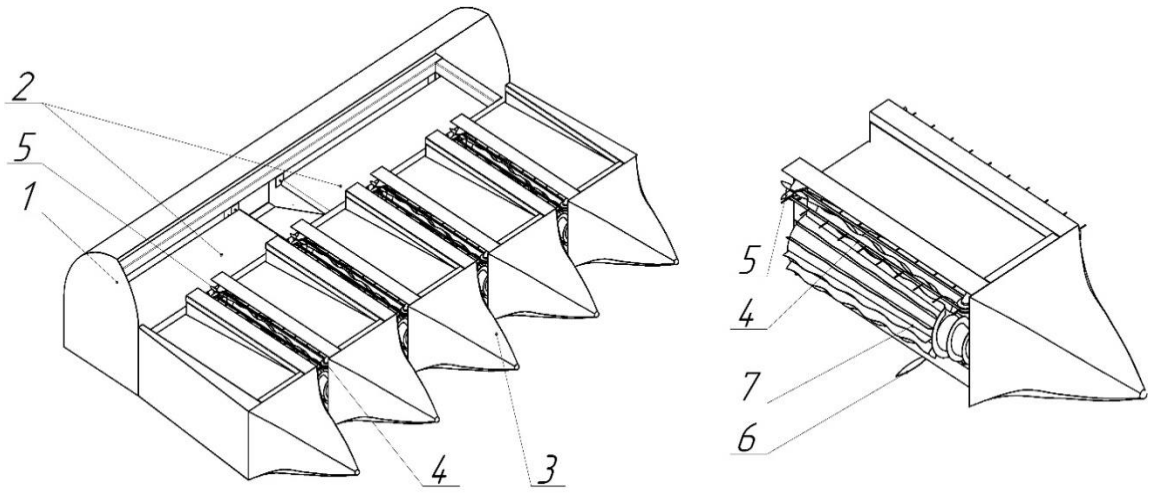

Fig. 1 - Scheme of a reaper

1– frame, 2 – belt conveyors, 3 – lifters, 4 – pass with captures, 5 – knives, 6 –rotating knives, 7 – rotor

The process of harvesting sunflower begins with the effect on the stems of the lateral surface of the reaper lifters. Consider how the interaction of the stems with the elevator is taking place. The regularities of the flow of this process need to be known in order to justify the parameters of the next technological operation - the transfer of stems with passes with grips *4* (Fig.1) in the pylons formed by rotors *7*. Consider the moment of contact of the stem with the elevator.

Assume that the stem contact occurs from the side *(ab)* of the elevator side surface (Fig. 2). The contact point of the stem with the lifter is denoted – C_n. The elevator moves at the speed of a combine with a combine harvester V_z and presses on the stem O_nC_n (Fig. 2). with a lateral surface. The stem, however, deviates in the vertical plane $O_nC_{n1}S_n$ the plane bends and slides along it.

The absolute velocity of the point of contact C_n is denoted V_a, the vector of which has a line of action perpendicular to the stem and lies in the plane of the stem bias $O_0C_1C_{np}$; V_r - vector of the relative speed of the point.

The position of the lateral face of the lifter, which affects the stalk, will be determined by the following parameters: h height of the nose, above the ground plane; γ – the angle between its projection onto the plane $x_0O_0Y_0$ and the axis Ox; α – half of an angle exacerbation of the lifter nose.

Friction force F_m between the stem and the side surface of the elevator has an action line that coincides with the action line of the vector of relative velocity V_r and is directed opposite. Action of vector line of common pressure N of the lateral surface of the lifter on the stem is directed perpendicular to the plane O_nab. Friction F between stem and lateral side of lifter has an action line which coinsides with vector of

action line of relative velocity $\overline{V_r}$ and directed opposite. The action line of this force is deviated from the normal to the angle φ in the direction of the slope of the stem with the side surface of the elevator.

Under the influence of force *F,* the resultant of the forces F_m and *N,* the stem will move. In order to determine the position of the stem, it was necessary to establish the angle dependence θ_1 (Fig.3) on the elevator parameters.

Consider the scheme given in Fig. 3. For further analysis, we introduce the initial coordinate system $x_0O_0y_0z_0$. Axis O_0z_0 passes through the elevator's spout (point a).

The needle moves in such a way that the nose does not touch, in most cases, the stems. This is due to the fact that the stems are located at a distance from the axis x_0O_0. For example, a stem situated at the distance y_c, from the point O_n (Fig.3). This stem, when moving the lifter slides on it. Slide plane marked $a_1O_nb_1$. Axis x_1 is directed parallel to x_0. Axis y_1 coincides with the axis y_0.

Coordinates of any point of the elevator face (a_1b_1) or stems $(x_1y_1z_1)$ in the system of coordinates $(x_1O_ny_1z_1)$ are connected with coordinates $(x_0y_0z_0)$ in the system of coordinates $(x_0O_0y_0z_0)$.

This connection can be represented by the following equations:

$$\left.\begin{aligned} x_1 &= x_0, \\ y_1 &= x_0 - y_{c,}, \\ z_1 &= z_0. \end{aligned}\right\} \quad . \tag{1}$$

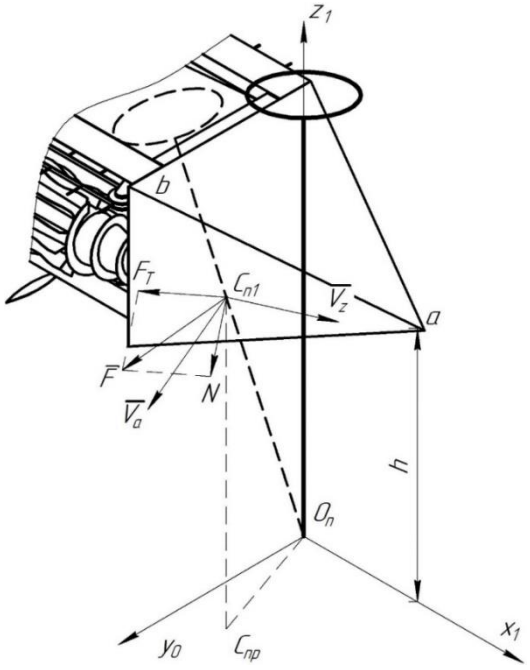

Fig. 2 - Scheme for analysing the interaction of sunflower stem with an lifter

RESULTS

It should be noted that the stem with the base at the point O_n will not interact with the entire lateral surface of the lifter, but only with that part which is located to the left of the point C_{n0} (the starting point of the stem and lifter contact).

In the scheme given in Figure 3, it is seen that distance aC_{n0} determine:

$$aC_{П0} = \frac{y_c}{\sin\alpha} \tag{2}$$

Thus, the stems whose roots are located with the displacement along the *y* axis does not affect the entire side of the lifter, but only that part that directly brings the stems to the next working body. Sliding plane equation $a_1O_nb_1$ will be written:

$$A_{1K}x_1 + B_{1K}y_1 + C_{1K}z_1 = 0 \tag{3}$$

where A_{1K}, B_{1K}, C_{1K} – coefficients of the equation.

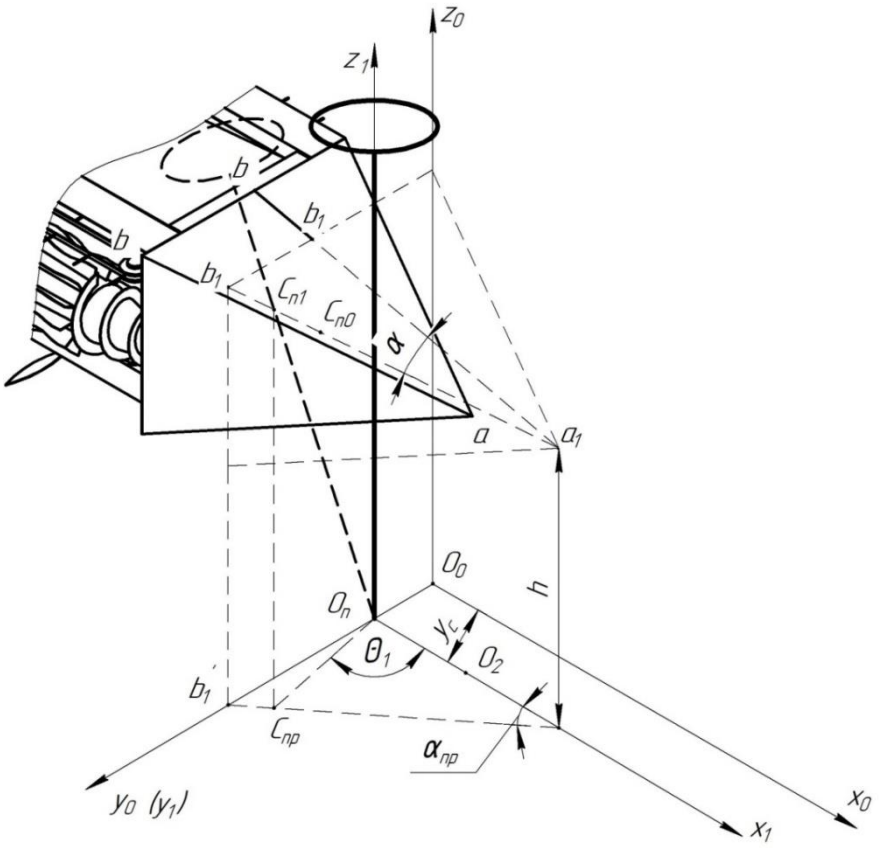

Fig. 3 - A diagram for the analysis of the stem movement

The determination of the coefficient data was carried out considering that:
- for a point C_{n0}:

$$\left.\begin{aligned} x_1 &= x_0, \\ y_1 &= 0, \\ z_1 &= y_c \cdot \sin\gamma \cdot ctg\alpha + h, \end{aligned}\right\} \tag{4}$$

- for a point *b*:

$$\left.\begin{aligned} x_1 &= l - \left(b_1b_1^{'}\right)\cdot\cos\gamma\cdot ctg\alpha, \\ y_1 &= \left(b_1b_1^{'}\right) - y_c, \\ z_1 &= h + \left(b_1b_1^{'} - y_c\right)\cdot\sin\gamma\cdot ctg\alpha, \end{aligned}\right\} \tag{5}$$

where *l* - move point C_0 in the system of coordinates $x_1O_{II}y_1z_1$.

Then the coefficients of equation (3) will look like:

$$\left.\begin{aligned} A_{K1} &= y_c\cdot\sin\gamma\cdot ctg\alpha + h, \\ B_{K1} &= \left(l\frac{\left(b_1b_1^{'}\right) - 2y_c}{\left(b_1b_1^{'}\right) - l}\cdot\sin\gamma + h\cdot\cos\gamma\right)\cdot ctg\alpha + y_c\cdot\sin\gamma\cdot\cos\gamma\cdot ctg^2\alpha, \\ C_{K1} &= -l. \end{aligned}\right\} \tag{6}$$

The displacement *l* depends on the displacement of the spout – *L* (fig. 4). Consider the scheme given in Fig.4, where we see two positions of the side surface of the elevator: *ab* and a_1b_1 – starting, which corresponds to the point of contact C_{n0} of stems and the following position which is characterized by the displacement of the elevator by the value of *l* and the displacement of the point C_{n0} in position C_{n1}.

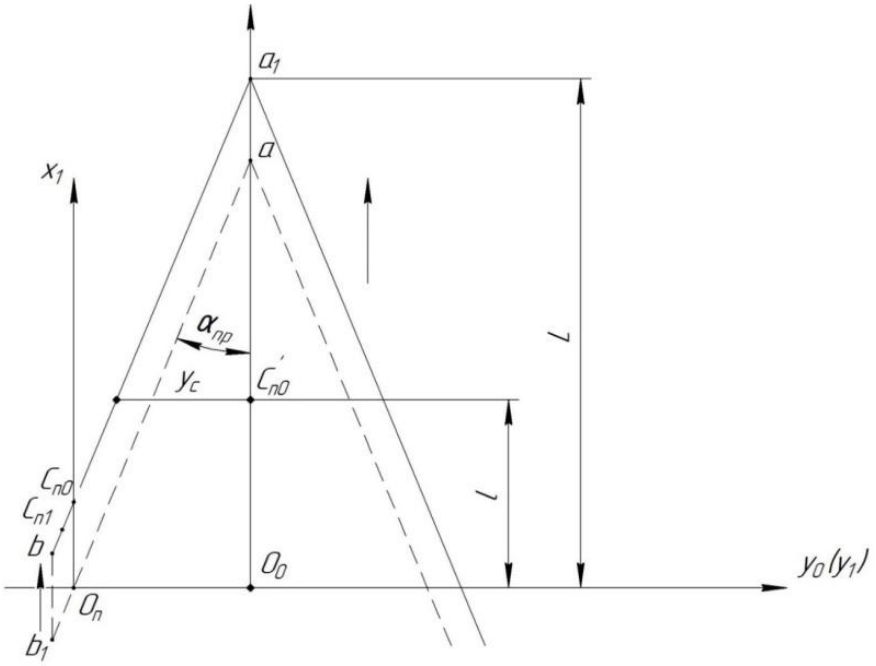

Fig. 4 - Top view of the lifter

In the scheme we see:

$$\left.\begin{aligned} aa_1 &= C_{\Pi O}C'_{\Pi O} = l, \\ L &= l + y_c \cdot ctg\alpha_{np}, \end{aligned}\right\} \tag{7}$$

where α_{np}– projection angle α on the surface $x_0O_0y_0$.

Based on the above we have:

$$l = L - y_c \cdot \cos\gamma \cdot ctg\alpha_{np} \tag{8}$$

As noted earlier, the stem slides along the side of the elevator and bends in the vertical plane. This plane passes for a stem with a root located in point O_n, through the axis O_nz_1 and point of C_n drop. This surface $C_nO_nC_{n0}$ deflected from the plane $y_1O_nz_1$ at some angle, which we will denote θ_1 (fig. 3).

Flat equation plane:

$$A_{1B}x_1 + B_{1B}y_1 = 0\,. \tag{9}$$

Points coordinate $C_{n1}(x_1; y_1)$:

$$x_1 = l - (C_{\Pi 0}C_{\Pi 1}) \cdot \cos\gamma \cdot \cos\alpha,$$
$$y_1 = (C_{\Pi 0}C_{\Pi 1}) \cdot \sin\alpha.$$

Distance $C_{n0}\,C_{n1}$ will be defined: $C_{n0}C_{n1} = (a_1C_{n1}) - \dfrac{y_c}{\sin\alpha}$.

Substituting these coordinates and solving the equation of type $\dfrac{H}{L}x + \dfrac{K}{L}y + z = 0$ *Efymov N.V., 1975)* will define coordinates:

$$\left.\begin{aligned} A_{1B} &= (a_1C_{\Pi 1}) \cdot \sin\alpha - y_c, \\ B_{1B} &= (a_1C_{\Pi 1}) \cdot \cos\gamma \cdot \sin\alpha - y_c \cdot \cos\gamma \cdot ctg\alpha - (L - y_c \cdot \cos\gamma \cdot ctg\alpha) \end{aligned}\right\} \tag{10}$$

Let's record the equation of the slip plane and the plane of the bend in the general case for the k-th stem. To do this, we will introduce the notation: y_{ck} – distance from the point O_0 to the basis k stems along the axis y_k;

- l_i – way of moving the nose of the elevator in the i-th coordinate system
- x_{ck}– distance from the point O_0 to the basis k stems along the axis x_k (for example, point O_2 fig.3).

In view of the above, we obtain the equation of the sliding and bending planes for the k-th stem.

Sliding plane equation:

$$A_{k\kappa}x_k + B_{k\kappa}y_k + C_{k\kappa}z_k = 0 \tag{11}$$

where the coefficients are determined by dependencies:

$$\left.\begin{aligned} A_{k\kappa} &= h + y_{ck}\cdot\sin\gamma\cdot ctg\alpha, \\ B_{k\kappa} &= -\left[\frac{1}{n}(h+t)\cdot(l_k - n\cdot\cos\gamma\cdot ctg\alpha) - l_k(h+m+t)\right], \\ C_{k\kappa} &= -(L - y_{ck}\cdot\cos\gamma\cdot ctg\alpha - x_{ck}). \end{aligned}\right\} \tag{12}$$

where $n = (b_1b_1') - y_{ck}$, $m = (b_1b_1')\cdot\sin\gamma\cdot ctg\alpha$, $t = y_{ck}\cdot\sin\gamma\cdot ctg\alpha$.

Trace l_k we deduct from the moment of touch of the stem with the lateral face of the elevator.

The flatness plane of the bend in the general form will be written down as:

$$A_{kB}x_k + B_{kB} = 0 \tag{13}$$

where coefficients are defined:

$$\left.\begin{aligned} A_{kB} &= (aC_{\Pi k})\cdot\sin\alpha - y_{ck}, \\ B_{kB} &= (aC_{\Pi k})\cdot\cos\gamma\cdot\cos\alpha - y_{ck}\cdot\cos\gamma\cdot ctg\alpha - l_k, \end{aligned}\right\} \tag{14}$$

where $l_k = L - y_{ck}\cdot\cos\gamma\cdot ctg\alpha$.

In order to obtain a mathematical model that reveals the legality of the movement of the k-th stem by lifter $aC_k=f(l_i)$ we deduce the equation of the force line F_T and N and their resulting point F.

For this purpose:

Based on the laws of analytic geometry *(Efymov N.V., 1975)* simultaneously considering equations (3) and (9), expressions have been obtained to determine the guiding parameters l_{k1}, m_{k1}, n_{k1} *(Efymov N.V., 1975)*;

Substituting the received expressions into the equations of the canonical form of the intersection of the slip and bending planes, we obtain the equations of the line of their intersection. It should be noted that this equation can be taken from the equation of the stem on which at the moment the lateral side of the elevator acts.

The resulting equation of the intersection of the sliding and bending planes in the general form (for k^{th} stem) has the form:

$$\frac{x_k}{-C_{k\kappa}\cdot B_{kB}} = \frac{y_k}{C_{k\kappa}\cdot A_{kB}} = \frac{z_k}{-A_{k\kappa}\cdot B_{kB} - B_{k\kappa}\cdot A_{kB}} \tag{15}$$

Similarly, determining the directional parameters of the action lines of the vectors of the absolute and relative velocities of the point C_{nk} we got the equation of their action lines. As indicated above, the equation of the action line of the relative velocity will be described as well as the action line of the frictional force F_T and they will look like:

$$\frac{x_k - x_{C_{\Pi k}}}{l_{kF_T}} = \frac{y_k - y_{C_{\Pi k}}}{m_{kF_T}} = \frac{z_k - z_{C_{\Pi k}}}{n_{kF_T}} \tag{16}$$

where l_{kF_T}, m_{kF_T}, n_{kF_T} – guiding parameters of the action line of the friction force.

The equation in the canonical form and the action line of the force of normal pressure, *N*, which is perpendicular to the sliding plane, passes through the point C_{nk}. Similarly, it was obtained using the coordinates of the vectors (a detailed description is not provided in the article):

$$\frac{x_k - x_{C_{\Pi k}}}{l_{kN}} = \frac{y_k - y_{C_{\Pi k}}}{m_{kN}} = \frac{z_k - z_{C_{\Pi k}}}{n_{kN}} \tag{17}$$

where l_{kN}, m_{kN}, n_{kN} – guiding parameters of the action line of the force of pressure.

The angle between the planes in which the force acts F_T and *N* equals angle *v* friction between the stem and the surface of the lifter. According to the formula known from *Efymov N.V. (1975),* we obtain:

$$\cos\vartheta = \frac{l_{kN} \cdot l_{kF_T} + m_{kN} \cdot m_{kF_T} + n_{kN} \cdot n_{kF_T}}{\sqrt{\left(l_{kN}^{\ 2} + m_{kN}^{\ 2} + n_{kN}^{\ 2}\right) \cdot \left(l_{kF_T}^{\ 2} + m_{kF_T}^{\ 2} + n_{kF_T}^{\ 2}\right)}}. \tag{18}$$

The mathematical model (18) reveals the relationship between the parameters:

- lifter: γ, α, ($b_1 b_1^{l}$);
- its installation: *α, h*;
- parameters of the position of the stems y_{ck}, x_{ck}, θ_k, αC_{nk}.

After the stem is removed from the lifter, it falls under the influence of the following working bodies (Fig. 1).

The distance between the adjacent surfaces of the rotors must be set in such a way as to prevent clogging. For that, stem should not be strongly deflected by the lateral faces on which they slip. This makes it impossible to cross them. The number of stems coming from the lifter will depend on the density of sunflower stems on the field, that is, the parameters y_{ci} and x_{ci}, which are included in the above-mentioned dependencies.

In order to determine the influence of the angle of inclination of the elevator lateral side, the angle of exacerbation of the elevator and the height of the installation of its nose over the surface of the soil on the magnitude of the angle between the lines of force F_T and *N,* depend on the conditions is constructed: α=5˚ - 25˚ and h_1=600 mm i h_2=800 mm.

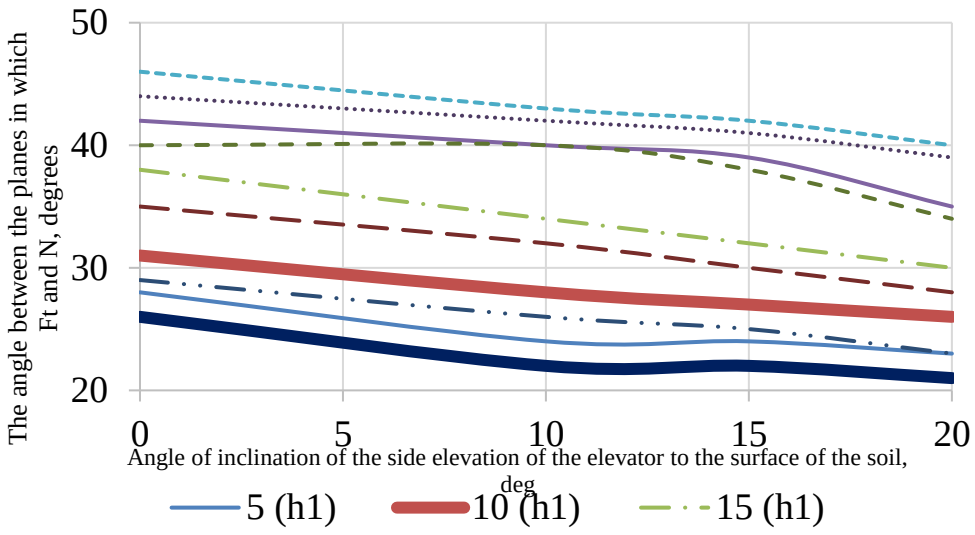

Fig. 5 - Dependence of the angle between the lines of force F_T and *N* and the angle of inclination of lateral side of the lifter

The performed analytical analysis gives grounds to assert that the process of interaction of the stems with the lateral side of the lifter depends on its constructive parameters, namely, the angle α and the lengths of the *ab* side and the technological parameters: the height of the installation and the angle of inclination to the surface of the field.

The analysis methodology of the analytical model, which allowed to determine the nature of the stem movement along the lateral sides of the sunflower header lifter in the process of their interaction, was obtained. This technique was used in the process of designing and further manufacturing a reaper for sunflower harvesting (fig. 1, 6). The lifters of the header have been adjusted in relation to the basic design and can be used to justify the parameters of lifters, in particular for the design of the header.

The resulting equality, considering the previous formulas, establishes the relationship between the parameters h, s_i, α, β_0, e_{x_i}, e_{y_i}, b, φ, ψ, AM_i.

Having solved this equation, one can determine the pattern of movement of the stem along the bar, namely, the function $AM_1=f(s_i)$ for other known parameters.

CONCLUSIONS

1. The method of substantiation of the analytical model is proposed, which allows to determine the nature of the stem movement on the lateral surface of the sunflower header elevator in the process of their interaction.

2. It is established that the angle between the planes in which the force acts F_T and N, which equals angle v friction between the stalk and the surface of the lifter decreases with a decrease in the angle α aggravation of its faces, increasing angle γ the slope of the lateral face of the lifter to the ground and the elevation of the elevator lifting height h.

3. It is recommended to take the angle of the elevator 40˚ (half of the angle $\alpha \leq 20^{\circ}$).

REFERENCES

[1] Anwar M.T., Gupta C. P., (1990), Performance evaluation of chick pea thresher in Pakistan, *Agricultural Mechanization in Asia, Africa and Latin America*, Vol. 21(3), pp. 23-28, Phnom Penh / Cambodia;

[2] Burianov M. A., (2011), Investigation of the interaction between the ear of a plant and the teeth of a single-drum hinged reaper when harvesting crops. (Исследование взаимодействия колоса растения с зубьями однобарабанной навесной на комбайн жаткой при уборке зерновых культур очесом), *Scientific Journal KubHAU*, No. 67, pp. 1–10, Kuban / Russia;

[3] Dalmist I.S., Kayisoglu B., Bayhan Y., Ulger P., Toruk F. and Durgut F., (2013), Development of a chopper unit for chopping of sunflower stalk during harvesting by combine harveater, *Bulgarian Journal of Agricultural Science,* Vol. 19, (no.5), pp. 1148-1154, Sofia / Bulgaria;

[4] Efymov N.V., (1975), *A short course of analytic geometry (Краткий курс аналитической геометрии)*, Moscow / Russia;

[5] Kapustyn, S.A., Kunakov V.P., (2004), *Analysis of losses during sunflower harvesting (Аналіз втрат при збирання соняшнику)*, Vestnyk THTU, no.3, pp. 773–778, Ternopil / Ukraine;

[6] Kepner R.A., (1978), *Principles of farm machinery 3rd edition*, Avi Pub Co, ISBN:087055252X, 527 p., Westport / Australia;

[7] Klenyn N. Y., Sakun V. A., (1980), *Agricultural and meliorative machines: Elements of the theory of work processes, calculation of adjusting parameters and operating modes (Сельськохозяйственные и мелиоративные машины: Элементы теории рабочих процессов, расчет регулировочных параметров и режимов работы),* Kolos, 671 p., Moscow / Russia;

[8] Kukhmazov K.Z., Fedorov V.V., (2013), *Reduction of losses of sunflower seeds during harvesting (Снижение потерь семян подсолнечника при уборке),* Nyva Povolzhia, no. 2, pp. 83–88, Penza / Russia;

[9] Letoshnev M.N., (1934), *Agricultural machines. Theory and calculation. (Сельскохозяйственные машины. Теория и расчет)*, Moscow / Russia;

[10] Lyon D., (1998), Sunflower residue weight and ground cover loss during summer fallow, *Journal of Soil and Water Conservation*, no. 53, ISSN: 1941-3300, pp. 71–73, Ankeny / USA;

[11] Makarov S.S., (2007), Determination of the optimal operating modes of the device with screw feeding of stems for harvesting sunflower (Определение оптимальных режимов работы приспособления со шнековой подачей стеблей для уборки подсолнечника), *Oilseeds. Scientific and Technical Bulletin of the All-Russian Research Institute of Oilseeds (Масличные культуры. Научно-технический бюллетень всероссийского научно-исследовательского института масличных культур)*, Vol. 1., pp. 119–123, Moscow / Russia;

[12] Maksoud A., El-Sayed M.A.F., Shalaby G.H., (2009), Modifying and testing a header system for cereal crop harvester to be suitable for sunflower harvesting, *Egyptian journal of agricultural research,* ISSN: 1110-6336, Cairo / Egypt;
[13] Martinez-Force E., (2015), *Sunflower: Chemistry, Production, Processing, and Utilization*, Presented at Urbana, Illinois / USA;
[14] Nalobina O., Markova O., Vasylchuk N., (2016), Application of morphological analysis and synthesis for the design of sunflower harvesting machines. WSEI scientific notebooks. Transport and IT series (Zastosowanie analizy i syntezy morfologicznej do projektowania maszyn do zbioru słonecznika. Zeszyty naukowe WSEI. Seria Transport I informatyka), Vol. 6 (1), *Lublin nnovatio Press Scientific Publisher of the University of Economics and Innovation (Lublin nnovatio Press Wydawnictwo Naukowe Wyższej Szkoły Ekonomii i Innowacji)*, pp. 45-52, Lublin / Poland;
[15] Nalobina O.O., (2017), *Sunflower harvesting knife (Жатка для збирання соняшнику).* Patent No. 118144, Rivne / Ukraine;
[16] Pacini C., Wossink A., Giesen G., Huirne R., (2004), Ecological-economic modelling to support multi-objective policy making: a farming systems approach implemented for Tuscany, Agriculture, ecosystems & Environment, Vol. 102, ISSN: 0167-8809, pp. 349-364, Amsterdam / The Netherlands;5
[17] Popov M., (2013), *Improvement of the technological process of sunflower harvesting by substantiating the structural and regime parameters of the auger-reel (Совершенствование технологического процесса уборки подсолнечника обоснованием конструктивных и режимных параметров шнека-мотовила),* PhD dissertation, Saratov Agrarian State University, Saratov / Russia;
[18] Shaforostov V.D., Makarov S.S., Pohorelov V.N., (2015), Header for a sunflower harvesting machine (Жатка к селекционному комбайну для уборки подсолнечника), *Oilseeds. Scientific and Technical Bulletin of the All-Russian Research Institute of Oilseeds (Масличные культуры. Научно-технический бюллетень всероссийского научно-исследовательского института масличных культур)*, Vol. 2, pp. 103–105, Moscow / Russia;
[19] Startsev A.S., (2017), Experimental-theoretical justification of the construction and diameter of the tube shaft of auger-reel scraper for harvesting sunflower (Экспериментально-теоретическое обоснование конструкции и диаметра трубного вала шнека-мотовила жатки для уборки подсолнечника), *Proceedings of the Orenburg State Agrarian University (Известия оренбургского государственного аграрного университета),* Vol. 1, pp. 70–74, Orenburg / Russia;
[20] Statistical bulletin, (2018), *«Harvesting of crops» (Статистичний бюлетень (2018 р.) "Збирання врожаю сільськогосподарських культур")*, URL: http://www.ukrstat.gov.ua/druk/publicat/Arhiv_u/07/Arch_zv_bl.htm.

KRAWTCHOUK MOMENT AND PARTICLE SWARM OPTIMIZED BP NEURAL NETWORK TO RECOGNIZE RICE PLANTHOPPER

/

基于 Krawtchouk 矩和 PSO 神经网络的稻飞虱识别研究

Assoc. Prof. Ph.D. Xiuguo Zou *[1], MEE. Stud. Siyu Wang [2], Assoc. Prof. Ph.D. Yan Qian [1], MAE. Stud. Shuaitang Zhang [1]

[1] College of Engineering, Nanjing Agricultural University / China;

[2] School of environmental science and Engineering, Nanjing University of Information Science and Technology / China

Tel: +862558606585; E-mail: xiuguozou@gmail.com

Keywords: *image processing, Krawtchouk moment, particle swarm optimized BP neural network, rice planthopper recognition*

ABSTRACT

Aimed at the problem of unreasonable spraying pesticide in paddy, machine vision can be used in the field identification technology of rice planthoppers. At first, gray processing of the planthopper images, the Gaussian algorithm, OTSU and mathematical morphology were applied for pre-processed images. Then Krawtchouk moment was used for features extraction, and the parameters were selected to optimize the particle swarm optimized neural network for training and testing. Experiments were implemented on MATLAB to train and test 100 Sogatella samples, 100 striatellus samples, and 100 brown planthopper samples. The results show that by using Krawtchouk moment to extract the shape features of the planthopper images and selecting parameters to improve particle swarm optimized BP neural network algorithm, the recognition rate reached 95%. Therefore, it can be used as the planthopper recognition algorithm.

摘要

针对大田中稻飞虱图像纹理和颜色效果不好的问题，研究了基于 Krawtchouk 矩提取形状特征值对稻飞虱进行分类识别。先对稻飞虱图像灰度化后用高斯算法滤波，再用大津法二值化，最后用数学形态学去噪；对预处理后的二值图像先采用 Krawtchouk 矩提取特征值，再用参数选择改进 PSO 优化神经网络的算法进行训练和测试。实验对白背飞虱、灰飞虱和褐飞虱各 100 个样本进行了训练和测试，结果表明 Krawtchouk 矩提取稻飞虱图像形状特征值后，用参数选择改进粒子群优化 BP 神经网络算法的整体识别率达到了 95%，而且收敛性很好，可以作为稻飞虱的识别算法。

INTRODUCTION

Aimed at the problem of unreasonable spraying pesticide in paddy, machine vision was used in the field recognition technology of rice planthoppers (*Finbarr G. H., 2015; Dale G. B., 2012)*. Some researchers of Nanjing Agricultural University have already used machine vision method to try to identify rice planthopper (*Zhao S., 2009; Liu D., 2012; Zou X., 2013*). Compared to the extraction of the texture features or color features, the planthopper shape feature extraction is easy and efficient, thus it plays an important role in real-time recognition. In this paper, the Krawtchouk invariant moment is adopted to extract the shape features of the planthopper. Krawtchouk moment is a discrete orthogonal moment proposed by (*Yap P. T., 2003*). Due to rotation and scale invariance of the moment variables, it is highly helpful for shape extraction of images. To the best of our knowledge, Krawtchouk moment has not been introduced to the recognition of insects such as planthopper before. When it is used for the description of the target images, the moment variable is the ideal feature of the planthopper images, because it provides an approach to image changes caused by the target's scale and position changes (*Yang L., 2008; Wang C., 2016*).

The PSO (Particle Swarm Optimization) algorithm is a fast search global optimization algorithm, which can return good optimization results. Like most evolutionary computation methods (e.g. genetic algorithm and ant colony optimization algorithm), PSO is also based on the swarm. But when the particles converge to the optimal positions, the fast convergence effect will occur among the particle swarm. As a result, it may be stuck in local extremum or cause premature convergence and low accuracy of results. Therefore, various countermeasures have been proposed (*Fang F., 2013*). In this paper, by selecting parameters, the particle swarm optimized BP neural network algorithm is improved for planthopper recognition.

MATERIALS AND METHODS

Image collection

The planthopper images were captured by the SunTime200A USB industrial camera equipped with the SunTimeT100 industrial lens, providing a focal length of 15:1. Three planthopper images are shown in Figure 1. In the next step, the images were sent to the computer for storage.

(a)Sogatella (b) Striatellus (c) Brown planthopper

Fig 1 - Sample images of rice planthoppers

Gray processing and Binarization

Let *R, G, B* denote the gray levels of the red, green and blue color components, and *Y* denotes the image brightness. Defining *Y* component as the gray level of the image pixels is suited for the human eye's perception of colors. The equation for converting color pixels to gray pixels is given in Equation 1.

$$Y = 0.299R + 0.587G + 0.114B \tag{1}$$

Binarization was done via OTSU, which is also known as the maximum between-cluster variance method commonly used to efficiently and easily convert gray images to binary images. By setting up a threshold *t* and according to the gray levels, OTSU classifies image pixels into two types: C_0 for 0 to *t*, and C_1 for *t*+1 to *l*—1, where *l* denotes the gray level of the image. The optimal threshold, t_0, can be determined by maximizing the equivalent decision criterion function of t in Equation 2 (*Wang H., 2012*).

$$\lambda = \frac{\sigma_B^2}{\sigma_W^2} \quad \eta = \frac{\sigma_B^2}{\sigma_T^2} \quad \kappa = \frac{\sigma_T^2}{\sigma_W^2} \tag{2}$$

where: *λ, η, κ* - the equivalent decision criterion function of *t; t*-OTSU threshold;

$\sigma_W^2, \sigma_B^2, \sigma_T^2$ denote the between-cluster, inter-cluster and total variance, respectively.

Gaussian filtering

The Gaussian filter is a linear smooth filter commonly used in image denoising. In this filter, a template is used to scan each pixel of the image, and the pixel at the center of the template is replaced with the weighted average of the gray levels of neighboring pixels. The form is given in Equation 3 (*Wan C., 2017*).

$$E(x, y) = e^{-D^2(x,y)/2\sigma^2} \tag{3}$$

where: *E*- the weighted average of the gray levels of neighboring pixels; *D*- the radius function of Gaussian filter; *x* - distance from the origin in the horizontal axis; *y* - distance from the origin in the vertical axis; *σ*- standard deviation of the Gaussian distribution;

$D(x, y)$ denotes the fuzzy radius $r^2 = D^2(x, y) = x^2 + y^2$. The filter that takes the Gaussian function as the weight function (*W*) is known as the Gaussian filter and its weight function is given in Equation 4.

$$W(r) = \frac{1}{\sqrt{2\pi\sigma}} e^{-r^2/2\sigma^2} \tag{4}$$

Where: *σ* denotes the distribution parameter. *r* - the radius of Gaussian filter; The 6*σ*-width area at the center of the Gaussian curve occupies 99.73% of the entire area under the curve. Thus, after stipulating that the weight function in this interval is dominant for filtering, the signals can be filtered by changing the value of σ.

Morphology-based denoising

After binarization, there may be noises around the truncus of the planthoppers, such as feet, antennae, and bristles. Hence, the morphology-based operations should be performed, which mainly refer to the erosion and dilation operations.

Erosion operations of binary images

Erosion operations can eliminate boundary points of objects as well as small and meaningless objects. It is based on the concepts of structural element, which is template for shrinking the object boundary to improve the recognition accuracy of planthoppers. If tiny connections exist between two objects, a sufficiently

large structural element will separate the two objects via erosion operations. Let $X\Theta S$ express erosion, so the equation is given as follows (*Mao W., 2008*).

$$X\Theta S = \{\chi \mid S[\chi] \subseteq X\} \tag{5}$$

where:

X denotes the set of pixels of target image, and *x* is each pixel point in *X*. *S* is the structural element, and *S*[*χ*] is the set that each pixel point of *S* moves the distance from the pixel point to *χ*.

Dilation operations of binary images

In dilation operations, each point *χ* in the image *X* is expanded to *S*[*χ*]. This operation is designed to merge the background points around the image into the object. If two objects are close to each other, then they can be connected via dilation operations, as it is very helpful in filling in the holes in the objects after image segmentation. Let $X \oplus S$ express the dilation operation, so the equation is given as follows (*Jufriadif N., 2017*).

$$X \oplus S = \{\chi \mid S[\chi] \cap \chi \neq \Phi\} \tag{6}$$

where: Φ is the empty set.

Features extraction method

The Krawtchouk moment invariant is derived from the Krawtchouk polynomial. The n^{th} weighted Krawtchouk polynomial at the discrete point *x* is defined as follows (*Yap P. T., 2003*).

$$K_n(x;p,N-1) = \sqrt{\frac{\omega(x;p)}{\rho(n;p)}} F_1\left(-n,-x;-(N-1);\frac{1}{p}\right) \tag{7}$$

where:

x, *n* = 0,1,2,…,*N*, *N*>0, *p*∈(0, 1).

$F_1(a,b;c;z) = \sum_{v=0}^{n} \frac{(a)_v (b)_v}{(c)_v} \frac{z^v}{v!}$ is the hypergeometric function, *a, b, c, z* are the formal parameters of the function, *v* is the argument in the range [0,*n*], $(a)_v$ denotes the reduced order power from *a*+*v*+1 to *a*. Definitions of $(b)_v$ and $(c)_v$ are similar to that of $(a)_v$.

$\omega(x;p) = \binom{N-1}{x} p^x (1-p)^{N-1-x}$ is the Binomial-distribution weight computation function.

$\rho(n;p)$ is the normalized coefficient and the equation is shown as follows:

$$\rho(n;p) = (-1)^n \left(\frac{1-p}{p}\right)^n \frac{n!}{-(N-1)_n} \tag{8}$$

With the above polynomial definition, the Krawtchouk moment can be defined according to the separability. An approximation of $f(x,y)$ is:

$$f(x,y) \cong \sum_{n=0}^{n_{max}} \sum_{n=0}^{m_{max}} Q_{nm} K_n(x;p_1,N-1) K_m(y;p_2,N-1) \tag{9}$$

According to Equation (9), the $(n+m)$th term of the Krawtchouk moment, Q_{nm}, is given as follows.

$$Q_{nm} = \sum_{x=0}^{N-1} \sum_{y=0}^{N-1} K_n(x;p_1,N-1) K_m(y;p_2,N-1) f(x,y) \tag{10}$$

where Q_{nm} is the Krawtchouk moment invariant.

PSO algorithm

The PSO algorithm originates from modelling the preying of birds and is based on the concepts of swarm and fitness. Each particle in the swarm can be characterized by position and speed and represents a possible solution by position. The quality of the position is measured by fitness in the algorithm. A group of particles is randomly initialized and the optimal solution is determined via iterations (*Yap P. T., 2003*).

In *H*-dimensional space, there are *M* particles, and *i*= 0,1,2,…,M, M>0, then the position and speed of the i^{th} particle are shown as Equation 11 and Equation 12.

$$u_i = (u_{i1}, u_{i2}, ...u_{iH}) \quad (11)$$

$$s_i = (s_{i1}, s_{i2}, ...s_{iH}) \quad (12)$$

During each iteration, the particle updates the following two solutions by tracking two extremums.

The first is the optimal solution of the particle itself, which is called the individual extremum, and the equation is shown as follows:

$$pb_i = (pb_{i1}, pb_{i2}, ..., pb_{iH}) \quad (13)$$

The second is the optimal solution that the entire population has found the optimal solution, which is called the global extremum, and the equation is shown as follows:

$$gb = (gb_1, gb_2, ..., gb_H) \quad (14)$$

While searching these two optimal values, the particle updates its position and speed in *H*-dimensional space using the following equations:

$$u_{ih}^{\ k} = u_{ih}^{\ k-1} + s_{ih}^{\ k-1} \quad (15)$$

$$s_{ih}^{\ k} = Ts_{ih}^{\ k-1} + c_1 \cdot rand() \cdot (pb_{ih}^{\ k-1} - u_{ih}^{\ k-1}) + c_2 \cdot rand() \cdot (gb_h^{\ k-1} - u_{ih}^{\ k-1}) \quad (16)$$

where:

h = 0, 1, 2 ,…, H, $u_{ih}^{\ k}$ and $s_{ih}^{\ k}$ denote the h^{th} dimensional components of the position and speed of the particle i at each iteration time k, pb_{id}^{k} is the best individual position of the particle i and gb_{id}^{k} are the best position of global particle position i at each iteration time k, *rand*( ) denotes the random number that follows (0,1) uniform distribution, T is the inertia weight, and c_1, c_2 are the acceleration coefficients.

Improved PSO neural network based on parameter selection

In PSO algorithm, when the particles converge to the optimal positions, the fast convergence effect will occur among the particle swarm, inclining it to be stuck in local extremum or causing premature convergence and low accuracy of results (*Zhang J., 2016*). So, the algorithms should be improved. In this paper, the PSO algorithm is improved via parameter selection. The improved algorithm is called Improved PSO. The parameters that need to be optimized include the maximum speed, two acceleration coefficients, and the constriction factor.

Step 1: Selection of the maximum speed.

The particle speed in Equation 16 is a random variable. The motion tracks generated by the particle position updating Equation 15 are uncontrollable, so the particles jump repeatedly in the problem space. To alleviate irregular jumping, the speed is usually bound by [$-s_{max}$, s_{max}]. A large s_{max} is helpful for global search, whereas a small s_{max} is helpful for local exploitation. But if s_{max} is too high, the motion tracks of particles may be irregular or even beyond the area of the optimal solutions. In this case, the algorithm can hardly converge and thus comes to a standstill. If s_{max} is too small, then the step of the particles may be also too small and the algorithm may be stuck in local extreme values. In this paper, s_{max} is set to 2.0 through the experiments. (*Hotaka Y., 2017*).

Step 2: Selection of acceleration coefficients.

The acceleration coefficients in Equation 16, c_1 and c_2, are used to make the particle move towards itself or the optimal position in the neighborhood, respectively. A time variable adaptive strategy is adopted: c_1 is linearly reduced from 2.5 to 0.5, and c_2 is linearly increased from 0.5 to 2.5 among evolutional generations.

Step 3: Selection of constriction factor.

If the PSO speed is updated according to Equation 17, then even though s_{max} and the two acceleration coefficients are selected properly, the particles are still likely to go beyond the problem space or even converge to the infinity, causing swarm explosion. The constriction factor A is properly selected to alleviate this problem.

The PSO algorithm with the constriction factor was proposed by (Kennedy, 1995), and the simplest version of the speed updating equation is given as follows.

$$s_{ih}^{\ k} = A\left[s_{ih}^{\ k-1} + c_1 \cdot rand() \cdot (pb_{ih}^{\ k-1} - u_{ih}^{\ k-1}) + c_2 \cdot rand() \cdot (gb_h^{\ k-1} - u_{ih}^{\ k-1}) \right] \quad (17)$$

where: A is the constriction factor, and the equation is shown as Equation (18).

$$A = \frac{2}{\left|2 - \varphi - \sqrt{\varphi^2 - 4\varphi}\right|}, \quad \varphi = c_1 + c_2, \varphi > 4 \tag{18}$$

The improved PSO optimized BP neural network algorithm is shown in Figure 2 (*Shi F., 2011*).

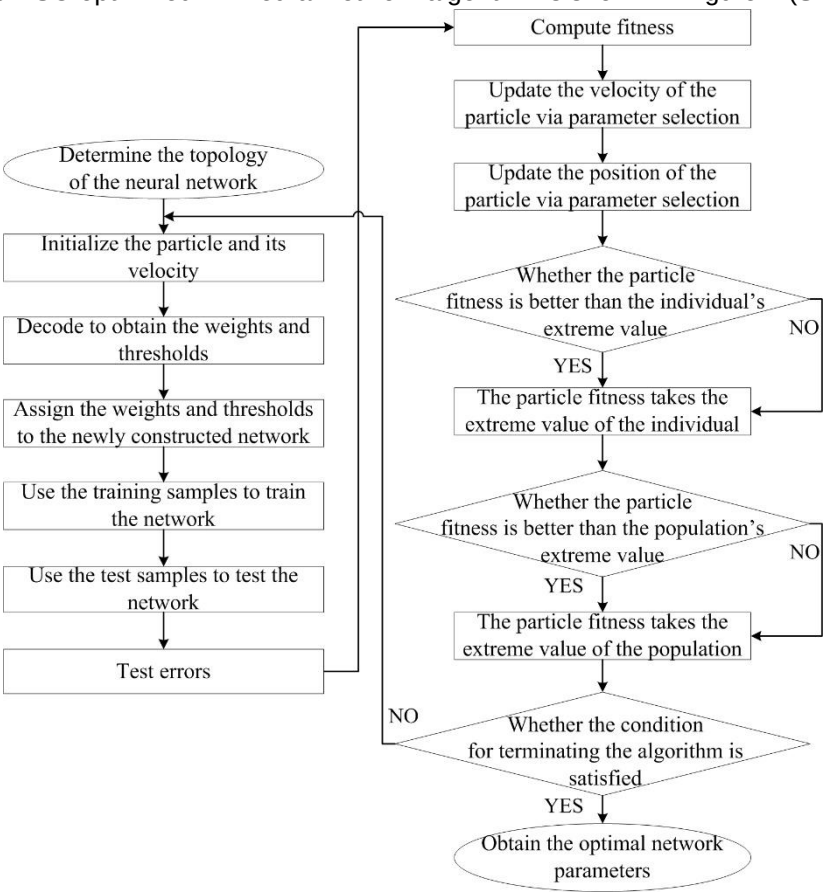

Fig. 2 - Flow chart of improved PSO optimized BP neural network

Planthoppers recognition using improved PSO optimized BP neural network algorithm

The steps for recognizing the planthoppers via the PSO optimized BP neural network algorithm are given as follows.

Step 1: Initialize a group of particles.

This step involves the size of the population, the neural network topology, random positions and speeds, acceleration coefficient, number of iterations, upper limit of errors, etc. For the BP neural network trained by PSO, the size of the population is set to 50. All the weights of the BP network and the thresholds of the hidden-layer nodes are defined as the initial positions of particles. Real numbers are used for particle coding, the initial number of nodes at the hidden layer is set to 5, and the largest number of nodes at the hidden layer is set to 20. The stepwise increase method is adopted for network training to increase the number of hidden-layer nodes until the requirements are satisfied. The maximum speed of particles is set to 2.0, and the number of iterations k is set to 2,000 (*Kim T. H., 2008*).

Step 2: Evaluate the fitness of each particle.

The fitness function is a performance measure of BP neural network. *MSE* of the neural network outputs is defined as the objective function, and its reciprocal is defined as the fitness function. (*Sun W., 2009*). The equation for computing function is shown as follows.

$$MSE = \frac{2}{IJ} \sum_{i=1}^{I} \sum_{j=1}^{J} \left(d_{ij} - w_{ij}\right) \tag{19}$$

where: I is the number of output nodes, J is the number of training samples, d_{ij} is the expected output of the network, and w_{ij} is the actual output of the network.

Step 3: Update each particle's speed and position via parameter selection.

By using the optimization parameters (i.e. the maximum speed, two acceleration coefficients, and the constriction factor), each particle's speed and position can be computed and updated according to Equation 15, Equation 16 and Equation 17.

The speed of each particle should be checked to see if it is in the range [$-s_{max}$, s_{max}], whereas the position of each particle should be checked to see if it is in the range [$-u_{max}$, u_{max}] (*Lei, Y., 2013*).

Step 4: Compare the fitness of each particle *i* with its previous extreme value pb_i. If it is better than pb_i, then it is defined as the current pb_i. Continue to compare it with the global extreme value *gb*. If it is better than *gb*, then *i* is defined as the current *gb* (*Shi B., 2010*).

Step 5: The number of evolution times is set to 100. If the fitness is sufficiently good or the preset maximum number of iteration is reached, then improved PSO neural network is constructed. Next, follow step 6, otherwise, increase the number of iteration times by 1 and jump to step 2.

Step 6: Use the improved PSO neural network to train and recognize the planthoppers.

RESULTS

After collecting planthopper images, gray processing, the Gaussian algorithm, OTSU and mathematical morphology were applied for pre-processed images. Figure 3 shows the gray-scale image and the binary image before and after Gaussian filtering.

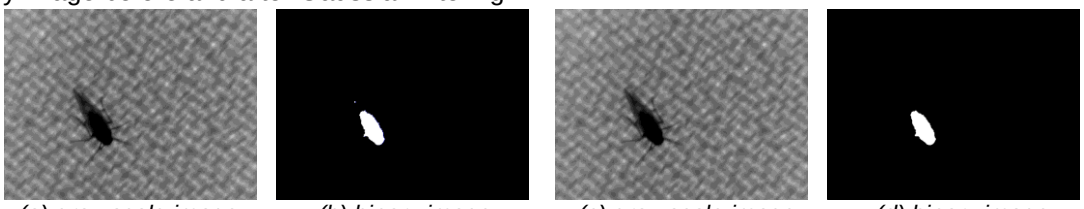

(a) gray-scale image before Gauss filtering *(b) binary image before Gauss filtering* *(c) gray-scale image after Gauss filtering* *(d) binary image after Gauss filtering*

Fig. 3 - Gray-scale images and binary images before and after Gauss filtering

Figure 4 shows the binary images that were processed by Gaussian filtered algorithm, OTSU binarized algorithm and denoised algorithm using the morphology-based method in sequence.

Fig. 4 - Binary images after denoising

After binarization, 6 Krawtchouk moment features can be extracted from each of the three types of planthopper images in Figure 1. The extracted feature values are listed in Table 1.

Table 1

Extracted features of rice planthoppers by Krawtchouk moment

Features of Krawtchouk moment	Sogatella	Striatellus	Brown planthopper
Krawtchouk20	4.054529	2.849234	3.498444
Krawtchouk02	2.597408	1.400971	2.323513
Krawtchouk30	2.360537	0.938745	1.899877
Krawtchouk03	2.659690	1.555703	2.514412
Krawtchouk40	5.547901	4.558641	5.240641
Krawtchouk04	1.405166	1.158586	1.099641

The 300 collected image samples were used in the experiment, consisting of 100 Sogatella samples, 100 striatellus samples, and 100 brown planthopper samples. The first 240 images were chosen as the training samples and the rest 60 images that consist of 20 Sogatella images, 20 striatellus images, and 20 brown planthopper images were chosen as the test samples. The training and test outputs are classified into

three types, and the values for the Sogatella, striatellus and brown planthopper are set to 100, 010 and 001, respectively. The algorithm was implemented on MATLAB.

When the BP neural network is trained by PSO, the size of the population is set to 50, the maximum speed of the particle: s_{max}=2.0, and the number of iterations k is set to 2,000. The trained network obtains the weights and thresholds that satisfy the requirements, whereas the number of evolution times is set to 100.

The test and actual results are compared in Figure 5.

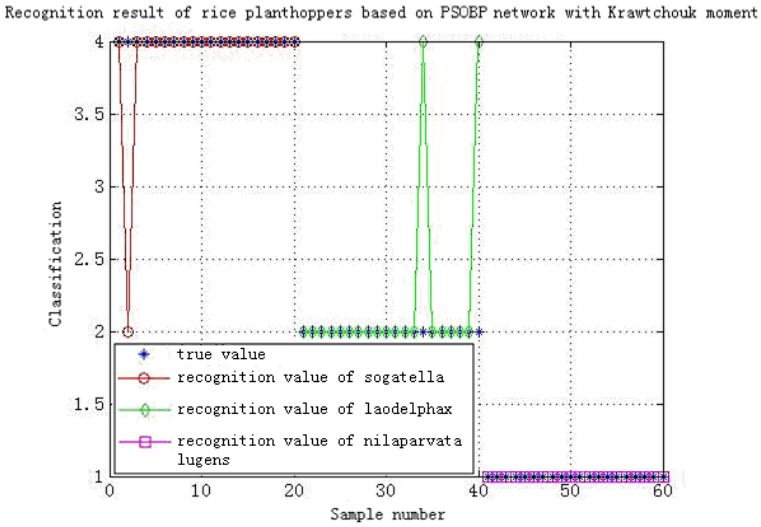

Fig. 5 - The actual value compared with test value by PSO optimized BP neural network

Figure 5 shows that the recognition rates for Sogatella, striatellus and brown planthopper are 95%, 90% and 100%, respectively. The overall recognition rate is up to 95%.

CONCLUSIONS

The collected planthoppers images can be used to yield the high-quality binary planthoppers images by gray processing, Gaussian filtering, OTSU binarization and morphology-based denoising. The images processed in this step facilitate features extraction and object recognition. The Krawtchouk moment-based extraction of shape features of planthopper images can represent global features and show good locality. Experiments prove that the recognition rate can be guaranteed if it is used for planthopper features extraction. In addition, if the Krawtchouk moment is used, only a small number of features will be extracted. So the computational complexity is low and helpful for real-time recognition. In PSO, particles may be stuck in local extremum or cause premature convergence and low accuracy of results. The parameter selection strategy is used to address this problem. Parameters are properly chosen to optimize the PSO algorithm and recognize planthoppers. The overall recognition rate is 95% while ensuring fast evolutionary rate and good convergence behavior. The proposed method is a good choice for real-time recognition of planthoppers.

ACKNOWLEDGEMENTS

This work was supported by China Postdoctoral Science Foundation (2015M571782), the Fundamental Research Funds for the Central Universities of China (KYTZ201661), and Jiangsu Agricultural Machinery Foundation (GXZ14002).

REFERENCES

[1] Carmine C., Luca P., Domenico G., (2017), Automatic target recognition of military vehicles with Krawtchouk moments, *IEEE Transactions on Aerospace and Electronic Systems,* Vol. 53, Issue 1, pp. 493-500, Piscataway, New Jersey/USA;

[2] Dale G.B., Kenneth G.S., (2012), Resurrecting the ghost of green revolutions past: The brown planthopper as a recurring threat to high-yielding rice production in tropical Asia, *Journal of Asia-Pacific Entomology,* Vol. 15, Issue 1, pp. 122-140, Suwon/South Korea;

[3] Fang F., Zhang Z., Zhang X. et al., (2013), Reduction in Activity/Gene Expression of Anthocyanin Degradation Enzymes in Lychee Pericarp is Responsible for the Color Protection of the Fruit by Heat and Acid Treatment, *Journal of Integrative Agriculture*, Vol. 12, Issue 9, pp. 1694-1702, Beijing/China;

[4] Finbarr G.H., Angelee F.R., Jagadish S.B. et al., (2015), Virulence of brown planthopper (Nilaparvata lugens) populations from South and South East Asia against resistant rice varieties, *Crop Protection*, Vol.78, Issue 11, pp. 222-231, Oxford/U.K.;

[5] Hotaka Y., Yoshikazu F., (2017), Parallel multi-population differential evolutionary particle swarm optimization for voltage and reactive power control in electric power systems, 56th Annual Conference of the Society of Instrument and Control Engineers of Japan, *IEEE*, Kanazawa/Japan;

[6] Jufriadif N., (2017), Edge detection on objects of medical image with enhancement multiple morphological gradient method, *4th International Conference on Electrical Engineering, Computer Science and Informatics*, *IEEE*, Yogyakarta/Indonesia;

[7] Kennedy, J., Russell C., (1995), Particle swarm optimization. *IEEE international conference on neural networks*, *Perth/ Australia;*

[8] Kim T.H., Maruta I. and Sugie T., (2008), Robust PID controller tuning based on the constrained particle swarm optimization, *Automatica*, Vol. 44, Issue 4, pp. 1104-1110,

[9] Lei Y., Xiaokang D., Jianlei K., (2013), Parameters optimization algorithms for improving the performance of obstacles identification in forest area, *INMATEH - Agricultural Engineering*, Vol. 40, Issue 2, pp. 43-52, Bucharest/Romania;

[10] Liu D., Zhao S., Ding W. et al., (2012), Identification method for rice planthoppers based on image spectral characteristics, *Transactions of the Chinese Society of Agricultural Engineering*, Vol. 28, Issue 7, pp. 184-188, Beijing/China;

[11] Mao W., Zheng Y., Yuan Y., (2008), Locust information extraction using Hue and shape feature, *Transactions of the Chinese Society for Agricultural Machinery*, Vol. 39, Issue 9, pp. 104-107, Beijing/China;

[12] Shi B., Li Y., Yu X., (2010), Long-term runoff forecast method based on dynamic adjustment particle swarm optimizer algorithm and Holt-Winters linear seasonal model, Transactions of the Chinese Society of Agricultural Engineering, Vol. 26, Issue 7, pp. 8-13, Beijing/China;

[13] Shi F., Wang H., Yu L., (2011), Matlab intelligent algorithm analysis of 30 cases, *Beijing University of Aeronautics and Astronautics Press*, Beijing/China;

[14] Sun W., Zhang W., Li X., (2009), Driving Fatigue Fusion Detection Based on T-S Fuzzy Neural Network Evolved by Subtractive Clustering and Particle Swarm Optimization, *Journal of Southeast University (English Edition),* Vol. 25, Issue 4, pp. 356-361, Nanjing/China;

[15] Wan C., Ye M., Yao C. et al., (2017), Brain MR image segmentation based on Gaussian filtering and improved FCM clustering algorithm, *10th International Congress on Image and Signal Processing, BioMedical Engineering and Informatics, IEEE* Shanghai/China;

[16] Wang C., Li Z., (2016), Weed recognition using SVM model with fusion height and monocular image features, *Transactions of the Chinese Society of Agricultural Engineering*, Vol. 32, Issue 15, pp. 165-174, Beijing/China;

[17] Wang H., Feng X., Li L., (2012), Detection algorithm of white foreign fibers based on improved two-dimensional maximum between-class variance method, *Transactions of the Chinese Society of Agricultural Engineering*, Vol. 28, Issue 8, pp. 214-219, Beijing/China;

[18] Yang L., Ding W., Liu D., et al., (2008), Study of feature measuring and extraction for delphacidae images, *Journal of Agricultural Mechanization Research,* Vol. 30, Issue 6, pp. 180-183, Haerbin/China;

[19] Yap P. T., Paramesran R., Omg S. H., (2003), Image analysis by Krawtchouk moments, *IEEE Transaction on Image Processing*, Vol. 12, Issue 11, pp. 1367-1377, Piscataway, New Jersey /USA;

[20] Zhang J., Qi L. and Ji R., (2016), Cotton diseases identification based on rough sets and BP neural network, *Transactions of the Chinese Society of Agricultural Engineering*, Vol. 47, Issue 7, pp. 35-41, Beijing/China;

[21] Zhao S., Ding W., Liu D., (2009), Rice hopper shape recognition based on Fourier descriptors, *Translations of the Chinese Society for Agricultural Machinery,* Vol. 40, Issue 8, pp. 181-184, Beijing/China;

[22] Zou X., Ding W., Liu D. et al., (2013), Recognition System of Rice Planthopper Based on Improved Hu Moment and Genetic Algorithm Optimized BP Neural Network, *Transactions of the Chinese Society for Agricultural Machinery*, Vol. 44, Issue 6, pp. 222-226, Beijing/China.

WRITING NORMS

Article Types

Three types of manuscripts may be submitted:

1. **Regular articles:** These should describe new and carefully confirmed findings, and experimental procedures should be given in sufficient detail for others to verify the work. The length of a full paper should be the minimum required to describe and interpret the work clearly (max.10 pages, even number);
2. **Short Communications:** A Short Communication is suitable for recording the results of complete small investigations or giving details of new models or hypotheses, innovative methods, techniques or apparatus. The style of main sections has not necessarily to be in accordance with that of full-length papers (max. 6 pages, even number);
3. **Reviews:** Submissions of reviews and perspectives covering topics of current interest are welcome and encouraged (max.10 pages, even number).

Manuscripts should be written in English (American or British usage is accepted, but not a mixture of these) and submitted **electronically** at the following e-mail addresses: ***inmatehjournal@gmail.com***
Please be sure to include your full affiliation and e-mail address (see Sample manuscript)
The authors are responsible for the accuracy of the whole paper and references.
There are allowed 2 papers by each first author.
The text layout should be in single-column format. To avoid unnecessary errors it is strongly advised to use the "spell-check" and "grammar check" functions of your word processor.

Review Process

All manuscripts are reviewed by 2 members of the Scientifically Review Office. Decisions will be made as rapidly as possible and the journal strives to return reviewers' comments to authors in approx.3 weeks.
The editorial board will re-review manuscripts that are accepted pending revision.

NOTE:

Submission of a manuscript implies: that the work described has not been published before (excepting as an abstract or as part of a published lecture or thesis) that it is not under consideration for publication elsewhere.

1. REGULAR ARTICLES

- Manuscripts should be concise, in ***1.15 line spacing***, and should have 2 cm all over margins. The font should be ***Arial 10 pt.*** Ensure that each new paragraph is clearly indicated, using **TAB at 1 cm**.
- Title will be ***Arial 12 pt***. and explicit figures will be ***Arial 9 pt***.
- Text will be written in English.
- Chapters' titles are written by ***Arial 10 pt, Bold, Uppercase*** (e.g. **INTRODUCTION, MATERIALS AND METHODS**), between chapters is left a space for 10 pt. At the beginning of each paragraph, TAB of 1 cm.
- The paper body will be written in ***Arial 10 pt., Justify alignment***.

TITLE ***Arial 12 pt., Uppercase, Bold, Center*** *(in English language)* and ***Bold Italic*** *(in native language).*
Should be a brief phrase describing the contents of the paper. Avoid long titles; a running title of no more than 100 characters is encouraged (without spaces).

AUTHORS ***ARIAL 9, Bold, Centre alignment***
Under the paper's title, after a space (enter) 9 pt., write ***authors' names*** and ***affiliations (Arial 8 pt.-Regular)***
When the paper has more than one author, their name will be followed by a mark (Arabic numeral) as superscript if their affiliation is different. Less than 6 authors.
Corresponding author's name (next row), ***(Arial 8 pt.)***. Should be added also: phone, fax and e-mail information, for the paper corresponding author (***font: 8 pt., Italic***).

KEYWORDS ***(In English)*** about 4 to 7 words that will provide indexing references should be listed (title: ***Arial 10pt, bold italic,*** text ***Arial 10 pt., italic***).

A list of non-standard *Abbreviations* should be added. In general, non-standard abbreviations should be used only when the full term is very long and used often. Each abbreviation should be spelled out and introduced in parentheses the first time it is used in the text. Standard abbreviations (such as ATP and DNA) need not to be defined.
ABSTRACT ***(in English and Native language, Arial 10 pt.)***, the title *bold*; the text of abstract: *italic*) should be informative and completely self-explanatory, briefly present the topic, state the scope of the experiments, indicate significant data, and point out major findings and conclusions. The Abstract should be max.250 words. Complete sentences, active verbs, and the third person should be used, and the abstract should be written in the past tense. Standard nomenclature should be used and abbreviations should be avoided. No literature should be cited.

INTRODUCTION (***Arial 10 pt.)*** should provide a clear statement of the problem, the relevant literature on the subject, and the proposed approach or solution. It should be understandable to colleagues from a broad range of scientific subjects. We should refer to the current stage of researches performed in the field of the paper to be published, by quoting up-to-date specialty studies, preferably published after 2006, excepting certain referential specialty books/studies, especially papers issued in magazines/journals/conferences/ISI quoted symposia or in other international data bases, which are well known and available.

MATERIALS AND METHODS (***Arial 10 pt.)*** should be complete enough to allow experiments to be reproduced. However, only truly new procedures should be described in detail; previously published procedures should be cited, and important modifications of published procedures should be mentioned briefly. Methods in general use need not be described in detail.

RESULTS (***Arial 10 pt.)*** should be clarity presented. The results should be written in the past tense when describing findings in the authors' experiments. Results should be explained, but largely, without referring to the literature. Discussion, speculation and detailed interpretation of data should not be included in the Results, but should be put into the Conclusions section.

CONCLUSIONS (***Arial 10 pt.)*** The main conclusions drawn from results should be presented in a short Conclusions section. Do not include citations in this section.

Formulae, symbols and abbreviations: Formulae will be typeset in Italics (preferable with the Equation Editor of Microsoft Office 2003) and should be written or marked as such in the manuscript, unless they require a different styling. They should be referred to in the text as Equation (4) or e.g. (4). The formulae should be numbered on the right side, between brackets ***(Arial 10 pt.)***:

$$P = F \cdot v \quad (1)$$

Terms of the equation and the unit measure should be explained, e.g.

P is the power, [W];
F – force, [N];
v – speed, [m/s]

SI units must be used throughout.

Tables should be self-explanatory without reference to the text. The details of the methods used in the experiments should preferably be described in the legend instead of in the text. The same data should not be presented both in table and graph form or repeated in the text.
Table's title will be typed***Arial 9 pt, Bold, Centered***
In the table, each row will be written Arial 9 pt, single-spaced throughout, including headings and footnotes.
The table should be numbered on the right side, between brackets ***(Arial 10 pt)***:

Figure (Arial 9 pt., Bold, Center)should be typed in numerical order (Arabic numerals). Graphics should be high resolution (e.g.JPEG).Figure number is followed by what represent the figure or graph e.g.:

Fig.1 – Test stand

Legend: Arial 8 pt, Italic, Center, e.g.

1 - plansifter compartments; 2- break rolls; 3 – semolina machines; 4 – reduction rolls; 5 – flour

ACKNOWLEDGMENTS (***Arial 10 pt.)*** of people, grants, funds etc should be brief (*if necessarily*).

REFERENCES (***Arial 10 pt.)***
(In alphabetical order, in English and in the original publication language).
Minimum 10 references, last 10 years, minimum 3 references from the last 2 years
It can be used"*References*" tool from the *Word Editor*.
References should be cited in the text in brackets as in the following examples:
(Babiciu P., Scripnic V., 2000)
All references must be provided in English with a specification of original language in round brackets.

Authors are fully responsible for the accuracy of the references.
References should be alphabetically, with complete details, as follows:
Examples:
Books: Names and initials of authors, year (between brackets), title of the book (Italic), volume number, publisher, place, pages number or chapter, ISSN/ISBN:

[1] Vlădut V., (2009), *Study of threshing process in axial flow apparatus (Studiul procesului de treier la aparatele cu flux axial),* vol.1, ISSN/ISBN ……., "Terra Nostra" Publishing House, Iaşi/Romania;

Journal Article: Names and initials of authors, year (between brackets), full title of the paper, full name of the journal (Italic), volume number, publisher, place, ISSN, page numbers:

[1] Lizhi Wu, Yan Di., (2005), Demonstrational study on the land consolidation and rehabilitation (LCR) project of saline-alkali soil in arid areas: a case study of Lubotan LCR project in Pucheng County, Shaanxi Province(干旱区盐碱化土地整理工程实证研究-以陕西蒲城县卤泊滩土地整理项目为例), *Transactions of the Chinese Society of Agricultural Engineering*,vol.21, no.1, pp.179-182, Madison/Wisconsin;

[2] Leonov I.P., (1973), Basic machine theory for tobacco stringing. Post-harvest care of tobacco and rustic tobacco (Основы теории машин для закрепления табака на шнуры. Послеуборочная обработка табака и махорки), *Collection of scientific articles (сборник научно-исследовательских работ)*, pp.37-45;

Conference or Symposium: Names and initials of authors, year (between brackets), full title of the paper (Regular), full name of the conference/symposium (Italic), volume number, publisher, place, ISSN, page numbers

[1] Bungescu S., Stahli W., Biriş S., Vlăduţ V.,Imbrea F., Petroman C., (2009), Cosmos program used for the strength calculus of the nozzles from the sprayers (Program Cosmos folosit pentru calculul de rezistență la zgomot al aparatelor de distribuție), *Proceedings of the 35 International Symposium on Agricultural Engineering "Actual Tasks on Agricultural Engineering",* pp.177-184, Opatija / Croatia;

Dissertation / Thesis: Names and initials of authors, year (between brackets), full name of the thesis (Italic), specification (PhD Thesis, MSc Thesis), institution, place;

[1] Popa L., (2004), *Research on the influence of structural and functional parameters of the braking system on the braking performance of agricultural trailers (Cercetări privind influența caracteristicilor constructive şi funcționale ale sistemelor de frânare asupra performanțelor de frânare ale remorcilor agricole)*, PhD dissertation, Transylvania University of Braşov, Braşov / Romania.

Patents: Names and initials of authors, year (between brackets), patent title (Italic), patent number, country:

[1] Grant P., (1989), *Device for Elementary Analyses*. Patent, No.123456, USA.

Legal regulations and laws, organizations: Abbreviated name, year (between brackets), full name of the referred text, document title/type (Italic), author, place:

[1] *** EC Directive, (2000), Directive 2000/76/EC of the European Parliament and of the Council of 4 December 2000, on the incineration of waste, Annex V, *Official Journal of the European Communities*, L332/91, 28.12.2000, Brussels.

Web references: The full URL should be given in text as a citation, if no other data are known. If the authors, year, and title of the documents are known and the reference is taken from a website, the URL address has to be mentioned after these data:

The title of the book, journal and conference must be written in Italic, the title of the article, chapter of the book, must be written Regular.

Citation in text

Please ensure that every reference cited in the text is also present in the reference list (and vice versa). Do not cite references in the abstract and conclusions. Unpublished results, personal communications as well as URL addresses are not recommended in the references list.

Making personal quotations (one, at most) should not be allowed, unless the paper proposed to be published is a sequel of the cited paper. Articles in preparation or articles submitted for publication, unpublished, personal communications etc. should not be included in the references list.

Citations style

Text: All citations in the text may be made directly (or parenthetically) and should refer to:

- ***single author:*** the author's name (without initials, unless there is ambiguity) and the year of publication:
  "as previously demonstrated *(Brown, 2010)*".
- ***two authors:*** both authors' names and the year of publication: *(Adam and Brown, 2008; Smith and Hansel, 2006; Stern and Lars, 2009)*
- ***three or more authors:*** first author's name followed by "et al." and the year of publication: "As has recently been shown *(Werner et al., 2005; Kramer et al., 2000)* have recently shown ...."

Citations of groups of references should be listed first alphabetically, then chronologically.

Units, Abbreviations, Acronyms

- Units should be metric, generally SI, and expressed in standard abbreviated form.
- Acronyms may be acceptable, but must be defined at first usage.

Edited by: INMA Bucharest
6 Ion Ionescu de la Brad Blvd., sect. 1, Bucharest, ROMANIA
Tel: +4021.269.32.60; Fax: +4021.269.32.73
http://www.inmateh.eu
e-mail: ***inmatehjournal@gmail.com***